GEOTRACK

VIVONNE-1 AND BORDA-1 WELLS, DUNTROON BASIN, OFFSHORE SOUTH AUSTRALIA

THERMAL HISTORY RECONSTRUCTION USING APATITE FISSION TRACK ANALYSIS AND VITRINITE REFLECTANCE

GEOTRACK REPORT #569

A report prepared for the Petroleum Division, Mines and Energy South Australia (MESA), Adelaide

Report prepared by: I. R. Duddy
AFTA determinations by: M. E. Moore
Vitrinite determinations by: Keiraville Konsultants

September 1995

Geotrack International Pty Ltd
A C N 006 821 209
PO Box 4120
Melbourne University
Victoria 3052 Australia

Telephone 61+3 9344 7214
Facsimile 61+3 9347 5938

Samples to:
Room 225 Earth Sciences Bldg
University of Melbourne
Cnr Swanston and Elgin St
Carlton Victoria 3052
Australia

VIVONNE-1 AND BORDA-1 WELLS, DUNTROON BASIN, OFFSHORE SOUTH AUSTRALIA

THERMAL HISTORY RECONSTRUCTION USING APATITE FISSION TRACK ANALYSIS AND VITRINITE REFLECTANCE

CONTENTS

GEOTRACK REPORT #569

TABLES

GEOTRACK REPORT #569

FIGURES

VIVONNE-1 AND BORDA-1 WELLS DUNTROON BASIN, OFFSHORE SOUTH AUSTRALIA

THERMAL HISTORY RECONSTRUCTION USING APATITE FISSION TRACK ANALYSIS AND VITRINITE REFLECTANCE

EXECUTIVE SUMMARY

Aims and Objectives

This study was commissioned by the **Petroleum Division, Mines and Energy South Australia (MESA)**, and was completed in September 1995. Principal objectives of the study were to determine the timing and nature of any episodes of heating and cooling affecting the Duntroon Basin. The report provides a thermal history framework for understanding the history of potential hydrocarbon occurrence in the **Vivonne-1 and Borda-1 wells, Duntroon Basin, offshore South Australia.**

Technical Summary

1. Thermal history reconstruction in the wells clearly reveals one major period of heating in the **Mid-Cretaceous** and, tentatively, a second period in the **Tertiary.**

2. The **Mid-Cretaceous** event is responsible for maximum paleotemperatures in the preserved Early Cretaceous (Borda Formation) sequence in Vivonne-1. Cooling from maximum paleotemperatures is constrained by integration of AFTA and VR data in Vivonne-1 to have begun between ~112 and 75 Ma, with a time around 95 Ma considered most likely on regional tectonic grounds. The observed Mid-Cretaceous heating is interpreted to result from a combination of increased heat flow (paleogeothermal gradient ~60°C/km) and deeper burial (~0.75 km), with cooling due to a combination of decline in heat flow and uplift and erosion.

3. A mild **Tertiary** heating event is tentatively identified in both the Vivonne-1 and Borda-1 wells, but the time of cooling is poorly constrained by a single sample from the Vivonne-1 well to some time within the last 60 Ma.

The nature of Tertiary heating is also poorly constrained, with moderately higher Tertiary heat flow, minor deeper burial or transient lateral heating from local hot fluid flow all possible explanations.

4. Integration of the results from Vivonne-1 and Borda-1 allows assessment of a general regional maturation model. For a site with a similar Late Cretaceous to Tertiary stratigraphy to Borda-1 and with a deeper Early Cretaceous section like Vivonne-1, maximum maturity in the deeper Early Cretaceous section would have been reached at ~95 Ma (112 to 75 Ma allowed by the AFTA data). Active hydrocarbon generation would have accompanied the rapid Early Cretaceous burial phase prior to rapid Mid-Cretaceous cooling. No hydrocarbon generation would have occurred in the deeper Early Cretaceous section since ~95 Ma, and only a relatively thin section at the top of the preserved Upper Borda Formation would have recommenced maturation during the Late Cretaceous to Recent burial phase.

5. The broad chlorine distributions measured and fission track age patterns in the five **Borda Formation** samples (Barremian to Aptian) from Vivonne-1 provide clear evidence of dominant derivation of detritus from a volcanogenic provenance. These data suggest derivation of the bulk of the detritus in the preserved Early Cretaceous section in the Duntroon Basin from a similar contemporaneous volcanogenic source to that responsible for the Otway and Strzelecki Group sediments deposited further east at the same time.

Recommendations

1. *Investigating the regional extent of Mid-Cretaceous high heat flow:* Thermal history reconstruction for Vivonne-1 has shown conclusively the occurrence of highly elevated paleo-heat flow in the Duntroon Basin, and demonstrated the marked similarity of this thermal history to that determined for the Otway Basin, which has important consequences for hydrocarbon exploration in the basin. It is recommended that AFTA and new VR data be collected on other existing wells in the basin to more fully document the elevated heat-flow event, as a method of focusing exploration on the most prospective areas.

2. *Investigating the cause of Tertiary heating*: Only limited AFTA results were obtained from analysis of two samples from the Borda-1 well, with no information obtained on timing of possible elevated paleotemperatures suggested by the VR data. Analysis of additional, larger samples from the Borda-1 section, or the Tertiary to Late Cretaceous section in related wells, could assist in resolution of this uncertainty. The interpretation of heating in Borda-1 is also hampered by a lack of detailed palaeontology of the shallow section, which becomes

essential in resolution of subtle thermal history problems. New determinations on the stratigraphic age of the Nullarbor Formation section would be desirable in each well studied, but this may be hampered by lack of samples collected in the upper section due to drilling practice.

Technical Results

Technical results of the thermal history reconstruction in Duntroon Basin wells Vivonne-1 and Borda-1 are summarised in Tables i to iii, while schematic illustrations of the main features of the thermal history reconstruction are presented in Figures i to iii. Full details of the interpretation, including discussion of reconstructed burial histories and maturation histories, are given in Sections 2 and 3.

Vivonne-1

1. Integration of AFTA and VR data from the Early Cretaceous section in Vivonne-1 show clear and consistent evidence of cooling from maximum paleotemperatures significantly higher than present temperatures in the Mid-Cretaceous, between ~112 and 75 Ma.

2. The AFTA results also tentatively reveal a second period or cooling from peak paleotemperatures marginally higher than present temperatures, beginning at some time in the Tertiary, between ~60 Ma and the present-day.

5. The Mid-Cretaceous paleotemperature results define a maximum likelihood estimate of the Mid-Cretaceous paleogeothermal gradient of 60.1°C/km (70.9 to 49.5°C/km at ±95% confidence limits), which is significantly higher than the present-day geothermal gradient of 30.2°C/km. This highly elevated paleogeothermal gradient is interpreted to result from higher heat flow associated with Early Cretaceous rifting.

6. The Tertiary paleotemperature results also define a maximum likelihood estimate of the Tertiary paleogeothermal gradient of 33.9°C/km (40.4 to 28.6°C/km at ±95% confidence limits), similar to the present-day geothermal gradient of 30.2°C/km. If present, the minor Tertiary heating may result from either slightly increased heat flow, deeper burial or localised hot fluid flow.

7. The thermal history results indicate that the entire Early Cretaceous section reached its maximum maturity prior to Mid-Cretaceous cooling and has not generated hydrocarbons since that time.

8. The thermal history results provide good constraints on the magnitude of removed section associated with Mid-Cretaceous cooling, with a best-fit estimate of 748 metres of Early Cretaceous section (514 to 1077 m at ±95% confidence limits) removed by uplift and erosion between ~ 112 Ma and 75 Ma. The data also provide a *maximum* estimate of 123 metres of Nullarbor Formation section (123 m at the upper 95% confidence limits), removed by uplift and erosion in the latest Tertiary to Recent. It should be borne in mind that other explanations other than deeper burial are possible for the Tertiary heating, including lateral heat transfer due to hot fluid movement without uplift and erosion.

Borda-1

1. AFTA data from the Borda-1 well are limited to one sample and provide no effective constraint on the thermal history. The VR data are difficult to interpret in detail with AFTA timing constraints, and a number of key questions concerning timing of maximum maturity remain unanswered.

2. At face value, the VR data through the Pidinga and Potoroo Formations indicate that maximum paleotemperatures were higher than the present temperatures at some time after the Maastrichtian-Eocene. However, with the lack of timing information noted in point 1, detailed interpretation depends on knowledge of the heating rate responsible for the observed VR levels, which it turn depends on a more detailed knowledge of the stratigraphic age of the Miocene-Recent Nullarbor Formation than we currently have.

3. Bearing the above point in mind, the VR paleotemperature results have been interpreted in terms of low and high heating rate cases which should encompass the range of geologically plausible scenarios. For the low heating rate case, the data define a maximum likelihood estimate for a Late Tertiary paleogeothermal gradient of 31.0°C/km (24.6 to 37.5°C/km at ±95% confidence limits), while for the high heating rate case, the data define a similar maximum likelihood estimate for a Late Tertiary paleogeothermal gradient of 32.1°C/km (25.5 to 38.8°C/km at ±95% confidence limits). Both estimates encompass the present-day geothermal gradient of 27.2°C/km. The simplest interpretation of the data is that there is little difference in heat flow between the Late Tertiary and the present day.

4. The thermal history results for the two heating rate cases provide maximum estimates (upper 95% confidence limits) of 220 and 728 metres of total uplift and erosion since the Late

Triassic-Early Jurassic, respectively, for the low and high heating rate cases. In both cases, a model with no uplift and erosion is possible.

5. Given the equivocal identification of past heating, it is therefore considered possible that the present day geothermal gradient is around 10% higher than the value of 27.3°C/km estimated from the corrected BHT data, and that the entire section is actually at maximum burial temperatures at the present-day.

6. The simplest interpretation of the thermal history results suggest that the deepest drilled section in Borda-1 (Potoroo Fm) reached its presently measured maturity level (VR ~0.5 to 0.6%) at some time within the last few million years (including the present-day), but scenarios involving local transient heating by hot fluid flow at any time in the Tertiary are allowed by the limited data currently available.

Table i: Paleotemperature analysis summary - AFTA and VR samples from wells Vivonne-1 and Borda-1, Duntroon Basin (Geotrack Report #569)

Sample number GC	Average depth (TVD) (m)	Present temperature*1 (°C)	Stratigraphic age (Ma)	Mid-Cretaceous episode (112 to 75 Ma)*2 Maximum paleotemperature (°C)	Mid-Cretaceous episode (112 to 75 Ma)*2 Onset of cooling (Ma)	Tertiary episode (60 to 0 Ma)*2 Peak paleotemperature (°C)	Tertiary episode (60 to 0 Ma)*2 Onset of cooling (Ma)
Vivonne-1							
569-14.1	923	38	42-29	Not applicable		39	-
569-15.1	1130	44	65-56	Not applicable		47	-
569-16	1182	46	65-56	Not applicable		<105	65-0
569-16.1	1217	47	65-56	Not applicable		47	-
569-17	1287	49	74-65	Not applicable		No apatite	
569-18.1	1318	50	74-65	Not applicable		59-74*3,4	-
569-19.1	1373	52	124-112	57-72*3,4	-	57-72*3,4	-
569-20.1	1470	54	124-112	57-72*3,4	-	57-72*3,4	-
569-21.1	1585	58	124-112	57-72*3,4	-	57-72*3,4	-
569-28	1699	61	124-112	80-100	112-50	No direct evidence	
SWC18	1718	62	132-124	79	-	Not applicable	
SWC16	1828	65	132-124	89	-	Not applicable	
569-29	1881	67	124-112	<110	112-0	No direct evidence	
569-22.1	2009	71	124-112	102	-	Not applicable	
SWC12	2058	72	132-124	98	-	Not applicable	
569-23	2068	73	124-112	95-115	112-65	<95	65-0
SWC9	2219	77	132-124	122	-	Not applicable	
SWC7	2312	80	132-124	131	-	Not applicable	
SWC4	2473	85	132-124	137	-	Not applicable	
569-30	2486	85	132-124	>110	124-75	85-110	60-0
569-24.1	2491	85	132-124	117	-	<100	60-0
569-25	2598	89	132-124	>89	124-75	No direct evidence	
SWC1	2660	90	132-124	136	-	Not applicable	
569-26.1	2687	91	132-124	134	-	Not applicable	
569-27.1	2823	95	132-124	117	-	Not applicable	
Borda-1							
569-1.1	1303	45	42-29	Not applicable		<35	-
569-2.1	1438	49	42-29	Not applicable		35	-
569-3.1	1623	54	42-29	Not applicable		55-70*3,4	-
569-4.1	1833	60	42-29	Not applicable		55-70*3,4	-
569-5.1	2035	65	42-29	Not applicable		63-77*3,4	-
569-6.1	2175	67	42-29	Not applicable		59-74*3,4	-
569-7.1	2175	69	65-56	Not applicable		73-88*3,4	-
569-9.1	2283	72	65-56	Not applicable		74-89*3,4	-
569-8	2296	72	65-56	Not applicable		No apatite	
SWC70	2302.5	73	65-56	Not applicable		91-107*3,4	-
569-10.1	2362	74	65-56	Not applicable		71-86*3,4	-
SWC63	2465	77	74-65	Not applicable		77-93*3,4	-
569-11.1	2539	79	74-65	Not applicable		81-96*3,4	-
SWC55	2582	80	74-65	Not applicable		81-96*3,4	-
SWC48	2652	82	74-65	Not applicable		88-104*3,4	-
569-12.1	2677	83	74-65	Not applicable		82-98*3,4	-
569-13	2752	85	74-65	Not applicable		<130*3,4	65-0
SWC33	2792	86	74-65	Not applicable		86-102*3,4	-

*1 See Appendix A for details of present temperature calculation.

*2 Derived from overlap of timing constraints from all AFTA samples

*3 Maximum paleotemperature estimates from VR data for two heating rates - see text.

*4 Timing of maximum paleotemperatures from VR data uncertain in these samples.

Table ii: Summary of paleogeothermal gradient estimates for wells Vivonne-1 and Borda-1, Duntroon Basin (Geotrack Report #569)

Well	Present day geothermal gradient (°C/km)	Paleogeothermal gradients (°C/km)*1 "Cretaceous"*2 (112 to 75 Ma)	Paleogeothermal gradients (°C/km)*1 "Tertiary"*2 (60 to 0 Ma)
Vivonne-1	30.2	60.1 (49.5 - 70.9)	33.9 (28.6 - 40.4)
Borda-1	27.2	Not applicable	31.0*3 (24.6 - 37.5)
		Not applicable	32.1*4 (25.5 - 38.8)

*1 Maximum likelihood value with ±95% confidence interval range in brackets.
*2 Timing of these heating episodes is constrained by AFTA data in Vivonne-1.
*3 Values from paleotemperature estimates based on a ***low*** heating rate prior to any cooling - see Table i and text.
*4 Values from paleotemperature estimates based on a ***high*** heating rate prior to any cooling - see Table i and text.

Table iii: Summary of removed section estimates for wells Vivonne-1 and Borda-1, Duntroon Basin (Geotrack Report #569)

Well	Removed section estimates (m)*1 "Cretaceous"*2 (112 to 75 Ma)	Removed section estimates (m)*1 "Tertiary"*2 (60 to 0 Ma)
Vivonne-1	748*3 (514 to 1077)	0 to 123*4
Borda-1	Not applicable	0 to 220*4,*5
		0 to 728*4, *6

*1 Maximum likelihood value with ±95% confidence interval range in brackets. Constant surface temperature of 15°C assumed.
*2 Timing of these heating episodes is constrained by AFTA data in Vivonne-1.
*3 Total removed section with respect to the top Upper Borda Formation unconformity.
*4 Total removed section with respect to the top of the Nullarbor Formation. Explicitly assumes that the minor "Tertiary" cooling possible in this well occurred after deposition of all of the preserved Nullarbor Formation. Cooling prior to deposition of the Nullarbor Formation would require an increased amount of removed section equivalent to the thickness of the subsequently deposited section - see text.
*5 Values from paleotemperature estimates based on a ***low*** heating rate prior to any cooling - see Table i and text.
*6 Values from paleotemperature estimates based on a ***high*** heating rate prior to any cooling - see Table i and text.

Notes: Details of maximum likelihood estimation of paleogeothermal gradient and section removed are provided in Section 1 and Appendix C (Section C.9). The allowed ranges of values of paleogeothermal gradient and section removed (within ±95% confidence limits) are highly correlated.

Estimation of section removed depends on the assumption that the paleogeothermal gradient is linear and can be extrapolated through the removed section to the paleo-surface temperature. If this assumption is not valid (e.g., if the paleo-thermal effects were due to fluid flow, with a higher paleogeothermal gradient in the shallower [removed] section), the estimated section removed will not be accurate.

The paleotemperature constraints (Table i) and the estimated paleogeothermal gradient through the preserved section (Table ii) are not affected by any of the assumptions required in order to estimate the amount of section removed, and can be regarded as reliable.

The amount of section removed has been estimated for an assumed paleo-surface temperature of 15°C. The resulting estimate can be adjusted to refer to other values of paleo-surface temperature simply by adding or subtracting the depth interval corresponding to the difference between the preferred value and 15°C, as appropriate, for the maximum likelihood value of paleogeothermal gradient.

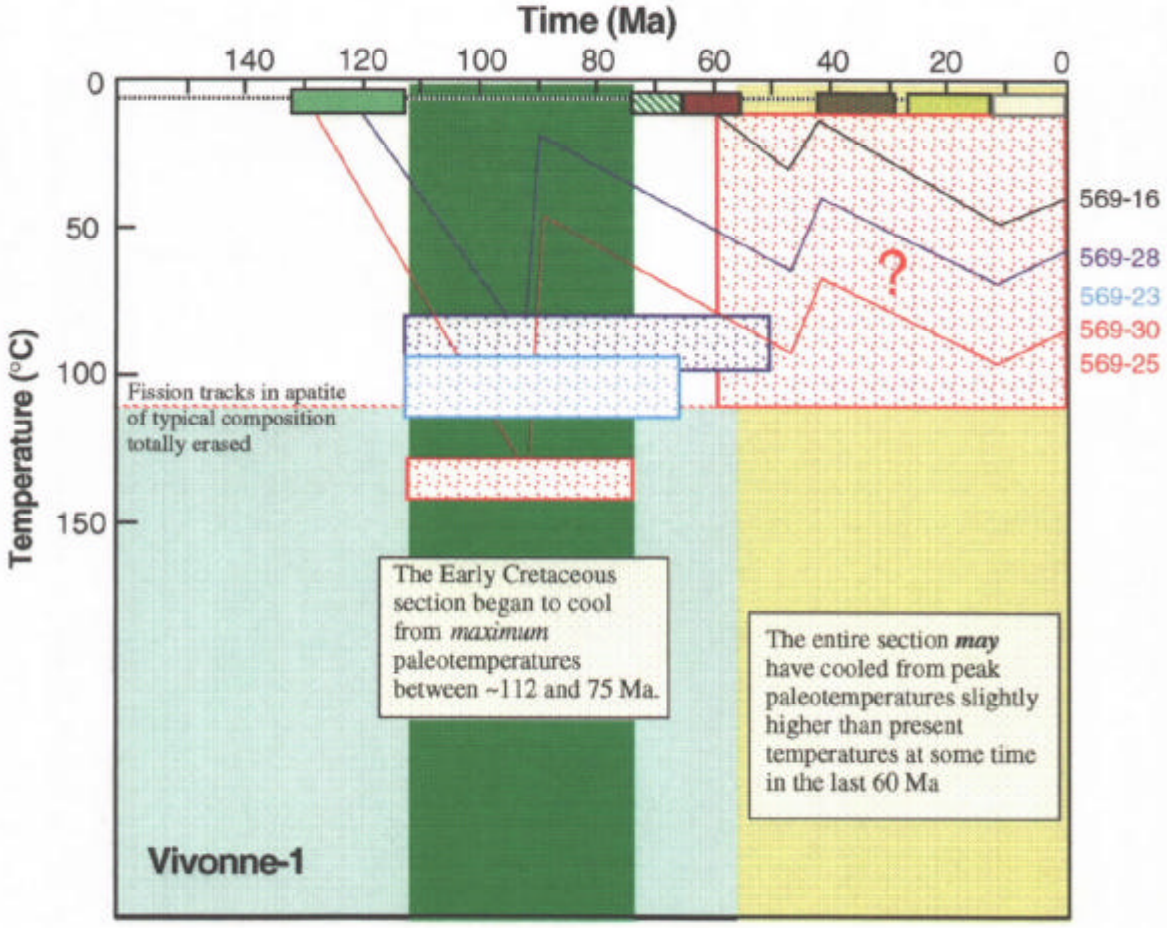

Figure i: Schematic illustration of the preferred thermal history interpretation for AFTA and VR data from the **Vivonne-1 well, Duntroon Basin** (only key data illustrated for clarity. Paleotemperatures and constraints on time of cooling are summarised in Table i. The Early Cretaceous Borda Formation section cooled from maximum paleotemperatures in the Mid-Cretaceous - see text.

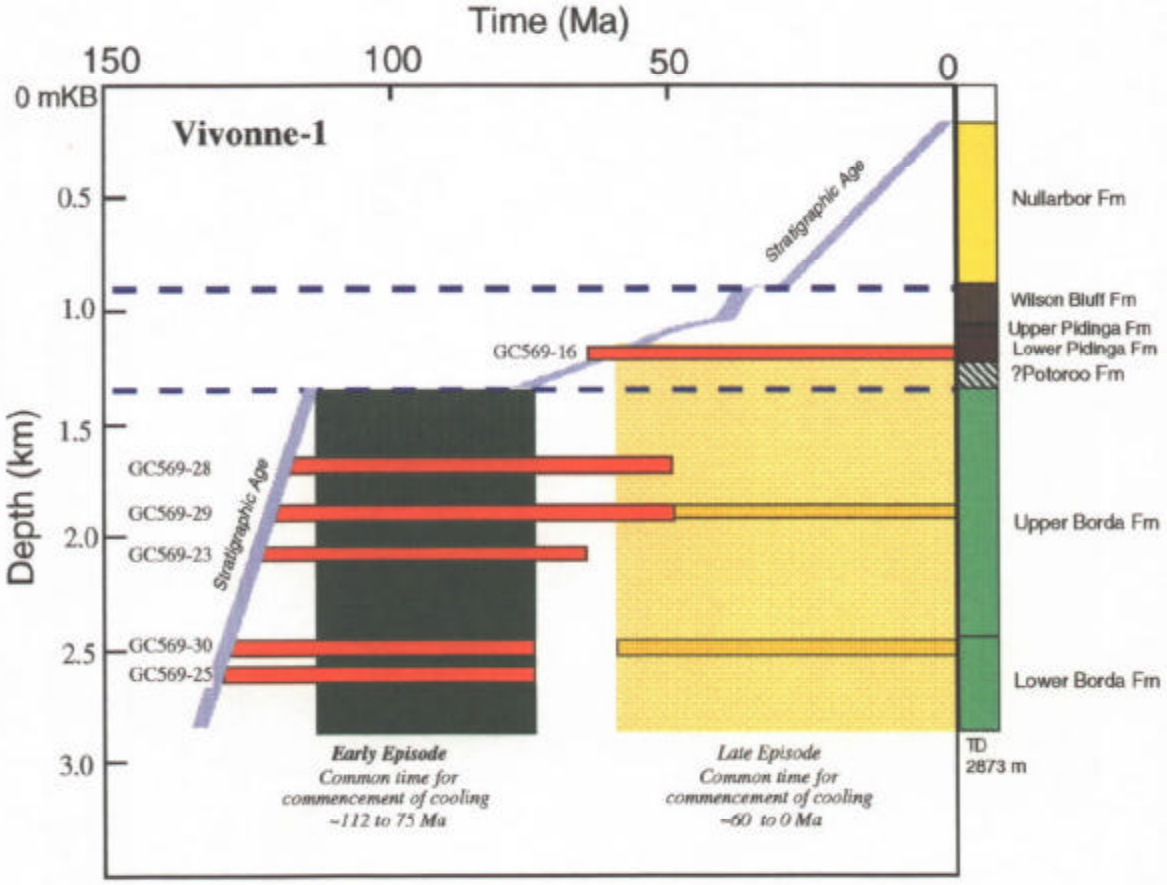

Figure ii: Constraints on time of cooling from the AFTA data in individual samples in the **Vivonne-1 well, Duntroon Basin.** The results indicate a major period of heating in the Mid-Cretaceous (~112 to 75 Ma) and tentatively indicate minor additional heating at some time in the Tertiary (~60 to 0 Ma) - see text.

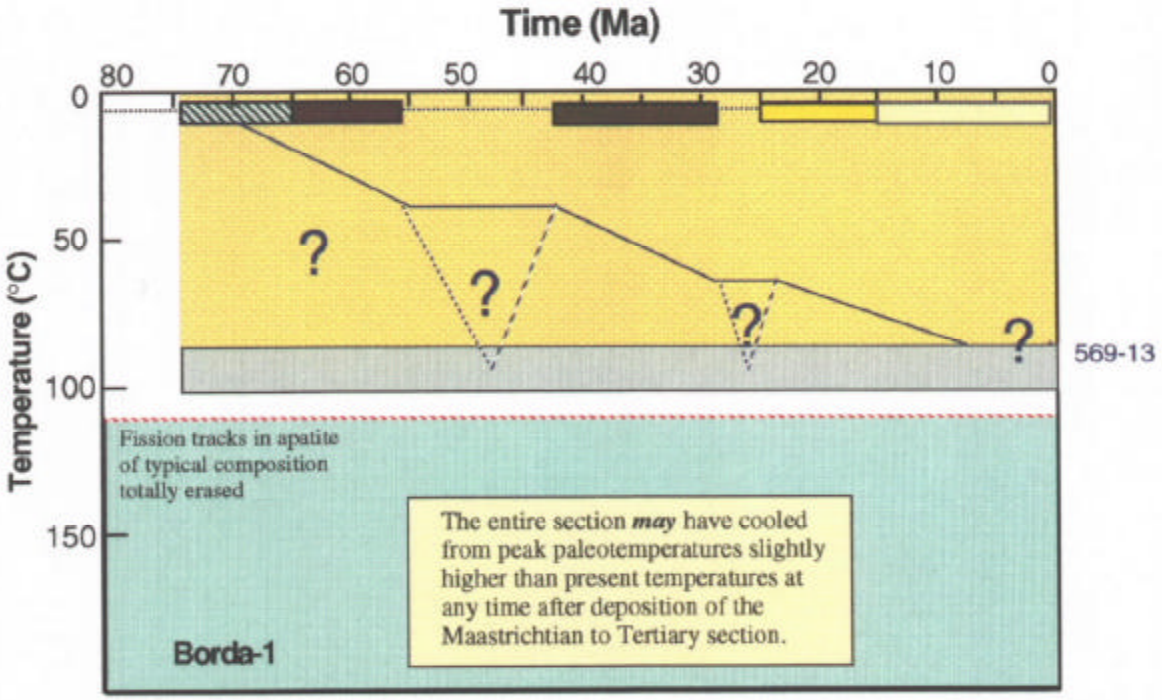

Figure iii: Schematic illustration of a possible thermal history interpretation for AFTA and VR data from the **Borda-1 well, Duntroon Basin.** Paleotemperatures and constraints on time of cooling are summarised in Table i. The data suggest minor cooling of the Maastrichtian to Eocene section at some time in the Tertiary, but the currently available data do not allow firm conclusions to be drawn - see text.

1. Introduction

1.1 Background and objectives of this report

This report describes the results of a study designed to provide a thermal history framework for understanding the structural and hydrocarbon generation history in the vicinity of the **Vivonne-1 and Borda-1 wells, Duntroon Basin, South Australia.** The study was commissioned by the **Petroleum Division, Mines and Energy South Australia** (MESA), and was completed in September 1995.

The study involves thermal history reconstruction using Apatite Fission Track Analysis (AFTA®) and Vitrinite Reflectance (VR). Seven AFTA samples from the **Vivonne-1 well** and two samples from the **Borda-1 well** were provided by **MESA,** in addition to 11 new samples for VR determination from each well. Open-file VR data on seven samples from Vivonne-1 and five samples from Borda-1 were also provided by MESA.

AFTA is used to identify any episodes of elevated paleotemperatures which have affected the region, to estimate the timing and magnitude of maximum paleotemperatures and to place constraints on any subsequent episodes of heating and cooling. VR data are also used to provide estimates of maximum paleotemperatures, the timing of which is interpreted on the basis of information provided by AFTA. Paleotemperature constraints from AFTA and VR are then integrated into a coherent thermal history synthesis. Estimates of maximum paleotemperature from AFTA and VR over a range of depths are used to constrain paleogeothermal gradients, which are used to infer the origins of the various episodes of heating and cooling (Section 1.7). Where possible, estimates of section removed by uplift and erosion are obtained from the paleotemperature constraints, allowing reconstruction of the burial history. Burial history reconstruction depends on a number of assumptions, with respect to the thermal structure of the eroded section, which are not directly known (Section 1.8). Therefore, the results should be regarded as indicative of the general magnitude and corroboration of the removed section estimates by other techniques (e.g., sonic velocity compaction studies, seismic reconstruction on structures, etc.) is always desirable. Comparison of data from all wells with the geological setting then allows a regional framework to be established, within which the implications of the regional variation of thermal history concerning patterns of hydrocarbon generation can be understood.

1.2 Report structure

The main conclusions of this report are summarised in the Executive Summary. The thermal history interpretations of AFTA and VR data for the three wells are summarised in Tables i, ii and iii, in terms of quantitative constraints on maximum paleotemperatures and timing of major thermal episodes, paleogeothermal gradients and magnitudes of removed section, respectively. Figures i and iii illustrate the constrained thermal history derived from AFTA and VR data in each of the two wells. Figure ii illustrates the constraints obtained from AFTA on the time of cooling from each sample in the Vivonne-1 well from which high-quality AFTA data were obtained.

In Section 1, introductory aspects of the report are discussed, including comments on data quality. The approach to thermal history reconstruction employed in this report is also described in Section 1. Sections 2 and 3 summarise the thermal history interpretation of the AFTA and VR data for the Vivonne-1 and Borda-1 wells, respectively, under various headings, including implications of the thermal history for source rock maturation and hydrocarbon exploration. Section 4 gives concluding remarks on the geological history of the Duntroon Basin. Section 5 discusses possibilities for further work, which might allow further insight into the thermal and hydrocarbon generation history on the wells analysed.

Supporting information is provided in four Appendices. Details of all AFTA samples, including depths, stratigraphic details and present temperatures in each well, are presented in Appendix A, together with the yields of detrital apatite obtained after mineral separation, apatite grain morphologies and apatite compositions (Cl contents). Sample preparation and analytical details are described in Appendix B, followed by the presentation of all AFTA data, including raw track counts and fission track ages for individual grains. Details of the presentation of data in the form of Tables and Figures throughout the report are also discussed in detail in Appendix B. Appendix C outlines the principles employed in interpreting the AFTA data in terms of thermal history. In Appendix D, the results of all new VR analyses obtained for this report, including sample details and analytical methods, are presented, along with a listing of open-file VR data used in this report. Appendix D also discusses the principles involved in integrating AFTA and VR data to provide coherent thermal history interpretations.

1.3 Data quality

AFTA data

The AFTA data generated for this report are generally of high quality. The yields of detrital apatite obtained after mineral separation from all samples processed are summarised in Table A.1. Yields of apatite varied from none to poor to excellent. The quality of the etched surfaces of the apatites obtained for analysis was high in all samples. The overall high quality of the AFTA data in key samples results in reliable thermal history interpretations for the Vivonne-1 well, but the lack of apatite in the two samples processed from Borda-1 leaves some key thermal history questions in this well unanswered.

VR data

Vitrinite reflectance data from Keiraville Konsultants, which were collected on 11 samples from the Vivonne-1 well and 11 samples from the Borda-1 well, were combined with a smaller number of open-file data to provide a comprehensive paleotemperature profile for each well. Comparison on mean maximum reflectance data from the new and open file datasets shows that VR levels for similar depths in each dataset are generally very consistent (Tables D.2 and D.3), giving confidence in the interpretation of all data in terms of maximum paleotemperatures using the Burnham and Sweeney (1989) algorithm (see Section 1.6 and Appendix D for further details). The majority of the vitrinite reflectance data used in this study are considered to be of high quality, with most samples yielding 20 or more measurements (Tables D.2 and D.3). A mean value based on 10 or more measurements from Keiraville Konsultants is considered reliable because of the way in which the VR data are gathered, with primary in-situ vitrinite identified on petrographic grounds within polished blocks (see Appendix D).

1.4 Apatite compositions

The annealing kinetics of fission tracks in apatite are affected by chemical composition, specifically the Cl content, as explained in more detail in Appendix C. Thus, an assessment of the chlorine content in apatite is essential in interpreting AFTA data, often providing greater accuracy in establishing the time and magnitude of thermal events.

For this study, chlorine compositions were determined for all individual apatite grains in which fission track ages were determined and lengths measured for the seven samples which provided apatite from the two wells studied.

The measured range of chlorine contents of dated grains and grains in which length were measured is shown in histogram format in Figure A.2. A plot of single grain age versus weight % chlorine is shown in Figure B.5. Chlorine contents, which are presented in numerical format for age grains, appear in the fission track age summary sheets in Appendix B.

1.5 Thermal history reconstruction and use of thermal gradients vs heat flow

Most approaches to thermal history reconstruction in sedimentary basins are based on consideration of the variation of heat flow through time, using models often based solely on theoretical grounds. However, this approach is beset by problems, particularly in sections which have been hotter in the past. Use of a heat flow-based approach depends critically on knowledge of thermal conductivities through the section. When considerable section has been removed, no information is available on lithologies (and hence thermal conductivities) in the removed section. In addition, large variation in thermal conductivities within similar lithological units (e.g., Corrigan, 1991) introduces considerable uncertainty into the relationship between heat flow and thermal gradient, even in relatively simple cases. For further illustration of these problems, see Waples et al. (1992). The influence of factors such as porosity, compaction and diagenesis is difficult to assess quantitatively, and the effects of greater depth of burial are unpredictable in a sequence affected by uplift and erosion, particularly when the magnitude of burial is unknown before the analysis. A heat flow-based approach to determining amounts of removed section is subject to considerable uncertainty because of problems such as these. This point has been discussed in greater detail by Duddy et al. (1991).

It is also important to realise the validity of theoretical heat-flow models is largely untested. High heat flow associated with rifting and early subsidence leaves no measurable effect if subsidence later in the basin's history has caused higher temperatures than those attained during the assumed high heat-flow episode. In many sedimentary basins, deep burial late in the subsidence history has caused maximum temperatures, and no record of earlier heat-flow variation is preserved either in the level of measured source rock maturity or in the AFTA parameters, as these data are dominated by the effects of maximum paleotemperature. Elevated heat-flow episodes associated with rifting are known to leave a measurable signature only where cooling

has occurred shortly after the initial rifting phase and where temperatures have subsequently remained low through to the present day (Duddy et al., 1991).

We have adopted an alternative approach, based on measurement of thermal gradients (present and past), using an integrated AFTA and VR methodology, because of these problems with a heat flow-based approach to thermal history reconstruction. This approach yields direct measurement of the time at which cooling from maximum paleotemperatures began (from AFTA), and the paleogeothermal gradient at that time (from AFTA and VR). The style of cooling from maximum paleotemperatures to present temperatures can also be constrained (from AFTA). This approach allows definition of all the major facets of the thermal history of a sedimentary section through time, and is *based on directly measurable parameters*, rather than on *assumed* values of highly unpredictable factors. The information provided can still ultimately be interpreted in terms of paleo-heat flow, if desired.

It should also be appreciated that the thermal history prior to the time at which cooling from maximum paleotemperatures begins cannot be constrained from any of the available in-situ paleotemperature indicators based on thermally activated reactions. This arises because of the dominance of temperature over time in the kinetics of the systems employed in this way (i.e., fission track annealing, vitrinite reflectance, etc.). For this reason, these data can only constrain the thermal history from the onset of cooling from maximum paleotemperatures to the present day. Information on the earlier history can only be obtained indirectly, e.g., from geological information, perhaps by reconstructing patterns of burial based on section preserved in neighbouring regions, from theoretical heat-flow models (given the above caveats), or possibly by more subtle means, such as the presence of residual hydrocarbon products generated during earlier heating to lower peak paleotemperatures.

1.6 Outline of our approach to interpretation of AFTA and VR data

Interpretation of AFTA and VR data in this report begins by assessing whether the AFTA and/or VR data in each sample could have been produced if the sample has never been hotter than its present temperature at any time since deposition. The burial history derived from the stratigraphy of the preserved sedimentary section and the present geothermal gradient are used to predict a "Default Thermal History" for each sample, which forms the basis of interpretation.

If the data show a greater degree of fission track annealing and/or a higher VR value than expected on the basis of this history, the sample must have been hotter at some time in the past. In this case, the AFTA data are analysed to provide estimates of the

magnitude of the maximum paleotemperature in that sample, and the timing of cooling from the thermal maximum. VR data provide an independent estimate of maximum paleotemperature. Paleotemperature estimates from both AFTA and VR are then used to reconstruct a paleogeothermal gradient, and, where appropriate, to estimate the amount of section removed by uplift and erosion.

The heating rate assumed in calculating paleotemperatures affects the magnitude of paleotemperature required to produce a given set of data. As AFTA and VR data do not independently constrain the heating rate, paleotemperatures are estimated by assuming simple linear heating between a point on the Default Thermal History and the maximum paleotemperature. This will not give the actual paleotemperature, in general, but this procedure at least allows AFTA and VR data to be analysed within a common thermal history framework in the absence of any other constraint on heating rate. If any evidence of the real time-scale of heating is available, this can easily be incorporated into the analysis. Note AFTA data provide some constraint on cooling rates, as explained in more detail in Appendix C.

Estimates of maximum paleotemperature from AFTA are often quoted in terms of a range of paleotemperatures, as the data can often be explained by a variety of scenarios. Paleotemperature estimates from VR are usually quoted to the nearest degree Celsius, as the value which predicts the measured reflectance. This is not meant to imply VR data can be used to estimate paleotemperatures to this degree of precision. VR data from individual samples typically show a scatter equivalent to a range of between ±5 and ±10°C. Estimates from a series of samples are normally used to define a paleotemperature profile in samples from a well, or a regional trend in paleotemperatures from outcrop samples.

If the data show a lower degree of fission track annealing and/or a lower VR value than expected on the basis of the Default Thermal History, this suggests either present temperatures may be overestimated or temperatures have increased very recently. In such cases, the data may allow an estimate of the true thermal gradient, or some estimate of the time over which temperatures have increased.

Further discussion of the methodology employed in interpreting AFTA and VR data are given in Appendices C and D.

AFTA data are interpreted using a new multi-compositional kinetic model for fission track annealing in apatite developed by Geotrack, details of which are provided in Appendix C. Vitrinite reflectance data are interpreted using the distributed activation energy model describing the evolution of VR, with temperature and time developed by

Burnham and Sweeney (1989) (see also Sweeney and Burnham, 1990), as implemented in the BasinMod™ software package of Platte River Associates (using version 3.15).

1.7 Paleogeothermal gradients

Basic principles

A series of paleotemperature estimates from AFTA and/or VR over a range of depths can be used to reconstruct a paleotemperature profile through the preserved section. The slope of this profile defines the paleogeothermal gradient. As explained by Bray et al. (1992), the shape of the paleotemperature profile and the magnitude of the paleogeothermal gradient provides unique insights into the origin and nature of the heating and cooling episodes expressed in the observed paleotemperatures.

Linear paleotemperature profiles with paleogeothermal gradients close to the present-day geothermal gradient provide strong evidence that heating was caused by greater depth of burial with no significant increase in basal heat-flow, implying in turn that cooling was due to uplift and erosion. Paleogeothermal gradients significantly higher than the present-day geothermal gradient suggest that heating was due, at least in part, to increased basal heat flow, while a component of deeper burial may also be important as discussed in the next section. Paleogeothermal gradients significantly lower than the present-day geothermal gradient suggest that a simple conductive model is inappropriate, and more complex mechanisms must be sought for the observed heating. One common cause of low paleogeothermal gradients is transport of hot fluids shallow in the section. However, the presence of large thicknesses of sediment with uniform lithology dominated by high thermal conductivities can produce similar paleotemperature profiles, and each case has to be considered individually.

A paleotemperature profile can only be characterised by a single value of paleogeothermal gradient when the profile is linear. Departures from linearity may occur where strong contrasts in thermal conductivities occur within the section, or where hot fluid movement or intrusive bodies have produced localised heating effects. In such cases, a single value of paleogeothermal gradient cannot be calculated. However, it is important to recognise that the validity of the paleotemperatures determined from AFTA and/or VR are independent of these considerations, and can still be used to control possible thermal history models.

Estimation of paleogeothermal gradients in this report

Paleogeothermal gradients have been estimated, using methods outlined in Appendix C, for each well analysed for this report in which paleotemperature estimates are available over a range of depths. These methods provide a best estimate of the gradient ("maximum likelihood value") and upper and lower 95% confidence limits on this estimate (analogous to ±2s limits). The "goodness of fit" is displayed in the form of a log-likelihood profile, which is expected to show good quadratic behaviour for a dataset which agrees with a linear profile. This analysis depends on the assumption that the paleogeothermal gradient through the preserved section is linear. Visual inspection is usually sufficient to confirm or deny this assumption.

1.8 Eroded section

Basic principles

Subject to a number of important assumptions, extrapolation of a linear paleotemperature profile to a paleo-surface temperature allows estimation of the amount of eroded section represented by an unconformity, as explained in more detail in Section C.9 (Appendix C).

Specifically, this analysis assumes:

- The paleotemperature profile through the preserved section is linear;
- The paleogeothermal gradient through the preserved section can be extrapolated linearly through the missing section;
- The paleo-surface temperature is known; and,
- The heating rate used to estimate the paleotemperatures defining the paleogeothermal gradient is correct.

It is important to realise that any method of determining the amount of eroded section based on thermal methods is subject to these and/or additional assumptions. For example, methods based on heat-flow modelling must assume values of thermal conductivities in the eroded section, which can never be known with confidence. Such models also require some initial assumption of the amount of eroded section to allow for the effect of compaction on thermal conductivity. Methods based on geothermal gradients, as used in this study, are unaffected by this consideration, and can therefore provide independent estimates of the amount of eroded section.

However, these estimates are always subject to the assumptions set out above and should be considered with this in mind.

Estimation of eroded section in this report

The analysis used to estimate paleogeothermal gradients is easily extended to provide maximum likelihood values of eroded section for an assumed paleo-surface temperature, together with ±95% confidence limits. These parameters are quoted for each well in which the paleotemperature profile suggests that heating may have been due, at least in part, to deeper burial.

However, it is emphasised that such interpretations are not unique, and alternative interpretations are always possible. For instance, the paleogeothermal gradient through the missing section may have been much higher than in the preserved section where the eroded section was dominated by units with high thermal conductivities, and extrapolation of a linear gradient will lead to overestimation of the eroded section.

For the wells analysed in this report, the estimates of eroded section are conditional on:

- A paleo-surface temperature equal to the present value of 15°C (for Vivonne-1 and Borda-1);
- Heating rates of 10°C/Ma in the first episode and 1°C/Ma in the second episode (for Vivonne-1); and,
- A range of heating rates from 1 to 10°C/Ma in each episode (for Borda-1),

as well as the other assumptions outlined above. The effects of higher paleo-surface temperatures can be simply allowed for by subtracting the depth increment corresponding to the increase in temperature, for the appropriate value of paleogeothermal gradient. For instance, if the paleogeothermal gradient was 45°C/km and the paleo-surface temperature was 10°C higher than the value assumed in this report, the estimated eroded section should be reduced by 222 metres. Different heating rates can be allowed for in similar fashion, with an order of magnitude change in heating rate equivalent to a 10°C change in paleotemperature (paleotemperatures increase for higher heating rates, and decrease for lower heating rates). For typical values, the assumed value of heating rate will not affect the shape or slope of the paleotemperature profile significantly.

2. Thermal history reconstruction in the Vivonne-1 well

2.1 Introduction

Geology

The Vivonne-1 well in the Duntroon Basin intersected a ~721 m thick section of Nullarbor Formation, of Pliocene-Late Oligocene age, unconformably overlying Late Eocene Wilson Bluff Formation ~175 m thick, in turn unconformably overlying Paleocene-Eocene Pidinga Formation ~182 m thick and Maastrichtian ?Potoroo Formation ~100 m thick. This Late Cretaceous to Tertiary package unconformably overlies 1531 m of Early Cretaceous Borda Formation, of Aptian age at the unconformity and Barremian age at TD of 2873 m (total vertical depth below RT). The generalised stratigraphy is shown in Figure 2.1. The present-day geothermal gradient is calculated from corrected BHT data at 30.2°C/km for a sea-bed temperature of 15°C (Appendix A).

AFTA data

Fission track parameters from five samples are summarised in Table 2.1, together with values of fission track age and mean track length predicted on the basis of the Default Thermal History (See Section 1.6). The calculation of these default values includes only those tracks formed after deposition of the sample, and therefore does not account for tracks inherited from sediment source areas. The use of these parameters in interpreting AFTA data is outlined in Section 1.6 and Appendix C. The range of measured apatite chlorine compositions used in calculating predicted values for AFTA samples is listed in Appendix B.

The measured AFTA data, which are also plotted in Figure 2.1, show a simple pattern, with fission track ages showing a general decrease from greater than to just less than the stratigraphic age, and track lengths decreasing from around 14 μm to ~11 μm with increasing depth.

VR data

Vitrinite reflectance data are available from 11 new samples analysed by Keiraville Konsultants (Table D.2) and open-file data on seven samples supplied by MESA (Table D.3).

$R_o$max values range from ~0.3% in the Wilson Bluff Formation to ~0.75% in the Lower Borda Formation, as shown in Figure 2.2, where they are plotted with respect

to depth. Also shown in Figure 2.2 is the VR profile predicted from the Default Thermal History, i.e., the thermal history of the well if the section has never been hotter than present temperatures. The burial history used in calculating this profile is shown in Figure 2.3.

2.2 Evidence for elevated paleotemperatures from AFTA data

Results of detailed kinetic modelling of the AFTA data, in conjunction with maximum paleotemperature estimates derived from associated VR levels, in the five Borda Formation samples clearly indicate cooling from paleotemperatures significantly higher than present temperatures at some time after deposition of the youngest preserved Early Cretaceous section (~112 Ma). Modelling of the AFTA data in the shallowest sample (GC569-16) from Lower Pidinga Formation show no direct evidence of elevated paleotemperatures after Paleocene deposition, but would allow paleotemperatures higher than present temperatures if required by other data.

Evidence for elevated paleotemperatures from each sample is summarised in Table 2.2.

2.3 Magnitude of paleotemperatures and time of cooling

Introduction

The thermal history interpretation of the AFTA data in each sample is summarised in Table 2.3. Estimates are quoted in terms of two paleo-thermal episodes - an **Early Episode** and a **Late Episode** - in the **Mid-Cretaceous** and the **Tertiary**, respectively. This arises because the synthesis of data from all samples from this well shows that while a Mid-Cretaceous event dominates the thermal history of the region, there is also tenuous, but consistent, evidence for a lower magnitude Tertiary event.

Paleotemperature estimates from each AFTA and VR sample for each time period are listed in Table i (Executive Summary) and plotted against depth in Figure 2.4. Results from all samples show a consistent overlap in timing for each event, constraining cooling to have begun in the first episode between ~112 Ma and 75 Ma (notionally, "Mid-Cretaceous"), and in the second episode between ~60 and 0 Ma ("Tertiary").

A schematic illustration of the main features of the thermal history in the Vivonne-1 well is presented in Figure i (Executive Summary), with the timing constraints obtained from AFTA in each sample illustrated in Figure ii (Executive Summary).

Mid-Cretaceous (112 to 75 Ma)

The best constraints on the timing of the Mid-Cretaceous event are obtained from modelling of the AFTA parameters in Borda Formation samples GC569-25 and 30 (and to a lesser extent sample GC569-23), in conjunction with the maximum paleotemperatures determined from the measured VR levels. In samples GC569-25 and 30, maximum paleotemperatures of ~130 to 140°C determined from the VR data (Tables 2.3 and i), are constrained by the AFTA data to have occurred after Barremian deposition (~132 to 124 Ma) and prior to ~75 Ma. Similarly, VR-derived maximum paleotemperatures of ~100°C in the vicinity of AFTA sample GC569-23 are constrained by the AFTA parameters to have occurred after Aptian deposition (~124 to 112 Ma) and prior to ~65 Ma.

As the paleotemperature estimates derived from the VR data form a consistent trend through the Upper and Lower Borda Formation, it is assumed that all of the data reflect a single heating event, between deposition of the youngest preserved Aptian section at ~112 Ma and 75 Ma. This event was experienced by the entire preserved Borda Formation section.

Tertiary (60 to 0 Ma)

Definite constraints on the timing of a Tertiary heating event are restricted to the AFTA data from sample GC569-30, from the Lower Borda Formation, where a peak paleotemperature of 85 to 110°C is indicated, prior to cooling commencing at some time within the last 60 Ma. Data from other samples would be consistent with some degree of Tertiary cooling, but do not require any such cooling episode.

2.4 Paleogeothermal gradients and the causes of heating and cooling

Introduction

The AFTA thermal history constraints indicate one major heating episode in the Mid-Cretaceous, with a possible minor heating episode at some time in the Tertiary (Figure ii). Estimated paleotemperatures in each episode are plotted against depth in Figure 2.4. Using the approach outlined in Section 1.7 and methods explained in Appendix C, paleogeothermal gradients are determined for each episode, as outlined below.

Mid-Cretaceous (112 to 75 Ma)

AFTA and VR-derived paleotemperature estimates (Early Cretaceous samples only) in individual samples for the ***Mid-Cretaceous*** episode depicted in Figure 2.4 are consistent with a common trend, suggesting they represent the same heating event, which is constrained by the stratigraphic age control and AFTA to have occurred between 112 and 75 Ma.

Fitting a linear gradient to the these paleotemperatures gives a maximum likelihood paleogeothermal gradient for this time of 60.1°C/km, with upper and lower 95% confidence limits of 70.9 and 49.5°C/km, respectively (Figure 2.5).

This range of paleogeothermal gradient is significantly higher than the present-day value of 30.2°C/km at the 95% confidence limits. This result indicates that an interpretation of heating in terms of higher heat-flow with cooling due, at least in part, to decline in geothermal gradient, is a viable explanation of the data. This interpretation does not exclude associated uplift and erosion; in fact, some is required, as discussed in Section 2.7.

Tertiary (60 to 0 Ma)

The paleotemperature results listed in Table i and depicted in Figure 2.4 show only tenuous evidence for **Tertiary** paleotemperatures being significantly higher than present temperatures. Only sample GC569-30 provides evidence for a distinct cooling event at some time within the last 60 Ma. The remaining samples provide only upper limits on estimates of maximum paleotemperature, with the data being equally consistent with the present temperatures being maximum at any time since 60 Ma. Nevertheless, the data does allow the estimation of a paleogeothermal gradient.

Fitting a linear profile to the **Tertiary** paleotemperatures derived from all AFTA data and VR data from the post-Early Cretaceous section gives a maximum likelihood paleogeothermal gradient of 33.9°C/km (Figure 2.6), with upper and lower 95% confidence limits of 40.4 and 28.6°C/km, respectively. This range of paleogeothermal gradients incorporates the present-day value of 30.2°C/km at the 95% confidence limits. Thus, one viable explanation of the data is that heating is due simply to minor deeper burial, followed by cooling due to uplift and erosion. However, an explanation involving a paleogeothermal gradient marginally higher than at present and no deeper burial is also possible, as discussed further in Section 2.7. Paleogeothermal gradient estimates are summarised in Table ii (Technical Summary).

2.5 Thermal history synthesis

The data presented in the previous sections allows us to constrain the thermal history for the Vivonne-1 well quite closely. The data indicates that the Early Cretaceous Upper and Lower Borda Formation began to cool from maximum paleotemperatures at some time between ~112 and 75 Ma - a time consistent with development of the marked unconformity to the overlying Maastrichtian Potoroo Formation. The AFTA data allow a reasonably good constraint on the timing, and it is likely that cooling commenced at around 95 Ma, based on the major regional tectonic episode at this time known more widely from AFTA and general geological studies in the Otway Basin and environs further to the east. Therefore, in the following diagrams, cooling is shown as beginning at 95 Ma, but the broader allowed time range should be borne in mind if other local data favours a different timing.

Figure 2.7 illustrates the constrained thermal history for the Vivonne-1 well, derived by using the maximum likelihood geothermal gradient of 60.1°C/km for the period prior to Mid-Cretaceous cooling, decreasing to a gradient of 30.2 °C/km for the period from 80 Ma to the present (consistent with the constraints on the Tertiary paleogeothermal gradient, but slightly lower than the maximum likelihood value).

The well-constrained thermal history shown in Figure 2.7 allows construction of a maturity profile in the preserved section at the Vivonne-1 well, as shown in Figure 2.8. The fit of the predicted VR-profile to the measured VR data is good, as expected.

2.6 Implications for source rock maturation at the well site

Figure 2.9 shows the variation of maturity (vitrinite reflectance) with time predicted from the constrained thermal history illustrates in Figure 2.7 (using Burnham and Sweeney, 1989). The plot graphically illustrates the cessation of maturation at the commencement of cooling at 95 Ma (allowable range of 112 to 75 Ma).

The plot implies that the **Borda Formation sequence with source rock potential** deposited at this location would have reached peak maturities within the conventional oil window (~0.5 to 0.8% $R_o$max) during the heating phase prior to Mid Cretaceous cooling, *and have not generated hydrocarbons since that time.* The same situation will apply to any deeper source rocks in the sequence (a notional Jurassic source, for instance), where more mature oils or dry gas will have been generated.

We can infer from these results that reservoiring of any hydrocarbons from this generation episode would rely on pre-Mid-Cretaceous traps, and that filling any

younger traps would rely on re-migration of early generation phases and not contemporary generation.

2.7 Estimates of removed section at the well site

Introduction

The methodology employed in estimating the magnitude of any removed section associated with each heating event is described in Section 1.8.

Limits on Mid-Cretaceous (~112 to 75 Ma) removed section

Removed section estimates for the Mid-Cretaceous cooling episode refer to the *total* amount of section missing at the level of the top Borda Formation unconformity at ~1350 m (TVD) bKB, with all depths on the accompanying figures referring to depth below this unconformity, not the present-day measured depth from KB.

Extrapolating the estimated Mid-Cretaceous paleogeothermal gradient to an assumed paleo-surface temperature of 15°C gives a maximum likelihood estimate of 748 metres for the *total* amount of **Early Cretaceous** (Albian and possible Aptian) section which has been removed by uplift and erosion, with upper and lower 95% confidence limits of 1077 m and 514 m, respectively, as illustrated in Figure 2.10.

Figure 2.11 provides a crossplot of the allowed range of paleogeothermal gradient and removed section for the Mid-Cretaceous, with the ±95% confidence interval contoured, which enables alternative paired values of uplift and erosion and paleogeothermal gradient to be obtained (see Sections 1.7 and 1.8).

Limits on Tertiary (~60 to 0 Ma) removed section

Removed section estimates for the Tertiary cooling episode refer to the *total* amount of section missing at the level of the top Nullarbor Formation at the sea-bed (~162 m bKB), with all depths on the accompanying figures referring to depths below the sea-bed, not the present-day measured depth from KB.

Extrapolating the estimated Tertiary paleogeothermal gradient to an assumed paleo-surface temperature of 15°C gives a maximum likelihood estimate of *minus* 104 metres for the *total* amount of **Nullarbor Formation and younger units** which have been removed by uplift and erosion, with no real lower limit and an upper 95% confidence limit of 123 m, as illustrated in Figure 2.12. Obviously, a negative magnitude of uplift and erosion is not possible, thus the data only provide an effective

upper limit for section missing at the top of the preserved Nullarbor Formation of 123 m.

Figure 2.13 provides a crossplot of the allowed range of paleogeothermal gradient and removed section for the Tertiary, with the ±95% confidence interval contoured, which enables alternative paired values of uplift and erosion and paleogeothermal gradient to be obtained (see Sections 1.7 and 1.8). This plot shows a burial history with no section removed during the Tertiary corresponds to paleogeothermal gradient values around 30 to 33°C/km (encompassing the present-day value of 30.2°C/km). This is a viable explanation of the paleotemperature data.

Removed section estimates for Vivonne-1 are listed in Table iii.

Burial history reconstruction

Figure 2.14 illustrates a possible burial history reconstruction for Vivonne-1 which is consistent with all of the thermal history constraints based on the estimated maximum likelihood paleogeothermal gradient of 60.1°C/km throughout the Early Cretaceous, declining to the present-day value of 30.2°C/km by 80 Ma. The plot shows the maximum likelihood value of 748 m of Early Cretaceous section removed in the Mid-Cretaceous event, commencing at 95 Ma, but no Tertiary erosion (as allowed by the data). This burial history faithfully reflects the major aspects of the constrained thermal history, but it is emphasised that other scenarios are possible for the Tertiary history, particularly involving some minor uplift and erosion during this period.

2.8 Concluding remarks

The AFTA data in Vivonne-1 clearly reveal one major period of heating - in the Mid-Cretaceous (112 to 75 Ma) - and tenuously reveal a second period at some time in the Tertiary (65 to 0 Ma). On this basis, the maximum maturity in the preserved Early Cretaceous section, including any deeper Jurassic section, must have been reached in the prior to ~75 Ma, probably at around 95 Ma, prior to cooling resulting from a combination of decline in paleogeothermal gradient (heat flow) and moderate uplift and erosion (~750 m).

Table 2.1: Summary of AFTA data in samples from the Vivonne-1 well, Duntroon Basin, South Australia (Geotrack Report #569)

Sample number	Average Depth*1 (m)	Present temperature*2 (°C)	Stratigraphic Age (Ma)	Mean track length (µm)	Default mean track length *3 (µm)	Apatite fission track age (Ma)	Default fission track age*3 (Ma)	Measured Ro (max)*4 (%)	Default Ro (max)*5 (%)
GC569-16	1182	46	65-56	14.48±0.94	13.9	192.1±55.0	56	0.34	0.32
GC569-17	1287	49	74-65	No apatite	—	No apatite	—	0.39	0.34
GC569-28	1699	61	124-112	12.24±0.31	13.4	117.1±11.8	106	0.42	0.38
GC569-29	1881	67	124-112	11.95±0.39	12.9	140.1±23.9	104	0.47	0.42
GC569-23	2068	73	124-112	11.07±0.36	12.5	132.0±24.5	101	0.55	0.45
GC569-30	2486	85	132-124	11.03±0.41	12.0	81.7±16.0	100	0.7	0.53
GC569-25	2598	89	132-124	11.11±0.72	11.6	108.9±25.9	95	0.75	0.56

*1 All depths quoted are total vertical depth (TVD) with respect to KB.

*2 See Appendix A for a discussion of present temperature estimation.

*3 AFTA values predicted from the "Default Thermal History" (Section 1.6); i.e., assuming that each sample is now at its maximum temperature since deposition. The values refer only to tracks formed after deposition. Samples may also contain tracks inherited from sediment provenance areas. Calculations for the ranges given refer to actual measured compositions of apatites analysed within a particular sample, which is discussed in Appendix A.

*4 Vitrinite reflectance values at the level of the AFTA sample either measured, or estimated, based on the VR determinations in the entire well where interpolation is possible.

*5 Vitrinite reflectance values predicted from the "Default Thermal History" (see point *3), using the Burnham and Sweeney (1989) algorithm - see Appendices C and D for discussion.

Table 2.2: Summary of thermal history interpretation of AFTA and VR data in samples from the Vivonne-1 well, Duntroon Basin, South Australia (Geotrack Report #569)

Sample number	Do AFTA data require revision of present temperature ?	Evidence of higher temperatures in the past from length data?	Evidence of higher temperatures in the past from fission track age data?	Evidence of higher temperatures in the past from vitrinite reflectance data?	Conclusion
569-16 1182 m	No 46°C	No [Mean track length is compatible within error of that predicted from Default History.]	No [Central fission track age and most individual grain ages are older than the age range predicted by the Default History.]	No [Measured vitrinite reflectance is similar to that predicted by the Default History.]	Sample is probably at, or close to, its maximum post-depositional temperature at the present day.
569-17 1287 m	No data 49°C	No apatite	No apatite	No [Measured vitrinite reflectance is similar to that predicted by the Default History.]	Sample is probably at, or close to, its maximum post-depositional temperature at the present day.
569-28 1699 m	No 61°C	Yes [Mean track length less than predicted from Default History and modelling of the AFTA parameters indicates paleotemperatures higher than present temperatures.]	No [Pooled fission track age is similar to the age range predicted by the Default History.]	Yes [Measured vitrinite reflectance is greater than predicted by the Default History.]	Sample has been hotter in the past.

Note: Interpretation of AFTA data is based on comparison of measured AFTA parameters with values predicted from the "Default Thermal History" (Section 1.6); i.e., assuming that each sample is now at its maximum temperature since deposition. The predicted values for each sample are summarised in Table 2.1, and refer only to tracks formed after deposition. Samples may also contain tracks inherited from sediment provenance areas, which has been allowed for in interpreting the data.

Table 2.2: Continued

Sample number	Do AFTA data require revision of present temperature ?	Evidence of higher temperatures in the past from length data?	Evidence of higher temperatures in the past from fission track age data?	Evidence of higher temperatures in the past from vitrinite reflectance data?	Conclusion
569-29 1881 m	No 67°C	No, equivocal [Mean track length less than predicted from Default History. Modelling the fission track age and length data indicate the observed shortening can be explained either by inheritance of all short tracks from sediment provenance terrains, or by paleotemperatures higher than present temperatures after deposition.]	No [Central fission track age and most individual grain ages are older than the age range predicted by the Default History.]	Yes [Measured vitrinite reflectance is greater than predicted by the Default History.]	Sample has been hotter in the past, but a number of grains show evidence of considerable inheritance of tracks from an older provenance terrain, resulting in a lack of observable age reduction.
569-23 2068 m	No 73°C	No, equivocal [Mean track length less than predicted from Default History. Modelling the fission track age and length data indicate the observed shortening can be explained either by inheritance of all short tracks from sediment provenance terrains, or by paleotemperatures higher than present temperatures after deposition.]	No [Central fission track age and most individual grain ages are older than the age range predicted by the Default History.]	Yes [Measured vitrinite reflectance is greater than predicted by the Default History.]	Sample has been hotter in the past, but a number of grains show evidence of considerable inheritance of tracks from an older provenance terrain, resulting in a lack of observable age reduction.

Note: Interpretation of AFTA data is based on comparison of measured AFTA parameters with values predicted from the "Default Thermal History" (Section 1.6); i.e., assuming that each sample is now at its maximum temperature since deposition. The predicted values for each sample are summarised in Table 2.1, and refer only to tracks formed after deposition. Samples may also contain tracks inherited from sediment provenance areas, which has been allowed for in interpreting the data.

Table 2.2: Continued

Sample number	Do AFTA data require revision of present temperature ?	Evidence of higher temperatures in the past from length data?	Evidence of higher temperatures in the past from fission track age data?	Evidence of higher temperatures in the past from vitrinite reflectance data?	Conclusion
569-30 2486 m	No 85°C	No [Mean track length similar to that predicted from Default History due to the high present temperatures. Modelling of the length parameters indicates paleotemperatures may have been higher than present temperatures, but are not required.]	Yes [Central fission track age and some individual grain ages are younger than the age range predicted by the Default History.]	Yes [Measured vitrinite reflectance is greater than predicted by the Default History.]	Sample has been hotter in the past.
569-25 2598 m	No 89°C	No [Mean track length similar to that predicted from Default History due to the high present temperatures. Modelling of the length parameters indicates paleotemperatures may have been higher than present temperatures, but are not required.]	Yes, equivocal [Central fission track age and most individual grain ages are similar to the age range predicted by the Default History, but one Cl-rich grain is younger suggesting paleotemperatures were higher than present temperatures. Two relatively F-rich grains are older than expected and appear to be contaminants, probably caved.]	Yes [Measured vitrinite reflectance is greater than predicted by the Default History.]	Sample has been hotter in the past, but fission track parameters in most grains are dominated by the present temperatures and show little direct evidence of this.

Note: Interpretation of AFTA data is based on comparison of measured AFTA parameters with values predicted from the "Default Thermal History" (Section 1.6); i.e., assuming that each sample is now at its maximum temperature since deposition. The predicted values for each sample are summarised in Table 2.1, and refer only to tracks formed after deposition. Samples may also contain tracks inherited from sediment provenance areas, which has been allowed for in interpreting the data.

Table 2.3: Estimates of timing and magnitude of elevated paleotemperatures from AFTA and VR data in samples from the Vivonne-1 well, Duntroon Basin, South Australia (Geotrack Report #569)

Sample number	Stratigraphic Age	Present temperature	Early episode (~112 to 75 Ma) Maximum paleo-temperature	Early episode (~112 to 75 Ma) Onset of cooling	Late episode (~65 to 0 Ma) Peak paleo-temperature	Late episode (~65 to 0 Ma) Onset of cooling	Comments
GC	(Ma)	(°C)	(°C)	(Ma)	(°C)	(Ma)	
569-16 1182 m	65 to 56 Paleocene Lower Pidinga	46	Not applicable		<105 AFTA VR ~46	65 to 0	Modelling of the AFTA parameters suggest that maximum paleotemperatures in the section must have been less than ~105°C after deposition, with no direct evidence that paleotemperatures were higher than present temperatures. Measured VR values in this part of the section indicate a maximum paleotemperature of ~47°C, indistinguishable from the present temperature of 46°C, suggesting little post-Paleocene cooling.
569-17 1287 m	74 to 65 Maastrichtian	49	No apatite				A measured VR value indicates a maximum paleotemperature of ~59 to 74°C, for a range of heating rates, a little higher than the present temperature of 49°C, suggesting some Tertiary cooling.
569-28 1699 m	124 to 112 Aptian Upper Borda	61	80 to 100 AFTA VR ~79°C	112 to 50	No direct evidence		AFTA data indicate cooling from a maximum paleotemperature of 80 to 100°C, similar to the maximum paleotemperature of ~79°C indicated by the VR data, commencing at some time after Aptian deposition (124 to 112 Ma) and prior to ~50 Ma. The AFTA data provide no direct evidence for any Late (post-Paleocene) cooling episode. The data would allow paleotemperatures in this interval on any value less than the maximum reached prior to 50 Ma, but do not require them.

Table 2.3: Continued

Sample number	Stratigraphic Age	Present temperature	Early episode (~112 to 75 Ma) Maximum paleo-temperature	Early episode (~112 to 75 Ma) Onset of cooling	Late episode (~65 to 0 Ma) Peak paleo-temperature	Late episode (~65 to 0 Ma) Onset of cooling	Comments
GC	(Ma)	(°C)	(°C)	(Ma)	(°C)	(Ma)	
569-29 1881 m	124 to 112 Aptian Upper Borda	67	<110 AFTA VR ~89 to 98°C	112 to 0 (112 to 50 favoured)	No direct evidence		AFTA data indicate cooling from a maximum paleotemperature less than ~110°C at any time after Aptian deposition, although the data favour the time prior to ~50 Ma. VR data from nearby samples indicate maximum paleotemperatures between ~89 and 98°C. The AFTA data provide no direct evidence of any additional period of post-Paleocene heating, but paleotemperatures of any value up to the maximum reached in the Early heating episode would be allowed but not required.
569-23 2068 m	124 to 112 Aptian	73	95 to 115 AFTA VR ~100°C	112 to 65	< 95	No direct evidence	AFTA data indicates cooling from maximum paleotemperatures in the range 95 to 115°C at some time between ~112 and 65 Ma. VR data from nearby samples indicate maximum paleotemperatures of ~100°C. The AFTA data provide no direct evidence of any additional period of post-Paleocene cooling, but paleotemperatures up to ~95°C would be allowed but not required.

Table 2.3: Continued

Sample number	Stratigraphic Age	Present temperature	Early episode (~112 to 75 Ma) Maximum paleo-temperature	Early episode (~112 to 75 Ma) Onset of cooling	Late episode (~65 to 0 Ma) Peak paleo-temperature	Late episode (~65 to 0 Ma) Onset of cooling	Comments
GC	(Ma)	(°C)	(°C)	(Ma)	(°C)	(Ma)	
569-30 2486 m	132 to 124 Barremian	85	>110 AFTA VR ~135°C	124 to 75	85 to 110	60 to 0	VR data indicate maximum paleotemperatures of ~135°C after deposition. The AFTA data indicates cooling from maximum paleotemperatures greater than ~110°C, which, when interpreted in terms of the maximum paleotemperature of ~135°C indicated by the VR data, shows that cooling must have occurred between ~124 (depositional age) and 75 Ma. The AFTA data also indicate a later cooling period, with cooling from paleotemperatures of ~85 to 110°C commencing at some time within the last 60 Ma. Data from this sample provide the best constraints on the timing of both the Early and Late heating episodes.
569-25 2598 m	132 to 124 Barremian	89	>89 AFTA VR ~140°C	124 to 75	<100	60 to 0	VR data indicate maximum a paleotemperature of ~140°C after deposition. The AFTA data also indicate cooling from maximum paleotemperatures higher than the present temperature at some time after deposition, which, when interpreted in terms of a VR-derived maximum paleotemperature of ~140°C, shows that cooling must have occurred between ~124 (depositional age) and 75 Ma. The AFTA data also indicate a later cooling period, with cooling from paleotemperatures up to 100°C commencing at some time within the last 60 Ma. Two relatively F-rich grains are older than expected, compatible with maximum paleotemperatures less than ~110°C. They appear to be contaminants, probably caved from a depth of ~2100 m or shallower.

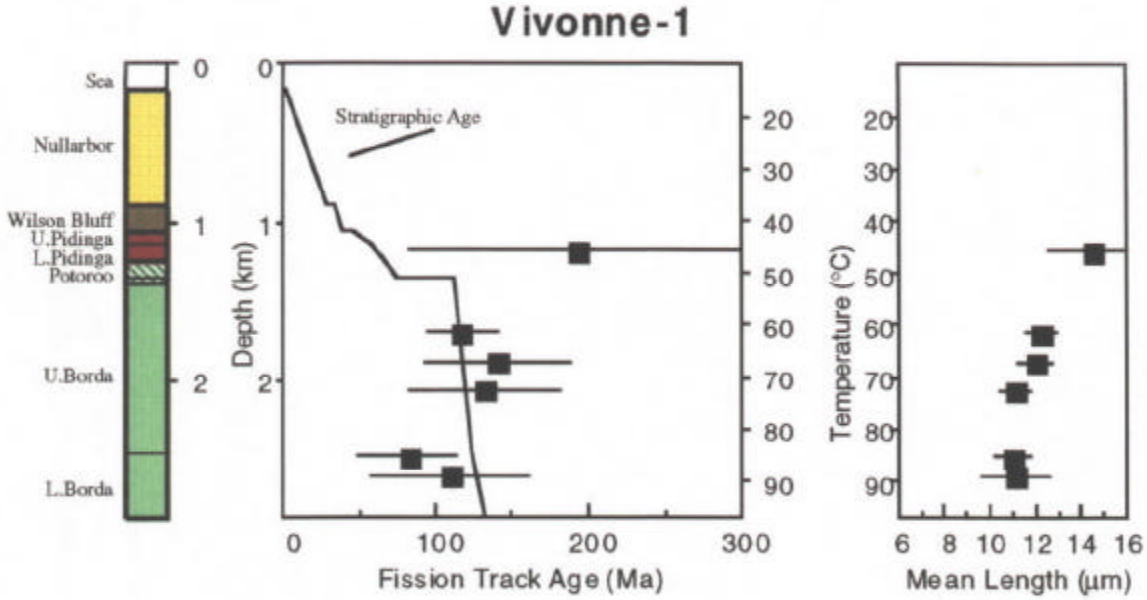

Figure 2.1: AFTA parameters plotted against sample depth and present temperature for samples from **well Vivonne-1, Duntroon Basin.** The variation of stratigraphic age with depth is also shown, as the solid line in the central panel.

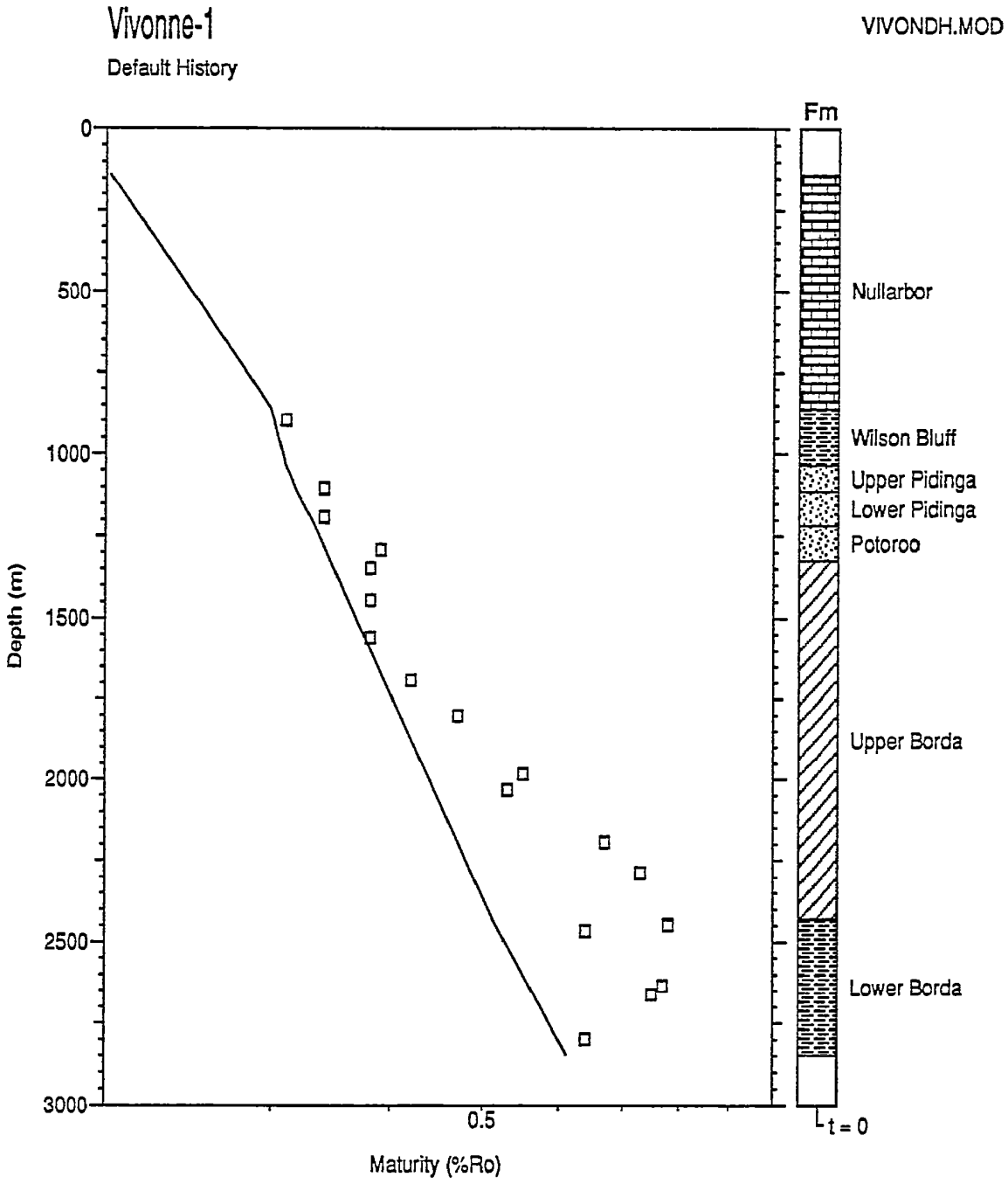

Figure 2.2: Predicted vitrinite reflectance profile for the **Vivonne-1 well, Duntroon Basin**, based on the "Default History" (Section 1.6), i.e., the profile expected if samples throughout the section are currently at their maximum temperature since deposition. The majority of data from the Borda Formation section fall above the predicted profile, indicating that samples have been hotter in the past. See text for details.

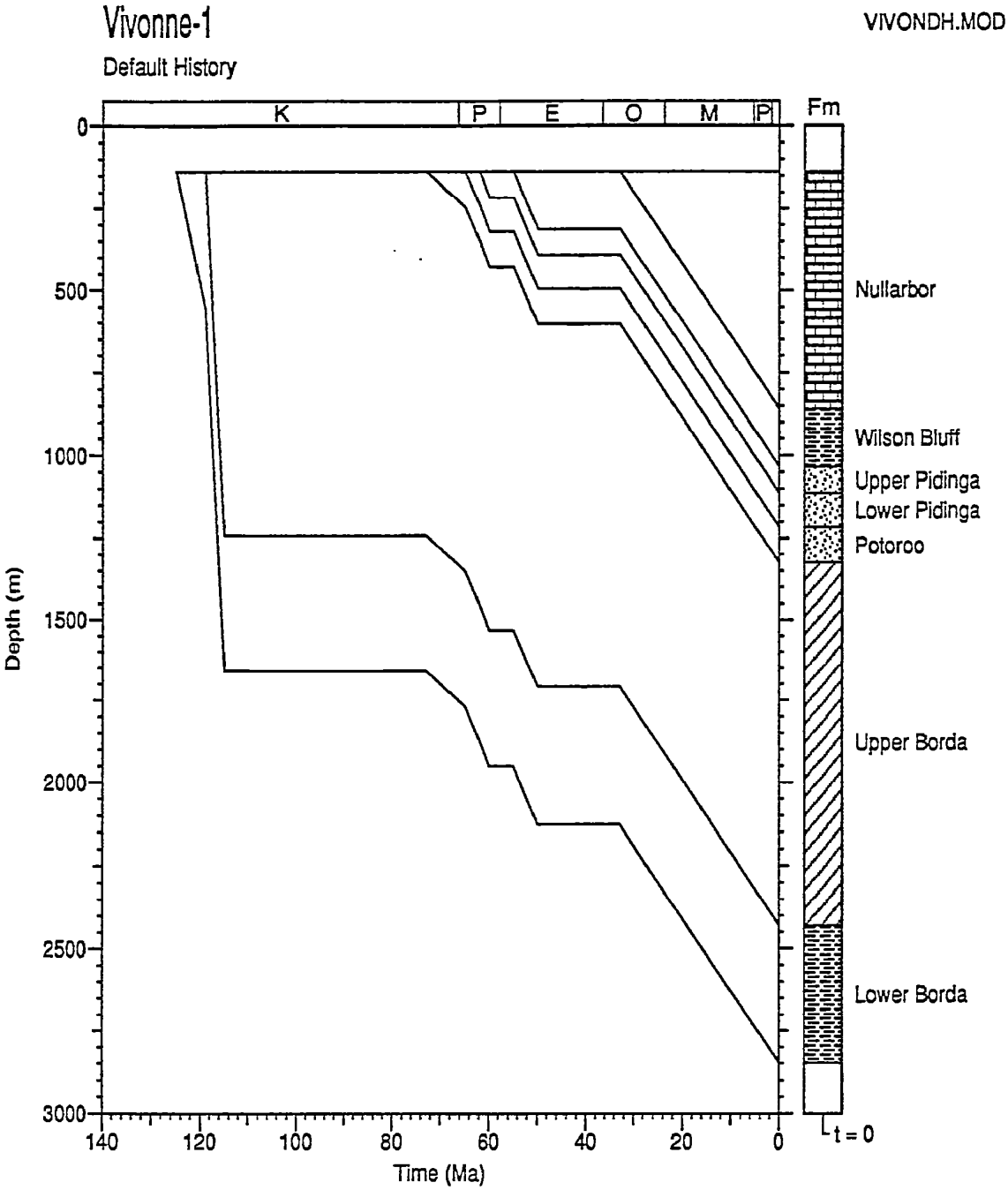

Figure 2.3: Default Burial History for the **Vivonne-1 well, Duntroon Basin**, derived from the preserved section, which, combined with a present-day linear geothermal gradient of 30.2°C/km (Appendix A), is used in predicting the VR profile shown in Figure 2.2.

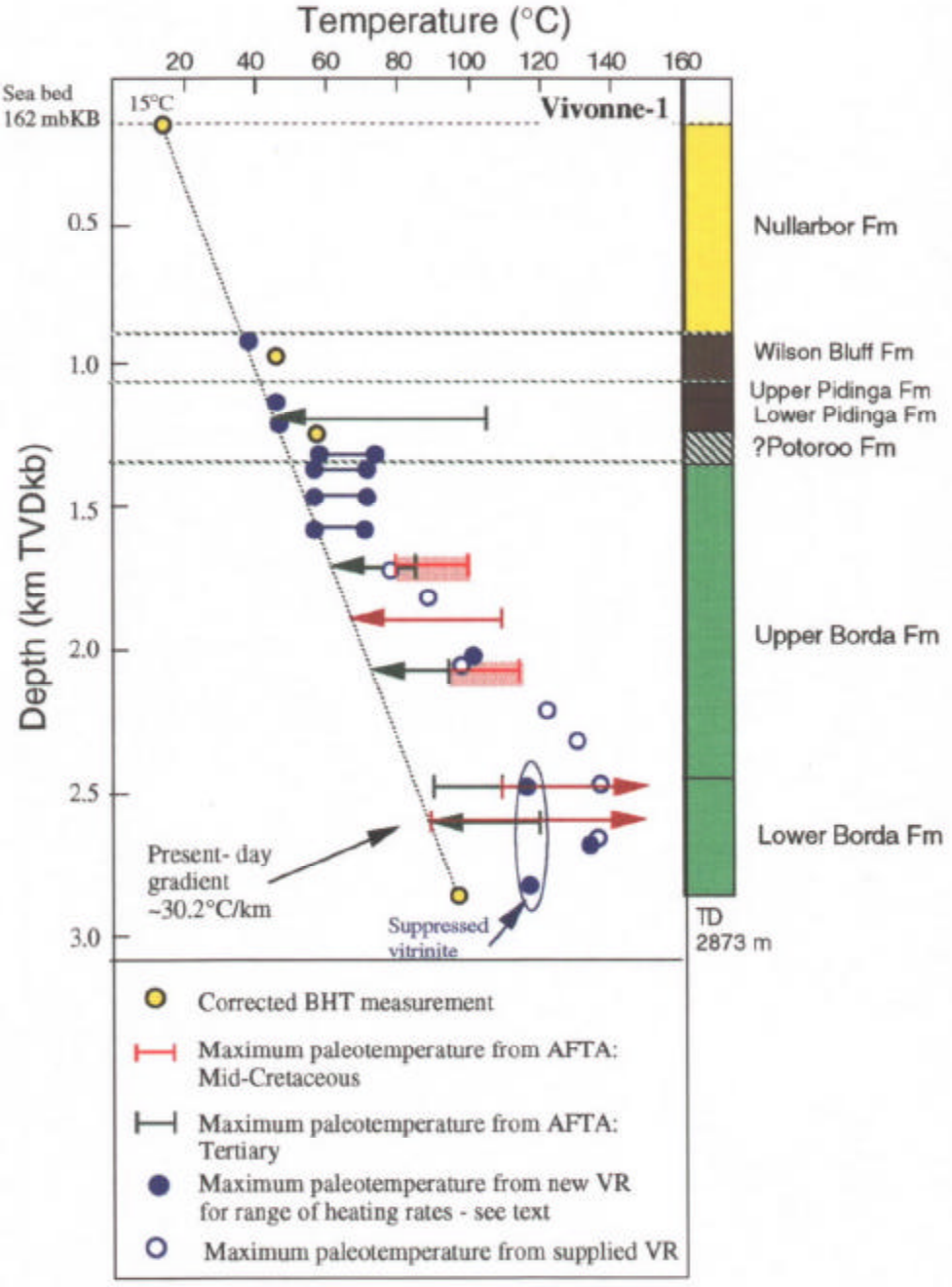

Figure 2.4: Plot of paleotemperatures derived from AFTA and VR data in the **Vivonne-1 well, Duntroon Basin**, against sample depth and the estimated present temperature profile for this well (see Appendix A). The AFTA and VR paleotemperature estimates give clear evidence of the sampled section having cooled from elevated paleotemperatures after deposition. Note the range of paleotemperatures given for a number of VR samples which reflect a range of heating rates, due to uncertainty in the time at which this part of the section cooled from maximum temperatures - see text.

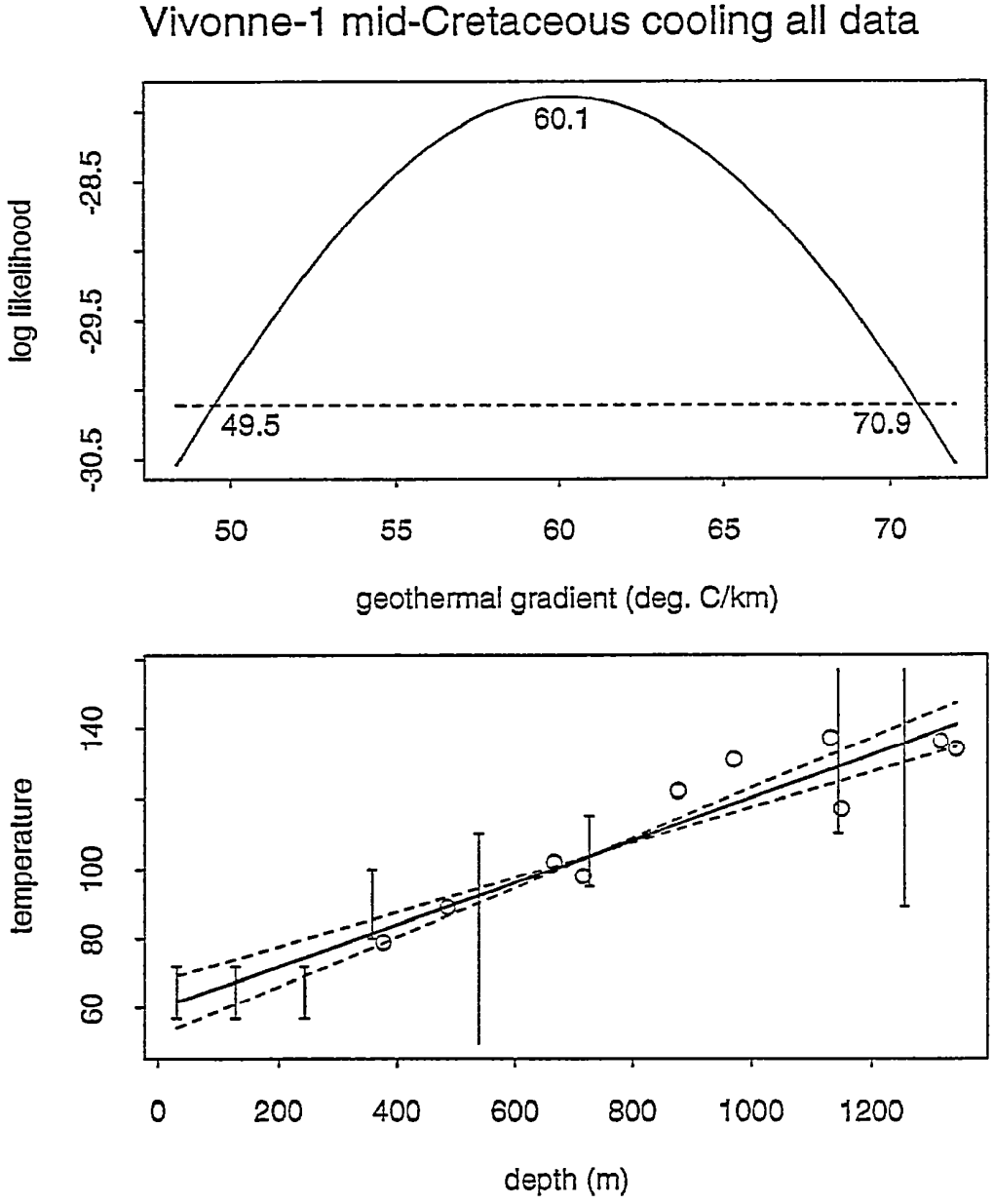

Figure 2.5: Upper: Maximum likelihood profile of linear paleogeothermal gradient fitted to the **Mid-Cretaceous** paleotemperature estimates from AFTA and VR data in the **Vivonne-1 well**. The profile shows good quadratic behaviour, suggesting a well-constrained value, with upper and lower 95% confidence limits of 70.9 and 49.5°C/km, respectively, and a best-fit value of 60.1°C/km. The methodology employed in deriving this profile is outlined in Appendix C.

Lower: Maximum paleotemperature estimates from AFTA (bars) and VR (circles) in the **Vivonne-1 well**, with fitted profile (solid line) and lines (dashed) representing upper and lower 95% confidence limits.

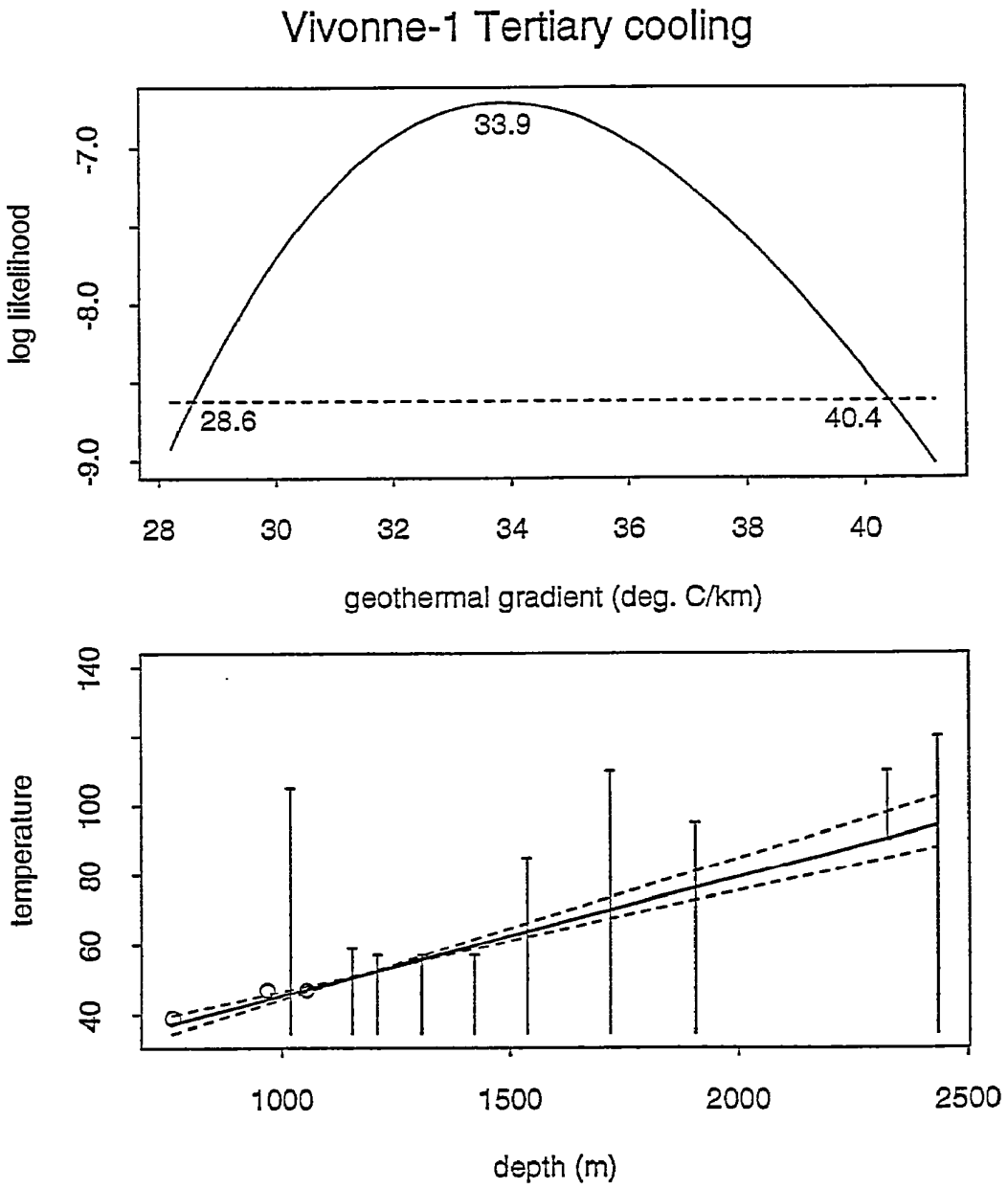

Figure 2.6: Upper: Maximum likelihood profile of linear paleogeothermal gradient fitted to the **Tertiary** paleotemperature estimates from AFTA data in the **Vivonne-1 well.** The profile shows good quadratic behaviour, suggesting a well-constrained value, with upper and lower 95% confidence limits of 40.4 and 28.6°C/km, respectively, and a best-fit value of 33.9°C/km. The methodology employed in deriving this profile is outlined in Appendix C.

Lower: Maximum paleotemperature estimates from AFTA (bars) in the **Vivonne-1 well,** with fitted profile (solid line) and lines (dashed) representing upper and lower 95% confidence limits.

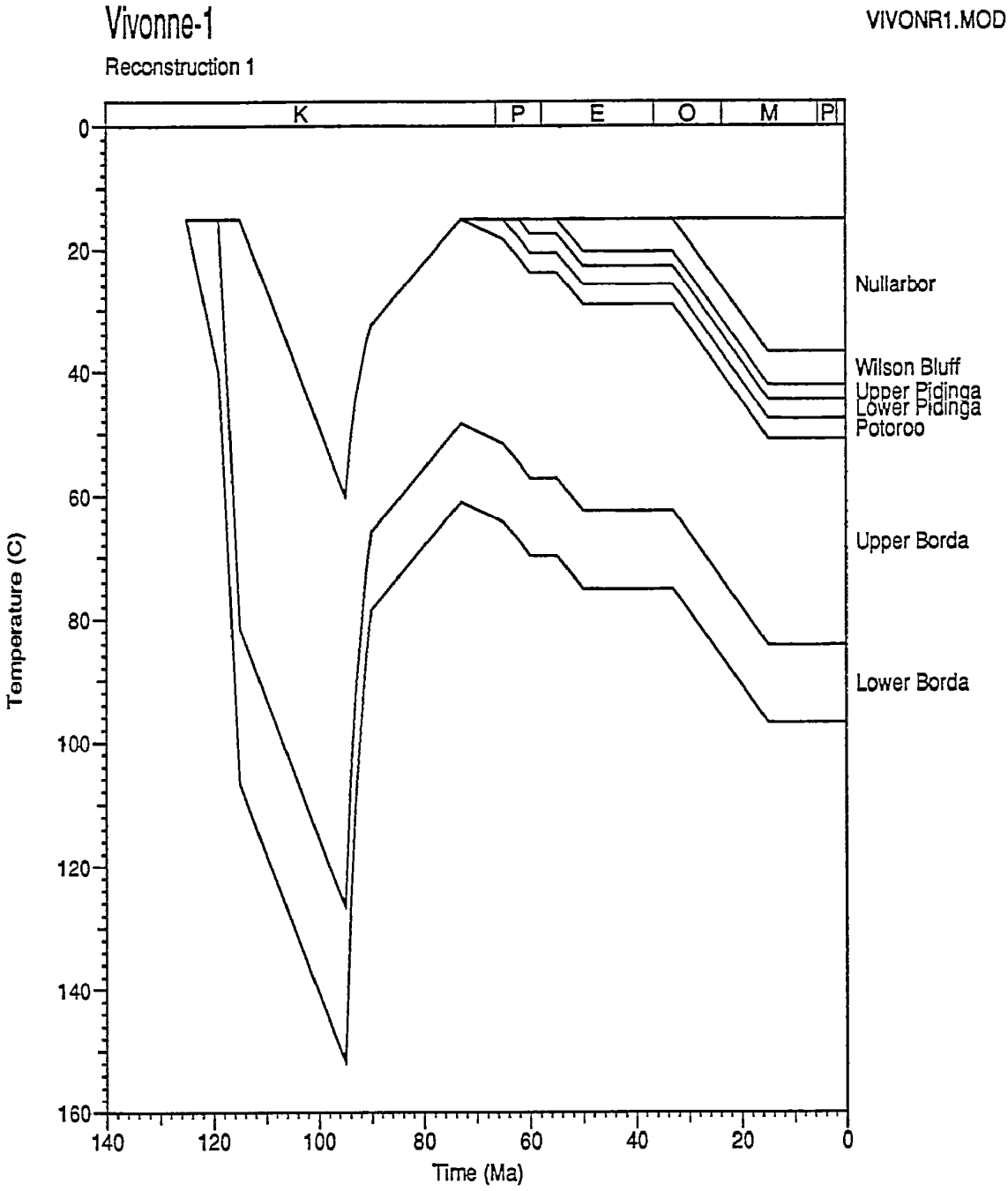

Figure 2.7: Reconstructed thermal history in the **Vivonne-1 well** derived from the AFTA and VR paleotemperature data, using the constrained maximum likelihood value for a paleogeothermal gradient of 60°.1°C/km through the Early Cretaceous until ~95 Ma, declining to the present-day level of 30.2°C/km by ~80 Ma.

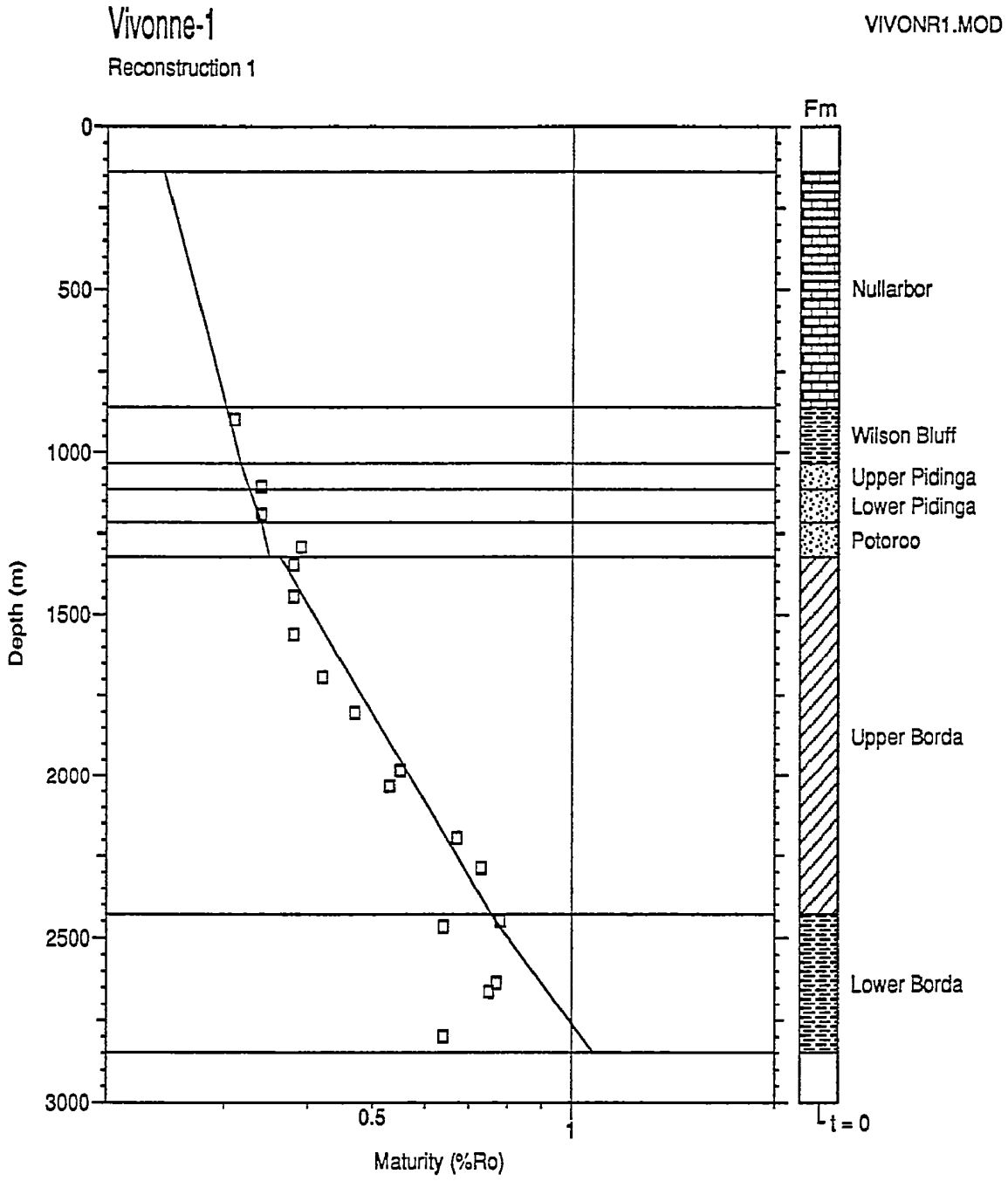

Figure 2.8: Measured vitrinite reflectance data (new Keiraville VR data as solid symbols) in samples from the **Vivonne-1 well**, and the VR profile predicted by the reconstructed thermal history shown in Figure 2.6. Most data show good agreement with the predicted profile, as expected.

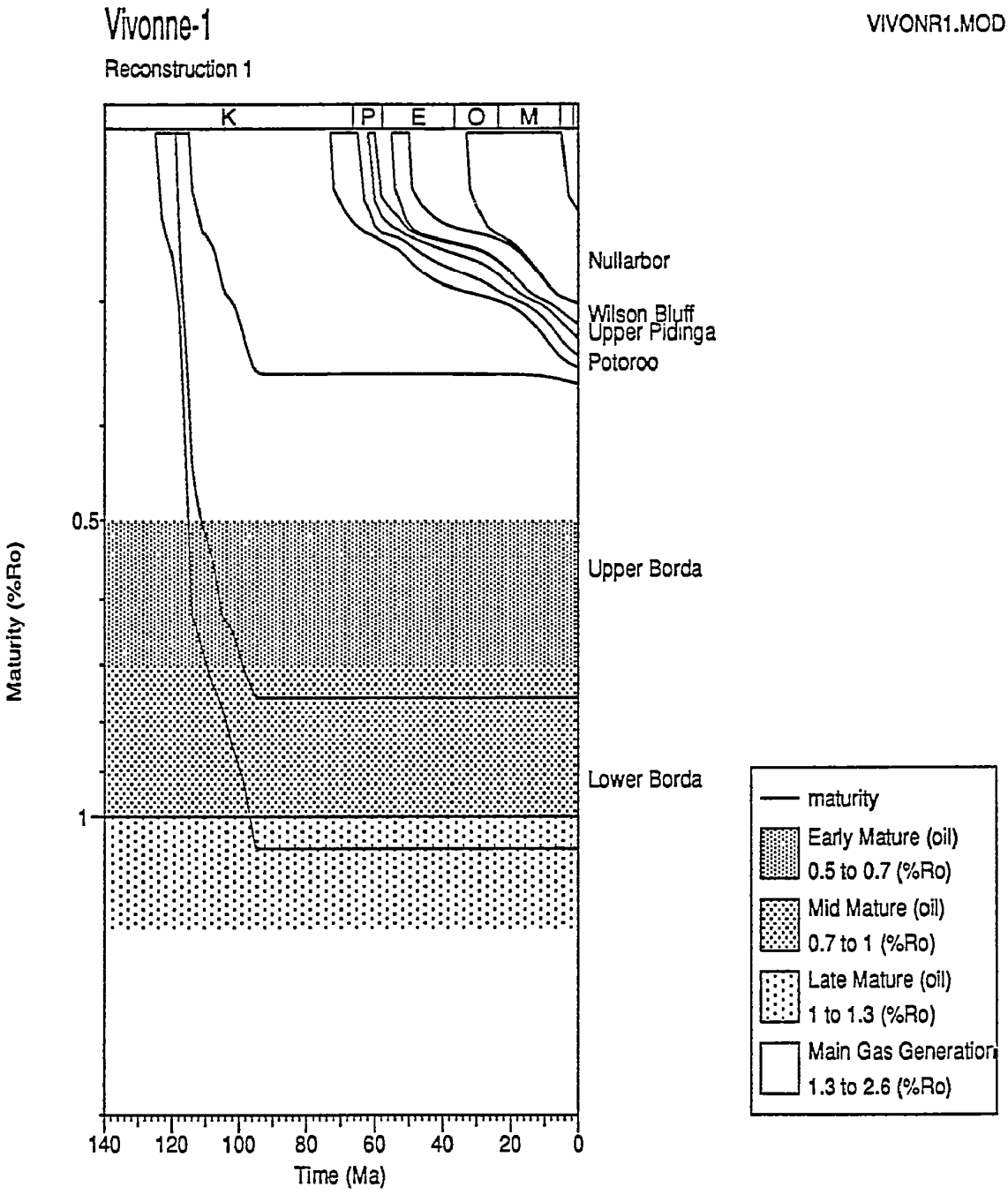

Figure 2.9: Predicted development of maturity with time in the **Vivonne-1 well, Duntroon Basin,** controlled by the AFTA and VR data. Potential Jurassic and Early Cretaceous source rocks reached maximum maturity prior to Mid-Cretaceous cooling (shown at ~95 Ma, but any time between 112 and 75 Ma allowed by AFTA). No significant hydrocarbon generation from Early Cretaceous source rocks has occurred since this time - see text.

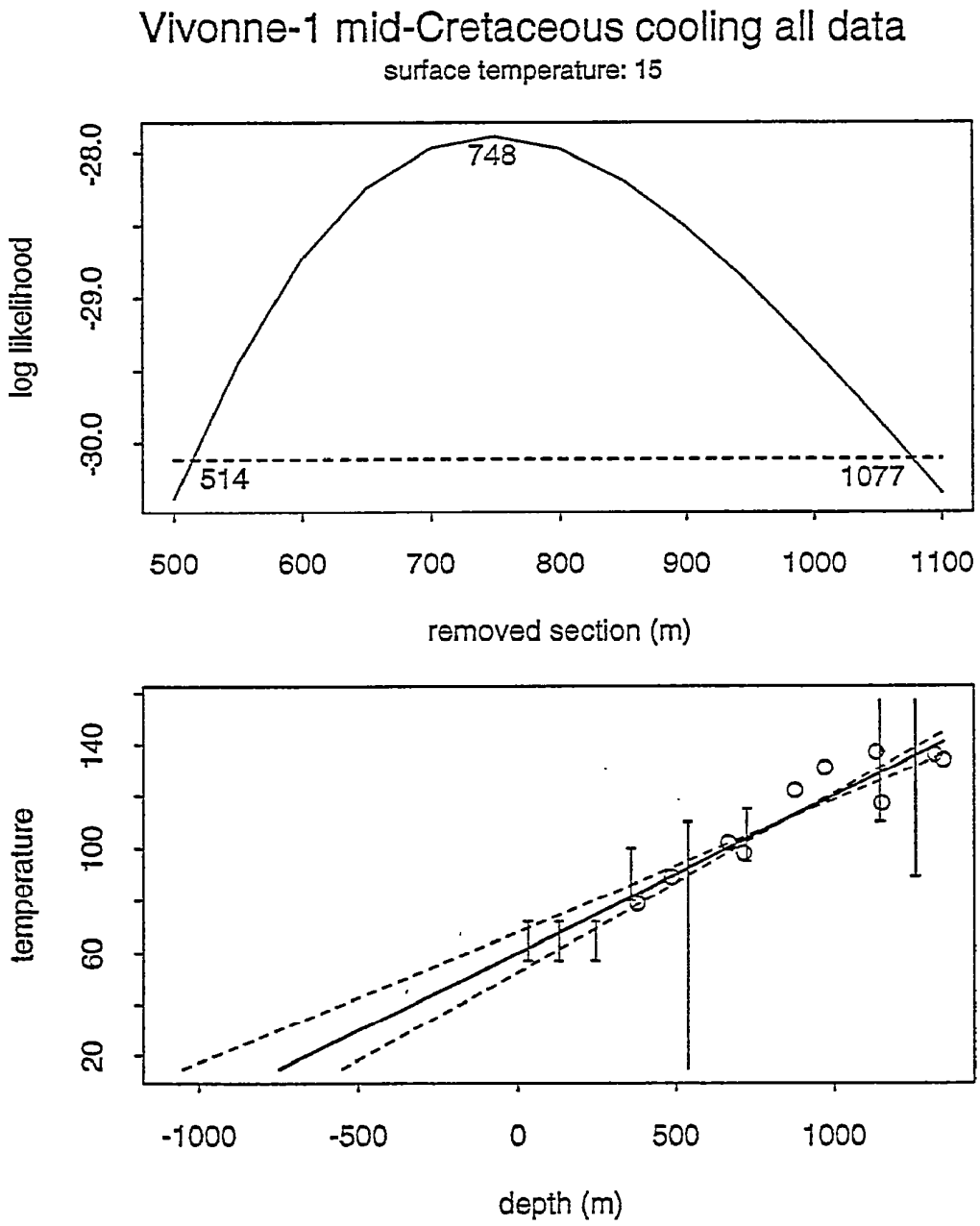

Figure 2.10: Upper: Maximum likelihood profile of estimated section removed by uplift and erosion since the **Mid-Cretaceous** in the **Vivonne-1 well**, derived from the paleogeothermal gradient shown in Figure 2.5, assuming a paleo-surface temperature of 15°C. The profile gives upper and lower 95% confidence limits of 1077 and 514 metres, respectively, and a best-fit value of 748 metres. The methodology employed in deriving this profile is outlined in Appendix C.

Lower: Maximum paleotemperature estimates from AFTA and VR data in the **Vivonne-1 well**, with fitted profile (solid line) and lines (dashed) representing upper and lower 95% confidence limits, extrapolated to the assumed paleo-surface temperature of 15°C.

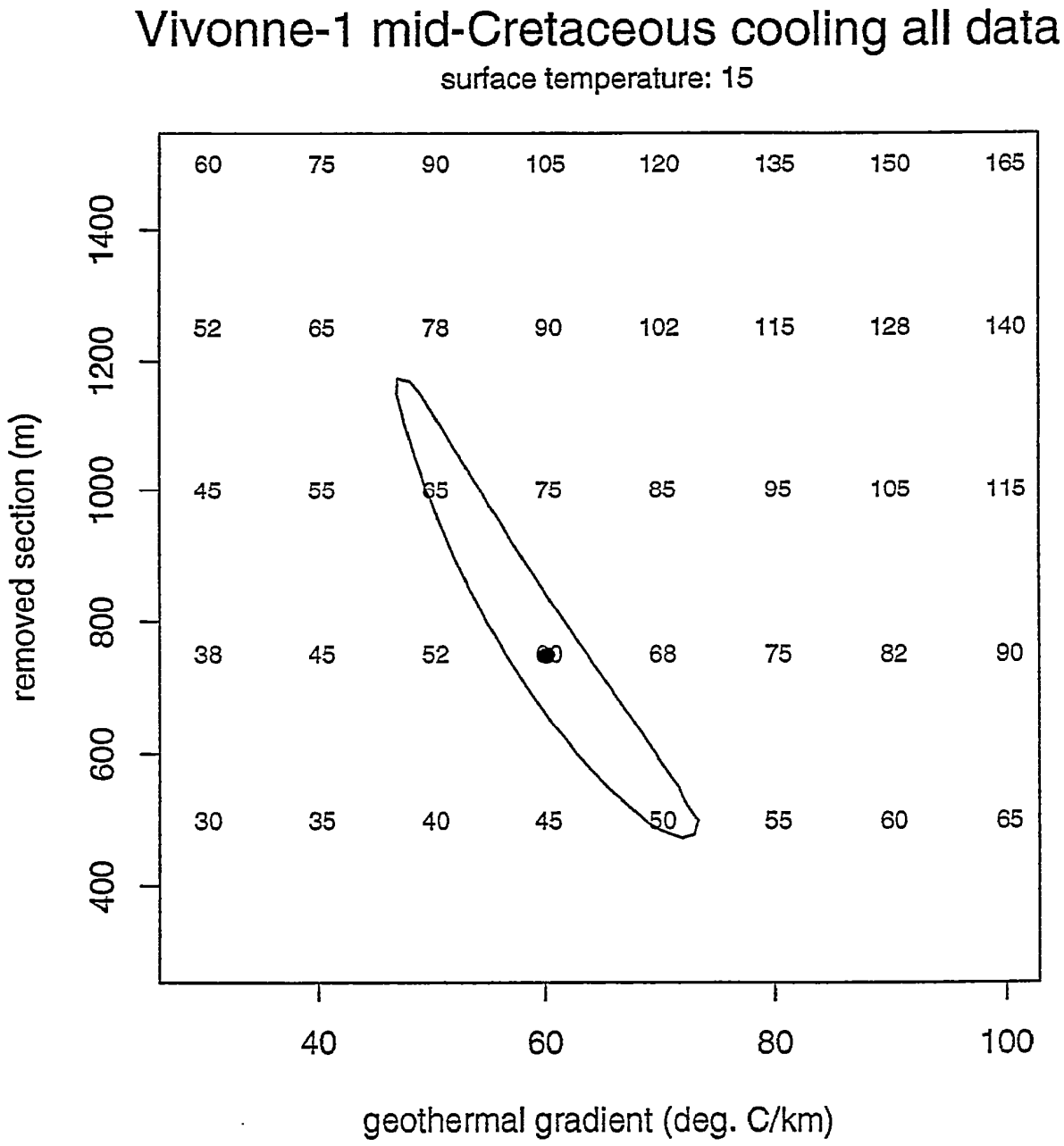

Figure 2.11: Crossplot of removed section against paleogeothermal gradient for the **Mid-Cretaceous** in the **Vivonne-1 well**, showing the range of values (within the contoured region) compatible with the maximum paleotemperatures derived from AFTA and VR, at the 95% confidence level. The numbers within the plot are paleotemperatures at the present ground surface corresponding to the specified values of removed section and paleo-gradient.

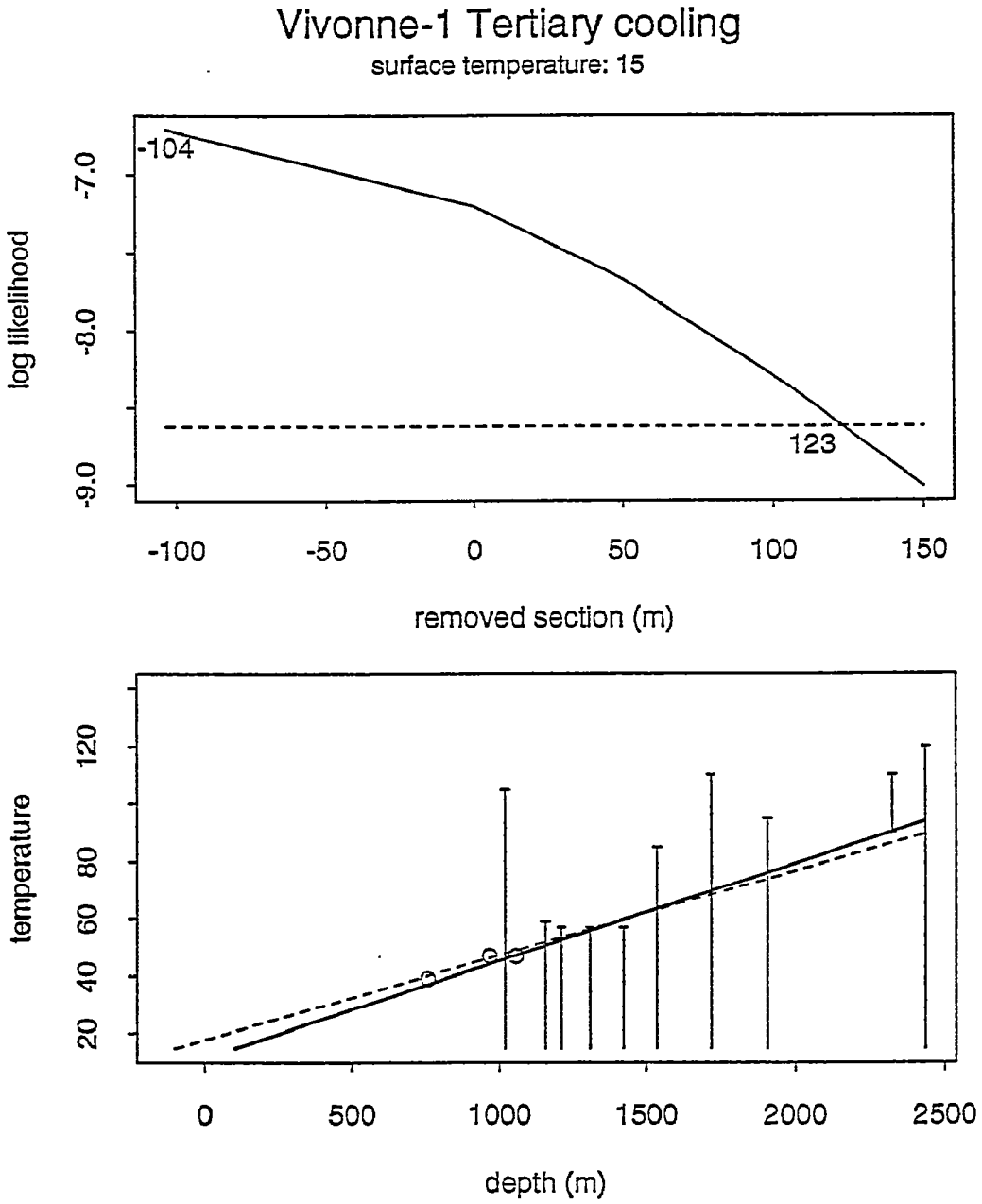

Figure 2.12: Upper: Maximum likelihood profile of estimated section removed by uplift and erosion since the **Mid-Cretaceous** in the **Vivonne-1 well**, derived from the paleogeothermal gradient shown in Figure 2.6, assuming a paleo-surface temperature of 15°C. The profile gives an upper 95% confidence limit of 123 metres, and an unreal best-fit value of -104 metres. The methodology employed in deriving this profile is outlined in Appendix C.

Lower: Maximum paleotemperature estimates from AFTA data in the **Vivonne-1 well**, with fitted profile (solid line) and lines (dashed) representing upper and lower 95% confidence limits, extrapolated to the assumed paleo-surface temperature of 15°C.

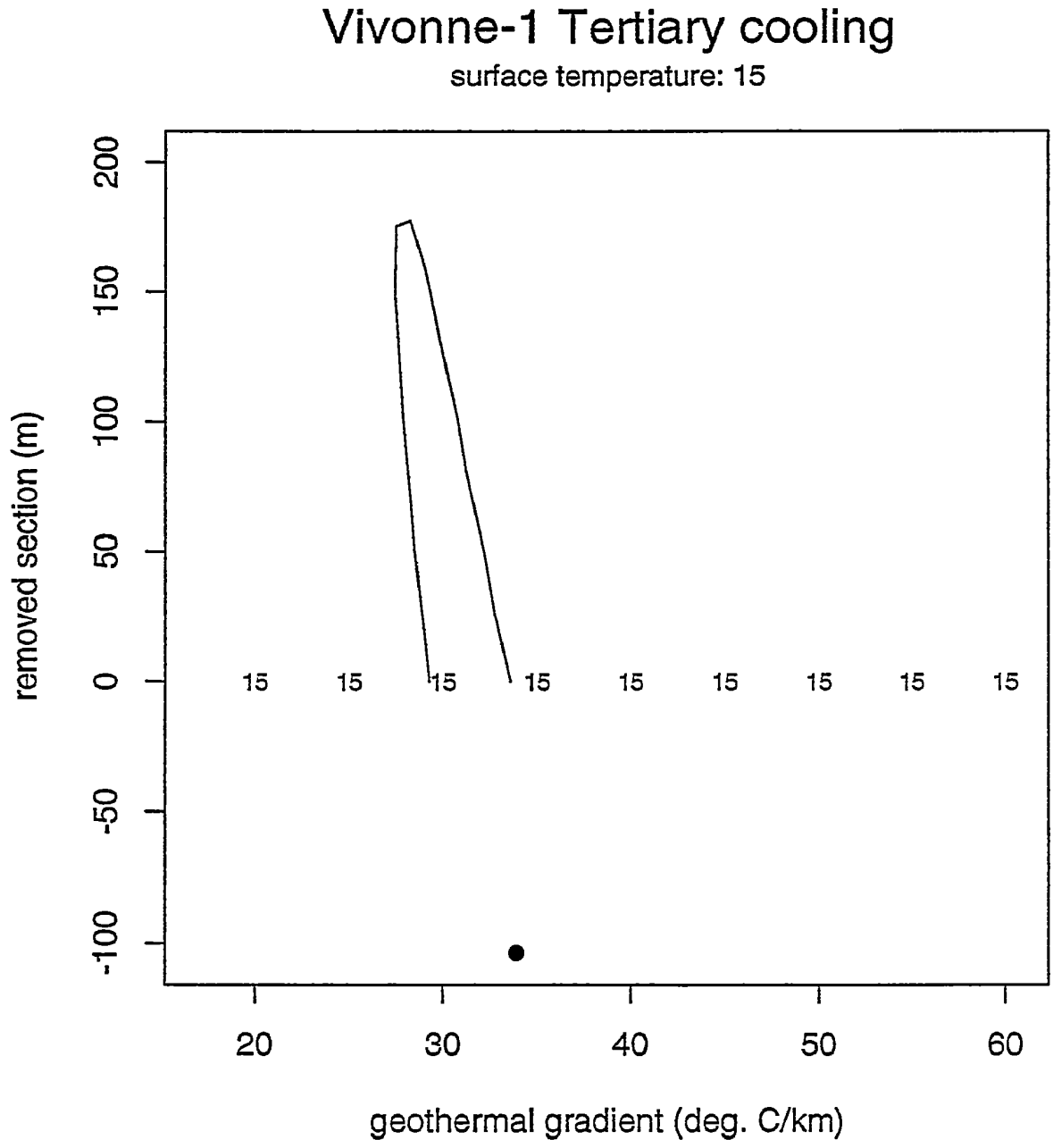

Figure 2.13: Crossplot of removed section against paleogeothermal gradient for the **Tertiary**, showing the range of values (within the contoured region) compatible with the maximum paleotemperatures derived from AFTA data in the **Vivonne-1 well** at the 95% confidence level. The numbers within the plot are paleotemperatures at the present sea-bed corresponding to the specified values of removed section and paleo-gradient.

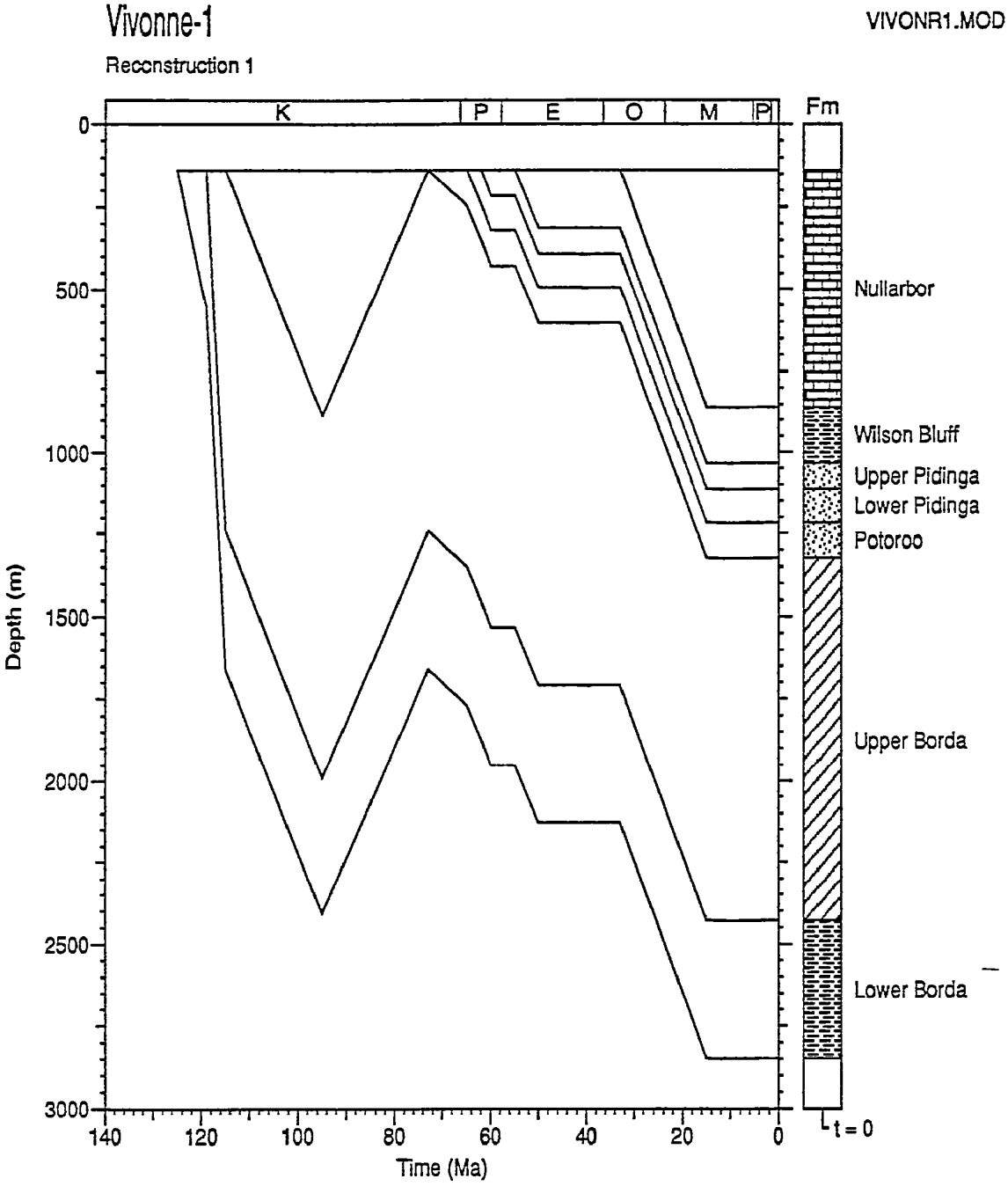

Figure 2.14: Possible burial history reconstructed from the paleotemperature data in the **Vivonne-1 well, Duntroon Basin,** using the maximum likelihood thermal and burial history parameters listed in Tables ii and iii and discussed in the text, with 748 m of Early Cretaceous section removed in the Mid-Cretaceous (at 95 Ma) and no subsequent uplift and erosion - see text for details.

3. Thermal history reconstruction in the Borda-1 well

3.1 Background

Geology

The Borda-1 well in the Duntroon Basin intersected a ~1048 m thick section of Nullarbor Formation of Pliocene-Late Oligocene age, unconformably overlying Late Eocene Wilson Bluff Formation ~916 m thick, in turn unconformably overlying Paleocene-Eocene Lower Pidinga Formation ~317 m thick and Maastrichtian ?Potoroo Formation ~337 m thick, with TD at 2800 m (measured depth below RT). The generalised stratigraphy is shown in Figure 3.1. The present-day geothermal gradient is calculated from corrected BHT data to be 27.2°C/km for a sea-bed temperature of 15°C (Appendix A).

AFTA data

Fission track parameters from one sample (a second sample failed to yield any apatite) are summarised in Table 3.1, together with values of fission track age and mean track length predicted on the basis of the Default Thermal History (see Section 1.6). The calculation of these default values includes only those tracks formed after deposition of the sample, and therefore does not account for tracks inherited from sediment source areas. The use of these parameters in interpreting AFTA data is outlined in Section 1.6 and Appendix C. The range of measured apatite chlorine compositions used in calculating predicted values for AFTA samples is listed in Appendix B.

The measured AFTA data are also plotted in Figure 3.1. The fission track age in the single sample of Potoroo Formation (GC569-13) is indistinguishable from the Maastrichtian stratigraphic age.

VR data

Vitrinite reflectance data on 11 samples from the Wilson Bluff, Lower Pidinga and Potoroo Formations, which were collected as a part of this study (Table D.2), were supplemented by data on a further five samples from the Lower Pidinga and Potoroo Formations supplied by MESA (Table D.3). All VR values are plotted with respect to depth in Figure 3.2. Also shown in Figure 3.2 is the VR profile predicted from the Default Thermal History, i.e., the thermal history of the well had the section never been hotter than present temperatures. The burial history used in calculating this profile is shown in Figure 3.3.

3.2 Evidence for elevated paleotemperatures

AFTA data

Kinetic modelling of the limited AFTA data in sample GC569-13 provide no clear evidence for paleotemperatures any higher than present temperatures after Maastrichtian deposition of the sample. Nonetheless, evidence for elevated paleotemperatures from this sample are summarised in Table 3.2.

VR data

The measured VR data in the deeper section of the Borda-1 well (particularly the Potoroo Formation samples) plot just above the profile predicted from the Default Thermal History (Figure 3.2), suggesting that this section has been hotter in the past. Data from the shallower Wilson Bluff Formation tend to plot closer to, or below, the predicted profile, showing no clear evidence for paleotemperatures higher than present temperatures. Note that in constructing the Default History, it has been assumed that the Nullarbor Formation in Borda-1 was continuously deposited from the Late Oligocene to the present day (see Figure 3.3), although specific information on the age of the youngest preserved Nullarbor Formation is unknown. This uncertainty will affect the estimation of maximum paleotemperatures from the VR data as discussed in Section 3.3.

Evidence for elevated paleotemperatures, shown by the VR level at the depth of each AFTA sample in Borda-1, is also summarised in Table 3.2.

3.3 Magnitude of maximum paleotemperatures and time of cooling from AFTA and VR

The thermal history interpretation of the AFTA data in a single sample is summarised in Table 3.3. Paleotemperature estimates are tentatively quoted in terms of a single paleo-thermal episode - **Tertiary** - as the synthesis of AFTA and VR data suggests that only a single event may be present.

The AFTA data from GC569-13 provide no conclusive evidence of even a single event, allowing, but not requiring, maximum paleotemperatures up to ~130°C, at any time after deposition.

Determination of maximum paleotemperatures from each VR sample depends on knowledge of the heating rate. In the Borda-1 well, there is neither specific data on the age of the Miocene-Pliocene Nullarbor Formation which would provide basic

burial rate information over the critical most recent part of the history, nor is there control on time of cooling from AFTA. In this situation, we have made estimates of maximum paleotemperature for each VR sample for two heating rates which will cover most typical geological situations (~ 1 and 5°C/Ma).

Maximum paleotemperatures estimated for the higher heating rate are significantly higher than the present temperatures in the deeper section. They mimic the trend shown on the maturity plot (Figure 3.2), which is a reflection of the relatively high heating rate created by assuming continuous deposition of the Nullarbor Formation over the last 30 Ma or so in constructing Figure 3.2 (see Section 3.2).

On the other hand, maximum paleotemperatures estimated for the lower heating rate are similar to the present temperatures, from which little if any cooling can be inferred for any of the drilled section. A low heating rate implies, however, that the youngest Nullarbor Formation in Borda-1 is around Middle Miocene or older (15 to 10 Ma, or so), and not Pliocene-Pleistocene.

More paleontological data are required to assess these possibilities adequately.

Estimates of maximum paleotemperature from the single AFTA and each VR sample for two heating rates are summarised in Table i (Executive Summary) and plotted against depth in Figure 3.4.

A schematic illustration of the main features of the thermal history in the Borda-1 well is presented in Figure iii (Technical Summary).

3.4 Paleogeothermal gradients and the cause of possible Tertiary heating

Paleotemperature estimates for a range of heating rates (see Section 3.3) derived from AFTA and VR data for the **possible Tertiary heating episode** are plotted with respect to depth in Figure 3.4. Using the approach outlined in Section 1.7 and methods explained in Appendix C, the paleogeothermal gradient has been determined for this episode, as outlined below. Depths for all calculations are with respect to the sea-bed at depth of 182 mbKB.

Regardless of heating rate, maximum paleotemperatures derived from the VR data for the Wilson Bluff to Potoroo Formation sections are generally consistent with a common trend, suggesting they represent the same heating event. The two shallower samples from the Wilson Bluff Formation plot at maximum paleotemperatures lower than present temperatures, which is attributed to uncertainties in the algorithm used

for converting very low maturity values (see Appendix D). Therefore, they have no thermal history significance.

The lack of any direct AFTA constraint means that no specific time can be assigned to these maximum paleotemperature estimates. Given the lack of any obvious breaks in the VR trend at known unconformities, we assume that any heating occurred after deposition of the entire drilled section. It is emphasised that other scenarios are also possible, with heating only affecting the Potoroo Formation, for instance, or the Pidinga and Potoroo Formations, etc., but detailed assessment of these possibilities awaits additional data.

Bearing these caveats in mind, fitting a linear gradient to the VR-derived maximum paleotemperatures for each heating rate for all samples from the Wilson Bluff to Potoroo Formations gives:

For the low heating rate: A maximum likelihood gradient of 31.0°C/km, with upper and lower 95% confidence limits of 37.5 and 24.6°C/km, respectively, as illustrated in Figure 3.5. The 95% confidence limit range of paleogeothermal gradient incorporates the present-day value of 27.2°C/km.

For the high heating rate: A maximum likelihood gradient of 32.1°C/km, with upper and lower 95% confidence limits of 38.8 and 25.5°C/km, respectively, as illustrated in Figure 3.6. The 95% confidence limit range of paleogeothermal gradient again incorporates the present-day value of 27.2°C/km.

Both results suggest that an interpretation of heating in terms of simple deeper burial with constant basal heat-flow through the Tertiary is a viable explanation of the data. On the other hand, a slightly higher basal heat-flow with a lower amount of additional burial is also possible, while there is not much scope for basal heat flow lower than indicated by the present-day measured temperature data.

3.5 Thermal history synthesis

The thermal history results discussed in the preceding sections allow a general reconstruction of the thermal history within the preserved stratigraphic section at the Borda-1 well site, but lacks detailed knowledge of the time of possible heating and the heating rate prior to any cooling.

Figure 3.7 illustrates a possible reconstructed thermal history for Borda-1, derived from the maximum likelihood value of paleogeothermal gradient for the high heating rate case only, with cooling assumed to have taken place after deposition of the

deposited Nullarbor Formation (*assumed* to have ceased at 2 Ma). The fit of the predicted VR profile for this thermal history is compared with the measured reflectance data in Figure 3.8. The profile shows good agreement with the majority of the VR results throughout the section, as expected, but again it should be borne in mind that other scenarios are possible, but cannot be resolved from the current dataset. The low heating rate case produces a similar set of figures but for simplicity these are not shown.

This possible thermal history allows the reconstruction of the maturation history, as described in Section 3.6, and, together with some simple assumptions, an indirect interpretation of the uplift and erosion history, as discussed in Section 3.7.

3.6 Implications for source rock maturation at the well site

The thermal history results presented above allow a general assessment of the possible maturation history at the Borda-1 well site.

Figure 3.9 shows the variation of vitrinite reflectance with time predicted (using the BasinMod™ implementation of Burnham and Sweeney, 1989) from the possible thermal history derived from the AFTA and VR data illustrated in Figure 3.7.

The plot shows the cessation of maturation in all drilled units at the commencement of cooling *assumed* to have occurred at 2 Ma (as noted above, no timing constraints could be obtained from the limited AFTA data).

The plot also illustrates that the maximum maturity reached by the Potoroo Formation section at TD was only sufficient for early oil generation. The data provide no direct constraint on maturation of possible **Early Cretaceous source rocks** below total depth drilled at this site, but some comments on this issue are made in Section 4.

3.7 Estimates of removed section and reconstructed burial history at the well site

Introduction

The methodology employed in estimating the magnitude of any removed section associated with each heating event is described in Section 1.8. In the following discussion of results from Borda-1, all estimates of erosion refer to the *total* amount of section missing at the level of the top Nullarbor Formation exposed at the sea-bed, ~182 mbKB. All depths on the accompanying Figures 3.10 to 3.13 refer to depth below sea-bed, not the present-day measured depth from KB.

The low heating rate case

Extrapolating the estimated **low heating rate "Tertiary"** paleogeothermal gradient to an assumed paleo-surface temperature of 15°C gives a maximum likelihood estimate of *minus* 276 metres for the *total* amount of **Nullarbor Formation and younger units** which have been removed by uplift and erosion, with no real lower limit, and an upper 95% confidence limit of 220 m, as illustrated in Figure 3.10. Obviously, a negative magnitude of uplift and erosion is not possible, thus the data only provide an effective upper limit for section missing at the top of the preserved Nullarbor Formation of 220 m.

Figure 3.11 provides a crossplot of the allowed range of paleogeothermal gradient and removed section for the Tertiary episode, with the ±95% confidence interval contoured, which enables alternative paired values of uplift and erosion and paleogeothermal gradient to be obtained (see Sections 1.7 and 1.8). This plot shows a burial history with no section removed during the Tertiary corresponds to paleogeothermal gradient values around 27 to 29°C/km (encompassing the present-day value of 27.2°C/km), and is a viable explanation of the paleotemperature data.

The high heating rate case

Extrapolating the estimated **high heating rate "Tertiary"** paleogeothermal gradient to an assumed paleo-surface temperature of 15°C gives a maximum likelihood estimate of 135 metres for the *total* amount of **Nullarbor Formation and younger units** which have been removed by uplift and erosion, with no real lower limit, and an upper 95% confidence limit of 728 m, as illustrated in Figure 3.12. Obviously, a negative magnitude of uplift and erosion is not possible, thus the data only provide an effective upper limit for section missing at the top of the preserved Nullarbor Formation of 728 m.

Figure 3.13 provides a crossplot of the allowed range of paleogeothermal gradient and removed section for the Tertiary episode, with the ±95% confidence interval contoured, which enables alternative paired values of uplift and erosion and paleogeothermal gradient to be obtained (see Sections 1.7 and 1.8). This plot shows a burial history with no section removed during the Tertiary corresponds to paleogeothermal gradient values around 32 to 35°C/km, which are greater than the present-day value of 27.2°C/km, suggesting that cooling through recent decline in basal heat flow is a viable explanation of the data.

Estimates of removed section for Borda-1 are listed in Table iii.

Burial history reconstruction

The data and interpretations presented above make it clear that the thermal history and hence burial history at the Borda-1 well site cannot be assessed independently of significant assumptions concerning the timing of possible heating. On this basis, we illustrate two possible burial history scenarios based on the low and high heating rate cases discussed in the preceding sections.

Figure 3.14 illustrates a possible burial history reconstruction for Borda-1 which is consistent with the thermal history constraints for the *low heating rate case.* In this case, we use a constant paleogeothermal gradient of 27.2°C/km throughout the Late Cretaceous to present-day, with no uplift and erosion (as allowed by the paleotemperature data) and with no significant burial over the last 15 Ma as one method of achieving a low heating rate. This burial history reflects the major aspects of the thermal history.

Figure 3.15 illustrates a second possible burial history reconstruction for Borda-1 which is consistent with the thermal history constraints for the *high heating rate case,* using the maximum likelihood paleogeothermal gradient of 32.1°C/km from the Late Cretaceous, declining to the present-day value at around 2 Ma, and with 135 m uplift and erosion at this time.

Both of these burial histories reflect the major aspects of the thermal history, but it is emphasised that other scenarios are possible for the Tertiary history, particularly involving heating prior to deposition of the Nullarbor Formation due to increased basal heat flow.

Table 3.1: Summary of AFTA data in samples from the Borda-1 well, Duntroon Basin, South Australia (Geotrack Report #569)

Sample number	Average Depth*1 (m)	Present temperature*2 (°C)	Stratigraphic Age (Ma)	Mean track length (µm)	Default mean track length *3 (µm)	Apatite fission track age (Ma)	Default fission track age*3 (Ma)	Measured Ro (max)*4 (%)	Default Ro (max)*5 (%)
GC569-8	2296	72	65-56	No apatite	—	No apatite	—	0.47	0.47
GC569-13	2752	85	74-65	10.01±1.12	12.1	65.5±23.3	60	0.56	0.51

*1 All depths quoted are total vertical depth (TVD) with respect to KB.

*2 See Appendix A for a discussion of present temperature estimation.

*3 AFTA values predicted from the "Default Thermal History" (Section 1.6); i.e., assuming that each sample is now at its maximum temperature since deposition. The values refer only to tracks formed after deposition. Samples may also contain tracks inherited from sediment provenance areas. Calculations for the ranges given refer to actual measured compositions of apatites analysed within a particular sample, which is discussed in Appendix A.

*4 Vitrinite reflectance values at the level of the AFTA sample either measured, or estimated, based on the VR determinations in the entire well where interpolation is possible.

*5 Vitrinite reflectance values predicted from the "Default Thermal History" (see point *3), using the Burnham and Sweeney (1989) algorithm - see Appendices C and D for discussion.

Table 3.2: Summary of thermal history interpretation of AFTA and VR data in samples from the Borda-1 well, Duntroon Basin, South Australia (Geotrack Report #569)

Sample number	Do AFTA data require revision of present temperature ?	Evidence of higher temperatures in the past from length data?	Evidence of higher temperatures in the past from fission track age data?	Evidence of higher temperatures in the past from vitrinite reflectance data?	Conclusion
569-8 2296 m	No data 72°C	No apatite	No apatite	Yes, equivocal [Measured vitrinite reflectance is close to, or greater than, that predicted by the Default History, depending on the true heating rate during the Late Tertiary]	Sample may have been hotter in the past, but resolution of this depends on a more detailed knowledge of the Late Tertiary stratigraphy (as this controls heating rate) than is currently available.
569-13 2752 m	No 85°C	No, equivocal [Only a few track length measured, but imprecise mean track length is similar to that predicted from Default History.)	No, equivocal [Fission track age of a single grain overlaps the age range predicted by the Default History.]	Yes, equivocal [Measured vitrinite reflectance is close to, or greater than, that predicted by the Default History, depending on the true heating rate during the Late Tertiary]	Sample may have been hotter in the past, but resolution of this depends on a more detailed knowledge of the Late Tertiary stratigraphy (as this controls heating rate) than is currently available.

Note: Interpretation of AFTA data is based on comparison of measured AFTA parameters with values predicted from the "Default Thermal History" (Section 1.6); i.e., assuming that each sample is now at its maximum temperature since deposition. The predicted values for each sample are summarised in Table 3.1, and refer only to tracks formed after deposition. Samples may also contain tracks inherited from sediment provenance areas, which has been allowed for in interpreting the data.

Table 3.3: Estimates of timing and magnitude of elevated paleotemperatures from AFTA and VR data in samples from the Borda-1 well, Duntroon Basin, South Australia (Geotrack Report #569)

Sample number	Stratigraphic Age	Present temperature	Early episode (74 to 0 Ma)*1 Maximum paleo-temperature	Early episode (74 to 0 Ma)*1 Onset of cooling	Cooling History Peak paleo-temperature	Cooling History Style of cooling	Comments
GC	(Ma)	(°C)	(°C)	(Ma)	(°C)		
569-8 2296 m	65 to 56 Paleocene Lower Pidinga	72	No apatite VR ~73 to 89		No apatite		VR data in the Lower Pidinga Fm indicate maximum paleotemperatures between ~73 and 89°C for a range of plausible heating rates (lower heating rate equates with lower maximum paleotemperature). At the lower end of the range (consistent with a low burial rate over the last 10 Ma, for example) the maximum paleotemperature is indistinguishable from the present temperature, suggesting little or no, post-Paleocene cooling. At the higher end of the range (consistent with high burial rate over the last 10 Ma), the maximum paleotemperature estimate suggests up to ~17°C of post-Paleocene cooling. A lack of AFTA data preclude a more precise estimate of timing.
569-13 2752 m	74 to 65 Maastrichtian Potoroo	85	<130 AFTA VR ~82 to 104	After deposition	No information		The poor apatite yield precludes detailed AFTA analysis. At face value, the data suggests maximum post-Maastrichtian temperatures did not exceed ~130°C (for a range of heating rates). VR data within the Potoroo Fm indicate maximum paleotemperatures between ~82 and 104°C for a range of heating rates. At the lower end of the range, the maximum paleotemperature is indistinguishable from the present temperature, suggesting little or no post-Paleocene cooling. At the higher end of the range, the maximum paleotemperature estimate suggests up to ~19°C of post-Paleocene cooling. If maximum paleotemperatures are at the high end of the range, the trend of the VR data throughout the well suggests that cooling is due to decline in the paleogeothermal gradient to the present-day value (see text).

*1 Based on the stratigraphic age of the samples that show evidence of elevated paleotemperatures in associated VR data.

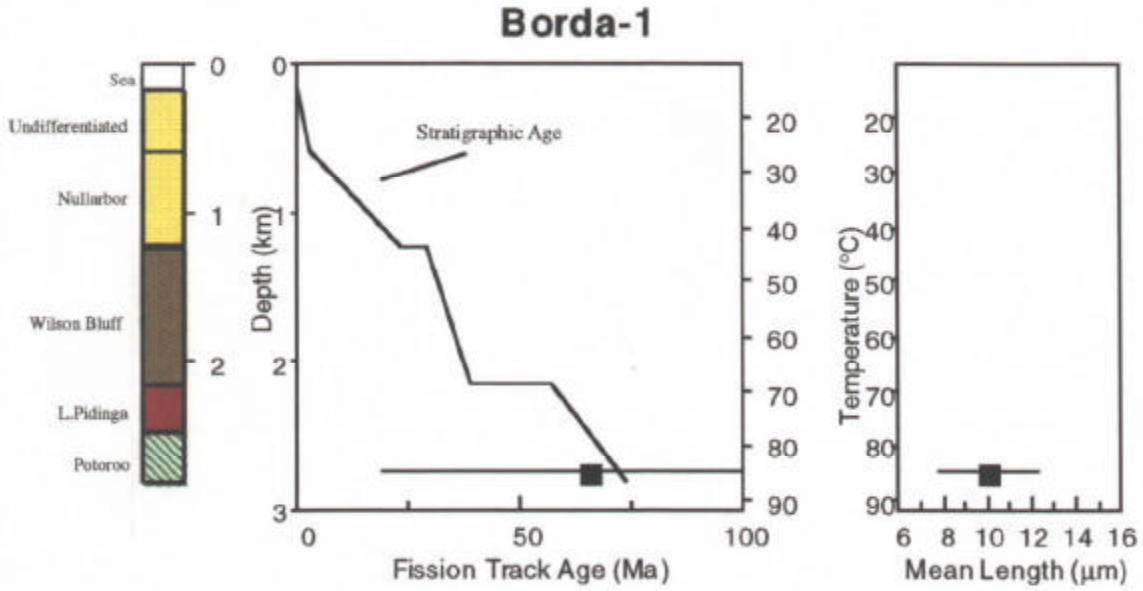

Figure 3.1: AFTA parameters plotted against sample depth and present temperature for samples from **well Borda-1, Duntroon Basin.** The variation of stratigraphic age with depth is also shown, as the solid line in the central panel.

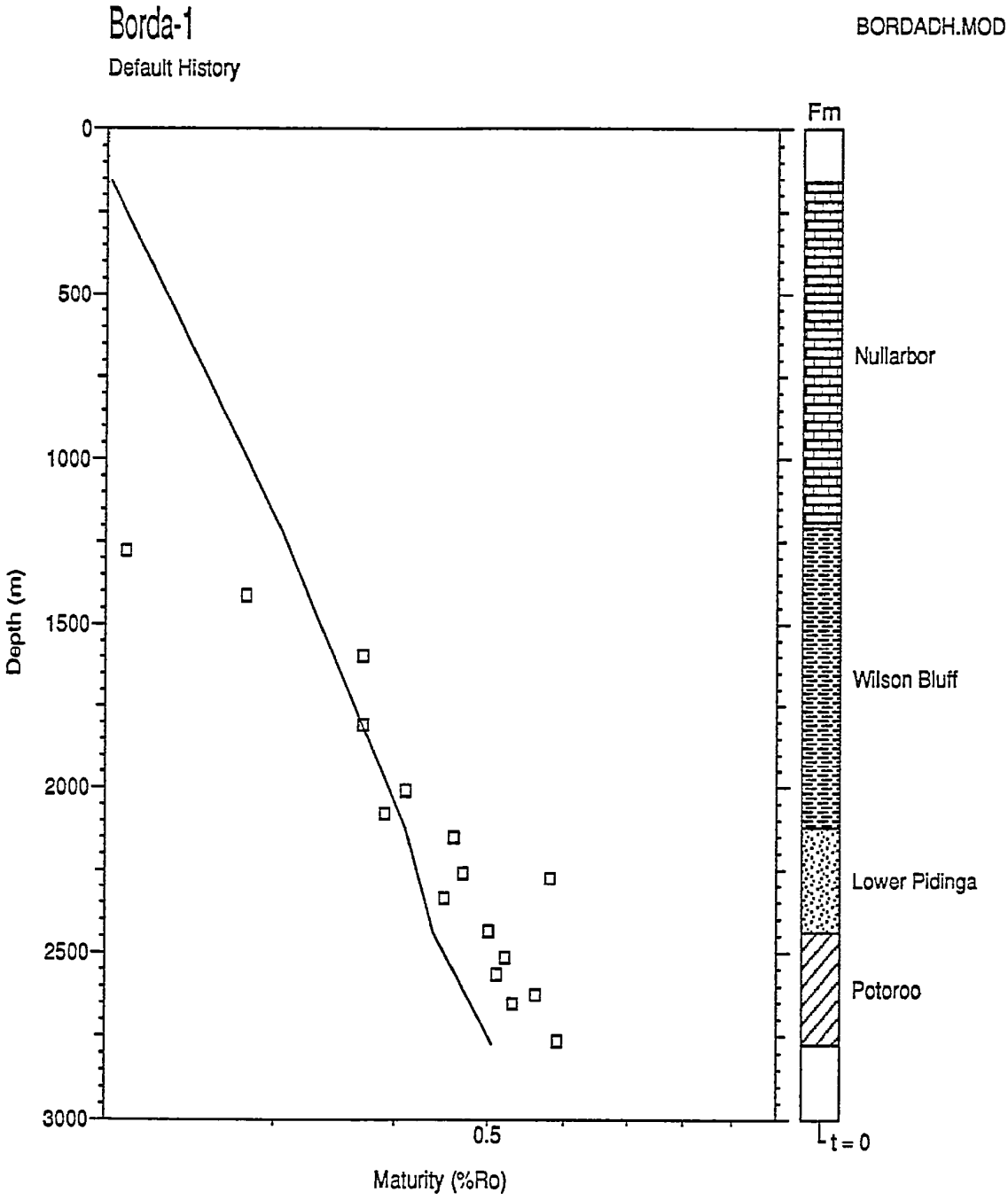

Figure 3.2: Vitrinite reflectance data in the **Borda-1 well, Duntroon Basin**, plotted against depth. The solid line shows the VR profile predicted by the "Default History" (Section 1.6), i.e., the profile expected if samples throughout the section are currently at their maximum temperature since deposition. The measured data gradually move from close to, to just above, the predicted profile with increasing depth, suggesting that the deeper section has been hotter in the past. See text for details.

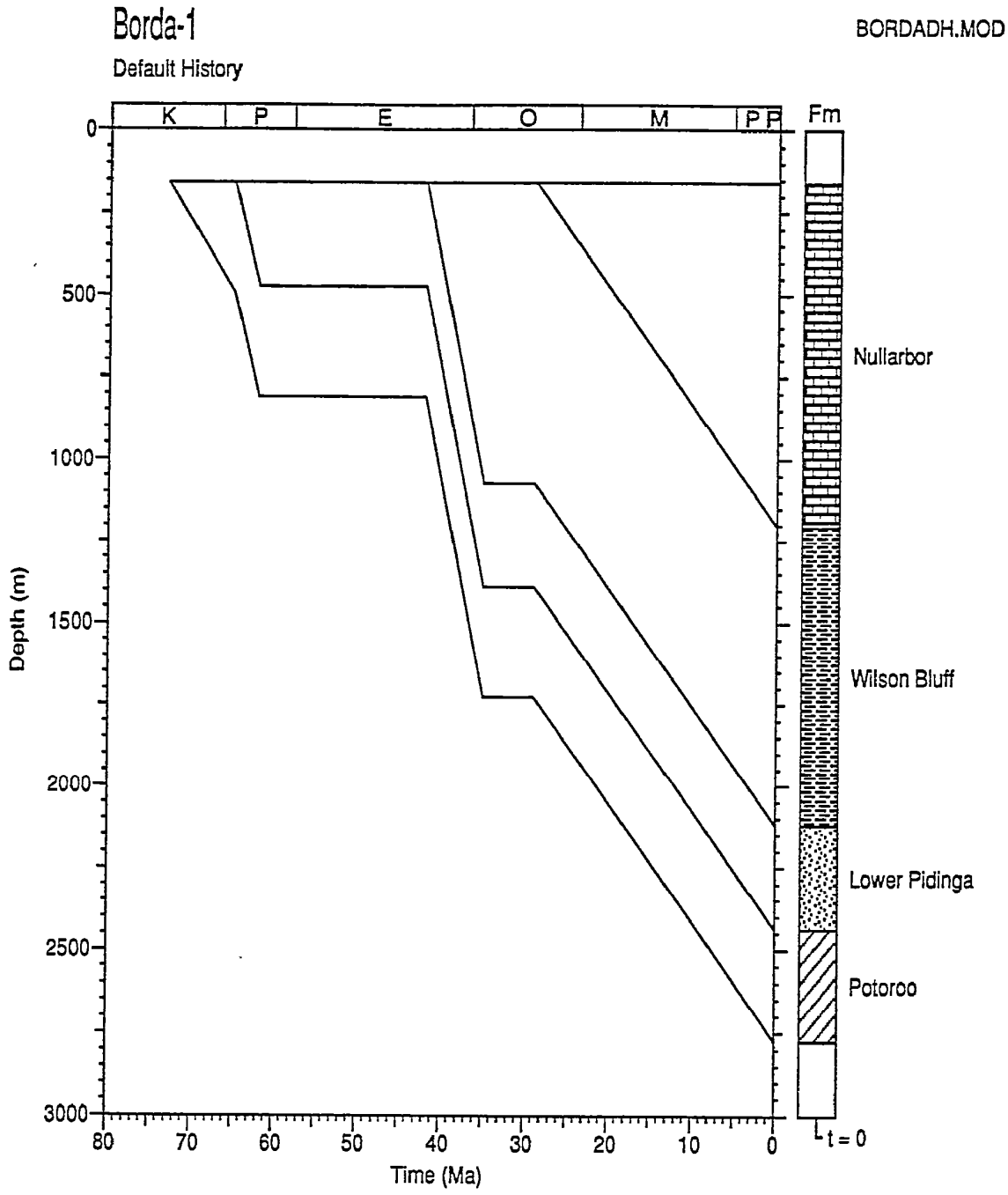

Figure 3.3: Default Burial History for the **Borda-1 well, Duntroon Basin**, derived from the preserved section, which, combined with the present-day linear geothermal gradient of 27.2°C/km (Appendix A), is used in predicting the VR profile shown in Figure 3.2.

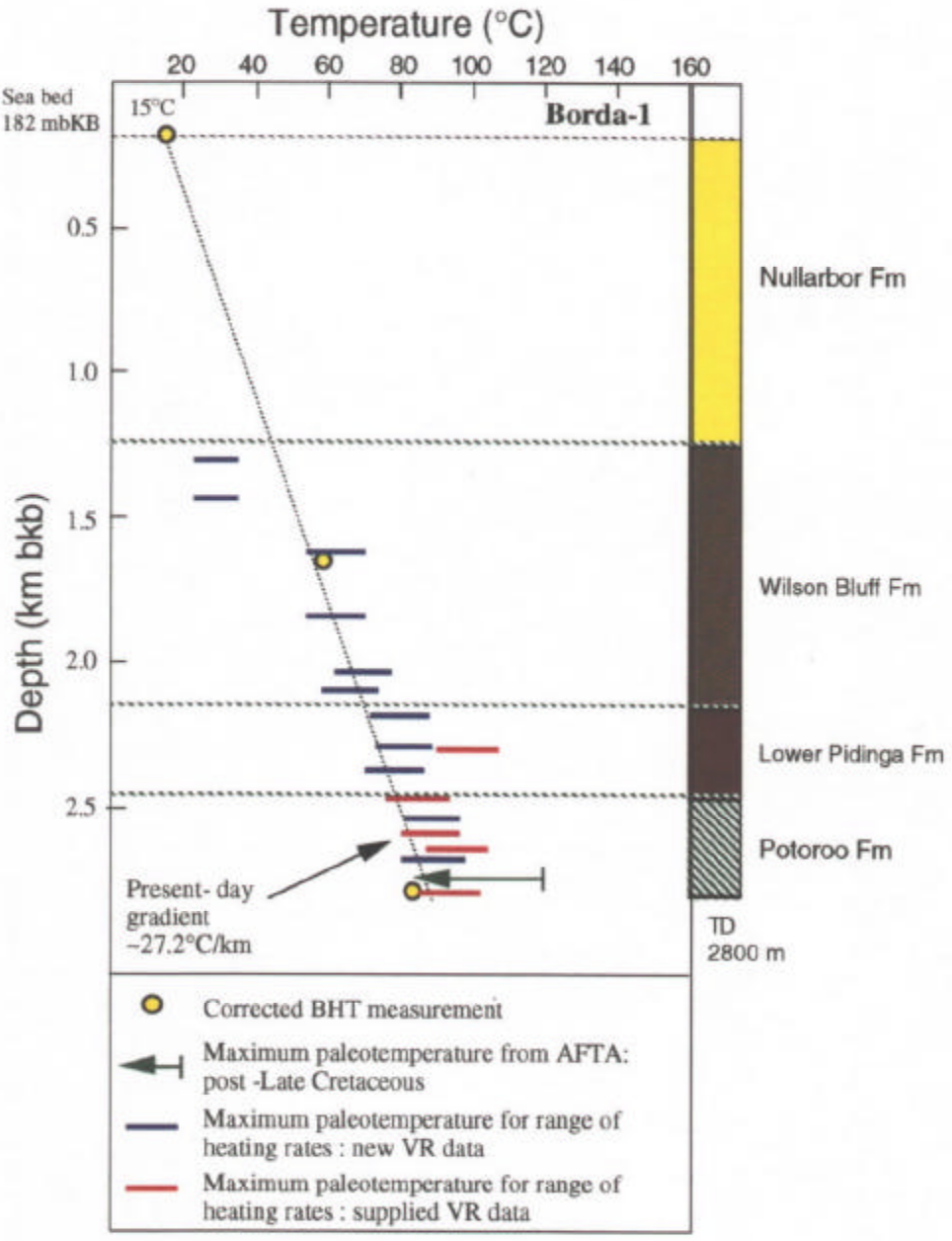

Figure 3.4: Plot of paleotemperatures for a range of heating rates derived from AFTA and VR data in the **Borda-1 well, Duntroon Basin**, against sample depth and the estimated present temperature profile for this well, including corrected BHT values (see Appendix A). The paleotemperature estimates give tentative evidence of the deeper part of the sampled section having cooled from elevated paleotemperatures after deposition - see text for details.

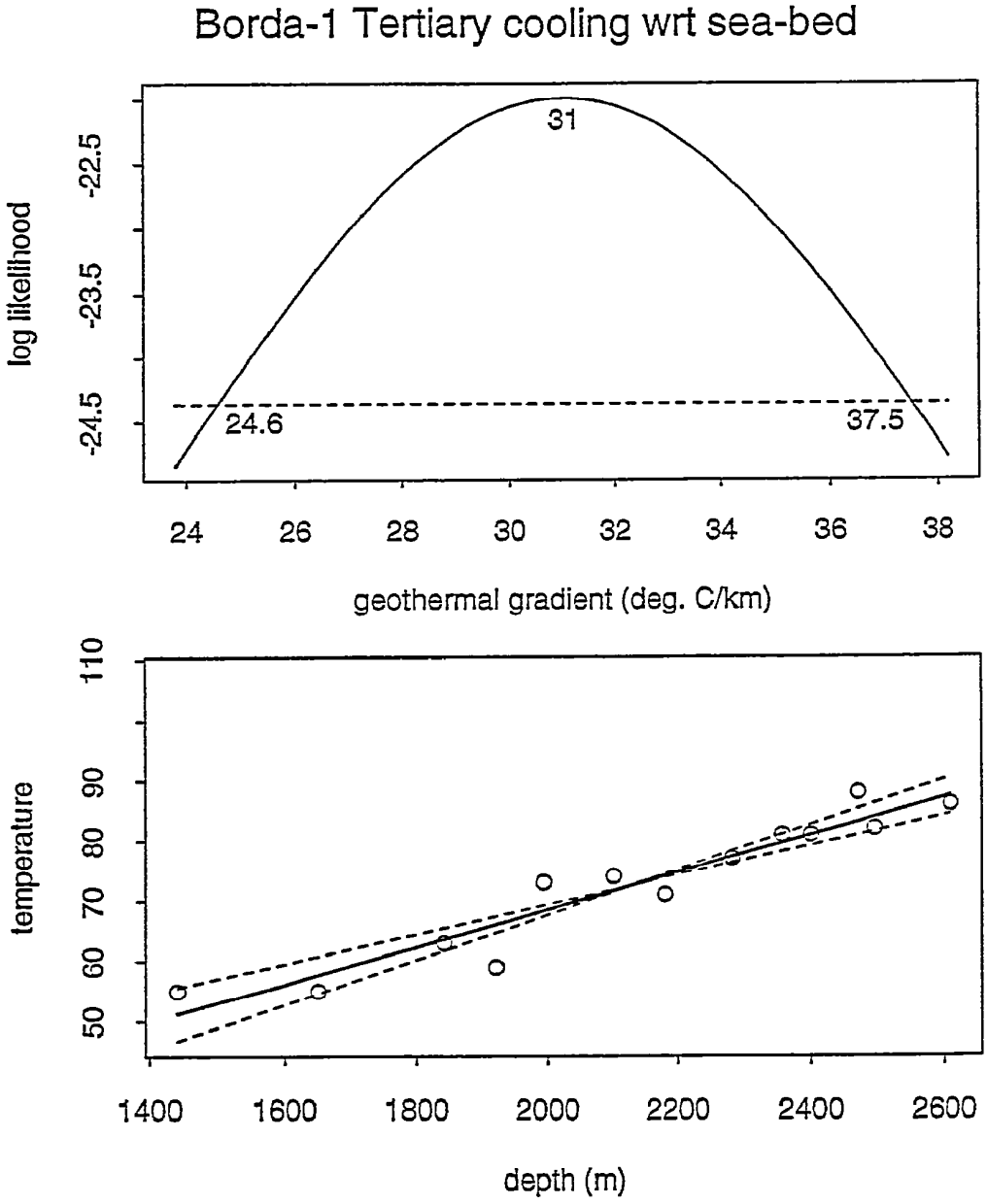

Figure 3.5: Upper: Maximum likelihood profile of linear paleogeothermal gradient fitted to the *low heating rate* **Tertiary** paleotemperature estimates from AFTA and VR data in the **Borda-1 well**. The profile shows good quadratic behaviour, defining upper and lower 95% confidence limits of 37.5 and 24.6°C/km and a best-fit value of 31.0°C/km. The methodology employed in deriving this profile is outlined in Appendix C.

Lower: Maximum paleotemperature estimates from AFTA and VR data in the **Borda-1 well**, with fitted profile (solid line) and lines (dashed) representing upper and lower 95% confidence limits.

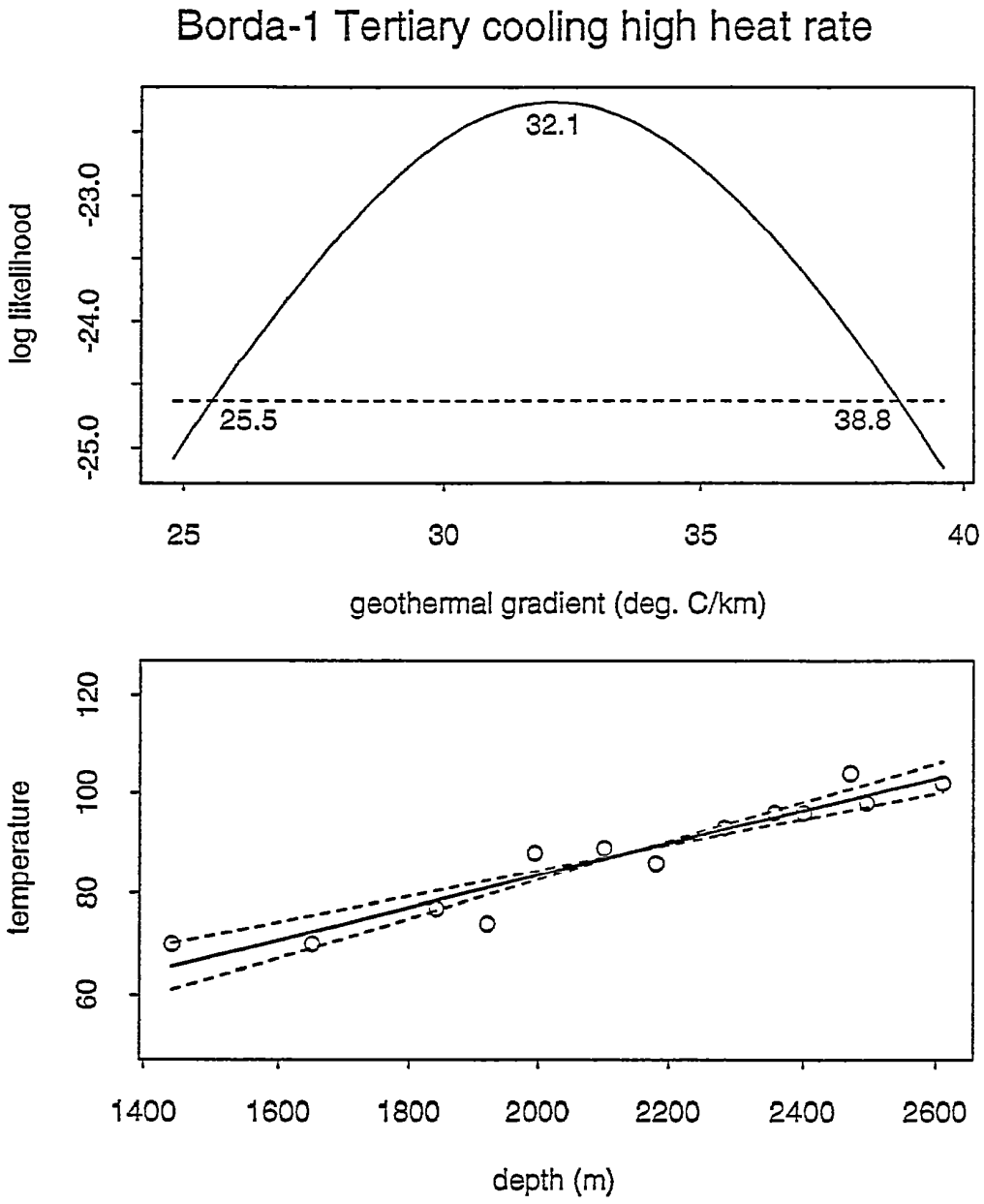

Figure 3.6: Upper: Maximum likelihood profile of linear paleogeothermal gradient fitted to the *high heating rate* **Tertiary** paleotemperature estimates from AFTA and VR data in the **Borda-1 well.** The profile shows good quadratic behaviour, defining upper and lower 95% confidence limits of 38.8 and 25.5°C/km and a best-fit value of 32.1°C/km. The methodology employed in deriving this profile is outlined in Appendix C.

Lower: Maximum paleotemperature estimates from AFTA and VR data in the **Borda-1 well,** with fitted profile (solid line) and lines (dashed) representing upper and lower 95% confidence limits.

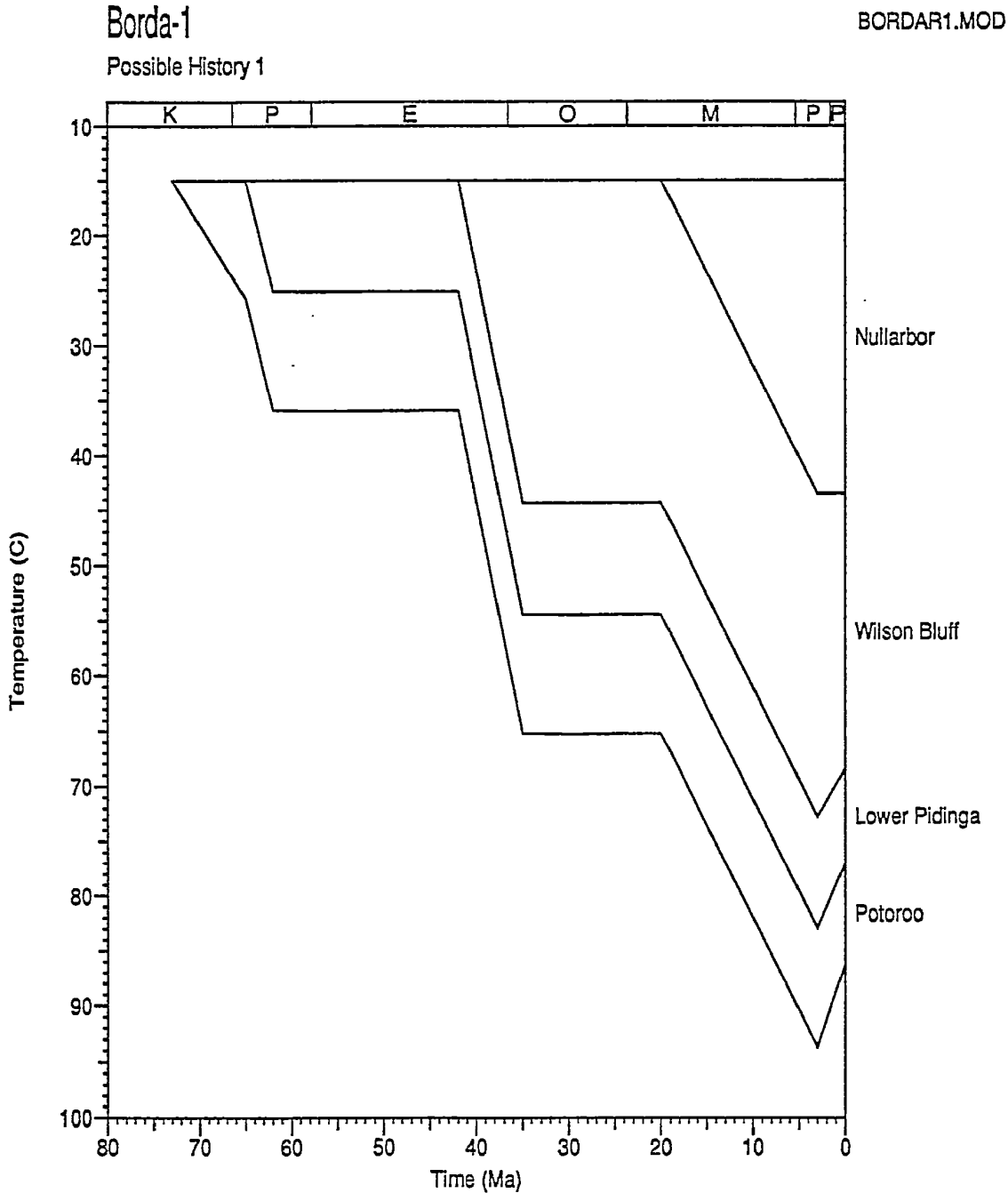

Figure 3.7: Possible thermal history reconstruction derived from the paleotemperature data in the **Borda-1 well, Duntroon Basin**, using the maximum likelihood paleogeothermal gradient of 32.1°C/km for the *high heating rate* case throughout the Tertiary to 2 Ma, then decreasing to the present-day value of 27.2°C/km. Note that although and event is shown at 2 Ma, the AFTA data provide no direct constraints on when the tentatively identified cooling may have occurred - see text.

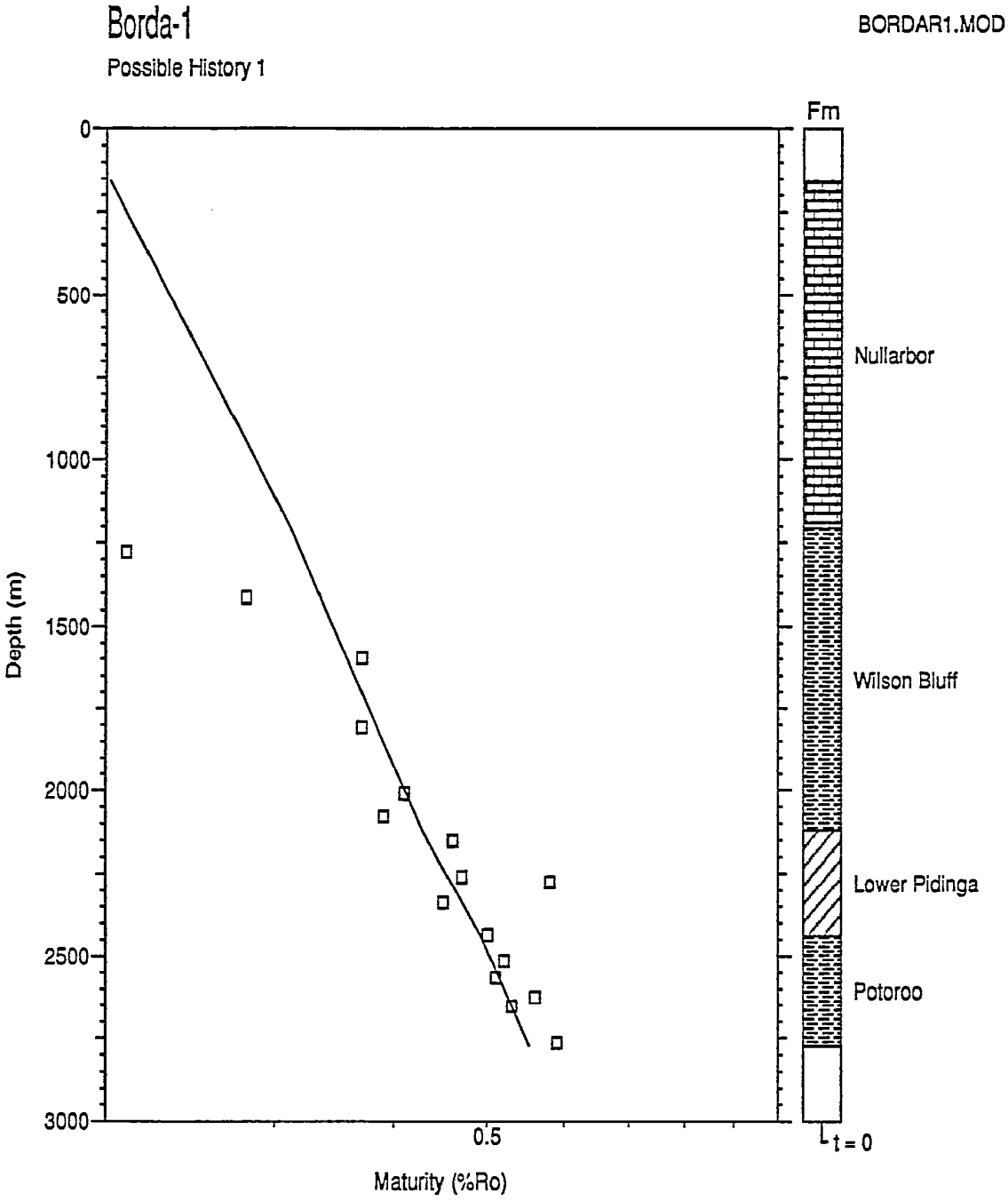

Figure 3.8: Measured vitrinite reflectance data in samples from the **Borda-1 well, Duntroon Basin**, and the VR profile predicted by the reconstructed thermal history shown in Figure 3.7. Most data show good agreement with the predicted profile, as expected.

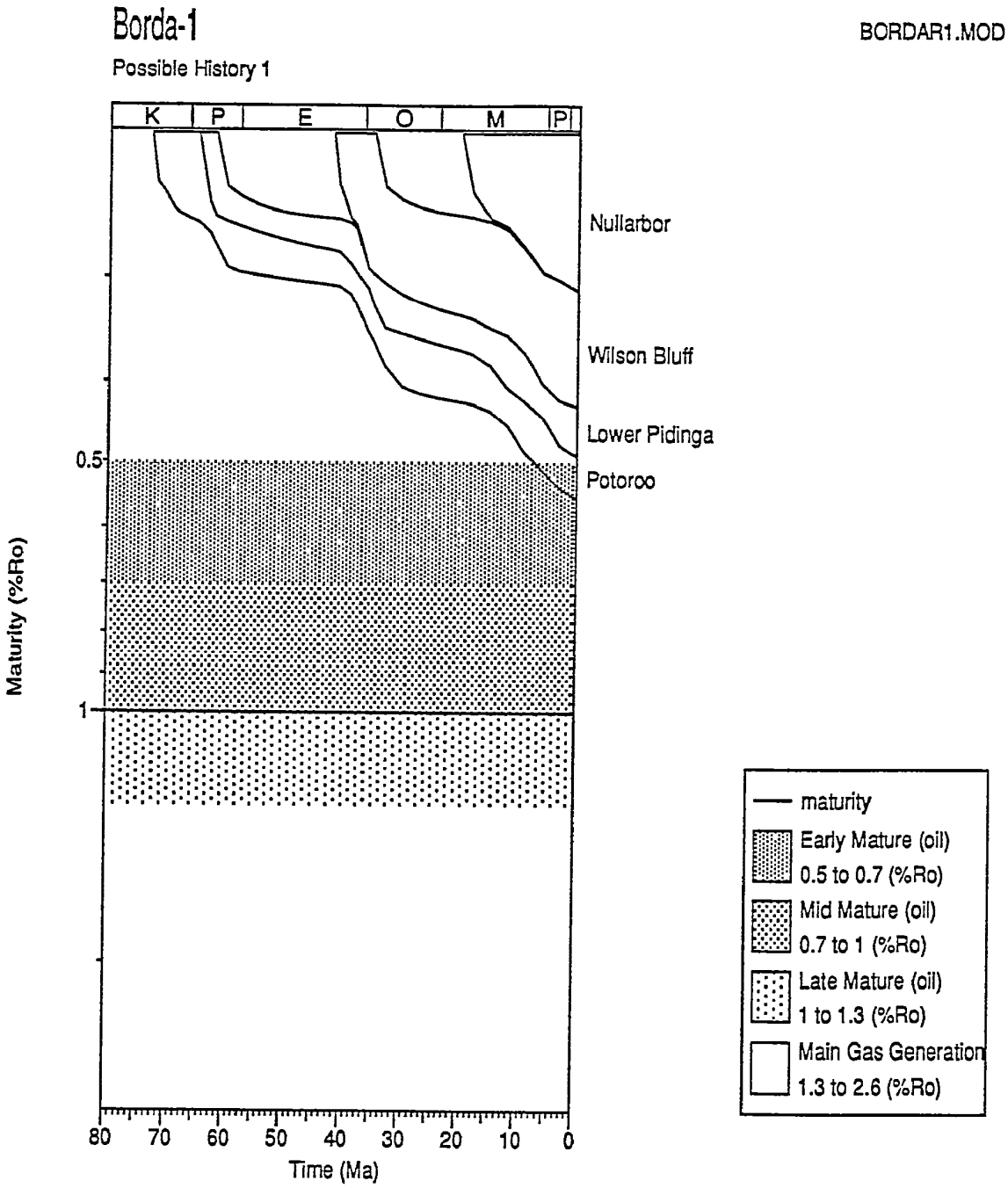

Figure 3.9: Possible development of maturity with time in the **Borda-1 well, Duntroon Basin.** Only low maturity has been reached by any of the drilled section, with maturation stopping at 2 Ma, coincident with the *assumed* time of cooling. More data are needed for this well before firm thermal history conclusion can be drawn - see text for details.

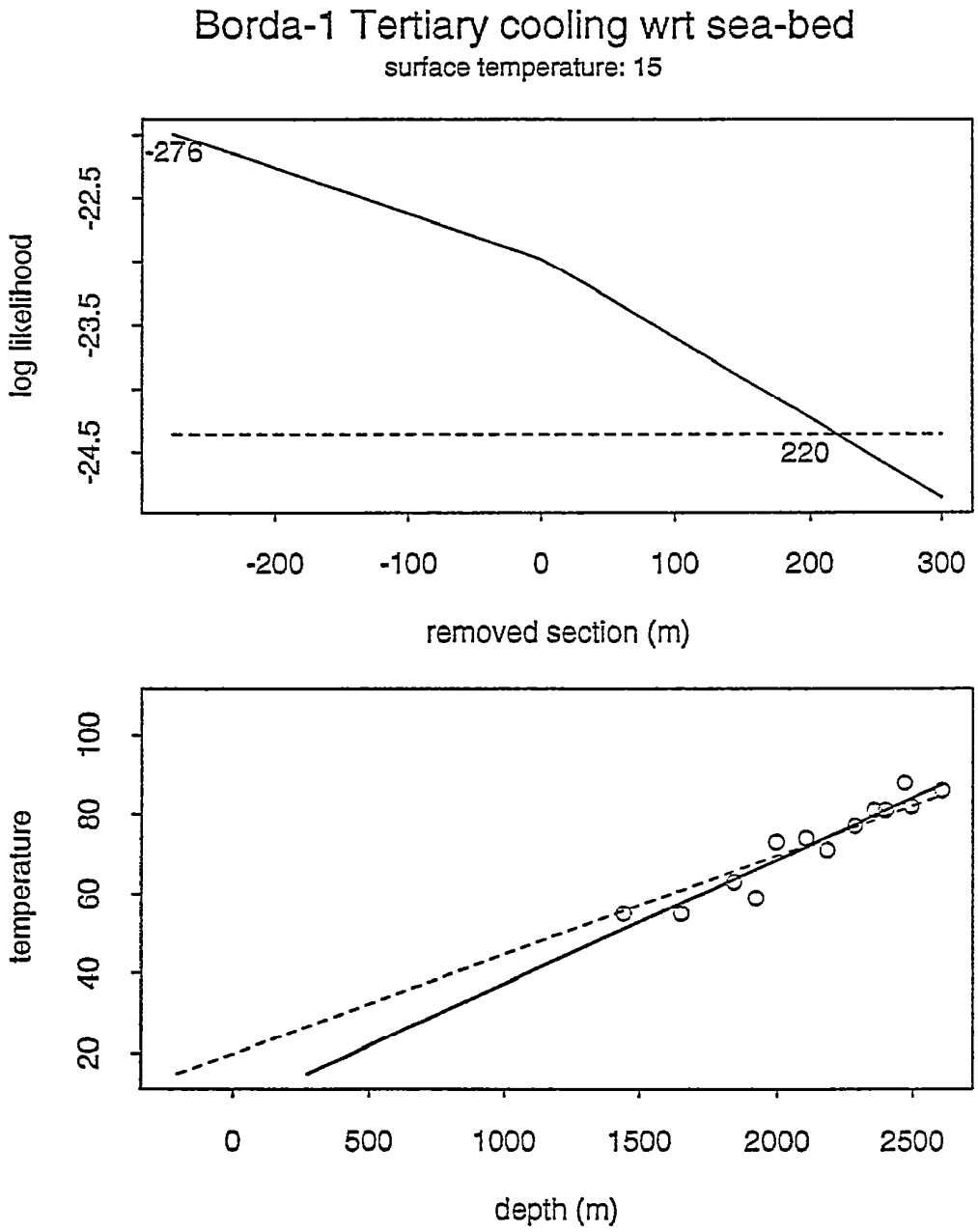

Figure 3.10: Upper: Maximum likelihood profile of estimated section removed by uplift and erosion since the **Tertiary** in the **Borda-1 well** for the *low heating rate* case derived from the paleogeothermal gradient shown in Figure 3.5, assuming a paleo-surface temperature of 15°C. The profile gives an upper 95% confidence limit of 220 metres, and an unreal best-fit value of -276 metres. The methodology employed in deriving this profile is outlined in Appendix C.

Lower: Maximum paleotemperature estimates from AFTA and VR data in the **Borda-1 well**, with fitted profile (solid line) and lines (dashed) representing upper and lower 95% confidence limits, extrapolated to the assumed paleo-surface temperature of 15°C.

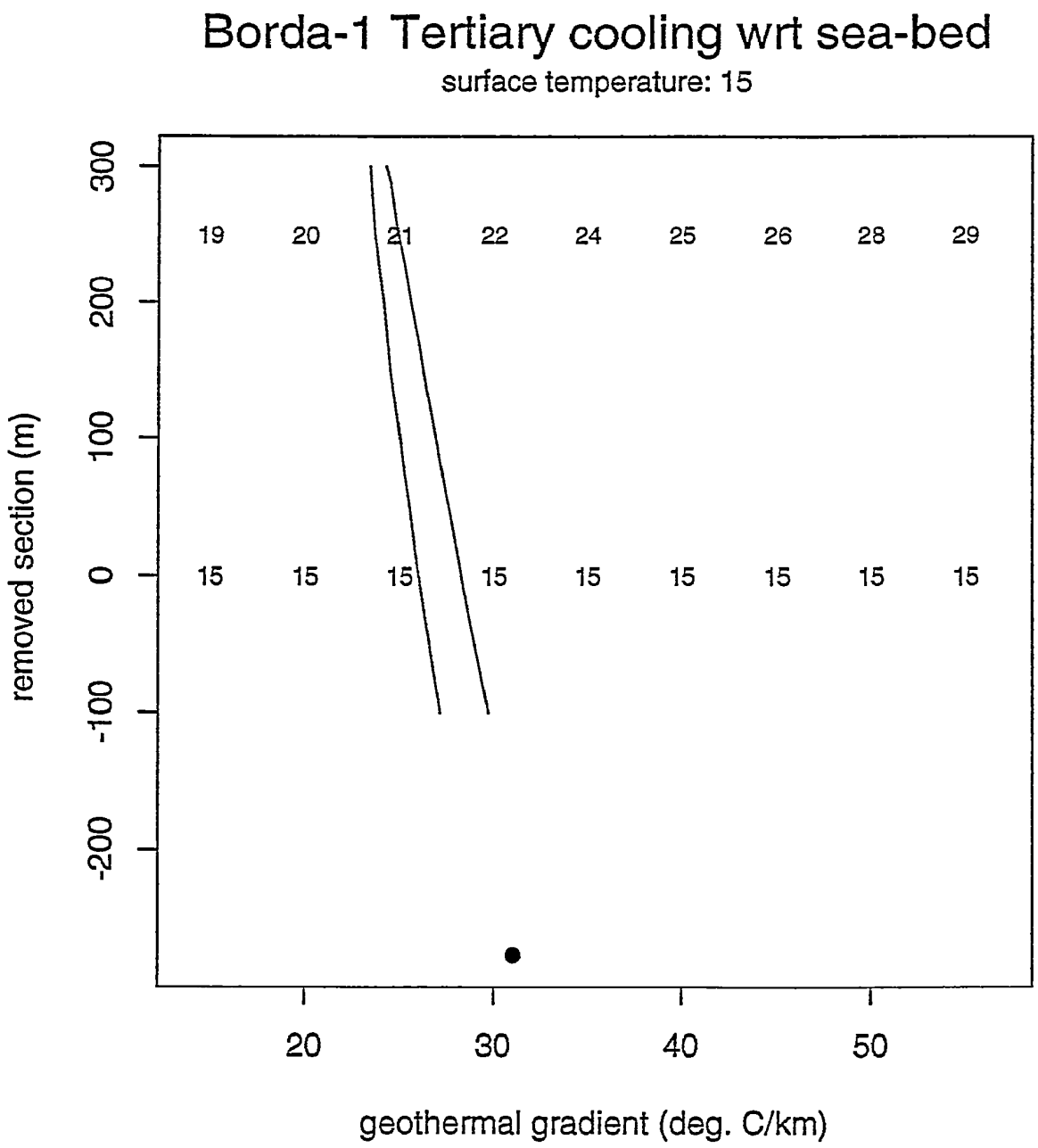

Figure 3.11: Crossplot of removed section against the *low heating rate* case paleogeothermal gradient for the **Tertiary**, showing the range of values (within the contoured region) compatible with the maximum paleotemperatures derived from AFTA and VR in the **Borda-1 well**, at 95% confidence level. The numbers within the plot are paleotemperatures at the present sea-bed corresponding to the specified values of removed section and paleo-gradient.

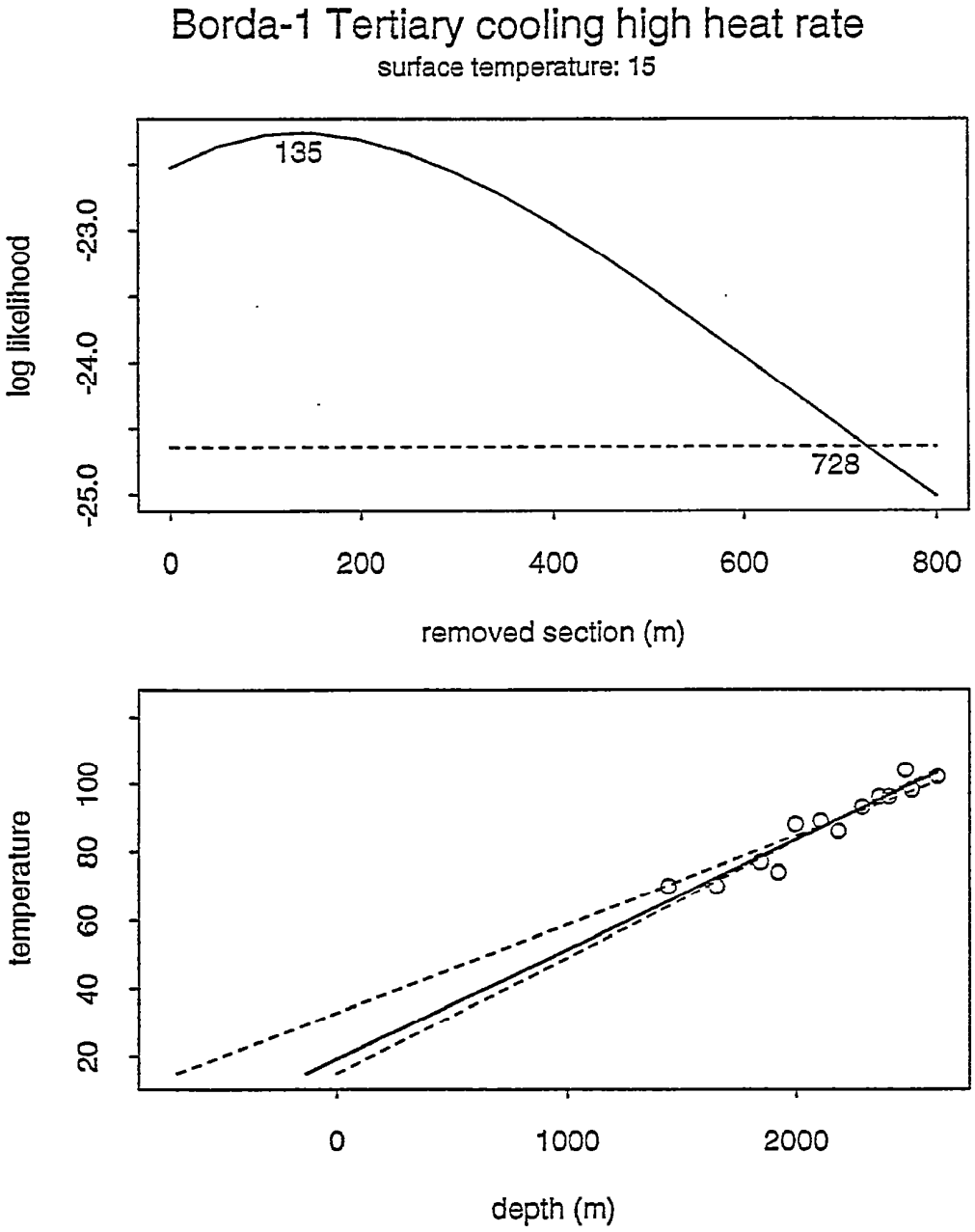

Figure 3.12: Upper: Maximum likelihood profile of estimated section removed by uplift and erosion since the **Tertiary** in the **Borda-1 well** for the *high heating rate* case derived from the paleogeothermal gradient shown in Figure 3.6, assuming a paleo-surface temperature of 15°C. The profile gives an upper 95% confidence limit of 728 metres and a best-fit value of 135 metres. The methodology employed in deriving this profile is outlined in Appendix C.

Lower: Maximum paleotemperature estimates from AFTA and VR data in the **Borda-1 well**, with fitted profile (solid line) and lines (dashed) representing upper and lower 95% confidence limits, extrapolated to the assumed paleo-surface temperature of 15°C.

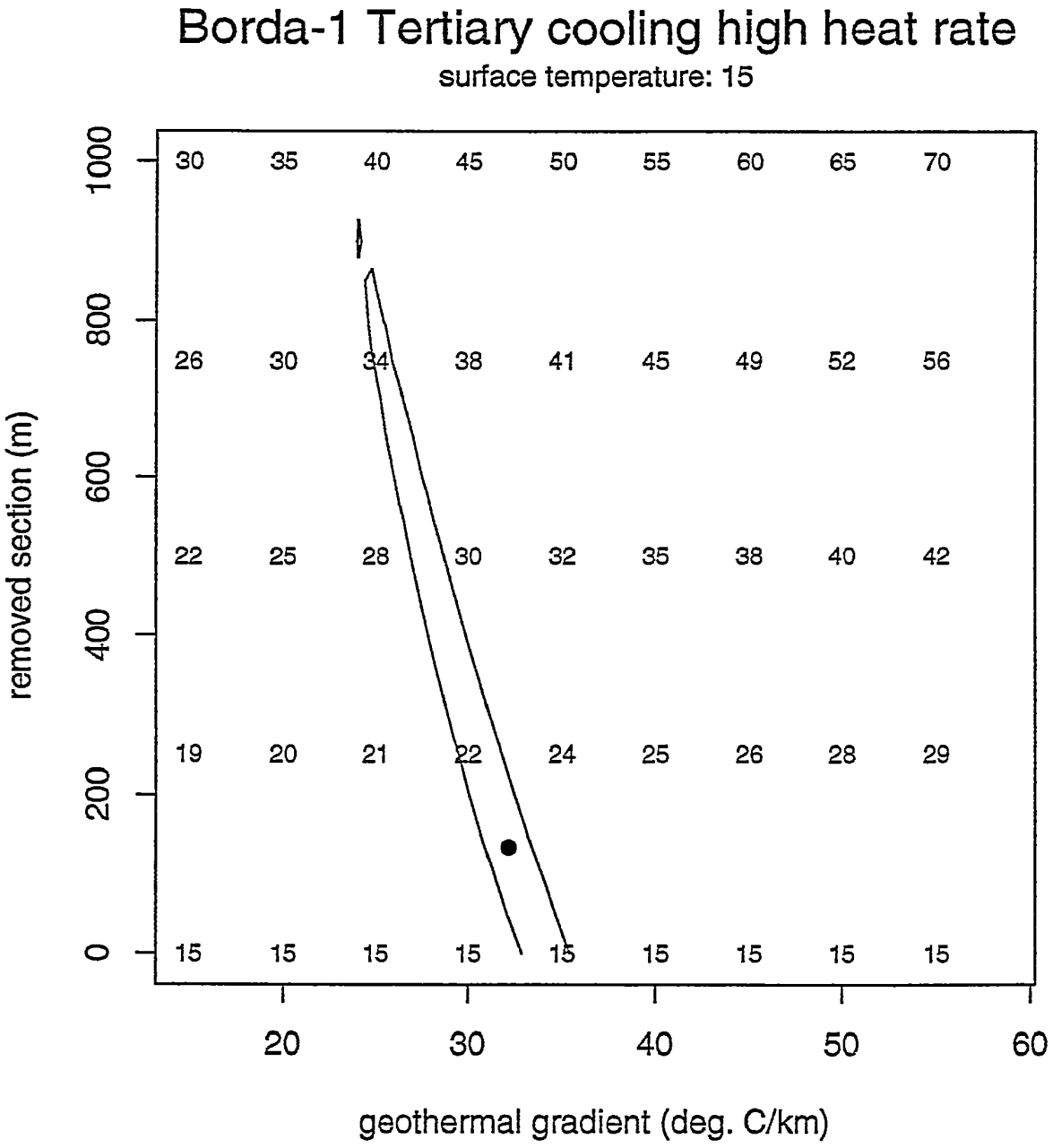

Figure 3.13: Crossplot of removed section against the *high heating rate* case paleogeothermal gradient for the **Tertiary**, showing the range of values (within the contoured region) compatible with the maximum paleotemperatures derived from AFTA data in the **Borda-1 well**, at 95% confidence level. The numbers within the plot are paleotemperatures at the present sea-bed corresponding to the specified values of removed section and paleo-gradient.

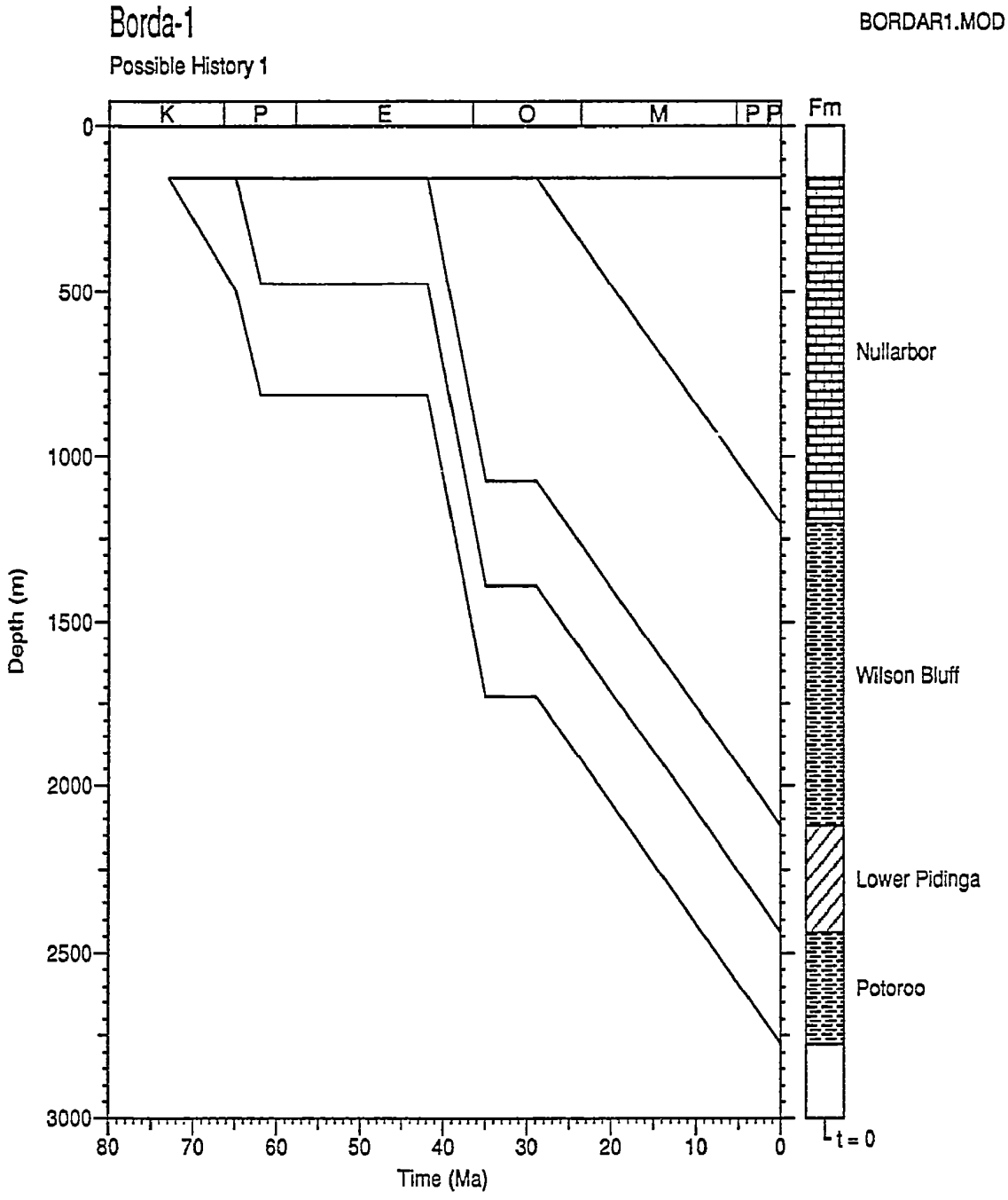

Figure 3.14: Possible burial history reconstructed from the paleotemperature data in the **Borda-1 well, Duntroon Basin**, for the *low heating rate* case, using a constant thermal gradient of 27.2°C/km from the Late Cretaceous to the present-day and no uplift and erosion (all parameter values within the ranges allowed by the thermal history data - see text for details).

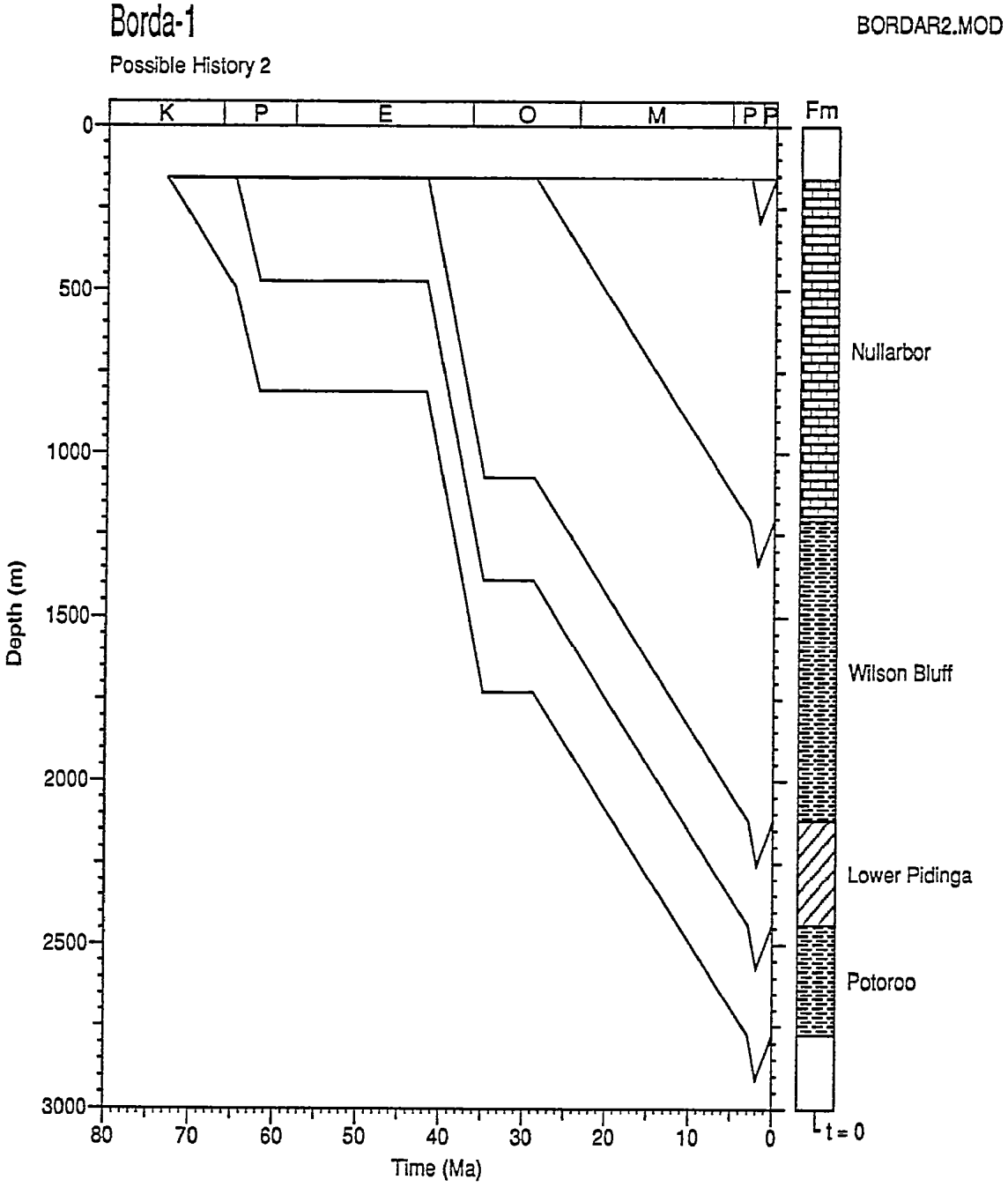

Figure 3.15: Alternative burial history reconstructed from the paleotemperature data in the **Borda-1 well, Duntroon Basin**, for the *high heating rate* case, using the maximum likelihood value of paleogeothermal gradient of 32.1°C/km from the Late Cretaceous until 2 Ma, then declining to the present day level of 27.2°C/km, with 135 m of associated uplift and erosion (all parameter values within the ranges allowed by the thermal history data - see text for details).

4. Concluding remarks on the geological history of the Duntroon Basin

4.1 Comments on Mid-Cretaceous heating - elevated heat flow

The significantly elevated Mid-Cretaceous paleogeothermal gradient identified in Vivonne-1 (a best-fit value of 60°C/km compared with a present-day value of ~30°C/km) implies highly elevated heat-flow during this period. Similarly elevated heat flow during this period has been identified in the Otway Basin much further to the east (Duddy, 1994), which contains a very similar sedimentary sequence to that found in the Duntroon Basin.

This elevated heat flow was operating until the Mid-Cretaceous, and is interpreted to reflect a fundamental regional feature of southern Australian margin basins, which was associated with the rifting mechanisms related to their formation. As such, highly elevated heat flow needs to be considered in assessing hydrocarbon maturation in these rift basins, even at the present day in locations where subsequent burial by thick Late Cretaceous and Tertiary sections has masked any direct evidence for it.

The major consequence of Early Cretaceous elevated heat-flow for hydrocarbon generation throughout these basins is that a large part of the potential Jurassic to Early Cretaceous source rock-bearing sequence will have generated much of its possible hydrocarbon yield prior to the Mid-Cretaceous, significantly decreasing volumes available for generation in the structurally more favourable Tertiary to Recent time period.

To illustrate this, Figures 4.1 and 4.2, show reconstructed thermal and burial histories for a hypothetical site similar to Borda-1, with a 2800 m Late Cretaceous to Tertiary section overlying a 3000 m Late Jurassic-Early Cretaceous sequence and with the regional Early Cretaceous thermal history derived from Vivonne-1. The paleogeothermal gradient of 60°C/km maintained until the Mid-Cretaceous results in maximum paleotemperatures at ~95 Ma, while maximum burial is in the Late Tertiary.

This constrained regional history was used to reconstruct the maturation-time plot shown in Figure 4.3. This plot shows that the notional Jurassic and Lower Borda Formations reached maximum maturity in range ~1 to 3% Ro(max) prior to cooling at 95 Ma, and would have therefore generated most of their oil and be well into dry gas generation by this time. This section has not generated further hydrocarbons during the subsequent Late Cretaceous to Tertiary burial phase because the associated burial heating was not sufficient to overcome the thermal effects of the high paleogeothermal gradient in the Mid-Cretaceous.

The plot also shows that the Upper Borda Formation (notionally divided into units A and B for clarity) reached maturities of ~0.5 to 1% prior to the 95 Ma cooling event, and remained at these levels until progressive burial/heating in the Tertiary allowed maturation to recommence, firstly in the shallowest Borda Formation in the Late Eocene and just starting at the base of the Upper Borda (B) in the last few million years. This "top-down-type" maturation history is characteristic of Australia's southern margin basins and is a major factor effecting hydrocarbon prospectivity.

4.2 Comments on provenance of the Upper and Lower Borda Formation

The chlorine content of detrital apatites in a sediment can provide unique information on the provenance (unpublished Geotrack data - see Appendix C). A link between the provenance of apatites in the Early Cretaceous Otway Group and chlorine content of contained apatite has been established for more than a decade. Sediments derived from contemporaneous volcanogenic sources show a wide range of Cl abundance in the derived apatites due to derivation from a range of igneous rock types, while sediment derived from a granitic basement-type provenance have a very narrow range of Cl-contents. Typical "volcanogenic-type" distributions based on a large number of samples from the volcanogenic Otway Group are shown in Figure C.4.c.

Distributions of Cl in apatite from the seven AFTA samples from Vivonne-1 and Borda-1 analysed in this study are given in Figures A.2 a and b (Appendix A).

The narrow Cl distributions in the Pidinga Formation sample (GC569-16, Fig. A.2a) are characteristic of basement derived apatites, consistent with the fission track ages older than stratigraphic ages (Fig. B.5a). The data from the Potoroo Formation sample (GC569-13, Fig. B.5b) are too limited for interpretation.

The broad chlorine distributions measured in the five Barremian-to-Aptian **Borda Formation** samples from Vivonne-1 provide clear evidence of derivation of detritus from a volcanogenic provenance (Fig. A.2a). These data suggest derivation of the bulk of the detritus in the preserved Early Cretaceous section from a similar, and coeval, contemporaneous volcanogenic provenance to that responsible for the Otway and Strzelecki Group sediments deposited further east.

The apatite age data in the least heated Borda Formation sample (GC569-28) support the interpretation of a dominant contemporaneous volcanogenic source, as the fission track ages for the majority of grains (especially those with Cl > 0.4 wt% typical of volcanogenic sources) are indistinguishable from the Aptian stratigraphic age (Figure B.5a). Only the fission track ages of a small number of Cl-poor grains are greater

than the stratigraphic age, showing they are derived from an older basement provenance. A small number of these older basement-derived Cl-poor grains are also found in Borda Formation samples GC569-29, 23 and 25 (although those in the latter have been attributed to cavings - see text), but again all Borda Formation samples are dominated by the Cl-rich volcanogenic grains (Figure B.5a).

Thus, massive explosive volcanism was present in the vicinity of the Duntroon Basin, at least from the Barremian to the Aptian, as shown by the stratigraphic ages of five samples analysed from Vivonne-1.

It is interesting to note that few sandy intervals were picked on the Vivonne-1 logs in the Borda Formation, and this was initially thought to be an impediment to application of AFTA which requires sand-sized detrital apatite. However, collection of composite cuttings samples at regular intervals through the Upper and Lower Borda Formations, without regard to picked sands, resulted in obtaining numerous sand-sized apatite suitable for AFTA (Table A.1). The lack of log-identified sands probably results from the pervasive diagenetic alteration involving various chlorite and zeolite secondary minerals, as well as enhanced compaction, which affects volcanogenic sandstones even at moderate burial depths (Duddy, 1983), producing low-resistivity sandstones.

4.3 Comments on Tertiary heating - hot fluid flow

There is only limited evidence of a Tertiary heating episode in the Vivonne-1 and Borda-1 wells. In Vivonne-1, AFTA data in a single sample (GC569-30) *require* Tertiary paleotemperatures higher than present temperatures, which might be due to local transient thermal effects, rather than a mechanism which affected the entire section. Lateral flow of heated fluids through suitable sandy sections could cause such transient thermal anomalies.

In the Borda-1 well, the VR data would allow maximum paleotemperatures higher than present temperatures at any time since the Maastrichtian (as controlled by the stratigraphic age of the samples showing the largest thermal anomalies. Cooling in the relatively recent past is the simplest way of achieving the measured VR levels as discussed above, but it should be borne in mind that transient lateral flow of heated fluids in an aquifer section in the vicinity of the Potoroo Formation section around TD could also produce similar maturity profiles.

4.4 Alternative interpretation of the Borda-1 paleotemperature profile

The corrected BHT data in the Borda-1 well (Appendix A) give an estimated present-day geothermal gradient of 27.2°C/km. If this gradient were underestimated by only 10% or so, this would be sufficient to explain the VR data with maximum paleotemperatures at the present day without the need for a Tertiary heating episode. Additional AFTA data from Borda-1, or analysis of the late Cretaceous section in other Duntroon Basin wells, may provide further insight into the Tertiary thermal history (see Section 5).

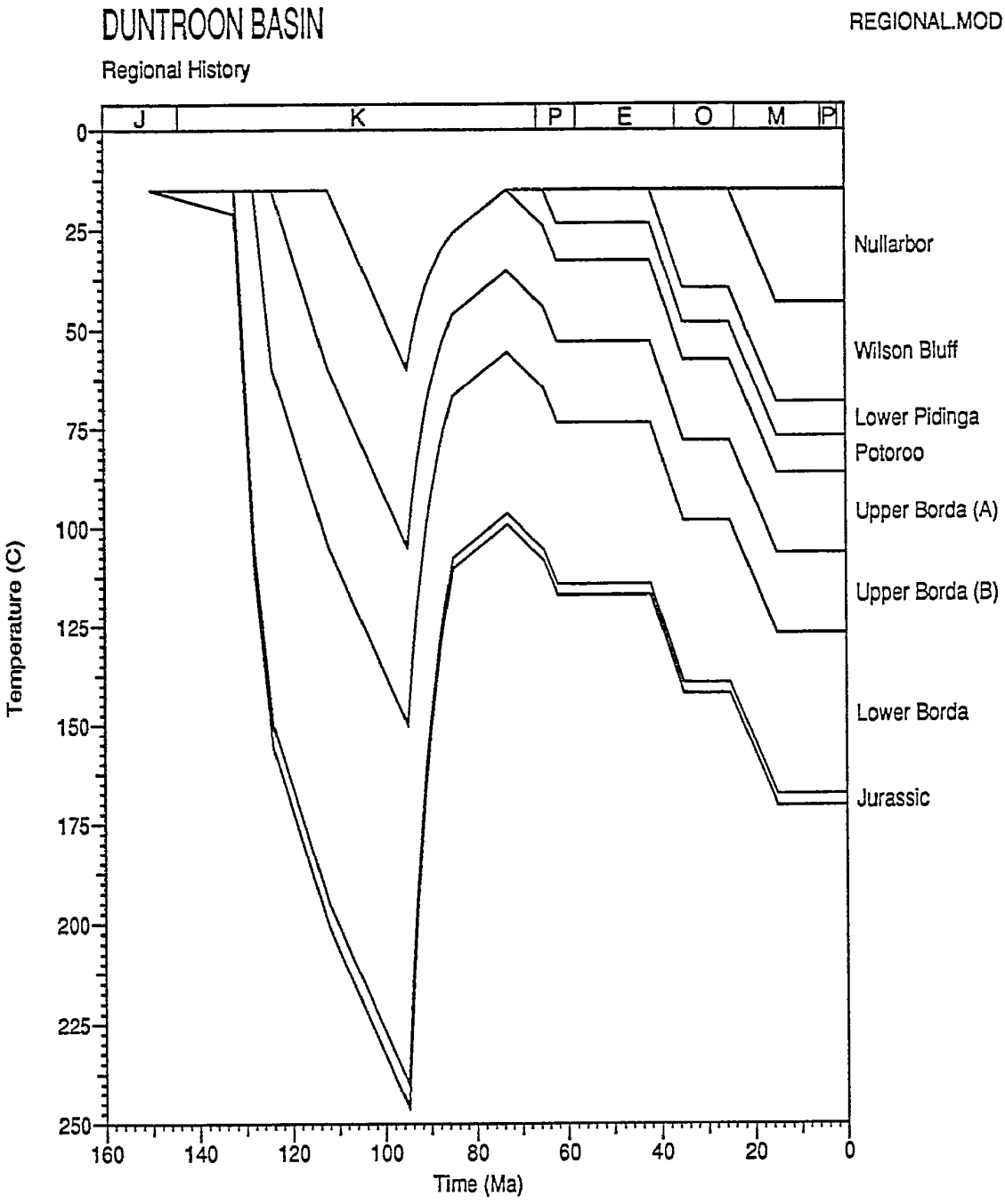

Figure 4.1: Preferred regional thermal history for the Duntroon Basin derived from interpretation of the data in the **Vivonne-1 and Borda-1 wells** presented in this report. This scenario uses the Late Cretaceous-Tertiary stratigraphy of Borda-1, combined with the an assumed Early Cretaceous stratigraphy and the reconstructed thermal history derived from the maximum likelihood thermal history parameters from Vivonne-1, as listed in Tables ii and iii.

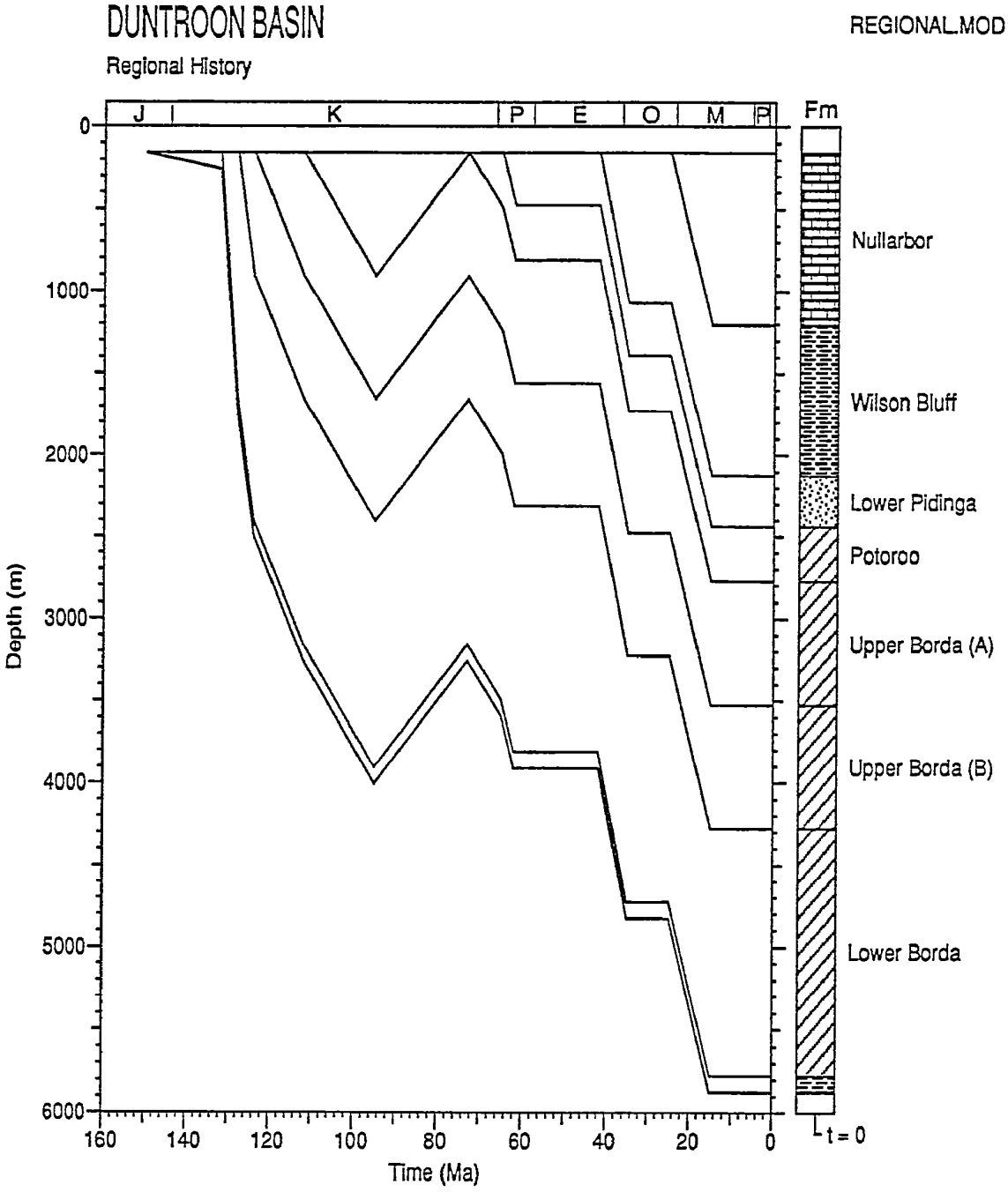

Figure 4.2: Possible regional burial history in the vicinity of the **Borda-1 well**, based on the reconstructed thermal history shown in Figure 4.1. Maximum burial occurred in the Late Tertiary to present day, while maximum heating occurred in the Mid-Cretaceous, as shown in Figure 4.1 - see text for details.

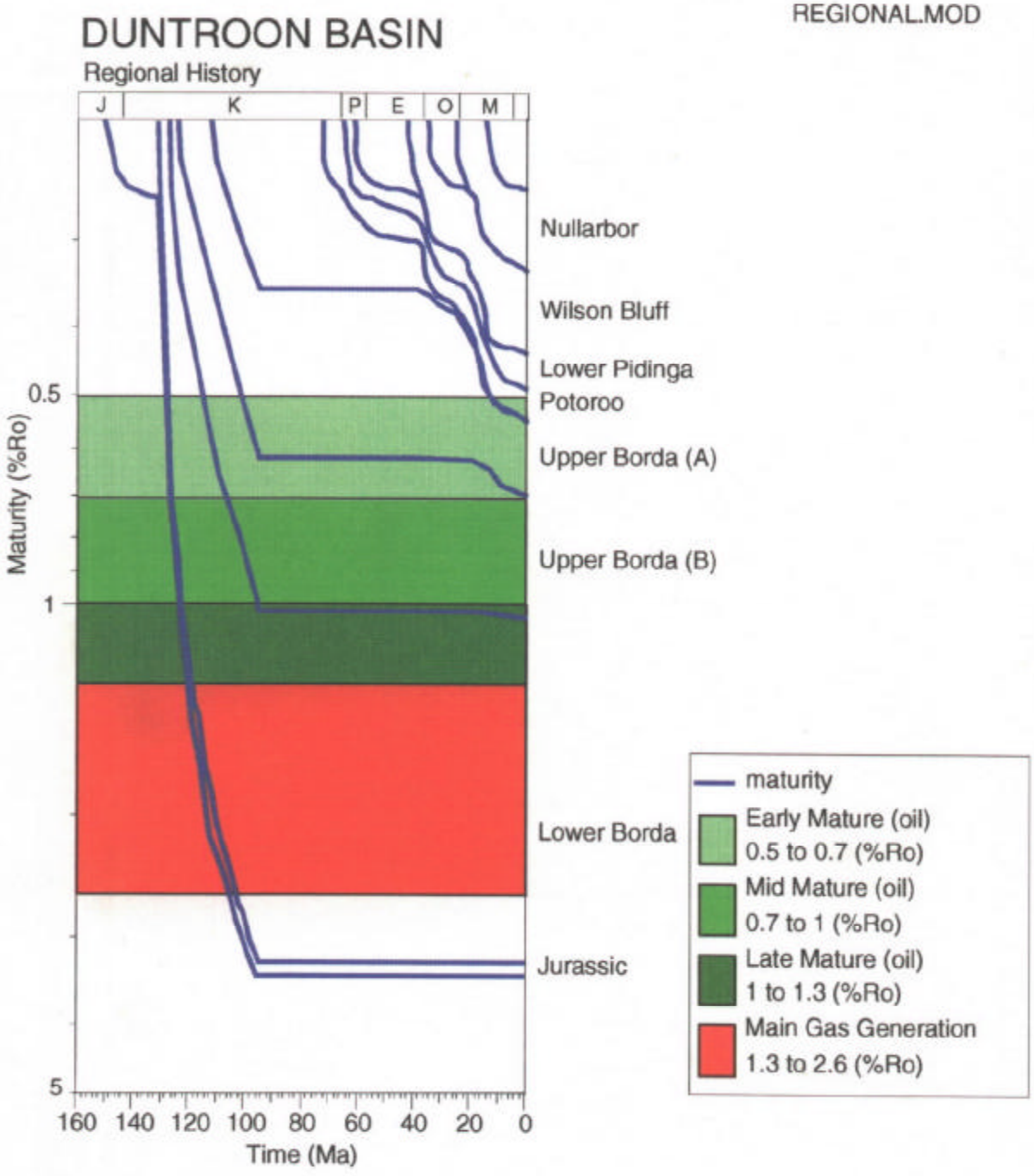

Figure 4.3: Preferred regional pattern of maturity development with time in the **Duntroon Basin**, based on the thermal history shown in Figure 4.1. The notional Jurassic and the deeper part of the Early Cretaceous section reached maximum maturity prior to cooling at ~95 Ma and have not increased in maturity since cooling took place. Only a small part of the Upper Borda Formation has increased in maturity during the Tertiary - see text for further details.

5. Further work which would significantly improve knowledge of the geological history of the region

5.1 Investigating the regional extent of Mid-Cretaceous high heat flow

Thermal history reconstruction for Vivonne-1 detailed in this report has conclusively shown the presence of highly elevated heat flow in the Duntroon Basin and demonstrated the marked similarity of the thermal history to that determined for the Otway Basin. These data suggest that this style of thermal history is regional in nature, which has important consequence for hydrocarbon exploration in the Duntroon Basin. It is recommended that AFTA and new VR data be collected on other existing wells in the basin to more fully document the elevated heat flow event as a method of focusing exploration on the most prospective areas of the basin.

5.2 Investigating the cause of Tertiary heating

Only very limited AFTA results were obtained from analysis of two samples from the Borda-1 well, with no information obtained on the timing of possible elevated paleotemperatures suggested by the VR data. Analysis of additional, larger samples from the Borda-1 section, or the Tertiary to Late Cretaceous section in related wells, could assist in resolution of this uncertainty.

The interpretation of heating in Borda-1 was also hampered by a lack of detailed palaeontology of the shallow section in Borda-1, which becomes essential in resolution of subtle thermal history problems. New determinations of the stratigraphic age of the Nullarbor Formation section would be desirable in each well studied, but this may be hampered by lack of samples collected in the upper section due to drilling practice.

References

Burnham, A. K. and Sweeney, J. J. (1989). A chemical kinetic model of vitrinite reflectance maturation. *Geochimica et Cosmochimica Acta.*, 53, 2649-2657.

Corrigan, J. D. (1991). Thermal anomalies in the Central Indian Ocean: Evidence for de-watering of the Bengal Fan. *Journal of Geophysical Research*, 96, 14263 - 14275.

Duddy, I. R. (1983). The geology, petrology and geochemistry of the Otway Formation volcanogenic sediments. Ph.D thesis, University of Melbourne (unpubl.), 426pp.

Duddy, I. R. (1994). The Otway Basin: Thermal, structural, tectonic and hydrocarbon generation histories. *In*: Finlayson, D. M. (*compiler*), NGMA/PESA Otway Basin Symposium, Melbourne, April 20, 1994. Australian Geological Survey Organisation, Record 1994/14.

Green, P. F., Duddy, I. R., Gleadow, A. J. W., Tingate, P. R. and Laslett, G. M. (1985). Fission track annealing in apatite: Track length measurements and the form of the Arrhenius Plot. *Nuclear Tracks*, 10, 323-328.

Duddy, I. R., Green, P. F., Hegarty, K. A. and Bray, R. J. (1991). Reconstruction of thermal history in basin modelling using Apatite Fission Track Analysis: what is really possible. Proceedings of the First Offshore Australia Conference (Melbourne). III-49 - III-61.

Green, P. F., Duddy, I. R. and Bray, R. J. (1995). Variation in thermal history styles around the Irish Sea and adjacent areas: implications for hydrocarbon occurrence and tectonic evolution. *In:* Petroleum Geology of the Irish Sea and adjacent areas. The Geological Society, Special Publication. Submitted 1995.

Sweeney, J. J. and Burnham, A. K. (1990). Evaluation of a simple model of vitrinite reflectance based on chemical kinetics. *The American Association of Petroleum Geologists' Bulletin,* 74, 1559 - 1570.

Waples, D. W., Kamata, H. and Suizu, M. (1992). The art of maturity modelling. Part 1: Finding a satisfactory geologic model. *The American Association of Petroleum Geologists' Bulletin*, 76, 31 - 46.

APPENDIX A

Sample Details, Apatite Compositions and Geological Data

A.1 Sample details

Nine samples from the **Vivonne-1 and Borda-1** wells, **Duntroon Basin,** were provided by the **Petroleum Division, Mines and Energy South Australia (MESA),** for Apatite Fission Track Analysis (AFTA®), along with 22 samples for Vitrinite Reflectance (VR) determinations (Table D.2, Appendix D).

In addition, open-file VR data on 12 samples (Table D.3, Appendix D) from both wells, which were supplied by MESA, have been re-interpreted in terms of maximum paleotemperature for this study in order to provide a more comprehensive assessment of the thermal history. The report was completed in September 1995.

Details of all samples, including depths and stratigraphic ages and present temperatures, (calculated using BHT data) supplied by MESA, are listed for each sample in Table A.1.

A.2 Stratigraphic details

The details of each stratigraphic interval in the preserved sections of Vivonne-1 and Borda-1 were supplied by MESA. Also supplied were the depths (mKB) of each AFTA sample. Based on the chronostratigraphic age, a numerical age (Ma) was assigned for each sample using Harland et al. (1989). The stratigraphic ages, or age ranges, of each AFTA sample are summarised in Table A.1.

A.3 Present temperatures

In application of any technique involving estimation of paleotemperatures, it is critical to control the present temperature profile, since estimation of maximum paleotemperatures proceeds from trying to see how much of the observed effect could be explained by the magnitude of present temperatures.

Time since circulation and time of circulation data was not available to allow Horner-correction procedures. For **Borda-1**, measured BHT data were corrected using a simplified correction procedure adapted from the literature (Oxburgh and Andrews-Speed, 1981; Andrews-Speed et al., 1984). Quoted BHT data were corrected by

increasing the difference between the sea-bed temperature (assumed to be 15°C) and the uncorrected BHT value by 20% for uncorrected temperatures below 150°F (66°C), and by 25% above 150°F. The first recorded BHT value was used where multiple temperature measurements were available at a given depth. While no doubt simplistic, this procedure has the advantage of allowing a common approach in all wells, and appears to give consistent results. Uncorrected and corrected BHT data from each well are summarised in Table A.2.

The corrected temperature values in **Borda-1** well define a broadly linear trend (Figure A.1). An average linear gradient of 27.2°C/km, constrained using all BHT data and a sea-bed temperature of 15°C, has been calculated, as summarised in Table A.2. Note that one interpretation of the Borda-1 paleotemperature data would suggest a present-day gradient of ~ 30°C/km (see Section 4.4).

For **Vivonne-1**, a corrected temperature of 97°C at TD (2873 m total vertical depth bRT) was supplied by MESA, and, combined with an assumed sea-bed temperature of 15°C, was used to calculate a present-day geothermal gradient of 30.2°C/km (Table A.2).

In general, the simple linear geothermal gradient in each well is considered to provide an adequate representation of the present-day geothermal regime, providing reasonable estimates of the present temperature for each AFTA and VR sample.

This is supported by the AFTA data in most samples, which are consistent with the present temperatures estimated in this way. Likely departures from this trend should not have any significant effect on the thermal history interpretations presented in this report.

A.4 Apatite yields

Yields of detrital apatite obtained after mineral separation from all samples processed are summarised in Table A.1. Yields varied from none to excellent, providing between one and more than 20 grains suitable for fission track age determination. Of the seven samples finally processed from Vivonne-1, the Lower Cretaceous Upper Borda Formation provided one excellent, one fair and two poor yields, the lower Borda Formation provided one excellent and one poor yield, while the Paleocene Lower Pidinga Formation gave a very poor yield and the Maastrichtian Potoroo Formation, none.

Of the two samples from Borda-1, the Maastrichtian Potoroo Formation gave a very poor yield and the Paleocene Lower Pidinga Formation none (Table A.1). These yields are fairly typical of the Mesozoic to Tertiary sequences of southern Australia in general, with the majority of the apatite found derived from first cycle Early Cretaceous volcanic

sources. The lack of apatite in Late Cretaceous and Tertiary units relates principally to derivation of the sediments from erosion of multi-cycle Paleozoic sediments which have an inherently low detrital apatite content.

Three of the six Vivonne-1 samples with apatite provided more than 30 confined track length measurements and are considered of very high quality, with the three remaining samples giving between nine and 12 measurements, which are adequate for general conclusions. Only four lengths were obtained from the single sample from Borda-1, resulting in poor control on the detail of the thermal history in this well. The quality of the etched surfaces of the apatites obtained for analysis was high in all samples, and the overall high quality of the AFTA data in key samples results in reliable thermal history interpretations for the two wells studied.

The AFTA data generated from Vivonne-1 for this report are considered to be of very high quality, while the unsatisfactory yields from the two Borda-1 samples have resulted in limited AFTA data and poorer thermal history constraints.

A.5 Apatite quality and grain morphologies

Apatite grains in all samples are generally characterised by euhedral to sub-rounded euhedral forms. The majority of apatite grain morphologies from the Early Cretaceous section are euhedral to sub-rounded euhedral forms, consistent with a provenance from contemporaneous volcanic activity, as well-documented for the similarly aged Otway Group section known further east (Duddy, 1983) - an interpretation supported by the broad range of chlorine contents for apatite from each sample.

The limited number of grains from the Maastrichtian and Palaeocene samples do not allow firm conclusions to be drawn concerning grain morphology.

A.6 Apatite compositions

The annealing kinetics of fission tracks in apatite are affected by chemical composition, specifically the Cl content, as explained in more detail in Appendix C. Compilation of data from a wide variety of geological environments from around the world suggests that apatites from common sedimentary rocks (such as quartzo-feldspathic sandstones) are characterised by a distribution of chlorine contents similar to the distribution shown in Figure C.4b. The majority of grains from quartzo-feldspathic sandstones have chlorine contents between 0 and 0.1 wt%, while a smaller number of grains give values up to ~0.5 wt%, close to the value found in the Durango apatite, on which Geotrack's original

kinetic model of fission track behaviour was based (Appendix C). Occasional grains may give Cl contents up to ~1 wt%, but higher amounts are unusual. On the other hand, apatite grains from volcanogenic sandstones have chlorine contents between 0 and ~3 wt%, as shown in Figure C.4c, indicative of derivation from a wide range of original volcanic rock types.

For this study, chlorine compositions were determined for all individual apatite grains in which fission track ages were determined and/or lengths were measured. Chlorine contents were measured using a semi-automated Jeol JXA-5A electron microprobe equipped with three wavelength dispersive crystal spectrometers, with an accelerating voltage of 15 KV and beam current of 25 nA. The beam was defocussed to 20μm to avoid the problems associated with apatite decomposition, which occur under a fully focussed 1μm - 2μm beam. The X-Y co-ordinates of apatite grains within the grain mount were transferred from the Autoscan Fission Track Stage to a file suitable for direct input into the electron microprobe. Pure rock salt (NaCl) was used as a standard for chlorine, which was the only element determined in each apatite grain. Count rates were converted to wt% Cl using an empirical correction factor determined specifically for apatite compositions. This allows for atomic number absorption and fluorescence matrix effects, which are normally calculated explicitly when analysing for all elements. Durango apatite (Melbourne University Standard APT151) was analysed at regular intervals throughout the analysis to monitor microprobe performance.

Using this approach, lower limits of detection for chlorine content have been calculated for typical analytical conditions (beam current, counting time, etc.) and are listed in Table A.3. Errors in wt% composition are given as a percentage and quoted at 1σ for chlorine determinations. A generalised summary of error values for various values of wt% chlorine is presented in Table A.4.

The measured range of chlorine contents of apatites (both age and length grains) within each sample is shown in histogram format in Figure A.3. Plots of single grain age versus weight % chlorine are shown in Figure B.5. Chlorine contents, which are presented in numerical format for dated grains only, appear in the fission track age summary sheets in Appendix B. The chlorine data are employed in interpreting the AFTA data for each sample, using methods outlined in Appendix C.

References

Andrews-Speed, C. P., Oxburgh, E. R. and Cooper, B. A. (1984). Temperatures and depth-dependent heat flow in the South-western North Sea. *In:* L. V. and Hobson, G. D. (*eds.*), The petroleum geology of the continental shelf of NW Europe, 3, 141-151.

Duddy, I. R. (1983). The geology, petrology and geochemistry of the Otway formation volcanogenic sediments. Ph.D thesis, University of Melbourne (unpubl.), 426pp.

Harland, W. B., Armstrong, R. L., Cox, A. V., Craig, L. E., Smith, A. G. and Smith, D. G. (1989). A geologic time scale 1989, Cambridge University Press.

Oxburgh, E. R. and Andrews-Speed, C. P. (1981). Temperatures and depth-dependent heat flow in the Western North Sea. *AAPG Bulletin*, 68, 1764-1781.

Table A.1: Details of AFTA samples and apatite yields - well samples from the Duntroon Basin (Geotrack Report #569)

Sample number	Depth (m)	Sample type	Stratigraphic subdivision	Stratigraphic age (Ma)	Present temperature *1 (°C)	Raw weight (g)	Washed weight (g)	Apatite yield *2
Vivonne-1								
GC569-16	1146-1218	cuttings	L.Pidinga Paleocene	65-56	46	1030	618	Very Poor
GC569-17	1263-1311	cuttings	Potoroo Maastrichtian	74-65	49	1020	761	None
GC569-28	1655-1743	cuttings	U.Borda Aptian	124-112	61	980	119	Excellent
GC569-29	1859-1903	cuttings	U.Borda Aptian	124-112	67	1010	166	Fair
GC569-23	2021-2115	cuttings	U.Borda Aptian	124-112	73	1020	178	Poor
GC569-30	2437-2535	cuttings	L.Borda Barremian	132-124	85	770	166	Excellent
GC569-25	2580-2616	cuttings	L.Borda Barremian	132-124	89	1130	286	Poor
Borda-1								
GC569-8	2252-2339	cuttings	L.Pidinga Paleocene	65-56	72	880	615	None
GC569-13	2708-2795	cuttings	Potoroo Maastrichtian	74-65	85	1020	654	Very Poor

*1 See Appendix A for discussion of present temperature data.

*2 Yield based on quantity of mineral suitable for age determination. Excellent: >20 grains; Very Good: ~20 grains; Good: 15-20 grains; Fair: 10-15 grains; Poor: 5-10 grains; Very Poor: <5 grains.

Note: All depths quoted are TVD with respect to KB.

Table A.2: Summary of present temperature measurements - Duntroon Basin wells (Geotrack Report #569)

	Sea bed	Depth (log)	Uncorrected temperature		Time since circulation	Depth	Corrected temperature	Geothermal gradient
	(m)	(ft)	(°F)	(°C)	(hrs)	(m)	(°C)	(°C/km)
Vivonne-1								
	162	3179*	106	41.0	-	969	46.2	30.2
		4068*	123	50.7	-	1240	57.8	
		8314*	178	81.0	-	2534	97.5	
					-	2873	97	
Borda-1								
	182	5436	126	52.0	-	1657	59.4	27.2
		9173	158	70.0	-	2796	83.8	

Quoted BHT values have been corrected by increasing the difference between sea bed temperature and measured BHT by 20% for measured temperatures <150°F (<66°C) and by 25% for temperatures >150°F (>66°C). A sea bed temperature of 15°C has been assumed.
All depths quoted are with respect to KB, except where otherwise stated.
* Measurements not used in calculation of Geothermal Gradient.

Table A.3: Lower Limits of Detection for Apatite Analyses (Geotrack Report #569)

Element	LLD (95% c.l.)		LLD (99% c.l.)	
	(wt%)	(ppm)	(wt%)	(ppm)
Cl	0.01	126	0.02	182

Table A.4: Per cent errors in chlorine content (Geotrack Report #569)

Chlorine content (wt%)	Error (%)
0.01	9.3
0.02	8.7
0.05	7.3
0.10	6.1
0.20	4.7
0.50	3.2
1.00	2.3
1.50	1.9
2.00	1.7
2.50	1.5
3.00	1.4

Errors quoted are at 1σ. See Appendix A for more details.

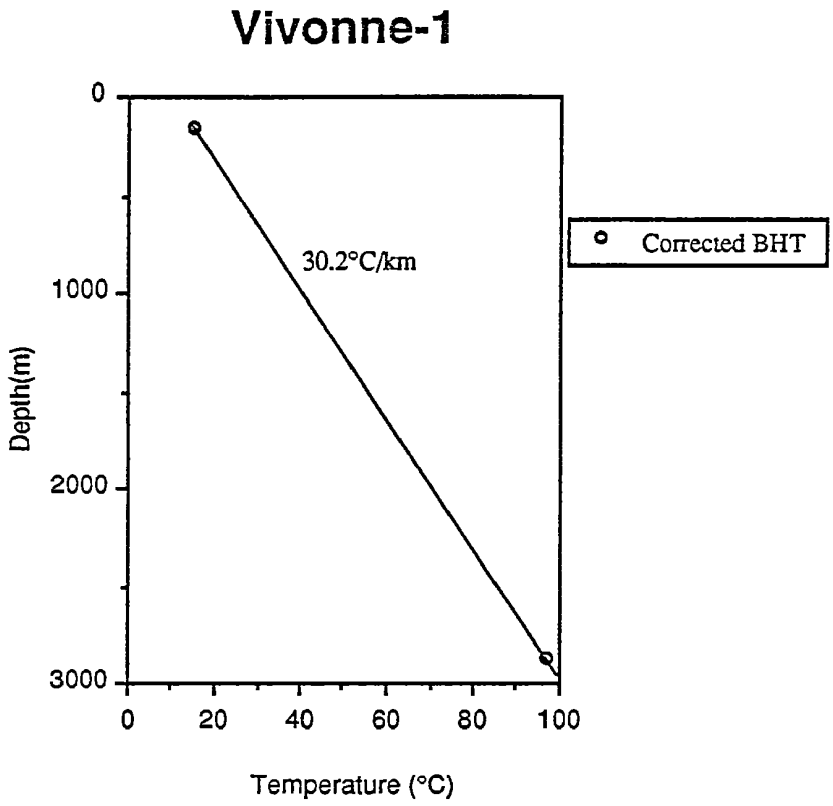

Figure A.1a: Present temperature profile calculated for **well Vivonne-1, Duntroon Basin.** See Table A.2 and Appendix A for more detail.

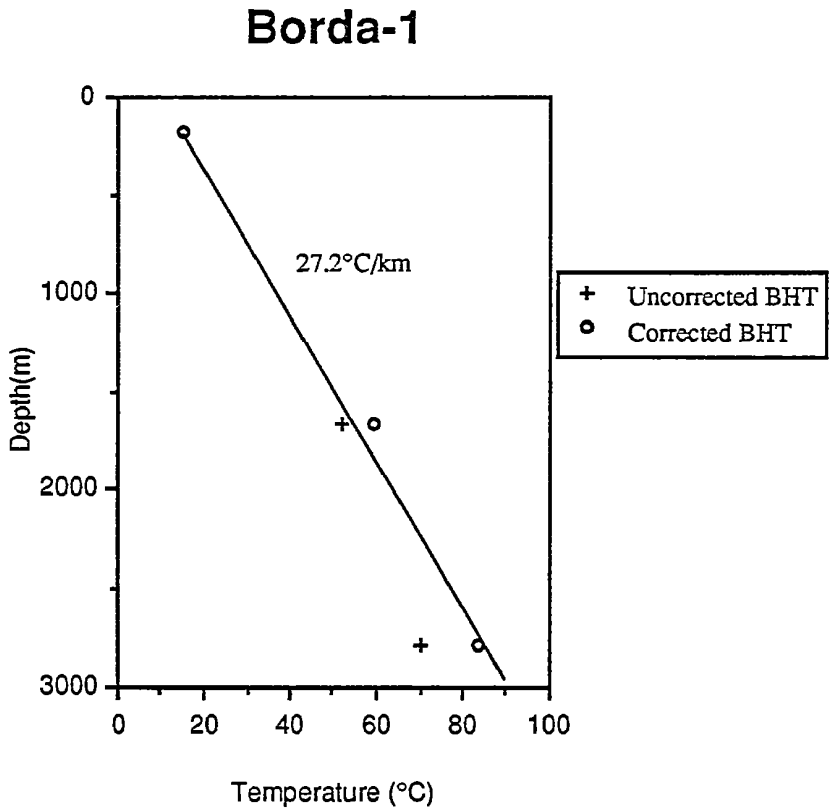

Figure A.1b: Present temperature profile calculated for **well Borda-1, Duntroon Basin.** See Table A.2 and Appendix A for more detail.

GC569-16

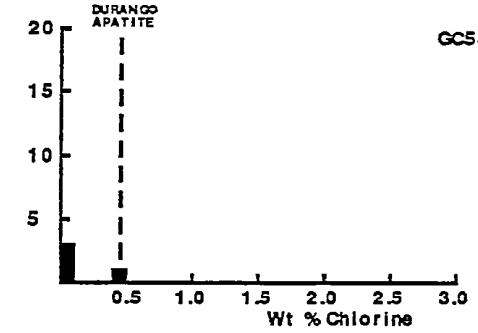

GC569-23

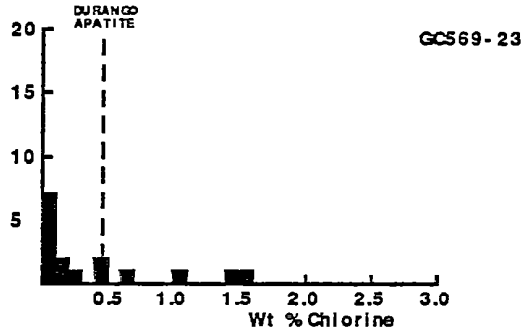

GC569-17

No Apatite

GC569-30

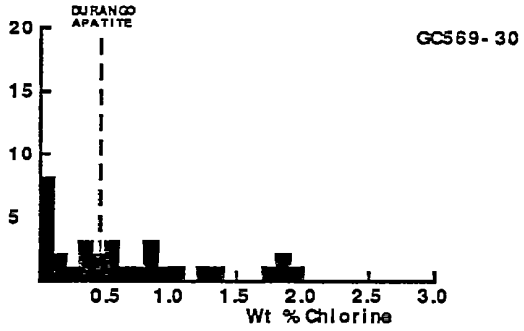

GC569-28

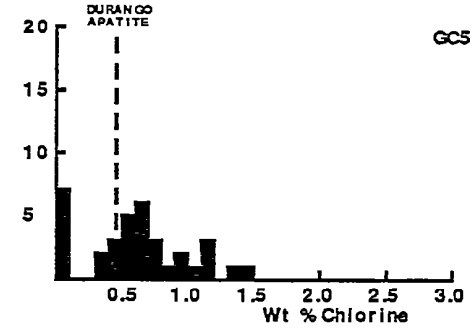

GC569-25

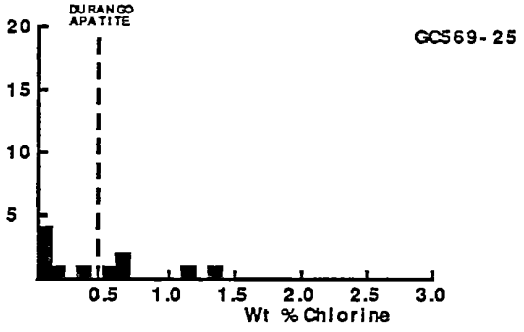

GC569-29

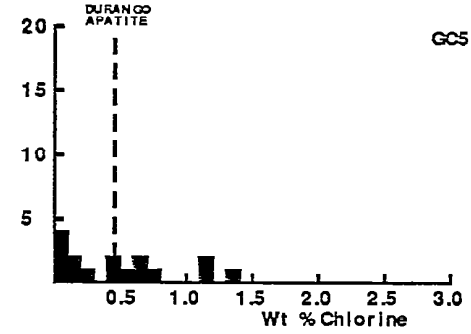

Figure A.2a: Distributions of chlorine content in samples from well **Vivonne-1, Duntroon Basin.**

GC569-8

No Apatite

GC569-13

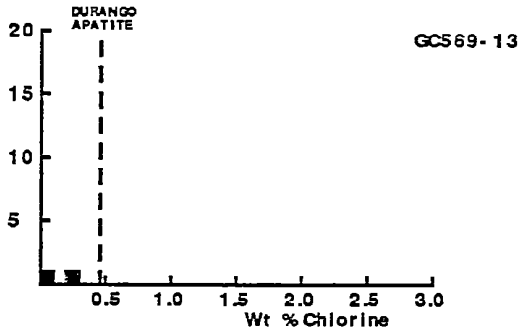

Figure A.2b: Distributions of chlorine content in samples from well **Borda-1, Duntroon Basin.**

APPENDIX B

Sample Preparation, Analytical Details and Data Presentation

B.1 Sample Preparation

Core and outcrop samples are crushed in a jaw crusher and then ground to sand grade in a rotary disc mill. Cuttings samples are washed and dried before grinding to sand grade. The ground material is then washed to remove dust, dried and processed by conventional heavy liquid and magnetic separation techniques to recover heavy minerals. Apatite grains are mounted in epoxy resin on glass slides, polished and etched for 20 sec in 5M HNO_3 at 20°C to reveal the fossil fission tracks.

After etching, all mounts are cut down to 1.5 X 1 cm, and cleaned in detergent, alcohol and distilled water. The mounts are then sealed in intimate contact with low-uranium muscovite detectors within heat-shrink plastic film. Each batch of mounts is stacked between two pieces of uranium standard glass, which has been prepared in similar fashion. The stack is then inserted into an aluminium can for irradiation.

After irradiation, the mica detectors are removed from the grain mounts and standard glasses and etched in hydrofluoric acid to reveal the fission tracks produced by induced fission of ^{235}U in the apatite and standard glass.

B.2 Analytical Details

Fission track ages

Fission track ages are calculated using the standard fission track age equation using the zeta calibration method (equation five of Hurford and Green, 1983), viz:

$$\text{F.T. AGE} = \frac{1}{\lambda_D} \ln \left[1 + \left(\frac{\zeta \lambda_D \rho_s g \rho_D}{\rho_i} \right) \right] \qquad \text{B.1}$$

where:
- λ_D = Total decay constant of ^{238}U (= 1.55125 x 10^{-10})
- ζ = Zeta calibration factor
- ρ_s = Spontaneous track density
- ρ_i = Induced track density
- ρ_D = Track density from uranium standard glass
- g = A geometry factor (= 0.5)

Fission track ages are determined by the external detector method or EDM (Gleadow, 1981). The EDM has the advantage of allowing fission track ages to be determined on single grains. In apatite, tracks are counted in 20 grains from each mount wherever possible. In those samples where the desired number is not present, all available grains are counted, the actual number depending on the availability of suitably etched and oriented grains. Only grains oriented with surfaces parallel to the crystallographic c-axis are analysed. Such grains can be identified on the basis of the etching characteristics, as well as from morphological evidence in euhedral grains. The grain mount is scanned sequentially, and the first 20 suitably oriented grains identified are analysed.

Tracks are counted within an eyepiece graticule divided into 100 grid squares. In each grain, the number of spontaneous tracks (N_S) within a certain number of grid squares (N_a) is recorded. The number of induced tracks (N_i) in the corresponding location within the mica external detector is then counted. Spontaneous and induced track densities (ρ_S and ρ_i, respectively) are calculated by dividing the track counts by the total area counted, given by the product of Na and the area or each grid square (determined by calibration against a ruled stage graticule or diffraction grating). Fission track ages may be calculated by substituting track counts (N_S and N_i) for track densities (ρ_S and ρ_i) in equation B.1, since the areas cancel in the ratio.

Translation between apatite grains in the grain mount and external detector locations corresponding to each grain is carried out using Autoscan™ microcomputer-controlled automatic stages (Smith and Leigh Jones, 1985). This system allows repeated movement between grain and detector, and all grain locations are stored for later reference if required.

Neutron irradiations are carried out in a well-thermalised flux (X-7 facility; Cd ratio for Au ~98) in the Australian Atomic Energy Commission's HIFAR research reactor. Total neutron fluence is monitored by counting tracks in mica external detectors attached to two pieces of NBS standard glass SRM612 included in the irradiation canister at each end of the sample stack. In determining track densities in external detectors irradiated adjacent to uranium standard glasses, 25 fields are normally counted in each detector. The total track count (N_D) is divided by the total area counted to obtain the track density (ρ_D). The positions of the counted fields are arranged in a 5 X 5 grid covering the whole area of the detector. For typical track densities of between ~5 X 10^5 and 5 X 10^6, this is a convenient arrangement to sample across the detector while gathering sufficient counts to achieve a precision of ~±2% in a reasonable time.

A small flux gradient is often present in the irradiation facility over the length of the sample package (note that this developed only in late 1991, after extended refurbishment

of the reactor, before which no detectable flux gradient was present). If a detectable gradient is present, the track count in the external detector adjacent to each standard glass is converted to a track density (ρ_D) and a value for each mount in the stack is calculated by linear interpolation. When no detectable gradient is present, the track counts in the two external detectors are pooled to give a single value of ρ_D, which is used to calculate fission track ages for each sample.

A Zeta calibration factor (ζ) has been determined empirically for each observer by analysing a set of carefully chosen age standards with independently known K-Ar ages, following the methods outlined by Hurford and Green (1983) and Green (1985).

All track counting is carried out using Zeiss(R) Axioplan microscopes, with an overall linear magnification of 1068 x using dry objectives.

For further details and background information on practical aspects of fission track age determination, see e.g., Fleischer, Price and Walker (1975), Naeser (1979) and Hurford (1986).

Track length measurements

For track length studies in apatite, the full lengths of "confined" fission tracks are measured. Confined tracks are those which do not intersect the polished surface but have been etched from other tracks or fractures, so that the whole length of the track is etched. Confined track lengths are measured using a digitising tablet connected to a microcomputer, superimposed on the microscope field of view via a projection tube. With this system, calibrated against a stage graticule ruled in 2 μm divisions, individual tracks can be measured to a precision of ± 0.2 μm. Tracks are measured only in prismatic grains, characterised by sharp polishing scratches with well-etched tracks of narrow cone angle in all orientations, because of the anisotropy of annealing of fission tracks in apatite (as discussed by Green et al., 1986). Tracks are also measured following the recommendations of Laslett et al. (1982), the most important of which is that only horizontal tracks should be measured. One hundred tracks are measured whenever possible. In apatite samples with low track density, or in those samples in which only a small number of apatite grains are obtained, fewer confined tracks may be available. In such cases, the whole mount is scanned to measure as many confined tracks as possible.

Integrated fission track age and length measurement

Fission track age determination and length measurement are now made in a single pass of the grain mount, in an integrated approach. The location of each grain in which tracks are

either counted or measured is recorded for future reference. Thus, track length measurements can be tied to age determination in individual grains. As a routine procedure we do not measure the age of every grain in which lengths are determined, as this would be much too time-consuming. Likewise we do not only measure ages in grain in which lengths are measured, as this would bias the age data against low track density grains. Nevertheless, the ability to determine the fission track age of certain grains from which length data originate can be a particularly useful aid to interpretation in some cases. Grain location data are not provided in this report, but are available on request.

B.3 Data Presentation

Fission track age data

Data sheets summarising the apatite fission track age data, including full details of fission track age data for individual apatite grains in each sample, together with the primary counting results and statistical data, are given in the following pages. Individual grain fission track ages are calculated from the ratio of spontaneous to induced fission track counts for each grain using equation B.1, and errors in the single grain ages are calculated using Poissonian statistics, as explained in more detail by Galbraith (1981) and Green (1981). All errors are quoted as $\pm 1\sigma$ throughout this report, unless otherwise stated.

The variability of fission track ages between individual apatite grains within each sample can be assessed using a chi-squared (χ^2) statistic (Galbraith, 1981), the results of which are summarised for each sample in the data sheets. If all the grains counted belong to a single age population, the probability of obtaining the observed χ^2 value, for ν degrees of freedom (where ν = number of crystals -1), is listed in the data sheets as $P(\chi^2)$ or P(chi squared).

A $P(\chi^2)$ value greater than 5% can be taken as evidence that all grains are consistent with a single population of fission track age. In this case, the best estimate of the fission track age of the sample is given by the "pooled age", calculated from the ratio of the total spontaneous and induced track counts in all grains analysed. Errors for the pooled age are calculated using the "conventional" technique outlined by Green (1981), based on the total number of tracks counted for each track density measurement (see also Galbraith, 1981).

A $P(\chi^2)$ value of less than 5% denotes a significant spread of single grain ages, suggesting real differences exist between the fission track ages of individual apatite grains. A significant spread in grain ages can result either from inheritance of detrital

grains from mixed source areas (in sedimentary rocks), or from differential annealing in apatite grains of different composition, within a narrow range of temperature.

Calculation of the pooled age inherently assumes that only a single population of ages is present, and is thus not appropriate to samples containing a significant spread of fission track ages. In such cases Galbraith, has recently devised a means of estimating the modal age of a distribution of single grain fission track ages which is referred to as the "central age". Calculation of the central age assumes that all single grain ages belong to a Normal distribution of ages, with a standard deviation (σ) known as the "age dispersion". An iterative algorithm (as yet unpublished) is used to provide estimates of the central age with its associated error, and the age dispersion, which are all quoted in the data sheets. Note that this treatment replaces use of the "mean age", which has used been in the past for those samples in which $P(\chi^2)<5\%$. For samples in which $P(\chi^2)>5\%$, the central age and the pooled age should be equal, and the age dispersion should be less than ~10%.

Table B.1 summarises the fission track age data in apatite from each sample analysed.

Construction of radial plots of single grain age data

Single grain age data are best represented in the form of radial plot diagrams (Galbraith, 1988, 1990). As illustrated in Figure B.1, these plots display the variation of individual grain ages in a plot of y against x, where:

$$y = (z_j - z_o)/\sigma_i \qquad x = 1/\sigma_j \qquad \text{B.2}$$

and; z_j = Fission track age of grain j
z_o = A reference age
σ_j = Error in age for grain j

In this plot, all points on a straight line from the origin define a single value of fission track age, and, at any point, the value of x is a measure of the precision of each individual grain age. Therefore, precise individual grain ages fall to the right of the plot (small error, high x), which is useful, for example, in enabling precise, young grains to be identified. The age scale is shown radially around the perimeter of the plot (in Ma). If all grains belong to a single age population, all data should scatter between y = +2 and y = -2, equivalent to scatter within $\pm 2\sigma$. Scatter outside these boundaries shows a significant spread of individual grain ages, as also reflected in the values of $P(\chi^2)$ and age dispersion.

In detail, rather than using the fission track age for each grain as in equation B.2, we use:

$$z_j = \frac{N_{sj}}{N_{ij}} \qquad \sigma_j = \{1/N_{sj} + 1/N_{ij}\} \qquad \text{B.3}$$

as we are interested in displaying the scatter within the data from each sample in comparison with that allowed by the Poissonian uncertainty in track counts, without the additional terms which are involved in determination of the fission track age (ρ_D, ζ, etc).

Zero ages cannot be displayed in such a plot. This can be achieved using a modified plot, (Galbraith, 1990) with:

$$z_j = \arcsin\sqrt{\left\{\frac{N_{sj}+3/8}{N_{sj}+N_{ij}+3/4}\right\}} \qquad \sigma_j = \frac{1}{2}\sqrt{\left\{\frac{1}{N_{sj}+N_{ij}}\right\}} \qquad \text{B.4}$$

Note that the numerical terms in the equation for z_j are standard terms, introduced for statistical reasons. Using this arc-sin transformation, zero ages plot on a diagonal line which slopes from upper left to lower right. Note that this line does not go through the origin. Figure B.2 illustrates this difference between conventional and arc-sin radial plots, and also provides a simple guide to the structure of radial plots.

Use of arc-sin radial plots is particularly useful in assessing the relative importance of zero ages. For instance, grains with $N_s = 0$, $N_i = 1$ are compatible with ages up to ~900 Ma (at the 95% confidence level), whereas grains with $N_s = 0$, $N_i = 50$ are only compatible with ages up to ~14 Ma. The two data would readily be distinguishable on the radial plot as the 0,50 datum would plot well to the right (high x) compared to the 0,1 datum.

In this report the value of z corresponding to the stratigraphic age of each sample (or the midpoint of the range where appropriate) is adopted as the reference value, z_0. This allows rapid assessment of the fission track age of individual grains in relation to the stratigraphic age, which is a key component in the interpretation of AFTA data, as explained in more detail in Appendix C.

Note that the x axis of the radial plot is normally not labelled, as this would obscure the age scale around the plot. In general labelling is not considered necessary, as we are concerned only with relative variation within the data, rather than absolute values of precision.

Radial plots of the single grain age data in apatite from each sample analysed in this report are shown in Figure B.3. Use of radial plots to provide thermal history information is explained in Appendix C and Figure C.7.

Smoothed probability distributions

The single grain ages within each sample are also shown in Figure B.3 in histogram form and also as smoothed probability distributions (Hurford et al., 1984). In constructing these distributions, each grain is represented by a normal probability curve, with mean equal to the single grain age, standard deviation given by the error on the single grain age and the contributions from all grains analysed in each sample summed to produce the plotted curve. These distributions are generally not as informative as the radial plot presentation of single grain age data as they convey little assessment of the relative precision of the fission track ages of different grains. However, they can be useful for portraying the general form of the distribution of ages within a sample.

Track length data

Distributions of confined track lengths in apatite from each sample are shown as simple histograms in Figure B.4. For every track length measurement, the length is recorded to the nearest 0.1 μm, but the measurements have been grouped into 1 μm intervals in the histograms in Figure B.4. Each distribution has been normalised to 100 tracks for each sample to facilitate comparison. A summary of the length distribution in each sample is presented in Table B.2, which also shows the mean track length in each sample and its associated error, the standard deviation of each distribution and the number of tracks (N) measured in each sample. The angle which each confined track makes with the crystallographic c-axis is also routinely recorded, as is the width of each fracture within which tracks are revealed. These data are not provided in this report, but can be supplied on request.

Breakdown of data into compositional groups

In Table B.3, AFTA data are grouped into compositional intervals of 0.1 wt% Cl width. Parameters for each interval represent the data from all grains with Cl contents within each interval. Also shown are the parameters for each compositional interval predicted from the Default Thermal History (see Section 2.1). These data form the basis of interpretation of the AFTA data, which takes full account of the influence of Cl content on annealing kinetics, as described in Appendix C.

Plots of fission track age against Cl content for individual apatite grains

In Figure B.5, fission track ages of single apatite grains within individual samples are plotted against the Cl content of each grain. These plots are useful in assessing the degree of annealing, as expressed by the fission track age data. For example, if grains with a range of Cl contents from zero give similar fission track ages which are significantly less

than the stratigraphic age, these compositions must have been totally annealed. Alternatively, if fission track age falls rapidly with decreasing Cl content, the sample displays a high degree of partial annealing.

B.4 A note on terminology

Note that throughout this report, the term "fission track age" is understood to denote the parameter calculated from the fission track age equation, using the observed spontaneous and induced track counts (either pooled for all grains or for individual grains). The resulting number (with units of Ma) should not be taken as possessing any significance in terms of events taking place at the time indicated by the measured fission track age, but should rather be regarded as a measure of the integrated thermal history of the sample, and should be interpreted in that light using the principles outlined in Appendix C. Use of the term "apparent age" is not considered to be useful in this regard, as almost every fission track age should be regarded as an apparent age, in the classic sense, and repeated use becomes cumbersome.

References

Fleischer, R. L., Price, P. B., and Walker, R. M. (1975). Nuclear tracks in solids, University of California Press, Berkeley.

Galbraith, R. F. (1981). On statistical models for fission-track counts. *Mathematical Geology*, 13, 471-488.

Galbraith, R. F. (1988). Graphical display of estimates having differing standard errors. *Technometrics*, 30, 271-281.

Galbraith, R. F. (1990). The radial plot: graphical assessment of spread in ages. *Nuclear Tracks*, 17, 207-214.

Gleadow, A. J. W. (1981). Fission track dating methods; what are the real alternatives? *Nuclear Tracks*, 5, 3-14.

Green, P. F. (1981). A new look at statistics in fission track dating. *Nuclear Tracks 5*, 77-86.

Green, P. F. (1985). A comparison of zeta calibration baselines in zircon, sphene and apatite. *Chem. Geol. (Isot. Geol. Sect.)*, 58, 1-22.

Green, P. F., Duddy, I. R., Gleadow, A. J. W., Tingate, P. R. and Laslett, G. M. (1986). Thermal annealing of fission tracks in apatite 1. A qualitative description. *Chem. Geol. (Isot. Geosci. Sect.)*, 59, 237-253.

Hurford, A. J. (1986). Application of the fission track dating method to young sediments: Principles, methodology and Examples. *In:* Hurford, A. J., Jäger, E. and Ten Cate, J. A. M. (*eds*), Dating young sediments, CCOP Technical Publication 16, CCOP Technical Secretariat, Bangkok, Thailand.

Hurford, A. J., Fitch, F. J. and Clarke, A. (1984). Resolution of the age structure of the detrital zircon populations of two Lower Cretaceous sandstones from the Weald of England by fission track dating. *Geological Magazine*, 121, 269-396.

Hurford, A. J. and Green, P. F. (1982). A user's guide to fission track dating calibration. *Earth. Planet. Sci Lett.* 59, 343-354.

Hurford, A. J. and Green, P. F. (1983). The zeta age calibration of fission track dating. *Isotope Geoscience* 1, 285-317.

Laslett, G. M., Kendall, W. S., Gleadow, A. J. W. and Duddy, I. R. (1982). Bias in measurement of fission track length distributions. *Nuclear Tracks*, 6, 79-85.

Naeser, C. W. (1979). Fission track dating and geologic annealing of fission tracks. *In:* Jäger, E. and Hunziker, J. C. (*eds*), Lectures in Isotope Geology, Springer Verlag, Berlin.

Smith, M. J. and Leigh-Jones, P. (1985). An automated microscope scanning stage for fission-track dating. *Nuclear Tracks*, 10, 395-400.

Table B.1: Apatite fission track analytical results - samples from the Duntroon Basin (Geotrack Report #569)

Sample number	Number of grains	Rho D x10^6 (ND)	Rho S x10^6 (Ns)	Rho I x10^6 (Ni)	Uranium content (ppm)	P(chi squared) (%)	Age dispersion (%)	Fission track age (Ma)
Vivonne-1								
GC569-16	3	1.318 (2112)	0.911 (51)	1.357 (76)	12	2	38	171.5 ± 31.4
								*192.1 ± 55.0**
GC569-17			No apatite					
GC569-28	20	1.302 (1987)	0.488 (158)	1.055 (342)	9	63	2	117.1 ± 11.8
GC569-29	14	1.297 (1987)	0.759 (130)	1.314 (225)	12	2	40	145.5 ± 16.6
								*140.1 ± 23.9**
GC569-23	9	1.324 (2112)	0.757 (153)	1.594 (322)	14	<1	44	122.5 ± 12.5
								*132.0 ± 24.5**
GC569-30	20	1.291 (1987)	0.300 (90)	0.796 (239)	7	2	58	94.8 ± 12.1
								*81.7 ± 16.0**
GC569-25	9	1.330 (2112)	0.620 (130)	1.241 (260)	11	<1	60	129.4 ± 14.4
								*108.9 ± 25.9**
Borda-1								
GC569-8			No apatite					
GC569-13	1	1.306 (2112)	1.589 (10)	6.197 (39)	54	-	-	65.5 ± 23.3

Rho S = spontaneous track density; Rho I = induced track density; Rho D = track density in glass standard external detector.
All track densities quoted in units of 1000000 tracks per square cm. Brackets show number of tracks counted.
Rho D and Rho I measured in mica external detectors; Rho S measured in internal surfaces.
* Central age, used where sample contains a significant spread of single grain ages—P(chi squared)<5%. Errors quoted at ±1 sigma.
Ages calculated using dosimeter glass CN5, with a zeta of 392.9±7.4 (Analyst: M. Moore)

Table B.2: Length distribution summary data - samples from the Duntroon Basin (Geotrack Report #569)

Sample number	Mean track length (µm)	Standard deviation (µm)	Number of tracks (N)	Number of Tracks in Length Intervals (µm) 1	2	3	4	5	6	7	8	9	10	11	12	13	14	15	16	17	18	19	20
Vivonne-1																							
GC569-16	14.48 ± 0.94	2.83	9	-	-	-	-	-	-	-	-	-	-	-	2	1	2	1	1	-	1	-	1
GC569-17	No apatite	-	-	-	-	-	-	-	-	-	-	-	-	-	-	-	-	-	-	-	-	-	-
GC569-28	12.24 ± 0.31	2.27	53	-	-	-	-	1	-	1	1	2	1	6	7	10	13	7	4	-	-	-	-
GC569-29	11.95 ± 0.39	1.16	9	-	-	-	-	-	-	-	-	-	1	1	1	5	1	-	-	-	-	-	-
GC569-23	11.07 ± 0.36	2.52	48	-	-	-	-	1	-	2	1	6	3	11	8	4	6	5	-	-	-	1	-
GC569-30	11.03 ± 0.41	2.48	37	-	-	1	-	-	-	-	1	5	2	9	8	3	4	3	1	-	-	-	-
GC569-25	11.11 ± 0.72	2.50	12	-	-	-	-	-	-	-	1	1	2	3	1	1	1	1	1	-	-	-	-
Borda-1																							
GC569-8	No apatite	-	-	-	-	-	-	-	-	-	-	-	-	-	-	-	-	-	-	-	-	-	-
GC569-13	10.01 ± 1.12	2.24	4	-	-	-	-	-	-	-	1	-	2	-	-	1	-	-	-	-	-	-	-

Track length measurements by M. Moore.

Table B.3: AFTA Data in Compositional Groups - (Geotrack Report #569)

Cl Wt %	Default fission track age* (Ma)	Measured fission track age (Ma)	Error in age (Ma)	P (χ 2)	Number of grains	Default fission track length* (µm)	Mean track length (µm)	Error in length (µm)	Std deviation (µm)	Number of lengths	Number of grains	Number of tracks in length interval (µm) 1	2	3	4	5	6	7	8	9	10	11	12	13	14	15	16	17	18	19	20
Vivonne-1																															
†569-16	56.5	192.1	54.7	2.0	3	13.9	14.5	0.9	2.8	9	3	0	0	0	0	0	0	0	0	0	0	0	2	1	2	1	1	0	1	0	1
0.0-0.1	56.2	279.7	72.0	89.0	2	13.8	14.4	1.4	2.7	4	2	0	0	0	0	0	0	0	0	0	0	0	1	1	0	0	1	0	1	0	0
0.1-0.2	-	-	-	-	-	-	-	-	-	-	-	-	-	-	-	-	-	-	-	-	-	-	-	-	-	-	-	-	-	-	-
0.2-0.3	-	-	-	-	-	-	-	-	-	-	-	-	-	-	-	-	-	-	-	-	-	-	-	-	-	-	-	-	-	-	-
0.3-0.4	-	-	-	-	-	-	-	-	-	-	-	-	-	-	-	-	-	-	-	-	-	-	-	-	-	-	-	-	-	-	-
0.4-0.5	57.3	103.9	28.3	100.0	1	14.1	14.6	1.4	3.2	5	1	0	0	0	0	0	0	0	0	0	0	0	1	0	2	1	0	0	0	0	1
†569-28	105.9	117.1	11.6	63.0	20	13.4	12.2	0.3	2.3	53	19	0	0	0	0	1	0	1	1	2	1	6	7	10	13	7	4	0	0	0	0
0.0-0.1	101.8	152.5	23.3	22.0	3	12.9	10.4	0.6	2.4	17	6	0	0	0	0	1	0	1	1	1	0	4	3	6	0	0	0	0	0	0	0
0.1-0.2	-	-	-	-	-	-	-	-	-	-	-	-	-	-	-	-	-	-	-	-	-	-	-	-	-	-	-	-	-	-	-
0.2-0.3	-	-	-	-	-	-	-	-	-	-	-	-	-	-	-	-	-	-	-	-	-	-	-	-	-	-	-	-	-	-	-
0.3-0.4	104.5	0.0	0.0	0.0	0	13.3	10.7	0.4	0.7	3	2	0	0	0	0	0	0	0	0	0	1	1	1	0	0	0	0	0	0	0	0
0.4-0.5	105.3	84.7	23.1	57.0	2	13.4	13.1	0.0	0.0	1	1	0	0	0	0	0	0	0	0	0	0	0	0	0	1	0	0	0	0	0	0
0.5-0.6	105.9	103.1	34.0	41.0	5	13.5	0.0	0.0	0.0	0	0	0	0	0	0	0	0	0	0	0	0	0	0	0	0	0	0	0	0	0	0
0.6-0.7	106.5	79.4	20.4	97.0	4	13.5	13.7	0.3	0.5	2	2	0	0	0	0	0	0	0	0	0	0	0	0	0	1	1	0	0	0	0	0
0.7-0.8	107.1	138.7	42.0	76.0	2	13.6	13.2	0.3	1.2	12	2	0	0	0	0	0	0	0	0	0	0	1	1	2	5	3	0	0	0	0	0
0.8-0.9	107.8	0.0	0.0	0.0	0	13.7	13.4	0.2	0.4	4	1	0	0	0	0	0	0	0	0	0	0	0	0	1	3	0	0	0	0	0	0
0.9-1.0	107.9	67.8	38.2	100.0	1	13.7	11.4	3.1	4.4	2	1	0	0	0	0	0	0	0	0	1	0	0	0	0	0	1	0	0	0	0	0
1.0-1.1	108.0	0.0	0.0	0.0	0	13.7	13.4	0.8	1.7	4	1	0	0	0	0	0	0	0	0	0	0	0	1	1	0	1	1	0	0	0	0
1.1-1.2	108.1	141.6	47.4	85.0	2	13.7	14.3	0.5	1.0	4	2	0	0	0	0	0	0	0	0	0	0	0	0	0	2	0	2	0	0	0	0
1.2-1.3	-	-	-	-	-	-	-	-	-	-	-	-	-	-	-	-	-	-	-	-	-	-	-	-	-	-	-	-	-	-	-
1.3-1.4	108.3	101.5	84.9	100.0	1	13.8	0.0	0.0	0.0	0	0	0	0	0	0	0	0	0	0	0	0	0	0	0	0	0	0	0	0	0	0
1.4-1.5	108.4	0.0	0.0	0.0	0	13.8	13.7	0.7	1.4	4	1	0	0	0	0	0	0	0	0	0	0	0	1	0	1	1	1	0	0	0	0

* Fission Track Age and Mean Track Length predicted from the Default Thermal History (i.e. if the sample has not been hotter in the past)

† Combined data for all compositional groups

Table B.3: Continued - (Geotrack Report #569)

Cl Wt %	Default fission track age* (Ma)	Measured fission track age (Ma)	Error in age (Ma)	P (χ 2)	Number of grains	Default fission track length* (µm)	Mean track length (µm)	Error in length (µm)	Std deviation (µm)	Number of lengths	Number of grains	Number of tracks in length interval (µm) 1	2	3	4	5	6	7	8	9	10	11	12	13	14	15	16	17	18	19	20
†569-29	104.1	140.1	23.6	2.0	14	12.9	11.9	0.4	1.2	9	7	0	0	0	0	0	0	0	0	0	1	1	1	5	1	0	0	0	0	0	0
0.0-0.1	100.2	302.6	67.5	18.0	3	12.5	11.5	0.8	1.6	4	2	0	0	0	0	0	0	0	0	0	1	1	0	1	1	0	0	0	0	0	0
0.1-0.2	101.3	121.8	28.2	33.0	2	12.7	11.8	0.5	0.7	2	2	0	0	0	0	0	0	0	0	0	0	0	1	1	0	0	0	0	0	0	0
0.2-0.3	102.5	93.2	41.2	100.0	1	12.8	0.0	0.0	0.0	0	0	0	0	0	0	0	0	0	0	0	0	0	0	0	0	0	0	0	0	0	0
0.3-0.4	-	-	-	-	-	-	-	-	-	-	-	-	-	-	-	-	-	-	-	-	-	-	-	-	-	-	-	-	-	-	-
0.4-0.5	104.6	117.8	27.1	25.0	2	13.1	12.6	0.0	0.0	1	1	0	0	0	0	0	0	0	0	0	0	0	0	1	0	0	0	0	0	0	0
0.5-0.6	105.3	200.6	95.3	100.0	1	13.2	12.5	0.0	0.0	1	1	0	0	0	0	0	0	0	0	0	0	0	0	1	0	0	0	0	0	0	0
0.6-0.7	106.0	101.1	84.6	100.0	1	13.3	13.0	0.0	0.0	1	1	0	0	0	0	0	0	0	0	0	0	0	0	1	0	0	0	0	0	0	0
0.7-0.8	106.8	151.1	110.4	100.0	1	13.3	0.0	0.0	0.0	0	0	0	0	0	0	0	0	0	0	0	0	0	0	0	0	0	0	0	0	0	0
0.8-0.9	-	-	-	-	-	-	-	-	-	-	-	-	-	-	-	-	-	-	-	-	-	-	-	-	-	-	-	-	-	-	-
0.9-1.0	-	-	-	-	-	-	-	-	-	-	-	-	-	-	-	-	-	-	-	-	-	-	-	-	-	-	-	-	-	-	-
1.0-1.1	-	-	-	-	-	-	-	-	-	-	-	-	-	-	-	-	-	-	-	-	-	-	-	-	-	-	-	-	-	-	-
1.1-1.2	107.9	80.5	35.0	16.0	2	13.5	0.0	0.0	0.0	0	0	0	0	0	0	0	0	0	0	0	0	0	0	0	0	0	0	0	0	0	0
1.2-1.3	-	-	-	-	-	-	-	-	-	-	-	-	-	-	-	-	-	-	-	-	-	-	-	-	-	-	-	-	-	-	-
1.3-1.4	108.2	56.4	44.1	100.0	1	13.5	0.0	0.0	0.0	0	0	0	0	0	0	0	0	0	0	0	0	0	0	0	0	0	0	0	0	0	0
†569-23	101.1	132.0	24.2	0.0	9	12.5	11.1	0.4	2.5	48	12	0	0	0	0	1	0	2	1	6	3	11	8	4	6	5	0	0	0	1	0
0.0-0.1	97.9	236.2	47.1	29.0	3	12.0	9.9	0.4	2.2	26	5	0	0	0	0	1	0	2	1	5	2	8	4	1	1	1	0	0	0	0	0
0.1-0.2	99.4	160.6	34.8	9.0	2	12.2	11.7	0.5	1.8	13	2	0	0	0	0	0	0	0	0	1	1	2	3	2	3	1	0	0	0	0	0
0.2-0.3	100.8	73.9	22.5	100.0	1	12.4	12.0	0.0	0.0	1	1	0	0	0	0	0	0	0	0	0	0	0	0	1	0	0	0	0	0	0	0
0.3-0.4	-	-	-	-	-	-	-	-	-	-	-	-	-	-	-	-	-	-	-	-	-	-	-	-	-	-	-	-	-	-	-
0.4-0.5	103.5	64.7	29.6	100.0	1	12.7	18.3	0.0	0.0	1	1	0	0	0	0	0	0	0	0	0	0	0	0	0	0	0	0	0	0	1	0
0.5-0.6	-	-	-	-	-	-	-	-	-	-	-	-	-	-	-	-	-	-	-	-	-	-	-	-	-	-	-	-	-	-	-
0.6-0.7	105.2	86.2	49.8	100.0	1	12.9	0.0	0.0	0.0	0	0	0	0	0	0	0	0	0	0	0	0	0	0	0	0	0	0	0	0	0	0
0.7-0.8	-	-	-	-	-	-	-	-	-	-	-	-	-	-	-	-	-	-	-	-	-	-	-	-	-	-	-	-	-	-	-
0.8-0.9	-	-	-	-	-	-	-	-	-	-	-	-	-	-	-	-	-	-	-	-	-	-	-	-	-	-	-	-	-	-	-
0.9-1.0	-	-	-	-	-	-	-	-	-	-	-	-	-	-	-	-	-	-	-	-	-	-	-	-	-	-	-	-	-	-	-
1.0-1.1	107.4	0.0	0.0	0.0	0	13.2	13.3	0.0	0.0	1	1	0	0	0	0	0	0	0	0	0	0	0	0	0	1	0	0	0	0	0	0
1.1-1.2	-	-	-	-	-	-	-	-	-	-	-	-	-	-	-	-	-	-	-	-	-	-	-	-	-	-	-	-	-	-	-
1.2-1.3	-	-	-	-	-	-	-	-	-	-	-	-	-	-	-	-	-	-	-	-	-	-	-	-	-	-	-	-	-	-	-
1.3-1.4	-	-	-	-	-	-	-	-	-	-	-	-	-	-	-	-	-	-	-	-	-	-	-	-	-	-	-	-	-	-	-
1.4-1.5	107.9	90.8	15.9	100.0	1	13.3	12.9	0.8	1.7	5	1	0	0	0	0	0	0	0	0	0	0	1	1	0	1	2	0	0	0	0	0
1.5-1.6	108.0	0.0	0.0	0.0	0	13.3	14.3	0.0	0.0	1	1	0	0	0	0	0	0	0	0	0	0	0	0	0	0	1	0	0	0	0	0

* Fission Track Age and Mean Track Length predicted from the Default Thermal History (i.e. if the sample has not been hotter in the past)
† Combined data for all compositional groups

Table B.3: Continued - (Geotrack Report #569)

Cl Wt %	Default fission track age* (Ma)	Measured fission track age (Ma)	Error in age (Ma)	P (χ 2)	Number of grains	Default fission track length* (μm)	Mean track length (μm)	Error in length (μm)	Std deviation (μm)	Number of lengths	Number of grains	Number of tracks in length interval (μm) 1	2	3	4	5	6	7	8	9	10	11	12	13	14	15	16	17	18	19	20
†569-30	99.6	81.7	15.8	2.0	20	12.0	11.0	0.4	2.5	37	17	0	0	1	0	0	0	0	1	5	2	9	8	3	4	3	1	0	0	0	0
0.0-0.1	90.9	19.5	9.1	36.0	6	10.7	9.9	0.4	0.6	2	1	0	0	0	0	0	0	0	0	0	1	1	0	0	0	0	0	0	0	0	0
0.1-0.2	93.4	84.0	36.7	100.0	1	11.0	8.1	0.2	0.4	4	1	0	0	0	0	0	0	0	1	3	0	0	0	0	0	0	0	0	0	0	0
0.2-0.3	95.9	0.0	0.0	0.0	0	11.3	11.1	0.0	0.0	1	1	0	0	0	0	0	0	0	0	0	0	0	1	0	0	0	0	0	0	0	0
0.3-0.4	98.3	147.9	39.0	7.0	2	11.6	11.7	0.7	2.2	9	3	0	0	0	0	0	0	0	0	2	0	1	2	1	2	1	0	0	0	0	0
0.4-0.5	100.4	92.4	32.6	100.0	1	11.8	15.0	0.0	0.0	1	1	0	0	0	0	0	0	0	0	0	0	0	0	0	0	0	1	0	0	0	0
0.5-0.6	101.7	0.0	0.0	110.0	1	12.0	9.7	1.5	3.8	6	2	0	0	1	0	0	0	0	0	0	0	2	2	1	0	0	0	0	0	0	0
0.6-0.7	103.0	94.4	45.3	100.0	1	12.2	10.4	0.3	0.4	2	1	0	0	0	0	0	0	0	0	0	0	2	0	0	0	0	0	0	0	0	0
0.7-0.8	104.3	0.0	0.0	110.0	1	12.3	0.0	0.0	0.0	0	0	0	0	0	0	0	0	0	0	0	0	0	0	0	0	0	0	0	0	0	0
0.8-0.9	105.7	125.6	153.9	100.0	1	12.5	10.6	0.4	0.7	4	2	0	0	0	0	0	0	0	0	0	1	2	1	0	0	0	0	0	0	0	0
0.9-1.0	105.9	167.0	76.3	100.0	1	12.5	13.4	0.0	0.0	1	1	0	0	0	0	0	0	0	0	0	0	0	0	0	1	0	0	0	0	0	0
1.0-1.1	106.1	117.3	53.8	100.0	1	12.5	14.4	0.3	0.5	3	1	0	0	0	0	0	0	0	0	0	0	0	0	0	1	2	0	0	0	0	0
1.1-1.2	-	-	-	-	-	-	-	-	-	-	-	-	-	-	-	-	-	-	-	-	-	-	-	-	-	-	-	-	-	-	-
1.2-1.3	106.5	279.3	135.9	100.0	1	12.6	0.0	0.0	0.0	0	0	0	0	0	0	0	0	0	0	0	0	0	0	0	0	0	0	0	0	0	0
1.3-1.4	106.7	0.0	0.0	0.0	0	12.6	11.7	0.0	0.0	1	1	0	0	0	0	0	0	0	0	0	0	0	1	0	0	0	0	0	0	0	0
1.4-1.5	-	-	-	-	-	-	-	-	-	-	-	-	-	-	-	-	-	-	-	-	-	-	-	-	-	-	-	-	-	-	-
1.5-1.6	-	-	-	-	-	-	-	-	-	-	-	-	-	-	-	-	-	-	-	-	-	-	-	-	-	-	-	-	-	-	-
1.6-1.7	-	-	-	-	-	-	-	-	-	-	-	-	-	-	-	-	-	-	-	-	-	-	-	-	-	-	-	-	-	-	-
1.7-1.8	107.5	72.1	57.8	100.0	1	12.7	11.7	0.0	0.0	1	1	0	0	0	0	0	0	0	0	0	0	0	1	0	0	0	0	0	0	0	0
1.8-1.9	107.7	161.1	68.9	100.0	1	12.7	11.4	0.7	0.9	2	1	0	0	0	0	0	0	0	0	0	0	1	0	1	0	0	0	0	0	0	0
1.9-2.0	107.8	100.7	84.3	100.0	1	12.7	0.0	0.0	0.0	0	0	0	0	0	0	0	0	0	0	0	0	0	0	0	0	0	0	0	0	0	0

* Fission Track Age and Mean Track Length predicted from the Default Thermal History (i.e. if the sample has not been hotter in the past)
† Combined data for all compositional groups

Table B.3: Continued - (Geotrack Report #569)

Cl Wt %	Default fission track age* (Ma)	Measured fission track age (Ma)	Error in age (Ma)	P (χ 2)	Number of grains	Default fission track length* (μm)	Mean track length (μm)	Error in length (μm)	Std deviation (μm)	Number of lengths	Number of grains	Number of tracks in length interval 1	2	3	4	5	6	7	8	9	10	11	12	13	14	15	16	17	18	19	20
												(μm)																			
†569-25	94.8	108.9	25.8	0.0	9	11.6	11.1	0.7	2.5	12	6	0	0	0	0	0	0	0	1	1	2	3	1	1	1	1	1	0	0	0	0
0.0-0.1	82.9	62.7	15.7	83.0	3	10.2	14.7	1.0	1.5	2	1	0	0	0	0	0	0	0	0	0	0	0	0	0	1	0	1	0	0	0	0
0.1-0.2	90.8	264.1	65.8	100.0	1	10.6	9.3	0.5	1.1	6	1	0	0	0	0	0	0	0	1	1	2	2	0	0	0	0	0	0	0	0	0
0.2-0.3	-	-	-	-	-	-	-	-	-	-	-	-	-	-	-	-	-	-	-	-	-	-	-	-	-	-	-	-	-	-	-
0.3-0.4	96.7	203.1	40.8	100.0	1	11.2	0.0	0.0	0.0	0	0	0	0	0	0	0	0	0	0	0	0	0	0	0	0	0	0	0	0	0	0
0.4-0.5	-	-	-	-	-	-	-	-	-	-	-	-	-	-	-	-	-	-	-	-	-	-	-	-	-	-	-	-	-	-	-
0.5-0.6	100.7	0.0	0.0	0.0	0	11.7	11.5	0.0	0.0	1	1	0	0	0	0	0	0	0	0	0	0	0	1	0	0	0	0	0	0	0	0
0.6-0.7	102.2	70.9	23.1	54.0	2	11.9	12.1	0.0	0.0	1	1	0	0	0	0	0	0	0	0	0	0	0	0	1	0	0	0	0	0	0	0
0.7-0.8	-	-	-	-	-	-	-	-	-	-	-	-	-	-	-	-	-	-	-	-	-	-	-	-	-	-	-	-	-	-	-
0.8-0.9	-	-	-	-	-	-	-	-	-	-	-	-	-	-	-	-	-	-	-	-	-	-	-	-	-	-	-	-	-	-	-
0.9-1.0	-	-	-	-	-	-	-	-	-	-	-	-	-	-	-	-	-	-	-	-	-	-	-	-	-	-	-	-	-	-	-
1.0-1.1	-	-	-	-	-	-	-	-	-	-	-	-	-	-	-	-	-	-	-	-	-	-	-	-	-	-	-	-	-	-	-
1.1-1.2	105.9	216.4	73.6	100.0	1	12.3	14.5	0.0	0.0	1	1	0	0	0	0	0	0	0	0	0	0	0	0	0	0	1	0	0	0	0	0
1.2-1.3	-	-	-	-	-	-	-	-	-	-	-	-	-	-	-	-	-	-	-	-	-	-	-	-	-	-	-	-	-	-	-
1.3-1.4	106.4	41.7	22.5	100.0	1	12.4	10.0	0.0	0.0	1	1	0	0	0	0	0	0	0	0	0	0	1	0	0	0	0	0	0	0	0	0
Borda-1																															
†569-13	59.8	65.5	23.3	100.0	1	12.1	10.0	1.1	2.2	4	1	0	0	0	0	0	0	0	1	0	2	0	0	1	0	0	0	0	0	0	0
0.0-0.1	-	-	-	-	-	-	-	-	-	-	-	-	-	-	-	-	-	-	-	-	-	-	-	-	-	-	-	-	-	-	-
0.1-0.2	-	-	-	-	-	-	-	-	-	-	-	-	-	-	-	-	-	-	-	-	-	-	-	-	-	-	-	-	-	-	-
0.2-0.3	59.8	65.5	23.3	100.0	1	12.1	10.0	1.1	2.2	4	1	0	0	0	0	0	0	0	1	0	2	0	0	1	0	0	0	0	0	0	0

* Fission Track Age and Mean Track Length predicted from the Default Thermal History (i.e. if the sample has not been hotter in the past)
† Combined data for all compositional groups

Estimates	z_i
Standard errors	σ_i
Reference value	z_o
Standardised estimates	$y_i = (z_i - z_o) / \sigma_i$
Precision	$x_i = 1 / \sigma_i$

PLOT y_i against x_i

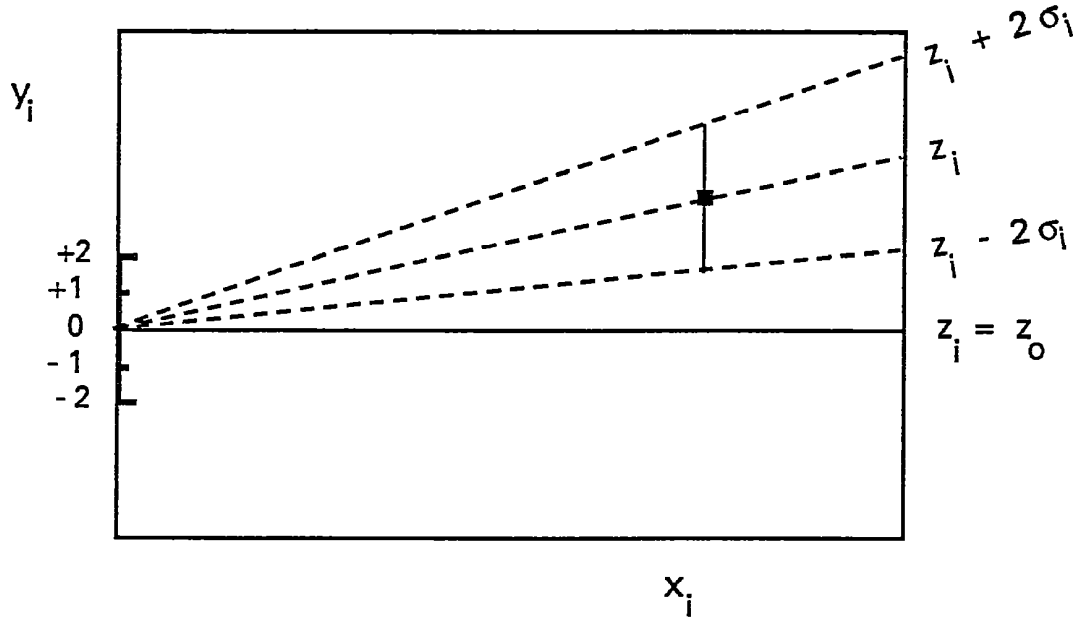

Slope of line from origin through data point $= y_i / x_i$

$= \{(z_i - z_o)/\sigma_i\} / \{1/\sigma_i\}$

$= z_i - z_o$

Key Points:

Radial lines emanating from the origin correspond to fixed values of z

Data points with higher values of x_i have greater precision.

Error bars on all points are the same size in this plot.

Figure B.1 Basic construction of a radial plot. In AFTA, the estimates z_i correspond to the fission track age values for individual apatite grains. Any convenient value of age can be chosen as the reference value corresponding to the horizontal in the radial plot. Radial lines emanating from the origin with positive slopes correspond to fission track ages greater than the reference value. Lines with negative slopes correspond to fission track ages less than the reference value.

Normal radial plot (equations B.2 and B.3)

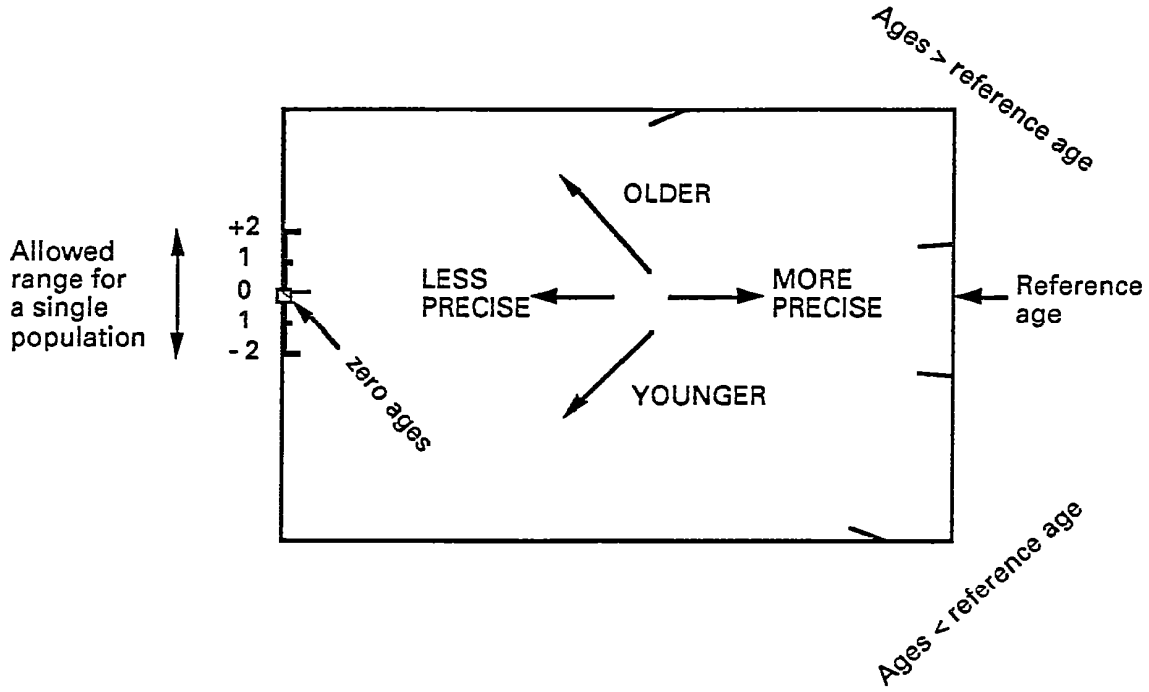

Arc-sin radial plot (equations B.2 and B.4)

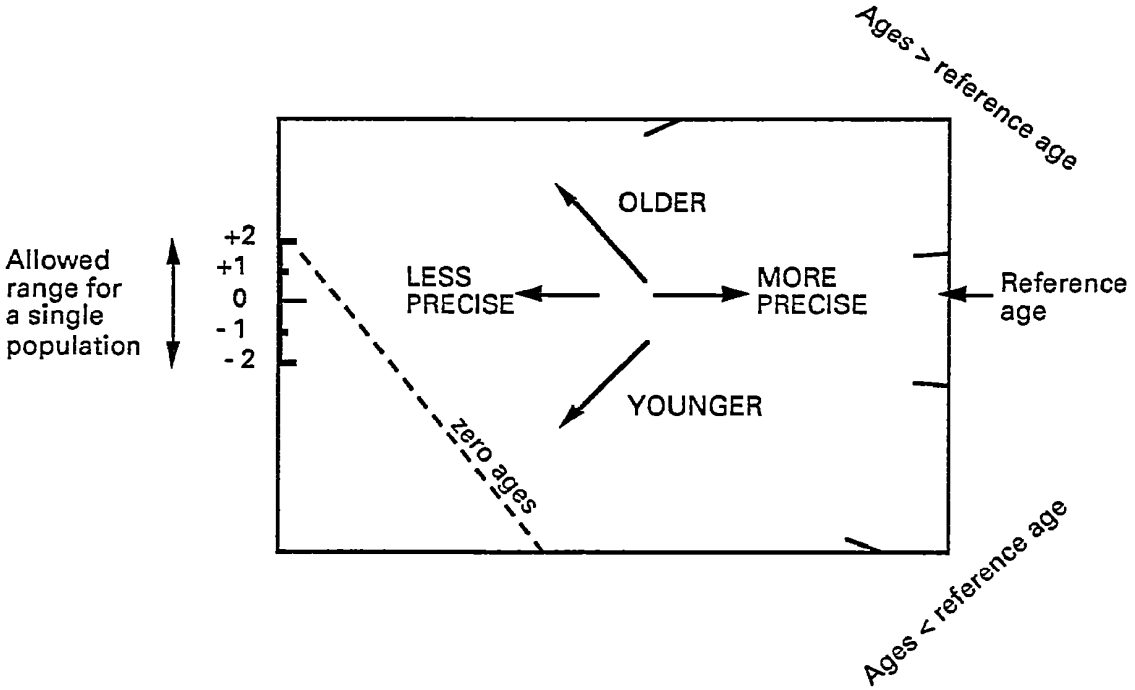

Figure B.2 Simplified structure of Normal and Arc-sin radial plots.

GC569-16

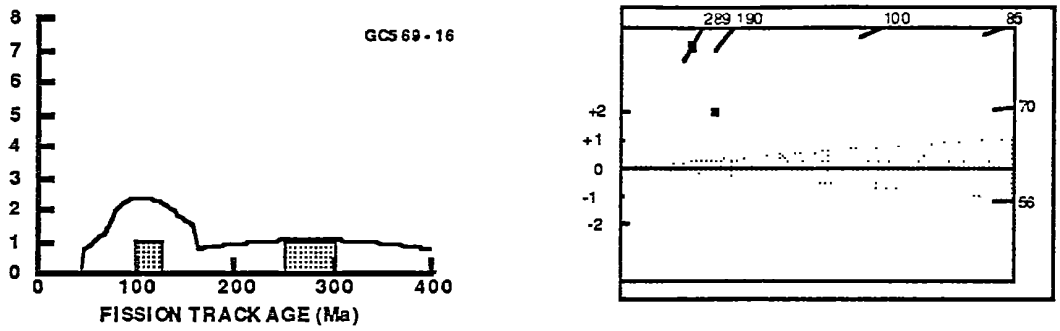

GC569-17
No Apatite

GC569-28

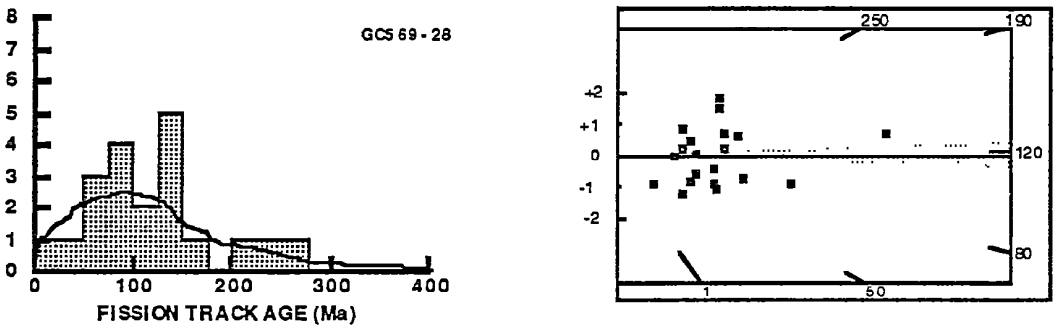

GC569-29

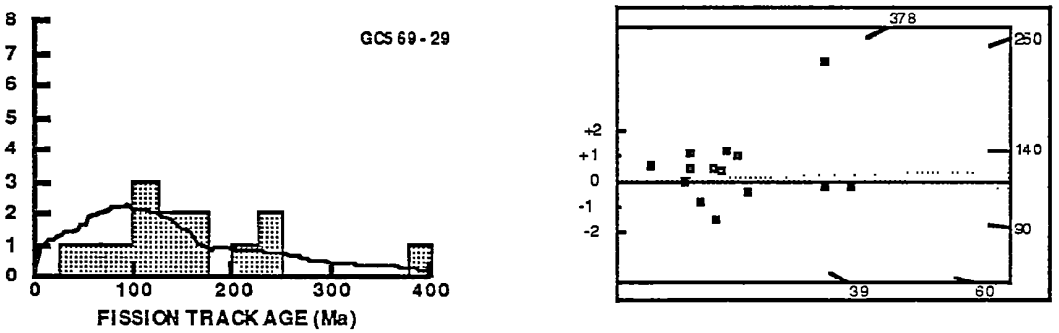

Figure B.3a: Single grain age figures for samples from **well Vivonne-1, Duntroon Basin.** See Appendix B for further details.

GC569-23

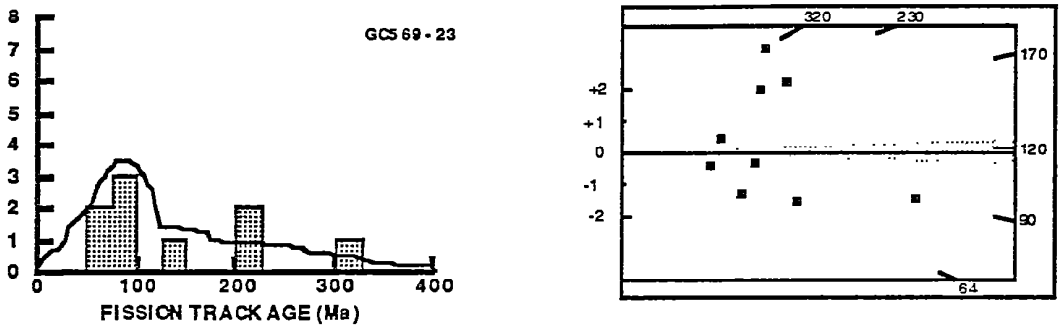

GC569-30

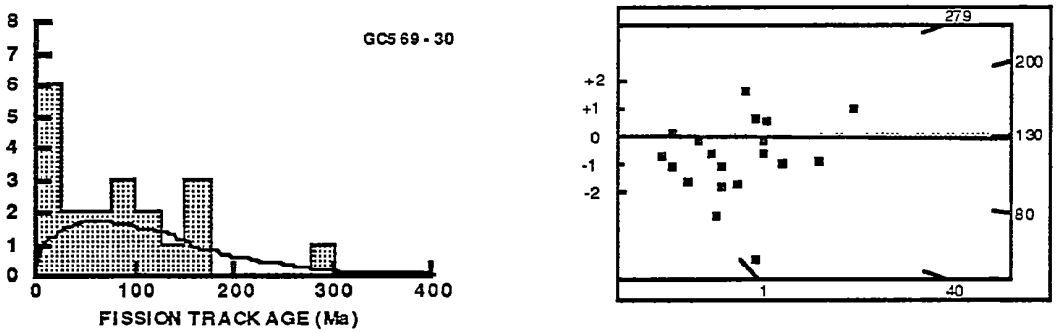

GC569-25

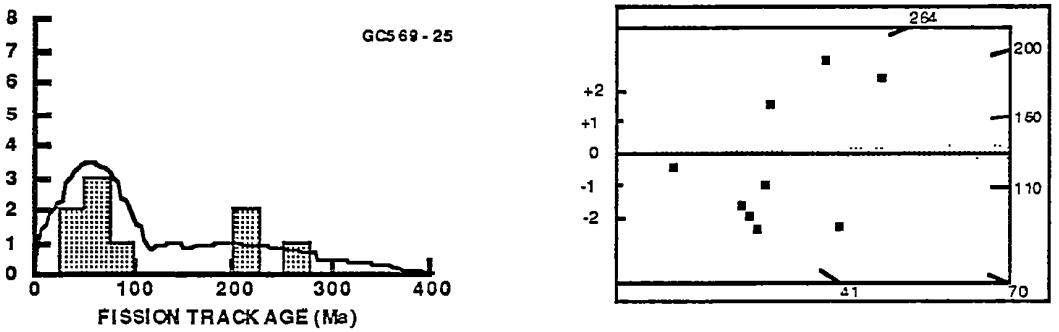

Figure B.3a: Continued.

GC569-8
No Apatite

GC569-13

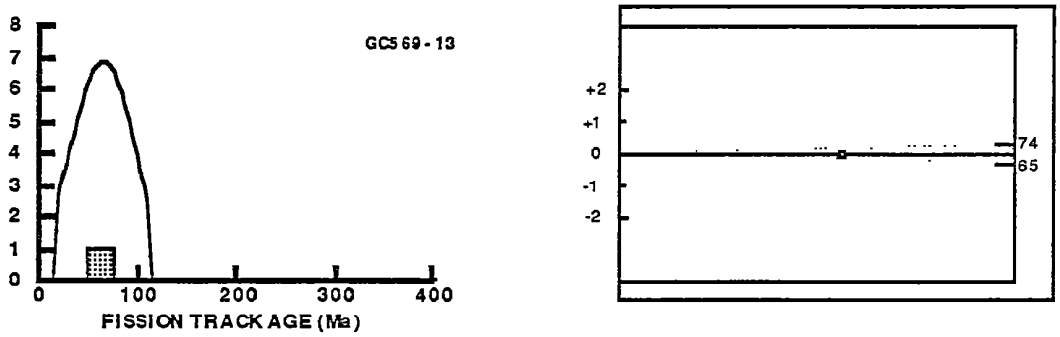

Figure B.3b: Single grain age figures for samples from **well Borda-1, Duntroon Basin.** See Appendix B for further details.

GC567-16

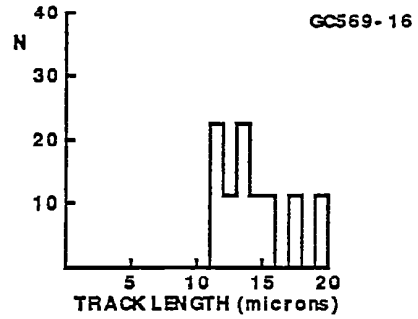

GC567-23

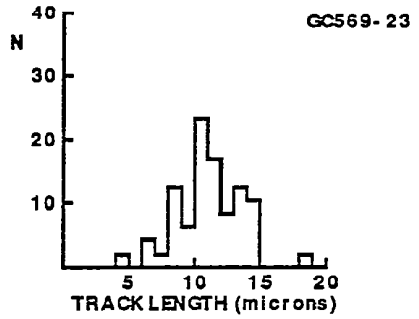

GC567-17

No Apatite

GC567-30

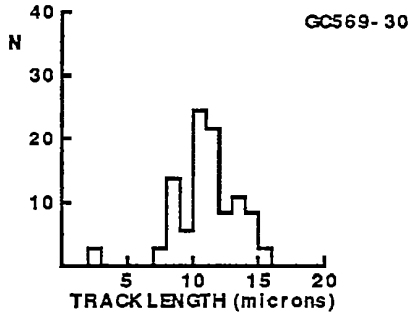

GC567-28

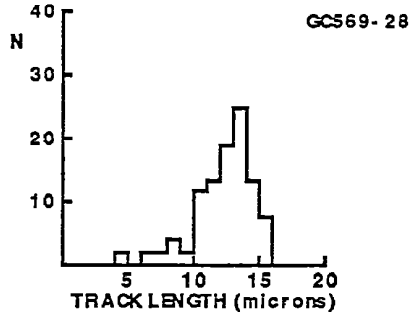

GC567-25

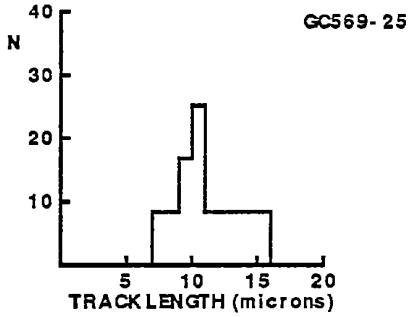

GC567-29

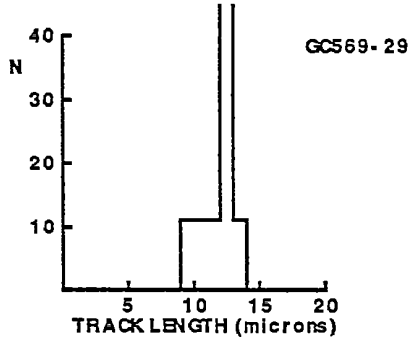

Figure B.4a: Length distributions in samples from well **Vivonne-1, Duntroon Basin.**

GC567-8

No Apatite

GC567-13

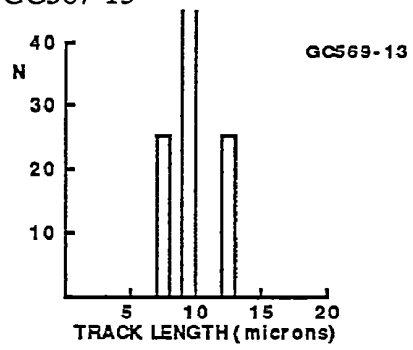

Figure B.4b: Length distributions in samples from well **Borda-1, Duntroon Basin.**

GC569-16

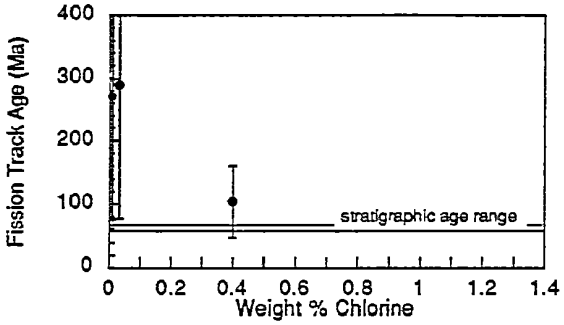

GC569-23

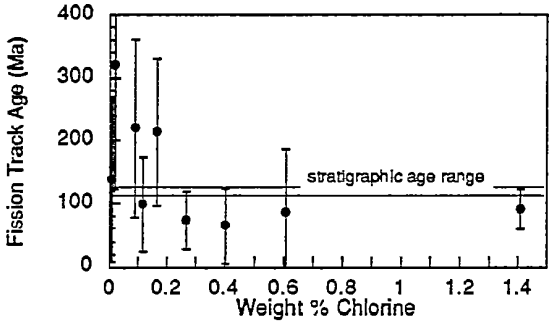

GC569-17

No Apatite

GC569-30

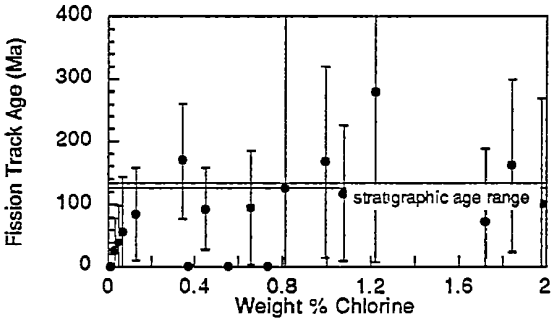

GC569-28

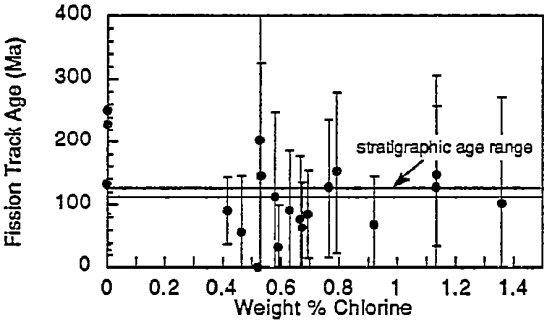

GC569-25

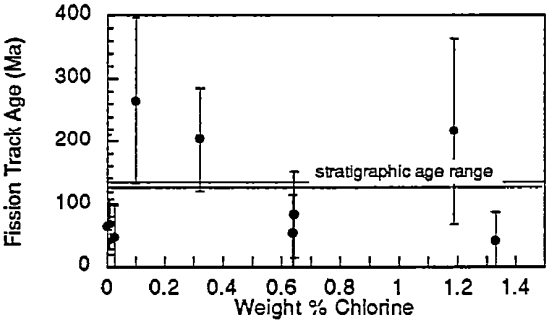

GC569-29

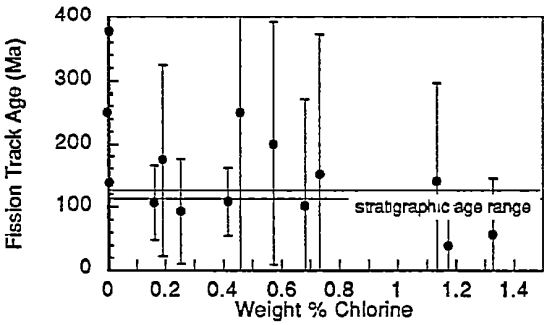

Figure B.5a: Plots of single grain age against weight percent chlorine for samples from well **Vivonne-1, Duntroon Basin.**

GC569-8

No Apatite

GC569-13

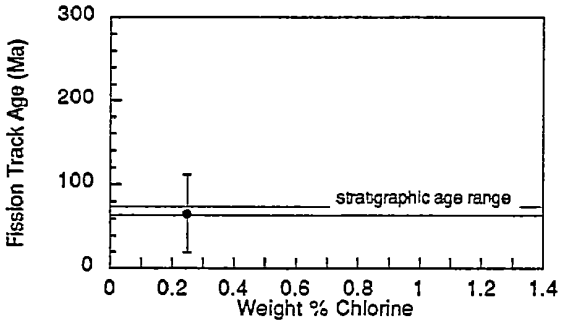

Figure B.5b: Plots of single grain age against weight percent chlorine for samples from well **Borda-1, Duntroon Basin.**

Fission Track Age Data Sheets - Glossary

Ns	=	Number of spontaneous tracks in Na grid squares
Ni	=	Number of induced tracks in Na grid squares
Na	=	Number of grid squares counted in each grain
RATIO	=	Ns/Ni
U (ppm)	=	Uranium content of each grain (= U content of standard glass * $\rho i/\rho_D$)
Cl (wt%)	=	Weight percent chlorine content of each grain
RHOs	=	Spontaneous track density (ρs) = Ns/ (Na*area of basic unit)
RHOi	=	Induced track density (ρi) = Ni/(Na*area of basic unit)
F.T. AGE	=	Fission track age, calculated using equation B.1
Area of basic unit	=	Area of one grid square
Chi squared	=	χ^2 parameter, used to assess variation of single grain ages within the sample
P(chi squared)	=	Probability of obtaining observed χ^2 value for the relevant number of degrees of freedom, if all grains belong to a single population
Correlation coefficient	=	Correlation coefficient between Ns and Ni
Variance of SQR(Ns)	=	Variance of square root of Ns values - should be ~ 0.25 for Poisson distribution; greater if additional variation present
Variance of SQR(Ni)	=	Variance of square root of Ni values - should be ~ 0.25 for Poisson distribution; greater if additional variation present
Age Dispersion	=	% variation in single grain ages - see discussion in text re "Central age"
Ns/Ni	=	Pooled ratio, total spontaneous tracks divided by total induced tracks for all grains
Mean ratio	=	Mean of (Ns/Ni) for individual grains
Zeta	=	Calibration constant, determined empirically for each observer
RhoD	=	Track density (ρ_D) from uranium standard glass (interpolated from values at each end of stack)
ND	=	Total number of tracks counted for determining ρ_D
POOLED AGE	=	Fission track age calculated from pooled ratio Ns/Ni. Valid only when $\chi^2 > 5\%$
CENTRAL AGE	=	Alternative to pooled age when $\chi^2 < 5\%$

GC569-13 APATITE

IRRADIATION G540
SLIDE NUMBER 2
COUNTED BY: MEM

Current grain no.	Ns	Ni	Na	RHOs	RHOi	RATIO	U (ppm)	Cl (wt%)	F.T. AGE (Ma)
3	10	39	10	1.589E+06	6.197E+06	0.256	54.1	0.26	65.5 ± 23.3
	10	39		1.589E+06	6.197E+06		54.1		

Area of basic unit = 6.293E-07 cm-2

Ns/Ni = 0.256 ± 0.091

Ages calculated using a zeta of 392.9 ± 7.4 for CN5 glass
Rho D = 1.306E+06cm-2; ND = 2112
Rho D interpolated between top of can; Rho D = 1.300E+06cm-2, ND = 1023
bottom of can; Rho D = 1.384E+06cm-2, ND = 1089

POOLED AGE = 65.5 ± 23.3 Ma

GC569-16 APATITE

IRRADIATION G540
SLIDE NUMBER 4
COUNTED BY: MEM

Current grain no.	Ns	Ni	Na	RHOs	RHOi	RATIO	U (ppm)	Cl (wt%)	F.T. AGE (Ma)
3	19	47	50	6.038E+05	1.494E+06	0.404	12.9	0.40	103.9 ± 28.4
4	16	15	24	1.059E+06	9.932E+05	1.067	8.6	0.01	270.5 ± 97.5
7	16	14	15	1.695E+06	1.483E+06	1.143	12.8	0.03	289.4 ± 106.2
	51	76		9.106E+05	1.357E+06		11.7		

Area of basic unit = 6.293E-07 cm-2

Chi Squared = 7.410 with 2 degrees of freedom
P(chi squared) = 2.5 %
Correlation Coefficient = 1.000
Variance of SQR(Ns) = 0.04
Variance of SQR(Ni) = 3.10
Age Dispersion = 37.709 %

Ns/Ni = 0.671 ± 0.121
Mean Ratio = 0.871 ± 0.235

Ages calculated using a zeta of 392.9 ± 7.4 for CN5 glass
Rho D = 1.318E+06cm-2; ND = 2112
Rho D interpolated between top of can; Rho D = 1.300E+06cm-2, ND = 1023
bottom of can; Rho D = 1.384E+06cm-2, ND = 1089

POOLED AGE = 171.5 ± 31.4 Ma
CENTRAL AGE = 192.1 ± 55.0 Ma

GC569-23 APATITE

IRRADIATION G540
SLIDE NUMBER 5
COUNTED BY: MEM

Current grain no.	Ns	Ni	Na	RHOs	RHOi	RATIO	U (ppm)	Cl (wt%)	F.T. AGE (Ma)
3	24	19	28	1.362E+06	1.078E+06	1.263	9.3	0.02	320.6 ± 98.9
6	14	49	32	6.952E+05	2.433E+06	0.286	20.9	0.27	73.9 ± 22.5
7	45	128	30	2.384E+06	6.780E+06	0.352	58.4	1.41	90.8 ± 16.0
8	10	26	40	3.973E+05	1.033E+06	0.385	8.9	0.12	99.3 ± 37.1
10	4	12	42	1.513E+05	4.540E+05	0.333	3.9	0.61	86.2 ± 49.8
11	6	24	25	3.814E+05	1.526E+06	0.250	13.1	0.40	64.7 ± 29.6
14	25	30	30	1.324E+06	1.589E+06	0.833	13.7	0.17	213.3 ± 58.1
20	7	13	40	2.781E+05	5.164E+05	0.538	4.4	0.01	138.6 ± 65.1
21	18	21	54	5.297E+05	6.180E+05	0.857	5.3	0.09	219.3 ± 70.7
	153	322		7.574E+05	1.594E+06		13.7		

Area of basic unit = 6.293E-07 cm-2

Chi Squared = 27.610 with 8 degrees of freedom
P(chi squared) = 0.1 %
Correlation Coefficient = 0.823
Variance of SQR(Ns) = 2.26
Variance of SQR(Ni) = 5.80
Age Dispersion = 43.930 %

Ns/Ni = 0.475 ± 0.047
Mean Ratio = 0.566 ± 0.115

Ages calculated using a zeta of 392.9 ± 7.4 for CN5 glass
Rho D = 1.324E+06cm-2; ND = 2112
Rho D interpolated between top of can; Rho D = 1.300E+06cm-2, ND = 1023
bottom of can; Rho D = 1.384E+06cm-2, ND = 1089

POOLED AGE = 122.5 ± 12.5 Ma
CENTRAL AGE = 132.0 ± 24.5 Ma

GC569-25 APATITE

IRRADIATION G540
SLIDE NUMBER 6
COUNTED BY: MEM

Current grain no.	Ns	Ni	Na	RHOs	RHOi	RATIO	U (ppm)	Cl (wt%)	F.T. AGE (Ma)
3	1	4	32	4.966E+04	1.986E+05	0.250	1.7	0.00	65.0 ± 72.7
4	8	25	42	3.027E+05	9.459E+05	0.320	8.1	0.64	83.1 ± 33.8
5	33	32	32	1.639E+06	1.589E+06	1.031	13.6	0.10	264.1 ± 66.0
8	4	25	40	1.589E+05	9.932E+05	0.160	8.5	1.33	41.7 ± 22.5
10	16	19	50	5.085E+05	6.038E+05	0.842	5.2	1.19	216.4 ± 73.7
11	15	57	32	7.449E+05	2.831E+06	0.263	24.3	0.01	68.4 ± 20.0
12	4	22	45	1.412E+05	7.769E+05	0.182	6.7	0.03	47.3 ± 25.8
13	45	57	30	2.384E+06	3.019E+06	0.789	25.9	0.32	203.1 ± 40.9
14	4	19	30	2.119E+05	1.006E+06	0.211	8.6	0.64	54.8 ± 30.2
	130	260		6.204E+05	1.241E+06		10.6		

Area of basic unit = 6.293E-07 cm-2

Chi Squared = 34.717 with 8 degrees of freedom
P(chi squared) = 0.0 %
Correlation Coefficient = 0.700
Variance of SQR(Ns) = 3.62
Variance of SQR(Ni) = 2.90
Age Dispersion = 59.583 %

Ns/Ni = 0.500 ± 0.054
Mean Ratio = 0.450 ± 0.113

Ages calculated using a zeta of 392.9 ± 7.4 for CN5 glass
Rho D = 1.330E+06cm-2; ND = 2112
Rho D interpolated between top of can; Rho D = 1.300E+06cm-2, ND = 1023
bottom of can; Rho D = 1.384E+06cm-2, ND = 1089

POOLED AGE = 129.4 ± 14.4 Ma
CENTRAL AGE = 108.9 ± 25.9 Ma

GC569-28 APATITE

IRRADIATION G547
SLIDE NUMBER 1
COUNTED BY: MEM

Current grain no.	Ns	Ni	Na	RHOs	RHOi	RATIO	U (ppm)	Cl (wt%)	F.T. AGE (Ma)
3	4	9	16	3.973E+05	8.938E+05	0.444	7.8	0.58	112.7 ± 67.8
4	11	19	40	4.370E+05	7.548E+05	0.579	6.6	1.14	146.4 ± 55.6
6	4	5	18	3.531E+05	4.414E+05	0.800	3.9	0.53	201.4 ± 135.2
7	11	11	15	1.165E+06	1.165E+06	1.000	10.2	0.00	250.8 ± 107.2
8	2	9	21	1.513E+05	6.810E+05	0.222	6.0	0.47	56.6 ± 44.3
9	8	16	40	3.178E+05	6.356E+05	0.500	5.6	0.77	126.6 ± 55.0
11	10	11	25	6.356E+05	6.992E+05	0.909	6.1	0.00	228.4 ± 100.0
12	5	14	30	2.648E+05	7.416E+05	0.357	6.5	0.63	90.7 ± 47.3
13	1	8	28	5.675E+04	4.540E+05	0.125	4.0	0.59	31.9 ± 33.8
14	8	24	48	2.648E+05	7.945E+05	0.333	7.0	0.70	84.7 ± 34.7
17	3	10	30	1.589E+05	5.297E+05	0.300	4.6	0.67	76.3 ± 50.3
18	4	16	40	1.589E+05	6.356E+05	0.250	5.6	0.67	63.6 ± 35.6
21	0	3	20	0.000E+00	2.384E+05	0.000	2.1	0.52	0.0 ± 0.0
22	16	45	15	1.695E+06	4.767E+06	0.356	41.7	0.42	90.3 ± 26.4
26	49	94	16	4.867E+06	9.336E+06	0.521	81.8	0.00	132.0 ± 23.6
30	3	6	16	2.980E+05	5.959E+05	0.500	5.2	1.13	126.6 ± 89.6
31	9	15	24	5.959E+05	9.932E+05	0.600	8.7	0.79	151.6 ± 64.1
32	4	15	25	2.542E+05	9.534E+05	0.267	8.3	0.92	67.8 ± 38.2
34	2	5	8	3.973E+05	9.932E+05	0.400	8.7	1.36	101.5 ± 85.0
35	4	7	40	1.589E+05	2.781E+05	0.571	2.4	0.53	144.5 ± 90.7
	158	342		4.875E+05	1.055E+06		9.2		

Area of basic unit = 6.293E-07 cm-2

Chi Squared = 16.449 with 19 degrees of freedom
P(chi squared) = 62.7 %
Correlation Coefficient = 0.960
Variance of SQR(Ns) = 2.00
Variance of SQR(Ni) = 3.17
Age Dispersion = 1.507 % (did not converge)

Ns/Ni = 0.462 ± 0.044
Mean Ratio = 0.452 ± 0.056

Ages calculated using a zeta of 392.9 ± 7.4 for CN5 glass
Rho D = 1.302E+06cm-2; ND = 1987
Rho D interpolated between top of can; Rho D = 1.302E+06cm-2, ND = 1024
bottom of can; Rho D = 1.224E+06cm-2, ND = 963

POOLED AGE = 117.1 ± 11.8 Ma
CENTRAL AGE = 117.1 ± 11.8 Ma

GC569-29 APATITE

IRRADIATION G547
SLIDE NUMBER 2
COUNTED BY: MEM

Current grain no.	Ns	Ni	Na	RHOs	RHOi	RATIO	U (ppm)	Cl (wt%)	F.T. AGE (Ma)
3	1	1	14	1.135E+05	1.135E+05	1.000	1.0	0.00	249.8 ± 353.4
4	7	19	30	3.708E+05	1.006E+06	0.368	8.8	0.25	93.2 ± 41.3
5	2	5	8	3.973E+05	9.932E+05	0.400	8.7	0.68	101.1 ± 84.6
8	38	25	24	2.516E+06	1.655E+06	1.520	14.6	0.01	376.0 ± 97.5
9	24	56	42	9.080E+05	2.119E+06	0.429	18.6	0.42	108.3 ± 26.6
10	2	13	9	3.531E+05	2.295E+06	0.154	20.2	1.18	39.1 ± 29.7
12	6	11	10	9.534E+05	1.748E+06	0.545	15.4	0.01	137.5 ± 69.9
14	2	9	16	1.986E+05	8.938E+05	0.222	7.9	1.33	56.4 ± 44.1
15	9	13	16	8.938E+05	1.291E+06	0.692	11.4	0.19	174.0 ± 75.6
16	4	4	24	2.648E+05	2.648E+05	1.000	2.3	0.46	249.8 ± 176.8
18	3	5	16	2.980E+05	4.966E+05	0.600	4.4	0.73	151.0 ± 110.4
20	8	10	30	4.238E+05	5.297E+05	0.800	4.7	0.57	200.6 ± 95.3
22	5	9	15	5.297E+05	9.534E+05	0.556	8.4	1.14	140.0 ± 78.2
23	19	45	18	1.677E+06	3.973E+06	0.422	34.9	0.16	106.7 ± 29.3
	130	225		7.595E+05	1.314E+06		11.6		

Area of basic unit = 6.293E-07 cm-2

Chi Squared = 25.884 with 13 degrees of freedom
P(chi squared) = 1.8 %
Correlation Coefficient = 0.719
Variance of SQR(Ns) = 2.25
Variance of SQR(Ni) = 3.18
Age Dispersion = 40.278 %

Ns/Ni = 0.578 ± 0.064
Mean Ratio = 0.622 ± 0.097

Ages calculated using a zeta of 392.9 ± 7.4 for CN5 glass
Rho D = 1.297E+06cm-2; ND = 1987
Rho D interpolated between top of can; Rho D = 1.302E+06cm-2, ND = 1024
bottom of can; Rho D = 1.224E+06cm-2, ND = 963

POOLED AGE = 145.5 ± 16.6 Ma
CENTRAL AGE = 140.1 ± 23.9 Ma

GC569-30 APATITE

IRRADIATION G547
SLIDE NUMBER 3
COUNTED BY: MEM

Current grain no.	Ns	Ni	Na	RHOs	RHOi	RATIO	U (ppm)	Cl (wt%)	F.T. AGE (Ma)
5	7	21	20	5.562E+05	1.669E+06	0.333	14.7	0.13	84.0 ± 36.8
6	0	3	24	0.000E+00	1.986E+05	0.000	1.8	0.02	0.0 ± 0.0
7	23	34	12	3.046E+06	4.502E+06	0.676	39.7	0.35	169.4 ± 46.0
8	1	10	24	6.621E+04	6.621E+05	0.100	5.8	0.03	25.3 ± 26.6
9	2	7	18	1.766E+05	6.180E+05	0.286	5.5	1.72	72.1 ± 57.8
10	6	16	28	3.405E+05	9.080E+05	0.375	8.0	0.66	94.4 ± 45.3
11	9	14	16	8.938E+05	1.390E+06	0.643	12.3	1.84	161.1 ± 69.0
12	0	10	35	0.000E+00	4.540E+05	0.000	4.0	0.01	0.0 ± 0.0
13	2	5	9	3.531E+05	8.828E+05	0.400	7.8	1.98	100.7 ± 84.3
14	0	2	28	0.000E+00	1.135E+05	0.000	1.0	0.56	0.0 ± 0.0
15	8	12	30	4.238E+05	6.356E+05	0.667	5.6	1.00	167.0 ± 76.4
17	9	8	24	5.959E+05	5.297E+05	1.125	4.7	1.22	279.3 ± 136.0
18	0	5	15	0.000E+00	5.297E+05	0.000	4.7	0.37	0.0 ± 0.0
19	0	3	18	0.000E+00	2.648E+05	0.000	2.3	0.73	0.0 ± 0.0
20	0	20	24	0.000E+00	1.324E+06	0.000	11.7	0.02	0.0 ± 0.0
21	2	9	42	7.567E+04	3.405E+05	0.222	3.0	0.07	56.1 ± 43.9
22	7	15	40	2.781E+05	5.959E+05	0.467	5.3	1.08	117.3 ± 53.8
24	11	30	40	4.370E+05	1.192E+06	0.367	10.5	0.45	92.4 ± 32.7
25	1	2	15	1.059E+05	2.119E+05	0.500	1.9	0.81	125.6 ± 153.9
26	2	13	15	2.119E+05	1.377E+06	0.154	12.2	0.05	38.9 ± 29.6
	90	239		2.998E+05	7.962E+05		7.0		

Area of basic unit = 6.293E-07 cm-2

Chi Squared = 34.130 with 19 degrees of freedom
P(chi squared) = 1.8 %
Correlation Coefficient = 0.784
Variance of SQR(Ns) = 1.98
Variance of SQR(Ni) = 1.59
Age Dispersion = 57.662 %

Ns/Ni = 0.377 ± 0.047
Mean Ratio = 0.316 ± 0.068

Ages calculated using a zeta of 392.9 ± 7.4 for CN5 glass
Rho D = 1.291E+06cm-2; ND = 1987
Rho D interpolated between top of can; Rho D = 1.302E+06cm-2, ND = 1024
bottom of can; Rho D = 1.224E+06cm-2, ND = 963

POOLED AGE = 94.8 ± 12.1 Ma
CENTRAL AGE = 81.7 ± 16.0 Ma

APPENDIX C

Principles of Interpretation of AFTA Data in Sedimentary Basins

C.1 Introduction

Detrital apatite grains are incorporated into sedimentary rocks from three dominant sources - crystalline basement rocks, older sediments and contemporaneous volcanism. Apatites derived from the first two sources will, in general, contain fission tracks when they are deposited, with AFTA parameters characteristic of the source regions. However, apatites derived from contemporaneous volcanism, or from rapidly uplifted basement, will contain no tracks when they are deposited. For now, we will restrict discussion to this situation, and generalise at a later point to cover the case of apatites which contain tracks that have been inherited from source regions.

C.2 Basic principles of Apatite Fission Track Analysis

Fission tracks are trails of radiation damage, which are produced within apatite grains at a more or less constant rate through geological time, as a result of the spontaneous fission of ^{238}U impurity atoms. Therefore, the number of fission events which occur within an apatite grain during a fixed time interval depends on the magnitude of the time interval and the uranium content of the grain. Each fission event leads to the formation of a single fission track, and the proportion of tracks which can intersect a polished surface of an apatite grain depends on the length of the tracks. Therefore, the number of tracks which are etched in unit area of the surface of an apatite grain (the "spontaneous track density") depends on three factors - (i) The time over which tracks have been accumulating; (ii) The uranium content of the apatite grain; and, (iii) The distribution of track lengths in the grain. In sedimentary rocks which have not been subjected to temperatures greater than ~50°C since deposition, spontaneous fission tracks have a characteristic distribution of confined track lengths, with a mean length in the range 14-15 μm and a standard deviation of ~1 μm. In such samples, by measuring the spontaneous track density and the uranium content of a collection of apatite grains, a "fission track age" can be calculated which will be equal to the time over which tracks have been accumulating. The technique is calibrated against other isotopic systems using age standards which also have this type of length distribution (see Appendix B).

In samples which have been subjected to temperatures greater than ~50°C after deposition, fission tracks are shortened because of the gradual repair of the radiation damage which

constitutes the unetched tracks. In effect, the tracks shrink from each end, in a process which is known as fission track "annealing". The final length of each individual track is essentially determined by the maximum temperature which that track has experienced. A time difference of an order of magnitude produces a change in fission track parameters which is equivalent to a temperature change of only ~10°C, so temperature is by far the dominant factor in determining the final fission track parameters. As temperature increases, all existing tracks shorten to a length determined by the prevailing temperature, regardless of when they were formed. After the temperature has subsequently decreased, all tracks formed prior to the thermal maximum are "frozen" at the degree of length reduction they attained at that time. Thus, the length of each track can be thought of as a maximum-reading thermometer, recording the maximum temperature to which it has been subjected.

Therefore, in samples for which the present temperature is maximum, all tracks have much the same length, resulting in a narrow, symmetric distribution. The degree of shortening will depend on the temperature, with the mean track length falling progressively from ~14 μm at 50°C, to zero at around 110°-120°C - the precise temperature depending on the timescale of heating and the composition of the apatites present in the sample (see below). Values quoted here relate to times of the order of 10^7-10^8 years and average apatite composition. If the effective timescale of heating is shorter than 10^7-10^8 years, the temperature responsible for a given degree of track shortening will be higher, depending in detail on the kinetics of the annealing process (Green et al., 1986; Laslett et al., 1987; Duddy et al., 1988; Green et al., 1989b). Shortening of tracks produces an accompanying reduction in the fission track age, because of the reduced proportion of tracks which can intersect the polished surface. Therefore, the fission track age is also highly temperature dependent, falling to zero at around 120°C due to total erasure of all tracks.

Complex thermal histories produce correspondingly complex length distributions and ages. Samples which have cooled from a thermal maximum (with peak temperature between ~50° and 120°C) at some time in the past will contain two populations of tracks. Those formed prior to the thermal maximum will all be shortened to more or less the same degree (the precise value depending on the peak temperature), while those formed during and after cooling will be longer, due to the lower prevailing temperatures. The length distribution in such samples will be broader than in the simple case, and the fission track age will be a reflection of the amount of length reduction which has occurred. In some cases, this kind of history produces a characteristic bimodal distribution of track lengths. If cooling is sufficiently rapid and the final temperature is low enough (<~50°C), tracks formed subsequently will have lengths of 14-15 μm and will contribute a fission track age component corresponding to the age of the cooling "event". If maximum temperatures exceed ~110 to 120°C, all pre-existing tracks will be erased, and all tracks now present will have formed

during and subsequent to cooling. Therefore, the fission track age in such samples relates directly to the time of cooling.

No information is preserved on the approach to maximum temperature, because temperature dominates the thermal response of tracks in apatite.. The only information available is the magnitude of the maximum temperature, the timing of cooling from that maximum and some indication of the thermal history since cooling.

In thermal history scenarios in which a heating episode is followed by cooling and then temperature increases again, the tracks formed during this second heating phase will undergo progressive shortening. The tracks formed prior to the initial cooling, which were shortened in the first heating episode, will not undergo further shortening until the temperature exceeds the maximum temperature reached in the earlier heating episode. (In practice, differences in timescale of heating can complicate this simple description. In detail, it is the integrated time-temperature effect of the two heating episodes which should be considered.) As temperature increases further, the two generations of tracks will be shortened to an identical degree and all information on the original heating phase will be lost.

C.3 Quantitative understanding of fission track annealing in apatite

Annealing kinetics and modelling the development of AFTA parameters

Our understanding of the behaviour of fission tracks in apatite during geological thermal histories is based on study of the response of fission tracks to elevated temperatures in the laboratory (Green et al., 1986; Laslett et al., 1987; Duddy et al., 1988; Green et al., 1989b), in geological situations (Green et al., 1989a), observations of the lengths of spontaneous tracks in apatites from a wide variety of geological environments (Gleadow et al., 1986), and the relationship between track length reduction and reduction in fission track age observed in controlled laboratory experiments (Green, 1988).

These studies resulted in the capability to simulate the development of AFTA parameters resulting from geological thermal histories for an apatite of average composition (Durango apatite, ~0.45 wt% Cl). Full details of this modelling procedure have been explained in Green et al. (1989b). The following discussion presents a brief explanation of the approach.

Geological thermal histories involving temperatures varying through time are broken down into a series of isothermal steps. The progressive shortening of track length through sequential intervals is calculated using the extrapolated predictions of an empirical kinetic model fitted to laboratory annealing data. Contributions from tracks generated throughout the history (remembering that new tracks are continuously generated through time as new fissions occur)

are summed to produce the final distribution of track lengths expected to result from the input history. In summing these components, care is taken to allow for various biases which affect revelation of confined tracks (Laslett et al., 1982). The final length reduction of each component of tracks is converted to a contribution of fission track age, using the relationship between track length and density reduction determined by Green (1988). These age contributions are summed to generate the final predicted fission track age.

This approach depends critically on the assumption that extrapolation of the laboratory-based kinetic model to geological timescales, over many orders of magnitude in time, is valid. This was assessed critically by Green et al. (1989b), who showed that predictions from this approach agree well with observed AFTA parameters in apatites of the appropriate composition in samples from a series of reference wells in the Otway Basin of south-east Australia (Gleadow and Duddy, 1981; Gleadow et al., 1983; Green et al., 1989a). This point is illustrated in Figure C.1. Green et al. (1989b) also quantitatively assessed the errors associated with extrapolation of the Laslett et al. (1987) model from laboratory to geological timescales (i.e., precision, as opposed to accuracy). Typical levels of precision are ~0.5 μm for mean lengths <~10 μm, and ~0.3 μm for lengths >~10 μm. These figures are equivalent to an uncertainty in estimates of maximum paleotemperature derived using this approach of ~10°C. Precision is largely independent of thermal history for any reasonable geological history. Accuracy of prediction from this model is limited principally by the effect of apatite composition on annealing kinetics, as explained in the next section.

Compositional effects

Natural apatites essentially have the composition $Ca_5(PO_4)_3(F,OH,Cl)$. Most common detrital and accessory apatites are predominantly Fluor-apatites, but may contain appreciable amounts of chlorine. The amount of chlorine in the apatite lattice exerts a subtle compositional control on the degree of annealing, with apatites richer in fluorine being more easily annealed than those richer in chlorine. The result of this effect is that in a single sample, individual apatite grains may show a spread in the degree of annealing (i.e., length reduction and fission track age reduction). This effect becomes most pronounced in the temperature range 90 - 120°C (assuming a heating timescale of ~10 Ma), and can be useful in identifying samples exposed to paleotemperatures in this range. At temperatures below ~80°C, the difference in annealing sensitivity is less marked, and compositional effects can largely be ignored.

Our original quantitative understanding of the kinetics of fission track annealing, as described above, relates to a single apatite (Durango apatite) with ~0.45 wt% Cl, on which most of our original experimental studies were carried out. Recently, we have extended this quantitative understanding to apatites with Cl contents up to ~3 wt%. This new, multi-compositional kinetic model is based both on new laboratory annealing studies on a range of apatites with

different F-Cl compositions (Figure C.2), and on observations of geological annealing in apatites from a series of samples from exploration wells in which the section is currently at maximum temperature since deposition. A composite model for Durango apatite composition was first created by fitting a common model to the old laboratory data (from Green et al., 1986) and the new geological data for a similar composition. This was then extended to other compositions on the basis of the multi-compositional laboratory and geological data sets. Full details of the development of the final multi-compositional model will be made available in the form of a Technical Note in the near future.

The multi-compositional model allows prediction of AFTA parameters for any Cl content between 0 and 3 wt%, using a similar approach to that used in our original single composition modelling, as outlined above. Then, for an assumed or measured distribution of Cl contents within a sample, the composite parameters for the sample can be predicted. The range of Cl contents from 0 to 3 wt% spans the range of compositions commonly encountered, as discussed in the next section.

Predictions of the new multi-compositional model are in good agreement with the geological constraints on annealing rates provided by the Otway Basin reference wells, as shown in Figure C.3. However, note that the AFTA data from these Otway Basin wells were among those used in construction of the new model, so this should not be viewed as independent verification, but rather as a demonstration of the overall consistency of the model.

Distributions of Cl content in common AFTA samples

Figure C.4a shows a histogram of Cl contents, measured by electron microprobe, in apatite grains from more than 100 samples of various types. Most grains have Cl contents less than ~0.5 wt%. The majority of grains with Cl contents greater than this come from volcanic sources and basic intrusives, and contain up to ~2 wt% Cl. Figure C.4b shows the distribution of Cl contents measured in randomly selected apatite grains from 61 samples of "typical" quartzo-feldspathic sandstone. This distribution is similar to that in Figure C.4a, except for a more rapid fall-off as Cl content increases. Apatites from most common sandstones give distributions of Cl content which are very similar to that in Figure C.4b. Volcanogenic sandstones typically contain apatites with higher Cl contents, with a much flatter distribution for Cl contents up to ~1.5%, falling to zero at ~2.5 to 3 wt%, as shown in Figure C.4c. Cl contents in granitic basement samples and high-level intrusives are typically much more dominated by compositions close to end-member Fluorapatite, although many exceptions occur to this general rule.

Information about the spread of Cl contents in samples analysed in this report can be found in Appendix A.

Alternative kinetic models

Recently, both Carlson (1990) and Crowley et al. (1991) have published alternative kinetic models for fission track annealing in apatite. Carlson's model is based on our own laboratory annealing data for Durango apatite (Green et al., 1986) and other (unpublished) data. In his abstract, Carlson claims that because his model is "based on explicit physical mechanisms, extrapolations of annealing rates to the lower temperatures and longer timescales required for the interpretation of natural fission track length distributions can be made with greater confidence than is the case for purely empirical relationships fitted to the experimental annealing data". As we have explained at length in a comment on Carlson's paper currently in press, all aspects of Carlson's model are in fact purely empirical, and his model is inherently no "better" for the interpretation of data than any other. In fact, detailed inspection shows that his model does not fit the laboratory data set at all well. Therefore, we recommend against use of this model to interpret AFTA data.

The approach taken by Crowley et al. (1991) is very similar to our own approach. They have fitted models to new annealing data in two apatites of different composition - one close to end-member Fluorapatite (B-5) and one having a relatively high Sr content (113855). The model developed by Crowley et al. (1991) from their own annealing data for the B-5 apatite gives predictions in geological conditions which are consistently higher than measured values, as shown in Figure C.5. Corrigan (1992) reported a similar observation in volcanogenic apatites in samples from a series of West Texas wells. Since the B-5 apatite is close to end-member Fluor-apatite, while the Otway Group apatites contain apatites with Cl contents from zero up to ~3 wt% (and the West Texas apatites have up to 1 wt%), the fluorapatites should have mean lengths rather less than the measured values. Therefore, the predictions of the Crowley et al. (1991) B-5 model appear to be consistently high.

We attribute this to the rather restricted temperature-time conditions covered by the experiments of Crowley et al. (1991), with annealing times between one and 1000 hours, in contrast to times between 20 minutes and 500 days in the experiments of Green et al. (1986). In addition, few of the measured length values in Crowley et al.'s study fall below 11 μm (in only five out of 60 runs in which lengths were measured in apatite B-5) and their model is particularly poorly defined in this region.

Crowley et al. (1991) also fitted a new model to our own annealing data for Durango apatite (from Green et al., 1986). Predictions of their fit to our data are not very much different to those from our own model (Figure C.6), increasing to ~1 μm at lengths at ~8 μm (from the Laslett et al. model). We have not pursued the differences between their model and ours in

detail because the advent of our multi-compositional model has rendered the single compositional approach obsolete.

C.4 Evidence for elevated paleotemperatures from AFTA

The basic principle involved in the interpretation of AFTA data in sedimentary basins is to determine whether the degree of annealing shown by tracks in apatite from a particular sample could have been produced if the sample has never been hotter than its present temperature at any time since deposition. To do this, the burial history derived from the stratigraphy of the preserved sedimentary section is converted to a thermal history using the present geothermal gradient and surface temperature (i.e., assuming these have not changed through time). This is termed the "Default Thermal History". The AFTA parameters predicted as a result of the Default Thermal History are then compared to the measured data. If the sample shows a greater degree of annealing that expected on the basis of this history, the sample must have been hotter at some time in the past. In this case, the AFTA data are analysed to provide estimates of the magnitude of the maximum paleotemperature in that sample, and the time at which cooling commenced from the thermal maximum.

The degree of annealing is assessed in two ways - from fission track age and track length data. The stratigraphic age provides a basic reference point for the interpretation of fission track age, because reduction of the fission track age below the stratigraphic age unequivocally reveals that appreciable annealing has taken place after deposition of the host sediment. Large degrees of fission track age reduction, with the pooled or central fission track age very much less than the stratigraphic age, indicate severe annealing, which requires paleotemperatures of at least ~100°C for any reasonable geological time-scale of heating (>~1 Ma). Note that this applies even when apatites contain tracks inherited from source areas. More moderate degrees of annealing can be detected by inspection of the single grain age data, as the most sensitive (fluorine-rich) grains will begin to give fission track ages significantly less than the stratigraphic age before the central or pooled age has been reduced sufficiently to give a noticeable signal. Note that this aspect of the single grain age data can also be used for apatites which have tracks inherited from source areas. If signs of moderate annealing (from single grain age reduction) or severe annealing (from the reduction in pooled or central age) are seen in samples in which the Default Thermal History predicts little or no effect, the sample must have been subjected to elevated paleotemperatures at some time in the past. Figure C.7 shows how increasing degrees of annealing are observable in radial plots of the single grain fission track age data.

Similarly, the present temperature from which a sample is taken, and the way in which this has been approached (as inferred from the preserved sedimentary section), forms a basic point of reference for track length data. The observed mean track length is compared with the mean

length predicted from the Default Thermal History (l_p). If the observed degree of track shortening in a sample is greater than that expected from the Default Thermal History, either the sample must have been subjected to higher paleotemperatures at some time after deposition, or the sample contains shorter tracks which were inherited from sediment source areas at the time the sediment was deposited. If shorter tracks were inherited from source areas, the sample should still contain a component of longer tracks corresponding to the tracks formed after deposition. In general, the fission track age should be greater than the stratigraphic age. This can be assessed quantitatively using the computer models for the development of AFTA parameters described in an earlier section. If the presence of shorter tracks cannot be explained by their inheritance from source areas, the sample must have been hotter in the past.

C.5 Determining maximum paleotemperatures using AFTA

The maximum paleotemperature in each sample is determined using a forward modelling approach based on the quantitative description of fission track annealing described in earlier sections. The Default Thermal History described above is used as the basis for this forward modelling, but with the addition of episodes of elevated paleotemperatures as required to explain the data. Initial guesses for the timing of these episodes can often be obtained from the fission track age data, as discussed in the next section.

AFTA parameters are modelled iteratively through successive thermal history scenarios in order to identify thermal histories that can account for observed parameters. The maximum paleotemperature is adjusted until it is sufficient to account for the degree of fission track age and track length reduction shown by those tracks formed prior to the onset of cooling.

In the past, estimation of maximum paleotemperatures based on extrapolation of a laboratory-based kinetic model to geological timescales introduced an uncertainty of ~±10°C to the paleotemperature estimates, as discussed by Green et al. (1989b). This aspect of the new multi-compositional modelling approach has not yet been quantitatively analysed, but uncertainty in paleotemperature estimation with this approach should be less than ±10°C, as the kinetic models are now constrained in both laboratory and geological conditions. As before, it should also be appreciated that relative differences in maximum paleotemperature can be identified with greater precision than absolute paleotemperatures, and it is only the estimation of absolute paleotemperature values to which the ±10°C uncertainty relates.

In addition, as illustrated earlier (see Figure C.3), comparison of the AFTA parameters predicted by the multi-compositional model - with measured values in samples which are currently at their maximum temperatures since deposition - shows a good degree of consistency, suggesting the uncertainty in application of the model is less than ±10°C.

In samples in which all tracks have been totally annealed at some time in the past, only a minimum estimate of maximum paleotemperature is possible. Total annealing can be identified from a number of lines of evidence. In a vertical sequence of samples showing increasing degrees of annealing, the transition from rapidly decreasing fission track age with increasing depth to more or less the same age over a range of depth denotes the transition from partial to total annealing of all tracks formed prior to the thermal maximum. In samples in which all tracks have been totally annealed, the single grain age data should show that none of the individual grain fission track ages are significantly older than the time of cooling. If the sample has cooled to sufficiently low temperatures, little annealing will have taken place since cooling, and all grains will give ages which are compatible with a single population around the time of cooling, as shown in Figure C.7. Total annealing can also be inferred from combining the age and length data, by modelling the form of the track length distributions likely to result from different scenarios. Often the observed length distribution can only be explained by invoking an episode of total annealing early in the history.

C.6 Determining the time of cooling from maximum paleotemperatures from AFTA

Timing of cooling from maximum paleotemperatures can be estimated from a number of lines of evidence. The most direct of these is "correction" of measured fission track ages for the observed degree of length reduction in samples which have been totally annealed. Such "corrected ages" provide an estimate of the time over which tracks have been retained in the sample. Corrected ages, which are shown for each sample in Table 1, are calculated using the relationship between length reduction and the reduction in fission track age during annealing reported by Green (1988). In samples which have been totally annealed prior to cooling and have undergone rapid cooling with little or no subsequent reheating, the corrected age should directly indicate the time of cooling. Any complexity in the thermal history leads to these "corrected ages" underestimating this parameter, but this procedure can often yield useful results. However, corrected ages can be very misleading, particularly in samples which have only been partially annealed, and must be used with caution.

Inspection of the distribution of single grain ages in partially annealed samples can often yield useful information on the time of cooling, as the most easily annealed grains (those richest in fluorine) may have been totally annealed prior to cooling, while more retentive (Cl-rich) compositions were only partially annealed (as in Figure 6, centre). The form of the track length distribution can also provide information, from the relative proportions of tracks with different lengths. Normally, all of these aspects of the data are employed in reaching a consistent thermal history interpretation.

C.7 Allowing for tracks inherited from source areas

The effect of tracks inherited from source areas, and present at the time the apatite is deposited in the host sediment, is often posed as a potential problem for AFTA. However, this can readily be allowed for in analysing both the fission track age and length data.

In assessing fission track age data to determine the degree of annealing, the only criterion used is the comparison of fission track age with stratigraphic age. From this point of view, inherited tracks do not affect the conclusion, since if a grain or a sample gives a fission track age significantly less than the stratigraphic age, the grain or sample has clearly undergone at least a moderate degree of annealing, whether the sample contained tracks when it was deposited or not. The absolute degree of annealing (age reduction) may be uncertain, but this does not significantly affect estimation of paleotemperatures because this is based on a number of lines of evidence.

The presence of inherited tracks does impose a limit on our ability to detect post-depositional annealing from age data alone. However, as in samples which contain a fair proportion of inherited tracks, moderate degrees of annealing may reduce the fission track age from the original value, but not to a value which is significantly less than the stratigraphic age. This is particularly noticeable in the case of Tertiary samples containing apatites derived from Paleozoic basement. In such cases, although fission track age data may show no evidence of post-depositional annealing, track length data may well show such evidence quite clearly.

The influence of track lengths inherited from source areas can be allowed for by comparison of the fission track age with the stratigraphic age and inspection of the length distribution. If the mean length is much less than the length predicted by the Default Thermal History (l_p), either the sample has been subjected to elevated paleotemperatures, sufficient to produce the observed degree of length reduction, or else the sample contains a large proportion of shorter tracks inherited from source areas. However, in the latter case, the sample should give a pooled or central fission track age correspondingly older than the stratigraphic age, while the length distribution should contain a component of longer track lengths corresponding to the value of l_p. It is important in this regard that the length of a track depends primarily on the maximum temperature to which it has been subjected, whether in the source regions or after deposition in the sedimentary basin. Thus, any tracks retaining a provenance signature will have lengths towards the shorter end of the distribution where track lengths will not have "equilibrated" with the temperatures attained since deposition.

In general, it is only in extreme cases that inherited tracks render track length data insensitive to post-depositional annealing. For example, if practically all the tracks in a particular sample were formed prior to deposition, perhaps in a Pliocene sediment in which apatites were

derived from a stable Paleozoic shield with fission track ages of ~300 Ma or more, the track length distribution will, in general, be dominated by inheritance, as only ~2% of tracks would have formed after deposition. Post-depositional heating will not be detectable as long as the temperature is insufficient to cause greater shortening than that which occurred in the source terrain. However, even in such extreme cases, once a sample is exposed to temperatures sufficient to produce greater shortening than that inherited from source areas, the inherited tracks and those formed after deposition will all undergo the same degree of shortening, and the effects of post-depositional annealing can be recognised. In such cases, the presence of tracks inherited from source areas is actually very useful, because the number of tracks formed after deposition is so small that little or no information would be available without the inherited tracks.

C.8 Plots of fission track age and mean track length vs depth and temperature

AFTA data from well sequences are usually plotted, as shown in Figure C.8. This figure shows AFTA data for two scenarios: one in which deposition has been essentially continuous from the Carboniferous to the present and all samples are presently at their maximum paleotemperature since deposition (Figure C.8a); and, one in which the section was exposed to elevated paleotemperatures prior to cooling in the Early Tertiary (Figure C.8b).

In both figures, fission track age and mean track length are plotted against depth and present temperature. Presentation of AFTA data in this way often provides insight into the thermal history interpretation, following principles outlined earlier in this Appendix.

In Figure C.8a, for samples at temperatures below ~70°C, the fission track age is either greater than or close to the stratigraphic age, and little fission track age reduction has affected these samples. Track lengths in these samples are all greater than ~13 μm. In progressively deeper samples, both the fission track age and mean track length are progressively reduced to zero at a present temperature of around 100 to 110°C, with the precise value depending on the spread of apatite compositions present in the sample. Track length distributions in the shallowest samples would be a mixture of tracks retaining information on the thermal history of source regions, while in deeper samples, all tracks would be shortened to a length determined by the prevailing temperature. This pattern of AFTA parameters is characteristic of a sequence which is currently at maximum temperatures.

The data in Figure C.8b show a very different pattern. The fission track age data show a rapid decrease in age, with values significantly less than the stratigraphic age at temperatures of ~40 to 50°C, at which such a degree of age reduction could not be produced in any geological timescale. Below this rapid fall, the fission track ages do not change much over ~1 km (30°C). This transition from rapid fall to consistent ages is diagnostic of the transition

from partial to total annealing. Samples above the "break-in slope" contain two generations of tracks: those formed prior to the thermal maximum, which have been partially annealed (shortened) to a degree which depends on the maximum paleotemperature; and, those formed after cooling, which will be longer. Samples below the break-in slope contain only one generation of tracks, formed after cooling to lower temperatures at which tracks can be retained. At greater depths, where temperatures increase to ~90°C and above, the effect of present temperatures begins to reduce the fission track ages towards zero, as in the "maximum temperatures now" case.

The track length data also reflect the changes seen in the fission track age data. At shallow depths, the presence of the partially annealed tracks shortened prior to cooling causes the mean track length to decrease progressively as the fission track age decreases. However, at depths below the break in slope in the age profile, the track length increases again as the shorter component is totally annealed and so does not contribute to the measured distribution of track lengths. At greater depths, the mean track lengths decrease progressively to zero once more due to the effects of the present temperature regime.

Examples of such data have been presented, for example, by Green (1989) and Kamp and Green (1990).

C.9 Determining paleogeothermal gradients and amount of section removed on unconformities

Estimates of maximum paleotemperatures in samples over a range of depths in a vertical sequence provides the capability of determining the paleogeothermal gradient immediately prior to the onset of cooling from those maximum paleotemperatures. The degree to which the paleogeothermal gradient can be constrained depends on a number of factors, particularly the depth range over which samples are analysed. If samples are only analysed over ~1 km, the paleotemperature difference over that range may be only ~20 to 30°C. Since maximum paleotemperatures can often only be determined within a ~10°C range, this introduces considerable uncertainty into the final estimate of paleogeothermal gradient (see Figure C.9)

Another important factor is the difference between maximum paleotemperatures and present temperatures ("net cooling"). If this is only ~10°C, which is similar to the uncertainty in absolute paleotemperature determination, only broad limits can be established on the paleogeothermal gradient. In general, the control on the paleogeothermal gradient improves as the amount of net cooling increases. However, if the net cooling becomes so great that many samples were totally annealed prior to the onset of cooling - so that only minimum estimates of maximum paleotemperatures are possible - constraints on the paleogeothermal gradient from AFTA come only from that part of the section in which samples were not totally

annealed. In this case, integration of AFTA data with VR measurements can be particularly useful in constraining the paleo-gradient, as explained in more detail in Appendix D.

Having constrained the paleogeothermal gradient at the time cooling from maximum paleotemperatures began, if we assume a value for surface temperature at that time, the amount of section subsequently removed by uplift and erosion can be calculated as shown in Figure C.10. The *net* amount of section removed is obtained by dividing the difference between the paleo-surface temperature (T_S) and the intercept of the paleotemperature profile at the present ground surface (T_i) by the estimated paleogeothermal gradient. The *total* amount of section removed is obtained by adding the thickness of section subsequently redeposited above the unconformity to the *net* amount estimated as in Figure C.10.

We have recently developed a method of deriving estimates of both the paleogeothermal gradient and the net amount of section removed using estimated paleotemperatures derived from AFTA and VR. Perhaps more importantly, this method also provides rigorous values for upper and lower 95% confidence limits on each parameter. The method is based on maximum likelihood estimation of the paleogeothermal gradient and the surface intercept, from a table of paleotemperature and depth values. The method is able to accept ranges for paleotemperature estimates (e.g., where the maximum paleotemperature can only be constrained to between, for example, 60 and 90°C), as well as upper and lower limits (e.g., <60°C for samples which show no detectable annealing; >110°C in samples which were totally annealed). Estimates of paleotemperature from AFTA and VR may be combined or analysed separately. Some results from this method have been reported by Bray et al. (1992). Full details of the methods employed are presented in a confidential, in-house, Geotrack research report, copies of which are available on request from the Melbourne office.

Results are presented in two forms. Likelihood profiles, plotting the log-likelihood as a function of either gradient or section removed, portray the probability of a given value of gradient or section removed. The best estimate is given by the value of gradient or section removed for which the log-likelihood is maximised. Ideally, the likelihood profiles should show a quadratic form, and values of gradient or section removed at which the log-likelihood has fallen by two from the maximum value define the upper and lower 95% confidence limits on the estimates. An alternative method of portraying this information is a crossplot of gradient against section removed, in which values which fall within 95% confidence limits (in two dimensions) are contoured. Note that the confidence limits defined by this method are rather tighter than those from the likelihood profiles, as the latter only reflect variation in one parameter, whereas the contoured crossplot takes variation of both parameters into account.

It must be emphasised that this method relies on the assumption that the paleotemperature profile was linear both throughout the section analysed and through the overlying section

which has been removed. While the second part of this assumption can never be confirmed independently, visual inspection of the paleotemperature estimates as a function of depth should be sufficient to verify or deny the linearity of the paleotemperature profile through the preserved section.

Results of this procedure are shown in this report if the data allow sufficiently well-defined paleotemperature estimates to justify use of the method. Where the AFTA data suggest that the section is currently at maximum temperature since deposition, or that the paleotemperature profile was non-linear, or where data are of insufficient quality to allow rigorous paleotemperature estimation, the method is not used.

References

Bray, R.J. Green, P.F. and Duddy, I.R. (1992). Thermal history reconstruction in sedimentary basins using apatite fission track analysis and vitrinite reflectance: a case study from the east Midlands of England and the Southern North Sea. *In:* Exploration Britain: Into the next decade. Geological Society Special Publication (in press).

Carlson, W.D. (1990). Mechanisms and kinetics of apatite fission-track annealing. American Mineralogist, 75, 1120 - 1139.

Corrigan, J. (1992). Annealing models under the microscope, On Track, 2, 9-11.

Crowley, K.D., Cameron, M. and Schaefer, R.L. (1991). Experimental studies of annealing of etched fission tracks in apatite. Geochimica et Cosmochimica Acta, 55, 1449-1465.

Duddy, I.R., Green, P.F. and Laslett G.M. (1988). Thermal annealing of fission tracks in apatite 3. Variable temperature behaviour. *Chem. Geol. (Isot. Geosci. Sect.)* , 73, 25-38.

Gleadow, A.J.W. and Duddy, I.R. (1981). A natural long-term track annealing experiment for apatite. *Nuclear Tracks*, 5, 169-174.

Gleadow, A.J.W., Duddy, I.R. and Lovering, J.F. (1983). Fission track analysis; a new tool for the evaluation of thermal histories and hydrocarbon potential. *APEA J*, 23, 93-102.

Gleadow, A.J.W., Duddy, I.R., Green, P.F. and Lovering, J.F. (1986). Confined fission track lengths in apatite - a diagnostic tool for thermal history analysis. *Contr. Min. Petr.*, 94, 405-415.

Green, P.F. (1988). The relationship between track shortening and fission track age reduction in apatite: Combined influences of inherent instability, annealing anisotropy, length bias and system calibration. *Earth Planet. Sci. Lett.*, 89, 335-352.

Green, P.F., Duddy, I.R., Gleadow, A.J.W., Tingate, P.R. and Laslett, G.M. (1986). Thermal annealing of fission tracks in apatite 1. A qualitative description. *Chem. Geol. (Isot. Geosci. Sect.)* , 59, 237-253.

Green, P.F., Duddy, I.R., Gleadow, A.J.W. and Lovering, J.F. (1989a). Apatite Fission Track Analysis as a paleotemperature indicator for hydrocarbon exploration. *In:* Naeser, N.D. and McCulloh, T. (*eds*), Thermal history of sedimentary basins - methods and case histories, Springer-Verlag, New York, 181-195.

Green, P.F., Duddy, I.R., Laslett, G.M., Hegarty, K.A., Gleadow, A.J.W. and Lovering, J.F. (1989b). Thermal annealing of fission tracks in apatite 4. Quantitative modelling techniques and extension to geological timescales. *Chem. Geol. (Isot. Geosci. Sect.)*, 79, 155-182

Laslett, G.M., Kendall, W.S., Gleadow, A.J.W. and Duddy, I.R. (1982). Bias in measurement of fission track length distributions. *Nuclear Tracks*, 6, 79-85.

Laslett, G.M., Green, P.F., Duddy, I.R. and Gleadow, A.J.W. (1987). Thermal annealing of fission tracks in apatite 2. A quantitative analysis. *Chem. Geol. (Isot. Geosci. Sect.)*, 65, 1-13.

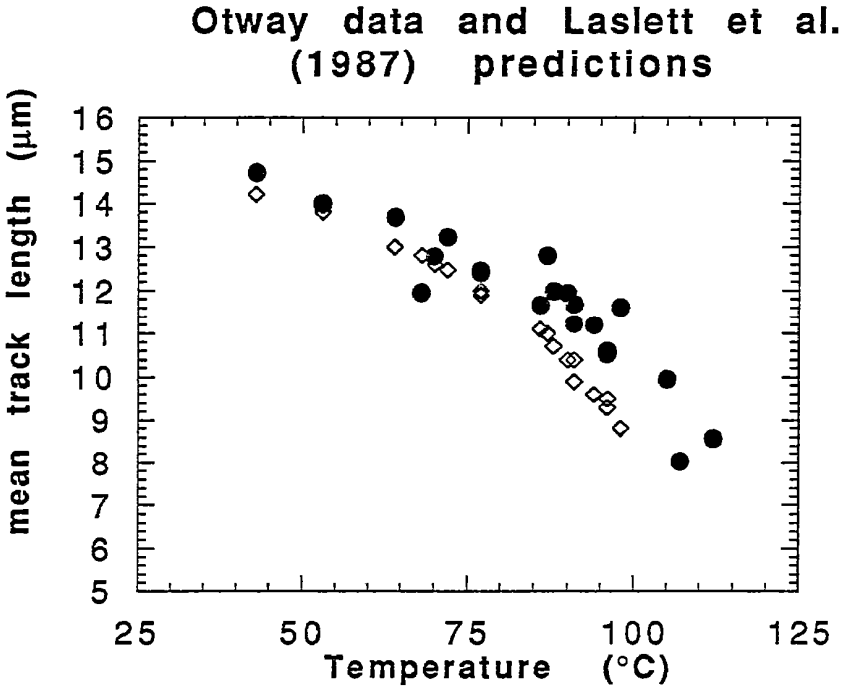

Figure C.1a Comparison of mean track length (solid circles) measured in samples from four Otway Basin reference wells (from Green et al, 1989a) and predicted mean track lengths (open diamonds) from the kinetic model of fission track annealing from Laslett et al. (1987). Although the predictions underestimate the measured values, they refer to an apatite composition that is more easily annealed than the majority of apatites in these samples, and therefore this is expected.

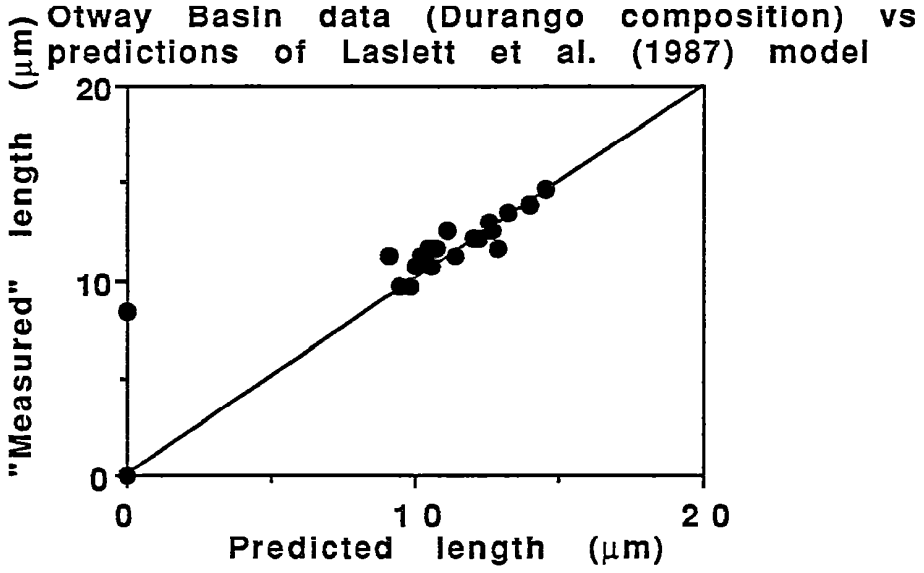

Figure C.1b Comparison of the mean track length in apatites of the same Cl content as Durango apatite from the Otway Group samples illustrated in figure C.1a, with values predicted for apatite of the same composition by the model of Laslett et al. (1987). The agreement is clearly very good except possibly at lengths below ~10 µm.

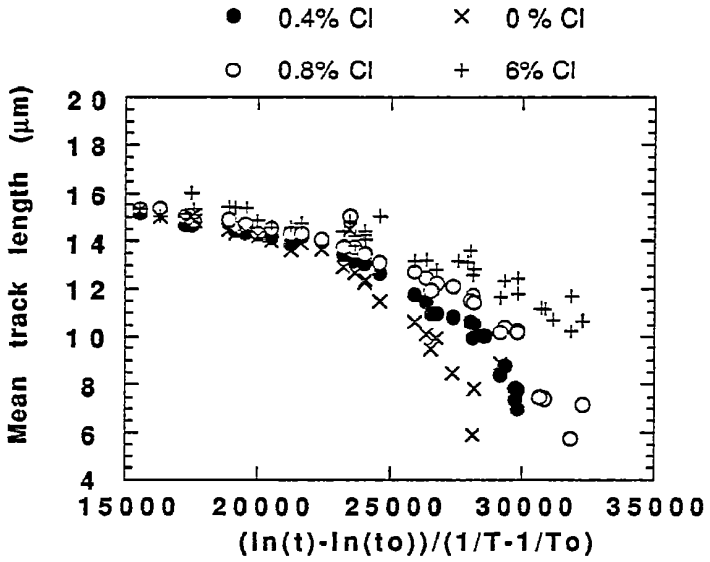

Figure C.2 Mean track length in apatites with four different chlorine contents, as a combined function of temperature and time, to reduce the data to a single scale. Fluorapatites are more easily annealed than chlorapatites, and the annealing kinetics show a progressive change with increasing Cl content.

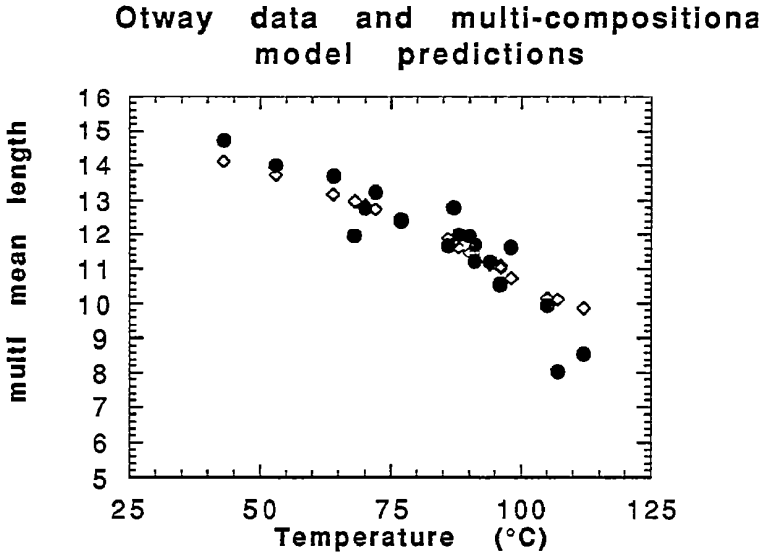

Figure C.3 Comparison of measured mean track length (solid circles) in samples from four Otway Basin reference wells (from Green et al, 1989a) and predicted mean track lengths (open diamonds) from the new multi-compositional kinetic model of fission track annealing desrcibed in Section C.3. This model takes into account the spread of Cl contents in apatites from the Otway Group samples and the influence of Cl content on annealing rate. The agreement is clearly very good over the range of the data.

All samples

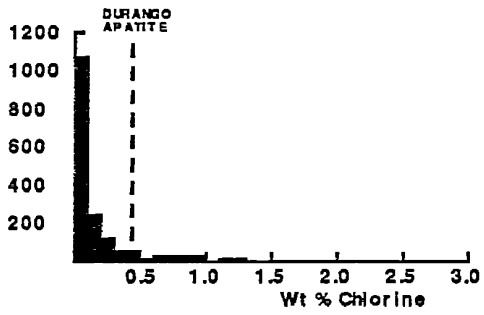

"Normal sandstones"

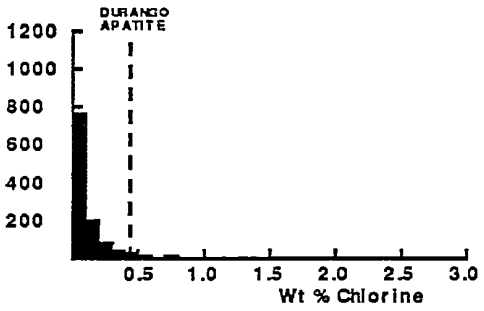

Volcanogenic sandstones

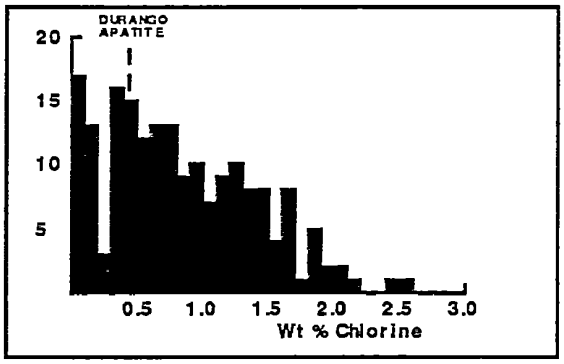

Figure C.4 **a:** Histogram of Cl contents (wt%) in over 1750 apatite grains from over 100 samples of various sedimentary and igneous rocks. Most samples give Cl contents below ~0.5 wt %, while those apatites giving higher Cl contents are characterisitic of volcanogenic sandstones and basic igneous sources.

b: Histogram of Cl contents (wt%) in 1168 apatite grains from 61 samples which can loosely be characterised as "normal sandstone". The distribution is similar to that in the upper figure, except for a lower number of grains with Cl contents greater than ~1%.

c: Histogram of Cl contents (wt%) in 188 apatite grains from 15 samples of volcanogenic sandstone. The distribution is much flatter than the other two, with much higher proportion of Cl-rich grains.

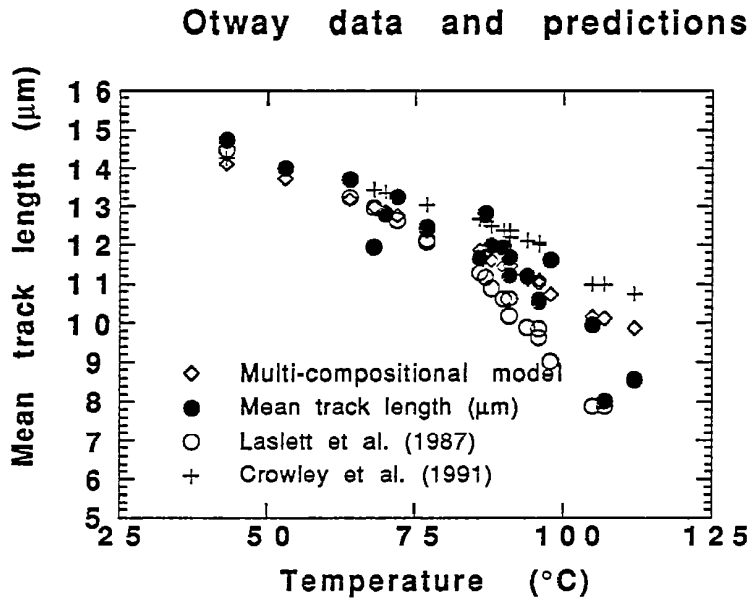

Figure C.5 Comparison of mean track length in samples from four Otway Basin reference wells (from Green et al, 1989a) and predicted mean track lengths from three kinetic models for fission track annealing. The Crowley et al. (1991) model relates to almost pure Fluorapatite (B-5), yet overpredicts mean lengths in the Otway Group samples which are dominated by Cl-rich apatites. The predictions of that model are therefore not reliable.

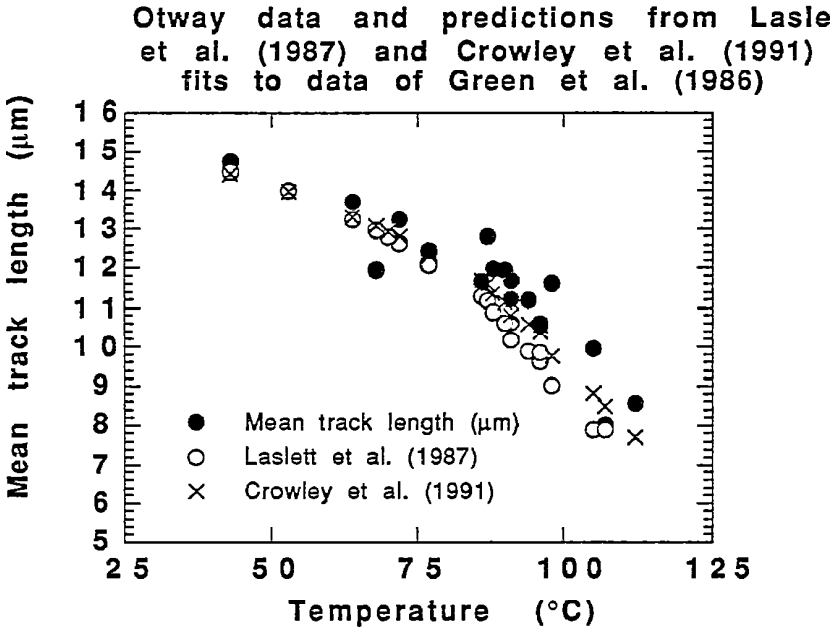

Figure C.6 Comparison of mean track length in samples from four Otway Basin reference wells with values predicted from Laslett et al. (1987) and the model fitted to the annealing data of Green et al. (1986) by Crowley et al. (1991). The predictions of the two models are not very different.

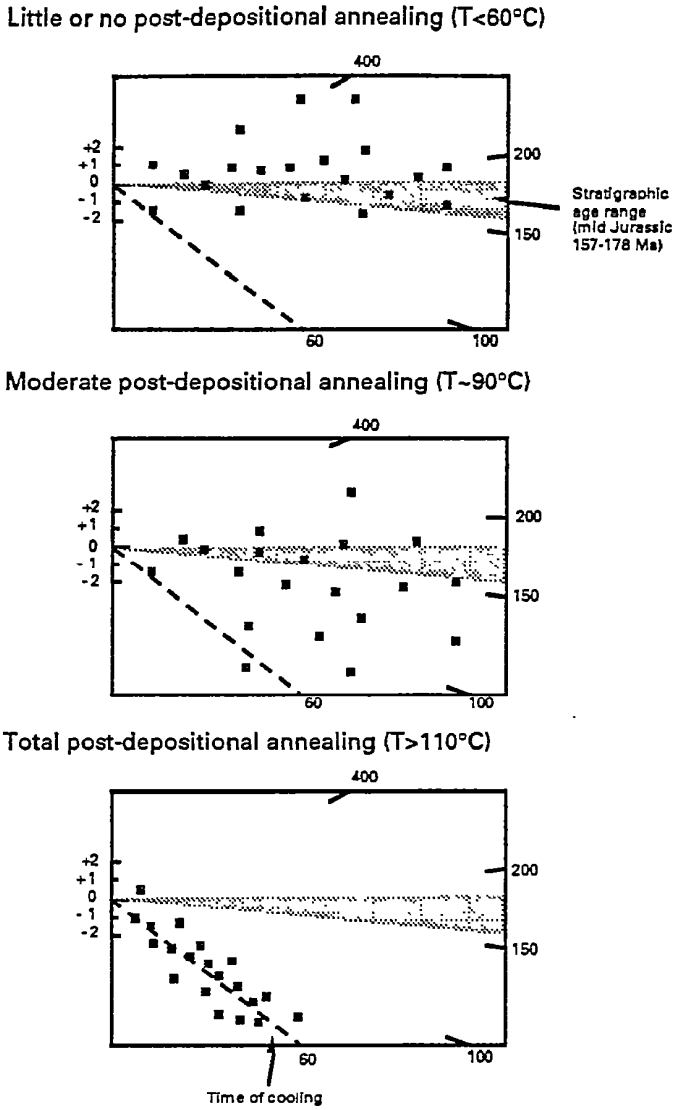

Figure C.7 Radial plots of single grain age data in three samples of mid-Jurassic sandstone that have been subjected to varying degrees of post-depositional annealing prior to cooling at ~60 Ma. The mid-point of the stratigraphic age range has been taken as the reference value (corresponding to the horizontal).

The upper diagram represents a sample which has remained at paleotemperatures less than ~60°C, and has therefore undergone little or no post-depositional annealing. All single grain ages are either compatible with the stratigraphic age (within $y = \pm 2$ in the radial plot) or older than the stratigraphic age ($y_i > 2$).

The centre diagram represents a sample which has undergone a moderate degree of post-depositional annealing, having reached a maximum paleotemperature of around ~90°C prior to cooling. While some of the individual grain ages are compatible with the stratigraphic age ($-2 < y_i < +2$) and some may be significantly greater than the stratigraphic age ($y_i > 2$), a number of grains give ages which are significantly less than the stratigraphic age ($y < 2$).

The lower diagram represents a sample in which all apatite grains were totally annealed, at paleotemperatures greater than ~110°C, prior to rapid cooling at ~60 Ma. All grains give fission track ages compatible with a fission track age of ~60 Ma (i.e. all data plot within ±2 of the radial line corresponding to an age of ~60 Ma), and most are significantly younger than the stratigraphic age.

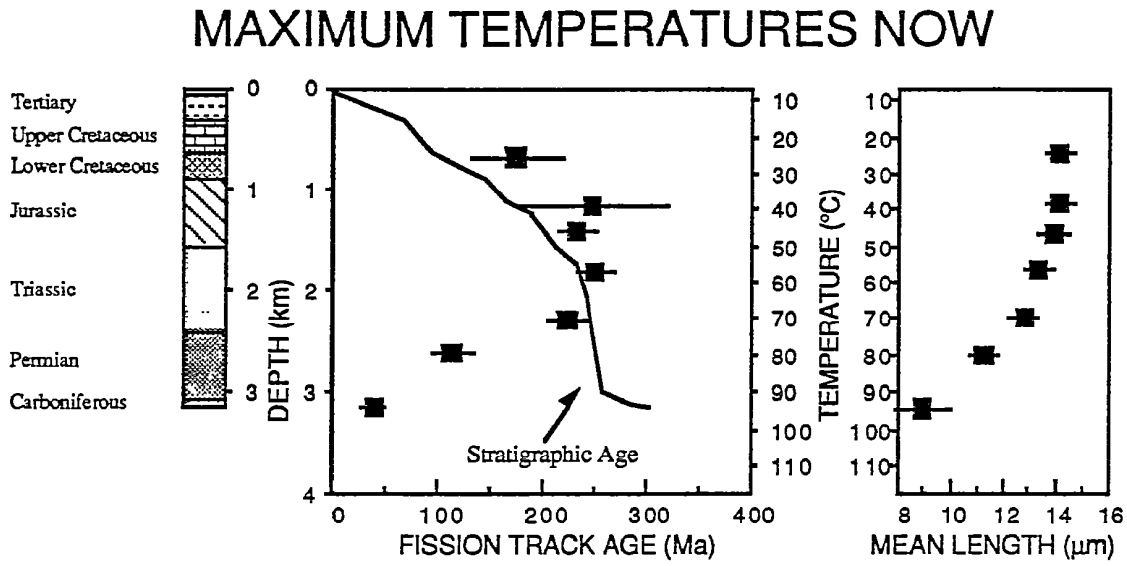

Figure C.8a Typical pattern of AFTA parameters in a well in which samples throughout the entire section are currently at their maximum temperatures since deposition. Both the fission track age and mean track length undergo progressive reduction to zero at temperatures of ~100 - 110°C, the actual value depending on the range of apatite compositions present.

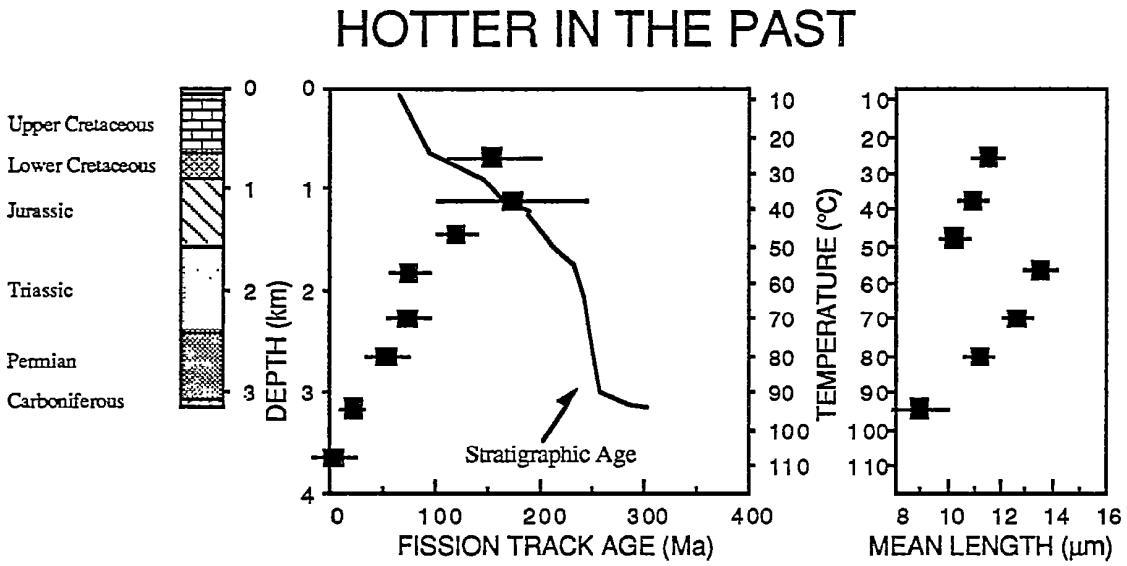

Figure C.8b Typical pattern of AFTA parameters in a well in which samples throughout the section were exposed to elevated paleotemperatures after deposition (prior to cooling in the Early Tertiary, in this case). Both the fission track age and mean track length show more reduction at temperatures of ~40 to 50°C than would be expected at such temperatures. At greater depths (higher temperatures), the constancy of fission track age and the increase in track length are both diagnostic of exposure to elevated paleotemperatures. See Appendix C for further discussion

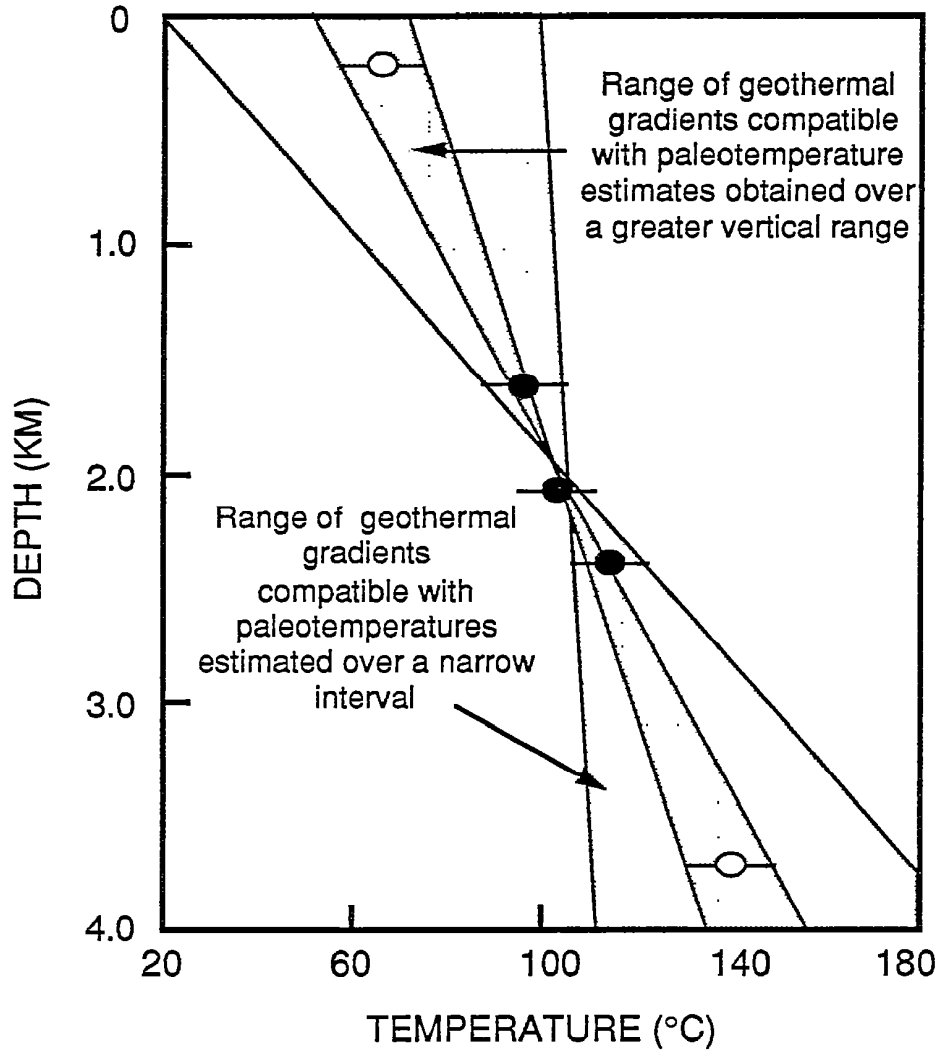

Figure C.9 It is important to obtain paleotemperature constraints over as great a range of depths as possible in order to provide a reliable estimate of paleogeothermal gradient. If paleotemperatures are only available over a narrow depth range, then the paleogeothermal gradient can only be very loosely constrained.

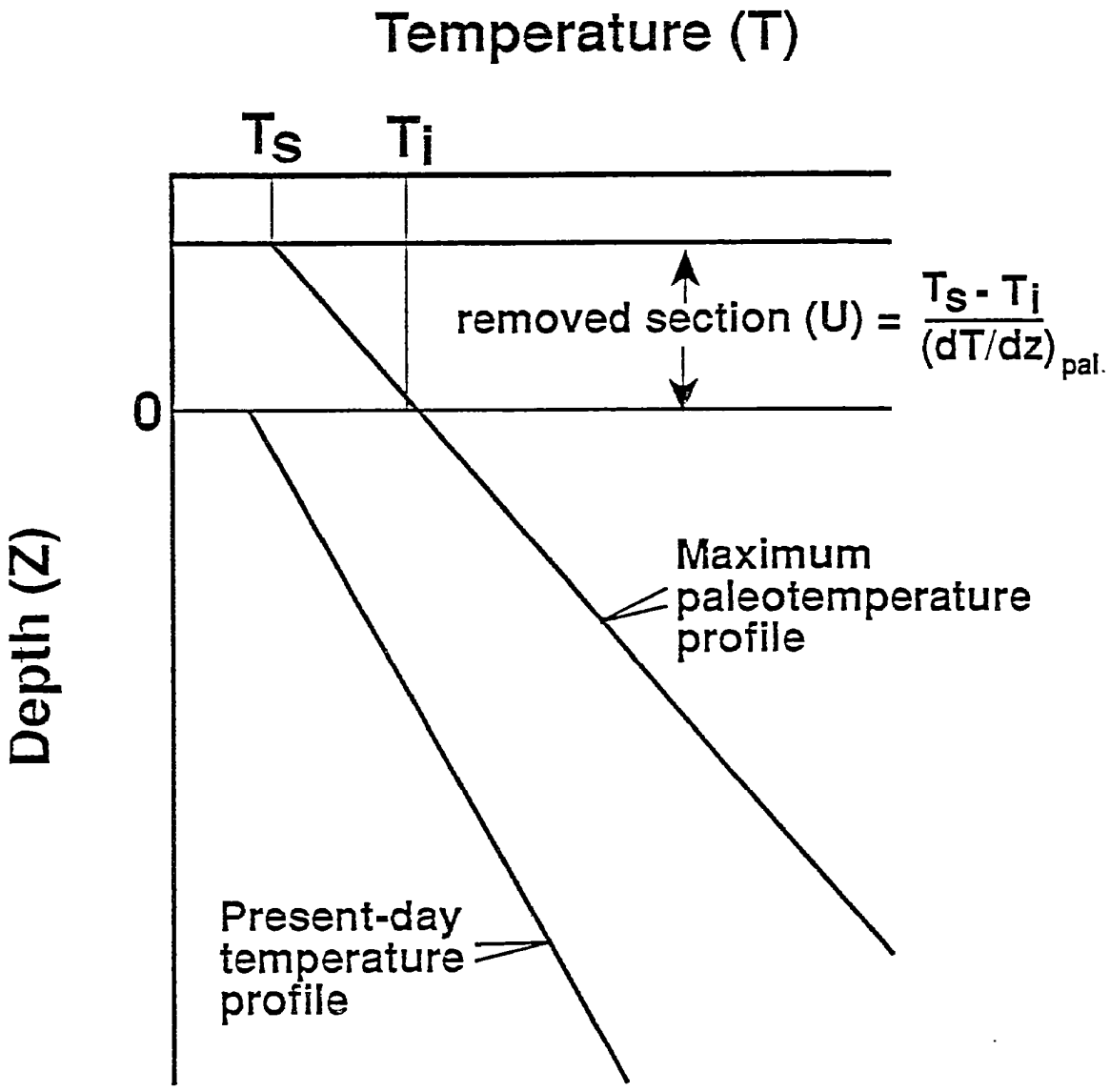

Figure C.10 If the paleogeothermal gradient can be constrained by AFTA and VR, as explained in the text, then for an assumed value of surface temperature, T_S, the amount of section removed can be estimated, as shown.

APPENDIX D

Vitrinite Reflectance Measurements

D.1 New vitrinite reflectance determinations

New vitrinite reflectance data were collected as part of this study, with details of determinations described in sections D.1 and D.2 below. In addition, further vitrinite reflectance data were supplied by the client, as summarised in section D.3.

Samples

Samples were submitted for vitrinite reflectance determination to Keiraville Konsultants, Australia. Results and sample details are summarised in Table D.2, while supporting data, including maceral descriptions and raw data sheets, are presented in the following pages.

Equipment

Leitz MPV1.1 photometer equipped with separate fluorescence illuminator, Swift point counter. Reflectance standards: spinel 0.42%, YAG 0.91%, GGG 1.72%, SiC standard for cokes and masked uranyl glass for measurement of intensity (I) in fluorescence mode. With the Keiraville Konsultants equipment, it is possible to alternate from reflectance to fluorescence mode to check for associated fluorescing liptinite, or importantly with some samples, to check for bitumen impregnation, or the presence, intensity, and source of oil-cut.

Sample preparation

Samples are normally mounted in cold setting polyester resin and polished using Cr_2O_3 and MgO polishing powders. Epoxy resins or araldite can be used if required. "Whole rock" samples are normally used but demineralisation can be undertaken. Large samples of coals and cokes can be mounted and examined.

Vitrinite Reflectance measurement

The procedure used generally follows Australian Standard (AS) 2486, but has been slightly modified for use with dispersed organic matter (DOM). For each sample, a minimum of 25 fields is measured (the number may be less if vitrinite is rare or if a

limited number of particles of vitrinite is supplied, as may be the case with hand-picked samples). If wide dispersal of vitrinite reflectances is found, the number of readings (N) is increased until a stable mean is obtained.

Vitrinite identification is made primarily on textural grounds, and this allows an independent assessment to be made of cavings and re-worked vitrinite populations. Histograms are only used for population definition when a cavings population significantly overlaps the range of the indigenous population. Where such data provides additional information, the mean maximum reflectance of inertinite and/or the mean maximum reflectance of liptinite (exinite) is reported. For each field, the maximum reflectance position is located and the reading recorded. The stage is then rotated by 180° which should give the same reading. In practice, the readings are seldom identical because of stage run-out and slight surface irregularities. If the readings are within ±5% relative, they are accepted. If not, the cause of the difference is sought and the results rejected. The usual source of differences is surface relief. The measurement of both maxima results in a total of 50 measurements being taken for the 25 fields reported. Thus, the 50 readings consist of 25 pairs of closely spaced readings which provide a check on the levelling of the surface and hence additional precision.

As the vitrinite reflectance measurements are being made, the various features of the samples are noted on a check sheet to allow a sample description to be compiled. When the reflectance measurements are complete, a thorough check is made of liptinite fluorescence characteristics. At the same time, organic matter abundance is estimated using a global estimate, a grain count method or point count method as required.

Data presentation

Individual sample results are reported in the following format:

KK No.	Depth (ft)	$\overline{R}_V$max*1	Range*2	N*3
x10324	3106	0.79	0.64 - 0.91	25

*1 Mean of all the maximum reflectance readings obtained.
*2 Lowest Rmax and highest Rmax of the population considered to represent the first generation vitrinite population.
*3 Number of fields measured (Number of measurements = 2N because 2 maximum values are recorded for each field)

Methods - Organic matter abundance and type.

After completion of vitrinite reflectance readings, the microscope is switched to fluorescence-mode and an estimate made of the abundance of each liptinite maceral. Fluorescence colours are also noted (BG 3 long UV excitation, TK400 dichroic mirror and a K490 barrier filter). The abundances are estimated using comparison charts. The categories used for liptinite (and other components) are:

Descriptor	%	Source potential
Absent	0	None
Rare	<0.1	Very poor
Sparse	0.1<x<0.5	Poor to fair
Common	0.5<x<2.0	Fair to good
Abundant	2.0<x<10.0	Good to very good
Major	10.0<x<40.0	Very good (excellent if algal)
Dominant	>40.0	Excellent

Dispersed Organic Matter (DOM) composition

At the same time as liptinite abundances are estimated, total DOM, vitrinite and inertinite abundances are estimated and reported in the categories listed above. Liptinite (exinite) fluorescence intensity and colour, lithology and a brief description of organic matter type and abundance are also recorded in a further column. Coal is described separately from dispersed organic matter (DOM). These data can be used to estimate the specific yield of the DOM and form a valuable adjunct to TOC data.

Lithological composition

The lithological abundances are ranked. For cuttings, these data can be useful in conjunction with geophysical logs in assessing the abundance and nature of cavings. For cores, it provides a record of the lithology examined and of the lithological associations of the organic matter.

Coal abundance and composition

Where coals are present, their abundance is recorded and their composition is reported as microlithotypes thus:

Coal major, Vitrinite>Inertinite>Exinite, Clarodurite>vitrite>clarite>inertite.

These data give an approximate maceral composition and information about the organic facies of the coal. Where coal is a major or dominant component, and more precise maceral composition data are required, point count analyses should be requested. However, the precision of the original sampling is commonly a limiting factor in obtaining better quality data.

Abundance factor analysis

Especially where cuttings samples are used, abundance factor analyses are used to obtain an assessment of the maceral assemblages in the various lithologies. This can be done by a combination analysis using a point counter, but a large number of categories is required, and the precision is low if DOM is less than about 10%. For an abundance factor analysis (for core, 50 microscope fields of view) we assess the abundance of DOM, coal and shaly coal in 50 grains. The data can be used to plot DOM and coal abundance profiles.

Analyst/Advisor: Professor A.C. Cook

Prior to transmittal of final results, all samples are examined and checked by A.C. Cook who has more than 30 years' experience of work on coals, cokes, source rocks and source rock maturation.

D.3 Integration of vitrinite reflectance data with AFTA

Vitrinite reflectance is a time-temperature indicator governed by a kinetic response in a similar manner to the annealing of fission tracks in apatite as described in Appendix C. In this study, vitrinite reflectance data are interpreted on the basis of the distributed activation energy model describing the evolution of VR with temperature and time described by Burnham and Sweeney (1989), as implemented in the BasinMod™ software package of Platte River Associates. In a considerable number of wells from around the world, in which AFTA has been used to constrain the thermal history, we have found that the Burnham and Sweeney (1989) model gives good agreement between predicted and observed VR data, in a variety of settings.

As in the case of fission track annealing, it is clear from the chemical kinetic description embodied in equation 2 of Burham and Sweeney (1989) that temperature is more important than time in controlling the increase of vitrinite reflectance. If the Burham and Sweeney (1989) distributed activation energy model is expressed in the form of an Arrhenius plot (a plot of the logarithm of time versus inverse absolute temperature), then

the slopes of lines defining contours of equal vitrinite reflectance in such a plot are very similar to those describing the kinetic description of annealing of fission tracks in Durango apatite developed by Laslett et al. (1987), which is used to interpret the AFTA data in this report. This feature of the two quite independent approaches to thermal history analysis means that for a particular sample, a given degree of fission track annealing in apatite of Durango composition will be associated with the same value of vitrinite reflectance regardless of the heating rate experienced by a sample. Thus paleotemperature estimates based on either AFTA or VR data sets should be equivalent, regardless of the duration of heating. As a guide, Table D.1 gives paleotemperature estimates for various values of VR for two different heating times.

One practical consequence of this relationship between AFTA and VR is, for example, that a VR value of 0.7% is associated with total annealing of all fission tracks in apatite of Durango composition, and that total annealing of all fission tracks in apatites of more Chlorine-rich composition is accomplished between VR values of 0.7 and ~0.9%.

Furthermore, because vitrinite reflectance continues to increase progressively with increasing temperature, VR data allow direct estimation of maximum paleotemperatures in the range where fission tracks in apatite are totally annealed (generally above ~110°C) and where therefore AFTA only provides minimum estimates. Maximum paleotemperature estimates based on vitrinite reflectance data from a well in which most AFTA samples were totally annealed will allow constraints on the paleogeothermal gradient that would not be possible from AFTA alone. In such cases the AFTA data should allow tight constraints to be placed on the time of cooling and also the cooling history, since AFTA parameters will be dominated by the effects of tracks formed after cooling from maximum paleotemperatures. Even in situations where AFTA samples were not totally annealed, integration of AFTA and VR can allow paleotemperature control over a greater range of depth, e.g. by combining AFTA from sand-dominated units with VR from other parts of the section, thereby providing tighter constraint on the paleogeothermal gradient.

D.2 Client-supplied vitrinite reflectance

Vitrinite reflectance and other data (if applicable) supplied by the client is summarised in Table D.3. Unless specified, this vitrinite reflectance data has been treated at face value, as if it were collected in the same manner as described for the new data, because detailed information is usually not available.

Table D.1: Paleotemperature - vitrinite reflectance nomogram based on Equation 2 of Burnham and Sweeney (1989)

Paleotemperature (°C/°F)	Vitrinite Reflectance (%) 1 Ma Duration of heating	10 Ma Duration of heating
40 / *104*	0.29	0.32
50 / *122*	0.31	0.35
60 / *140*	0.35	0.40
70 / *158*	0.39	0.45
80 / *176*	0.43	0.52
90 / *194*	0.49	0.58
100 / *212*	0.55	0.64
110 / *230*	0.61	0.70
120 / *248*	0.66	0.78
130 / *266*	0.72	0.89
140 / *284*	0.81	1.04
150 / *302*	0.92	1.20
160 / *320*	1.07	1.35
170 / *338*	1.23	1.55
180 / *356*	1.42	1.80
190 / *374*	1.63	2.05
200 / *392*	1.86	2.33
210 / *410*	2.13	2.65
220 / *428*	2.40	2.94
230 / *446*	2.70	3.23

References

Burnham, A. K. and Sweeney, J. J. (1989). A chemical kinetic model of vitrinite reflectance maturation. *Geochim. et Cosmochim. Acta*, 53, 2649-2657.

Laslett, G. M., Green, P. F., Duddy, I. R. and Gleadow, A. J. W. (1987). Thermal annealing of fission tracks in apatite 2. A quantitative analysis. *Chem. Geol. (Isot. Geosci.Sect.)*, 65, 1-13.

Table D.2: Vitrinite reflectance sample details and results - well samples from the Duntroon Basin (Geotrack Report #569)

Sample number	Depth (m)	Sample type	Stratigraphic subdivision	Stratigraphic age (Ma)	Present temperature *1 (°C)	VR %	N
Vivonne-1							
GC569-14.1	920-925	cuttings	Wilson Bluff U.Eocene - L.Oligocene	42-29	38	0.31 (0.22-0.43)	23
GC569-15.1	1128-1131	cuttings	L.Pidinga Paleocene	65-56	44	0.34 (0.27-0.39)	25
GC569-16.1	1215-1218	cuttings	L.Pidinga Paleocene	65-56	47	0.34 (0.28-0.42)	7
GC569-18.1	1316-1319	cuttings	U.Borda Aptian	124-112	50	0.39 (0.31-0.44)	27
GC569-19.1	1371-1374	cuttings	U.Borda Aptian	124-112	52	0.38 (0.30-0.49)	17
GC569-20.1	1468-1471	cuttings	U.Borda Aptian	124-112	54	0.38 (0.32-0.44)	15
GC569-21.1	1583-1586	cuttings	U.Borda Aptian	124-112	58	0.38 (0.31-0.46)	26
GC569-22.1	2007-2010	cuttings	U.Borda Aptian	124-112	71	0.55 (0.43-0.65)	25
GC569-24.1	2489-2492	cuttings	L.Borda Barremian	132-124	85	0.64 (0.53-0.77)	27
GC569-26.1	2685-2688	cuttings	L.Borda Barremian	132-124	91	0.75 (0.63-0.86)	26
GC569-27.1	2822-2825	cuttings	L.Borda Barremian	132-124	95	0.64 (0.51-0.77)	27

Table D.2: Continued

Sample number	Depth (m)	Sample type	Stratigraphic subdivision	Stratigraphic age (Ma)	Present temperature *1 (°C)	VR %	N
Borda-1							
GC569-1.1	1300-1305	cuttings	Wilson Bluff U.Eocene - L.Oligocene	42-29	45	0.21 (0.17-0.24)	6
GC569-2.1	1435-1440	cuttings	Wilson Bluff U.Eocene - L.Oligocene	42-29	49	0.28 (0.25-0.32)	6
GC569-3.1	1620-1625	cuttings	Wilson Bluff U.Eocene - L.Oligocene	42-29	54	0.37 (0.27-0.48)	10
GC569-4.1	1830-1835	cuttings	Wilson Bluff U.Eocene - L.Oligocene	42-29	60	0.37 (0.31-0.51)	13
GC569-5.1	2033-2036	cuttings	Wilson Bluff U.Eocene - L.Oligocene	42-29	65	0.41 (0.32-0.51)	21
GC569-6.1	2102-2105	cuttings	Wilson Bluff U.Eocene - L.Oligocene	42-29	67	0.39 (0.30-0.52)	13
GC569-7.1	2174-2177	cuttings	L.Pidinga Paleocene	65-56	69	0.46 (0.41-0.49)	7
GC569-9.1	2282-2285	cuttings	L.Pidinga Paleocene	65-56	72	0.47 (0.41-0.50)	3
GC569-10.1	2360-2363	cuttings	L.Pidinga Paleocene	65-56	74	0.45 (0.44-0.45)	3
GC569-11.1	2537-2540	cuttings	Potoroo Maastrichtian	74-65	79	0.52 (0.45-0.59)	15
GC569-12.1	2675-2678	cuttings	Potoroo Maastrichtian	74-65	83	0.53 (0.46-0.62)	29

Note: Some samples may contain both vitrinite and inertinite. Only vitrinite data is shown for these samples.

*1 See Appendix A for discussion of present temperature data.

Table D.3: Vitrinite reflectance data supplied by client - well samples from the Duntroon Basin (Geotrack Report #569)

Sample number	Depth (m)	Stratigraphic subdivision	Stratigraphic age (Ma)	Present temperature *1 (°C)	VR %	N
Vivonne-1						
SWC-18	1718	U.Borda Aptian	124-112	62	0.42 (0.31-0.53)	25
SWC-16	1828	U.Borda Aptian	124-112	65	0.47 (0.37-0.59)	25
SWC-12	2058	U.Borda Aptian	124-112	72	0.53 (0.43-0.63)	25
SWC-9	2219	U.Borda Aptian	124-112	77	0.67 (0.55-0.80)	27
SWC-7	2312	U.Borda Aptian	124-112	80	0.73 (0.63-0.80)	25
SWC-4	2473	L.Borda Barremian	132-124	85	0.78 (0.69-0.87)	25
SWC-1	2660	L.Borda Barremian	132-124	90	0.77 (0.63-0.93)	25
Borda-1						
SWC-70	2302	L.Pidinga Paleocene	65-56	73	0.58 (0.51-0.68)	12
SWC-63	2465	Potoroo Maastrichtian	74-65	77	0.50 (0.35-0.64)	26
SWC-55	2582	Potoroo Maastrichtian	74-65	80	0.52 (0.42-0.66)	26
SWC-48	2652	Potoroo Maastrichtian	74-65	82	0.56 (0.48-0.69)	29
SWC-33	2792	Potoroo Maastrichtian	74-65	86	0.55 (0.46-0.67)	25

*1 See Appendix A for discussion of present temperature data.

JOB # 569, MESA, VIVONNE-1

KK/Ref. No.	Depth(m) Type	$\dot{R}_v$ max	Range	N	Description Including Liptinite (Exinite) Fluorescence
					WILSON BLUFF
T1419 14.1	920-925 Ctgs	0.31	0.22-0.43	23	Sparse lamalginite, green to yellow, rare liptodetrinite, bright yellow. (Carbonate>>claystone. Dom sparse, L>V>I. Vitrinite and liptinite sparse, inertinite rare. Mineral fluorescence pervasive, weak green to orange. Forams and other fossils abundant. Glauconite common. Iron oxides rare. Pyrite common.)
					LOWER PIDINGA
T1420 15.1	1128-1131 Ctgs	0.34	0.27-0.39	25	Rare sporinite, orange, rare lamalginite, yellow to orange, rare liptodetrinite, yellow to orange. (Sandstone>carbonate> siltstone. Dom sparse, V>I>L. Vitrinite sparse, inertinite and liptinite rare. Mineral fluorescence patchy, weak green to yellow. Glauconite sparse. Iron oxides rare. Pyrite common.)
T1421 16.1	1215-1218 Ctgs	0.34	0.28-0.42	7	Rare liptodetrinite, yellow. (Siltstone>>claystone. Dom rare, V>I>L. All three maceral groups rare. Mineral fluorescence patchy, yellow to orange. Iron oxides common. Pyrite sparse.)
					POTOROO-UPPER BORDA
T1422 18.1	1332-1335 Ctgs	0.39	0.31-0.44	27	Common cutinite and liptodetrinite, yellow to dull orange, sparse lamalginite, sporinite and resinite, yellow to orange. (Clayey siltstone>sandstone>coal. Coal abundant, vitrite. Mineral-free maceral group composition of the coal: vitrinite - 100%, inertinite - tr., liptinite - tr. Dom abundant, L>V>>I. Liptinite and vitrinite common, inertinite rare. Mineral fluorescence pervasive, moderate yellow to orange. Iron oxides common. Pyrite sparse.)
					UPPER BORDA
T1423 19.1	1392-1395 Ctgs	0.38	0.30-0.49	17	Sparse lamalginite and liptodetrinite, bright yellow to orange, rare cutinite and sporinite, yellow to orange. (Silty claystone>>carbonate. Dom common, I>L>V. All three maceral groups sparse. Mineral fluorescence pervasive, moderate yellow to weak orange. Iron oxides sparse. Pyrite abundant.)
T1424 20.1	1497-1500 Ctgs	0.38	0.32-0.44	15	Sparse lamalginite, yellow to orange, rare liptodetrinite, yellow to orange, rare sporinite, orange, rare Botryococcus-related telalginite, bright yellow. (Clayey siltstone. Dom sparse, L>I>V. Liptinite and inertinite sparse, vitrinite rare. Mineral fluorescence pervasive, moderate orange. Iron oxides abundant. Pyrite common.)
T1425 21.1	1623-1626 Ctgs	0.38	0.31-0.46	26	Sparse lamalginite, greenish yellow to orange, rare liptodetrinite, yellow. (Clayey siltstone. Dom common, I>L=V. Inertinite common, liptinite and vitrinite sparse. Mineral fluorescence pervasive, moderate orange. Iron oxides abundant. Pyrite sparse.)

JOB # 569, MESA, VIVONNE-1

KK/Ref. No.	Depth(m) Type	$\bar{R}_v$max	Range	N	Description Including Liptinite (Exinite) Fluorescence
					UPPER BORDA
T1426 22.1	2085-2088 Ctgs	0.55	0.43-0.65	25	Sparse cutinite and sporinite, yellow to orange, rare resinite, yellow, rare lamalginite, bright yellow, rare suberinite, weak brown, rare liptodetrinite, yellow to orange. (Clayey siltstone>>carbonate>coal. Coal abundant, V>>L>I. Vitrite>duroclarite. Mineral-free maceral group composition of the coal: vitrinite - 90%, inertinite - <0.1%, liptinite - 10%. Dom common, V>L>I. All three maceral groups sparse. Mineral fluorescence pervasive, yellow to orange. Iron oxides sparse. Pyrite common.)
					LOWER BORDA
T1427 24.1	2610-2613 Ctgs	0.64	0.53-0.77	27	Sparse cutinite and sporinite, yellow to orange, rare liptodetrinite, yellow to orange. (Clayey siltstone>>carbonate> coal. Coal sparse, V>>L>I. Vitrite>clarite. Dom common, V>I>L. Vitrinite common, inertinite and liptinite sparse. Mineral fluorescence pervasive, yellow to orange. Iron oxides common. Pyrite sparse.)
T1428 26.1	2823-2826 Ctgs	0.75	0.63-0.86	26	Sparse cutinite and sporinite, yellow to orange, rare liptodetrinite, yellow to orange. (Siltstone>>coal. Coal sparse, V>>L. Vitrite>clarite. Dom common, L>V>I. Liptinite common, vitrinite and inertinite sparse. Oil drops sparse, greenish yellow. Mineral fluorescence pervasive, yellow to orange. Iron oxides common. Pyrite sparse.)
T1429 27.1	2973-2976 Ctgs	0.64	0.51-0.77	27	Common liptodetrinite, yellow to orange, sparse cutinite and sporinite, yellow to orange. (Silty claystone>shaly coal. Shaly coal common, V>>L, vitrite>>clarite. Dom abundant, V>>L>>I. Vitrinite abundant, liptinite common, inertinite sparse. Mineral fluorescence pervasive, moderate green to yellow. Iron oxides sparse. Pyrite sparse.)

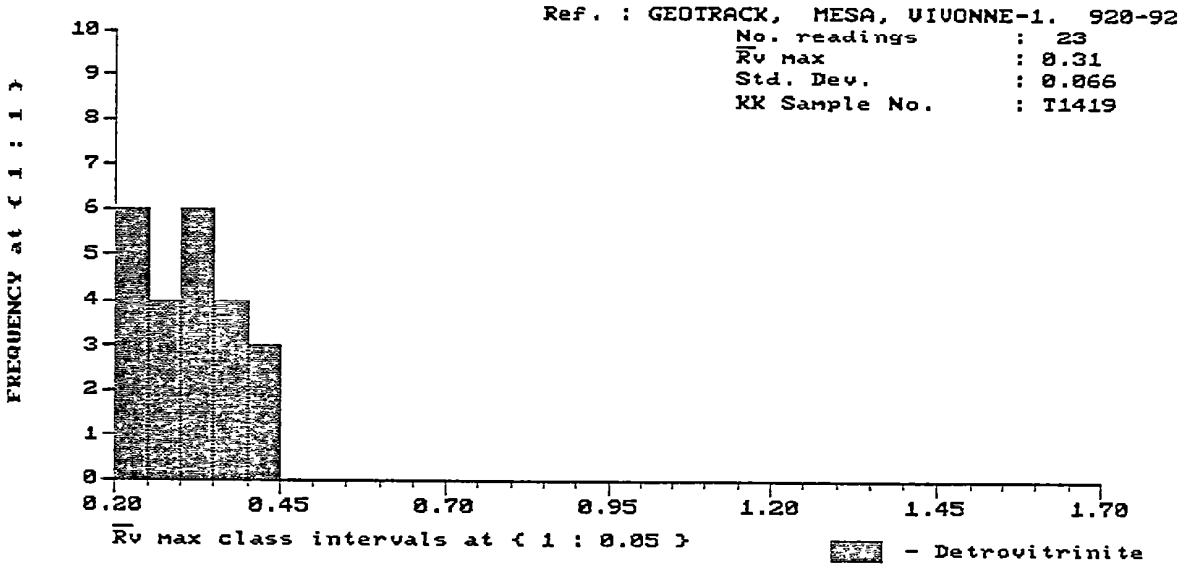

Keiraville Konsultants Pty. Ltd.

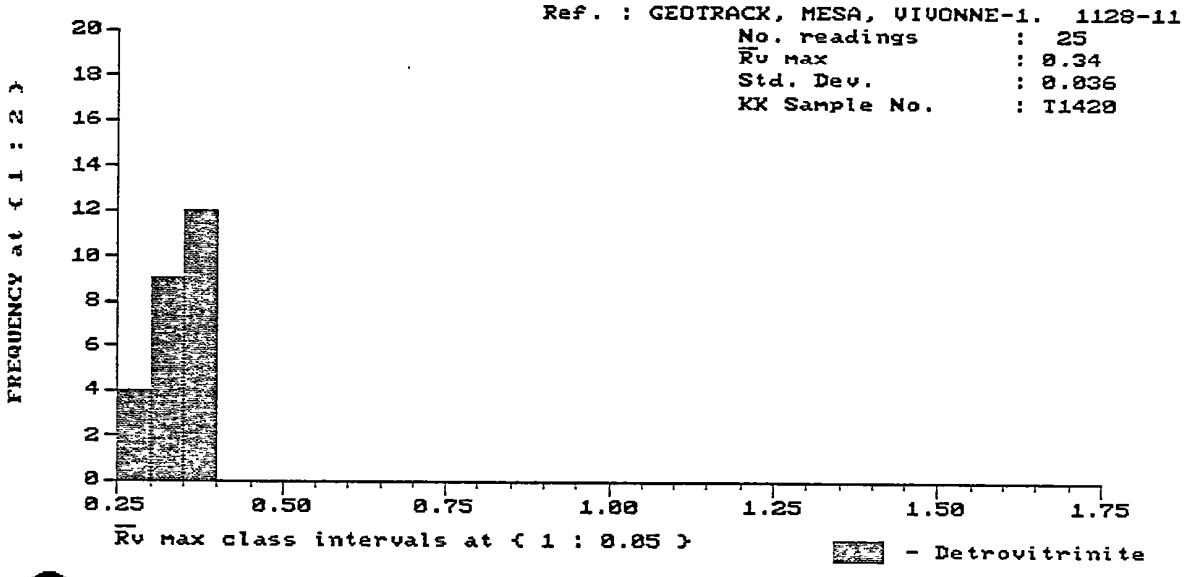

Keiraville Konsultants Pty. Ltd.

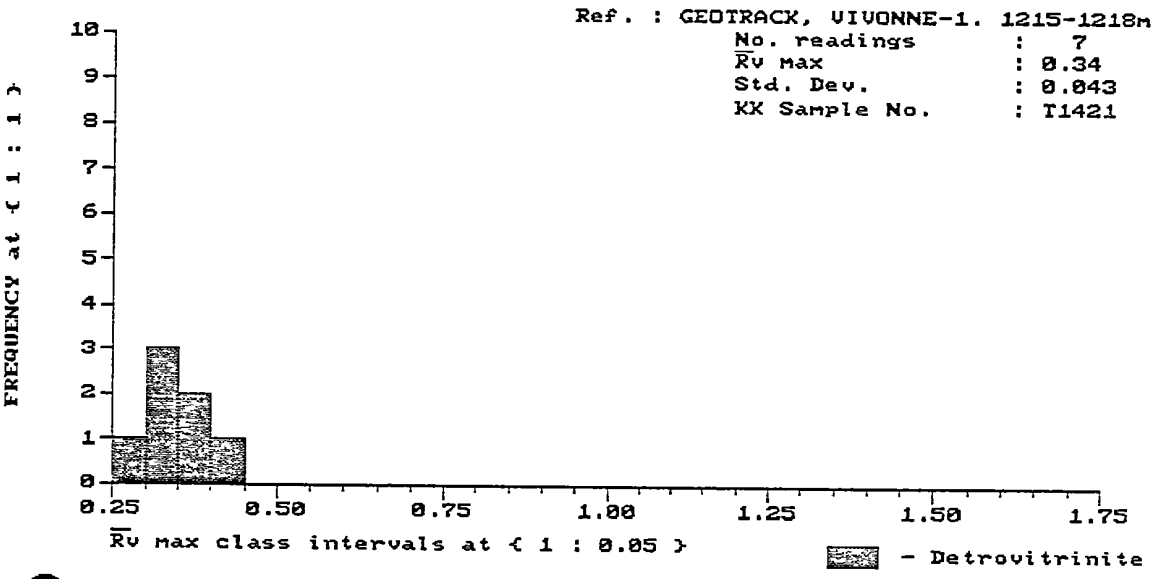

Keiraville Konsultants Pty. Ltd.

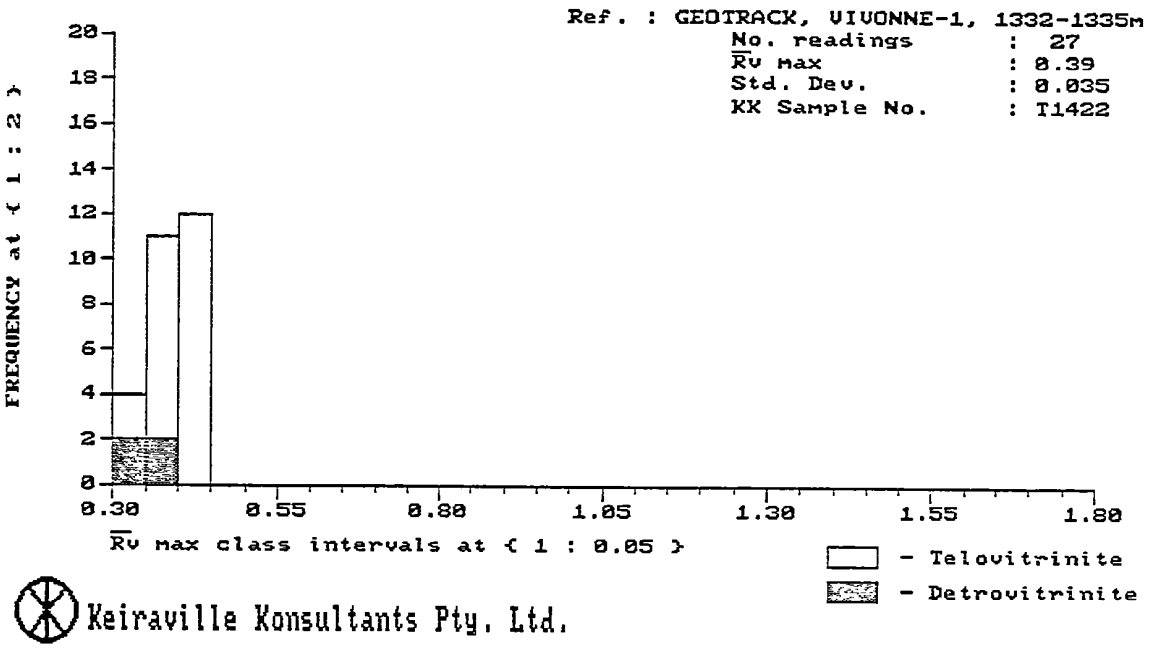
Ref. : GEOTRACK, VIVONNE-1, 1332-1335m
No. readings : 27
Rv max : 0.39
Std. Dev. : 0.035
KK Sample No. : I1422
FREQUENCY at (1 : 2)
0
2
4
6
8
10
12
14
16
18
20
0.30
0.55
0.80
1.05
1.30
1.55
1.80
Rv max class intervals at (1 : 0.05)
- Telovitrinite
- Detrovitrinite
Keiraville Konsultants Pty. Ltd.

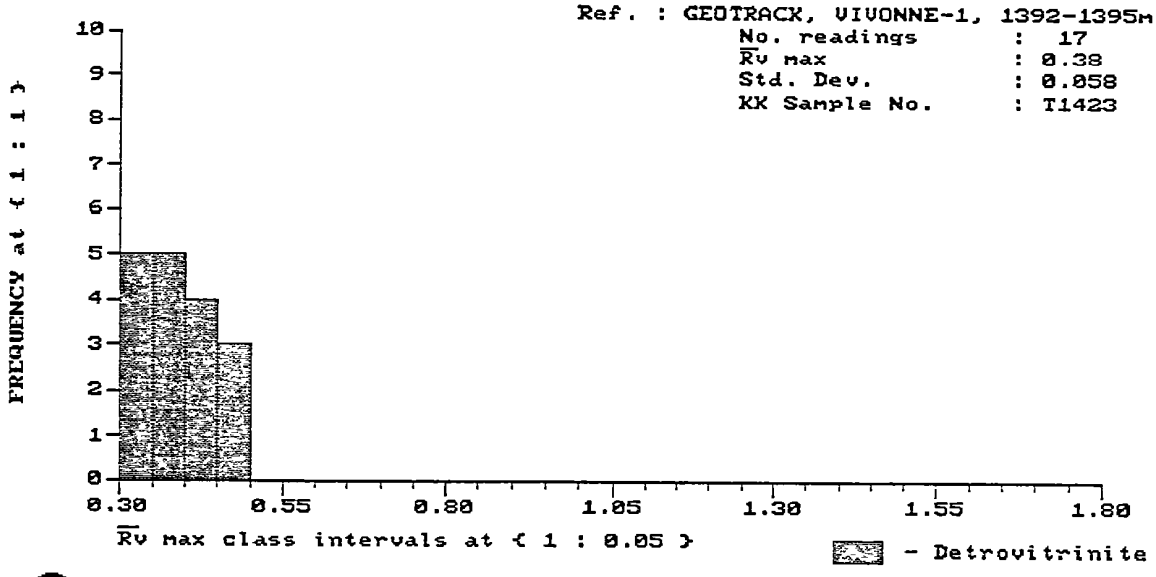

Keiraville Konsultants Pty. Ltd.

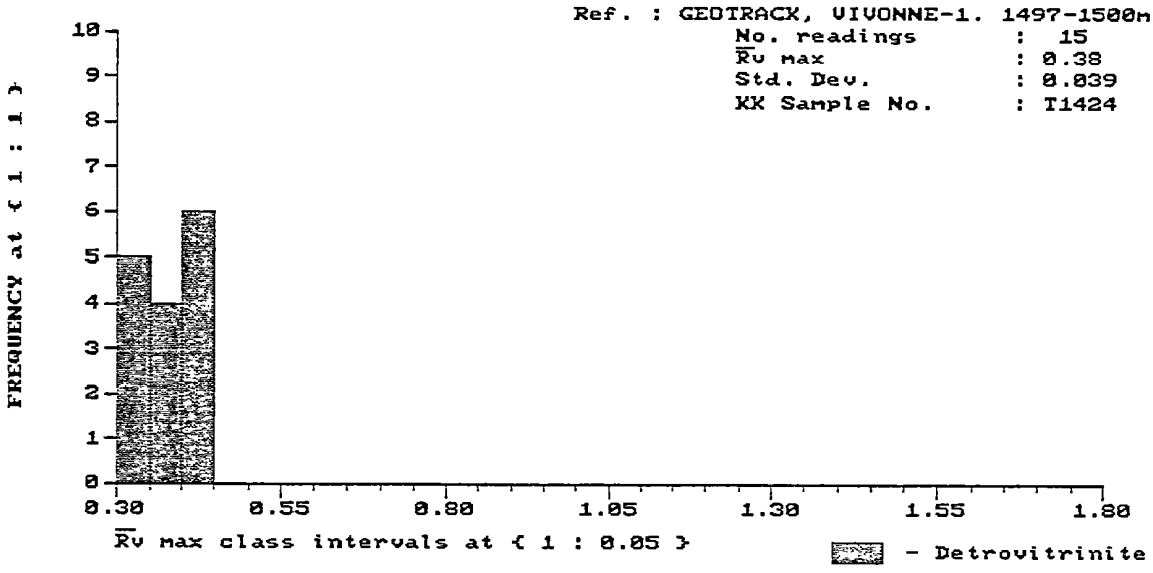

Keiraville Konsultants Pty. Ltd.

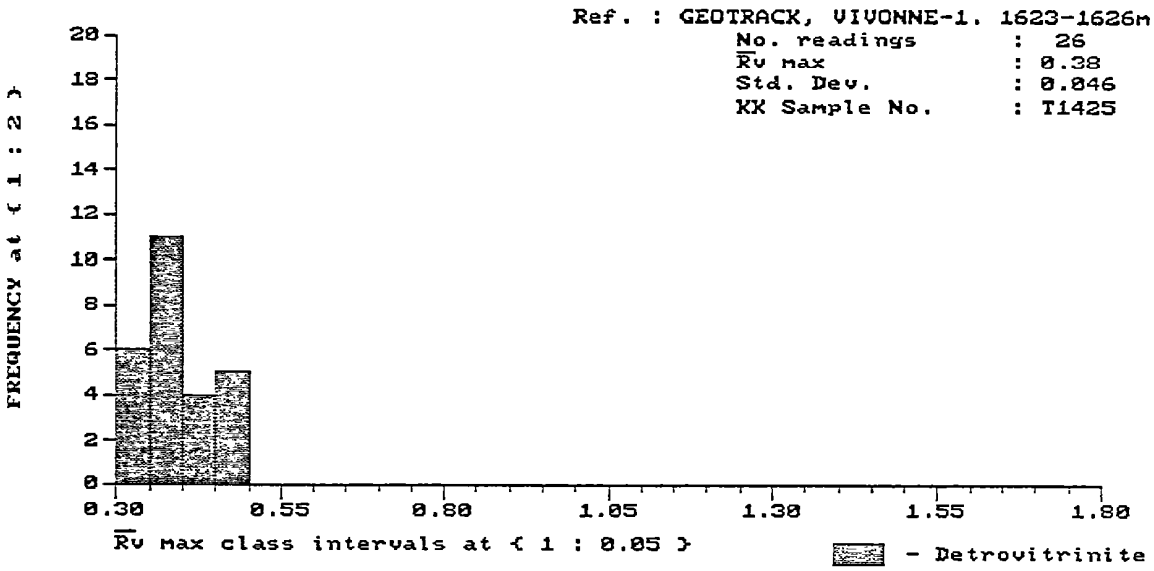

Keiraville Konsultants Pty. Ltd.

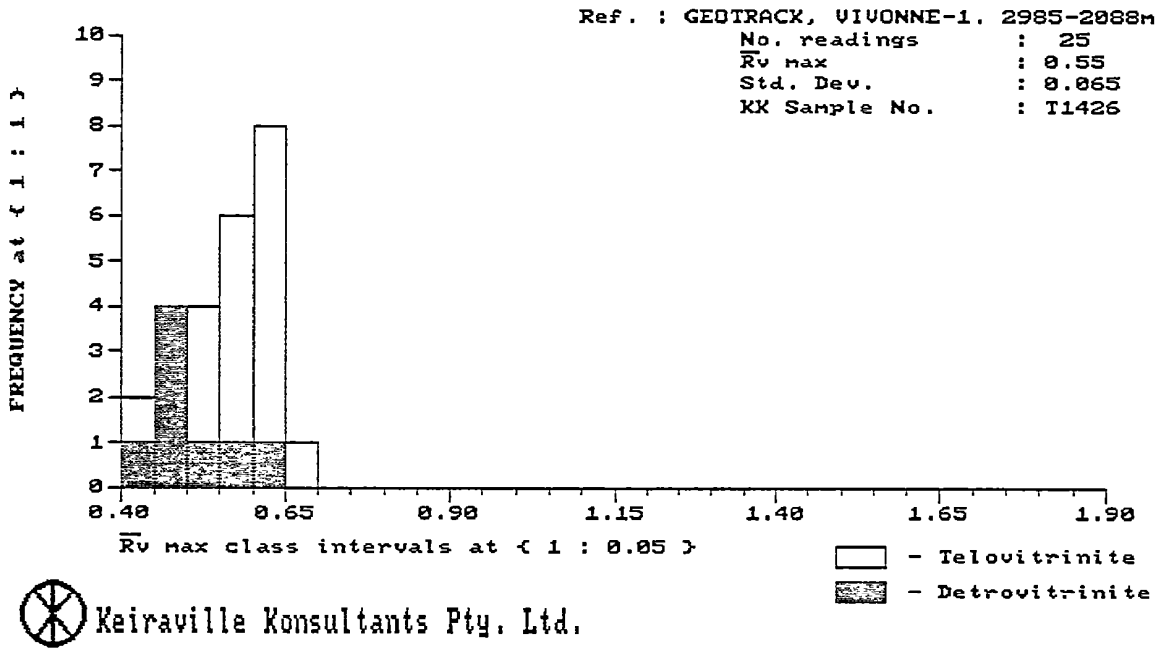

Keiraville Konsultants Pty. Ltd.

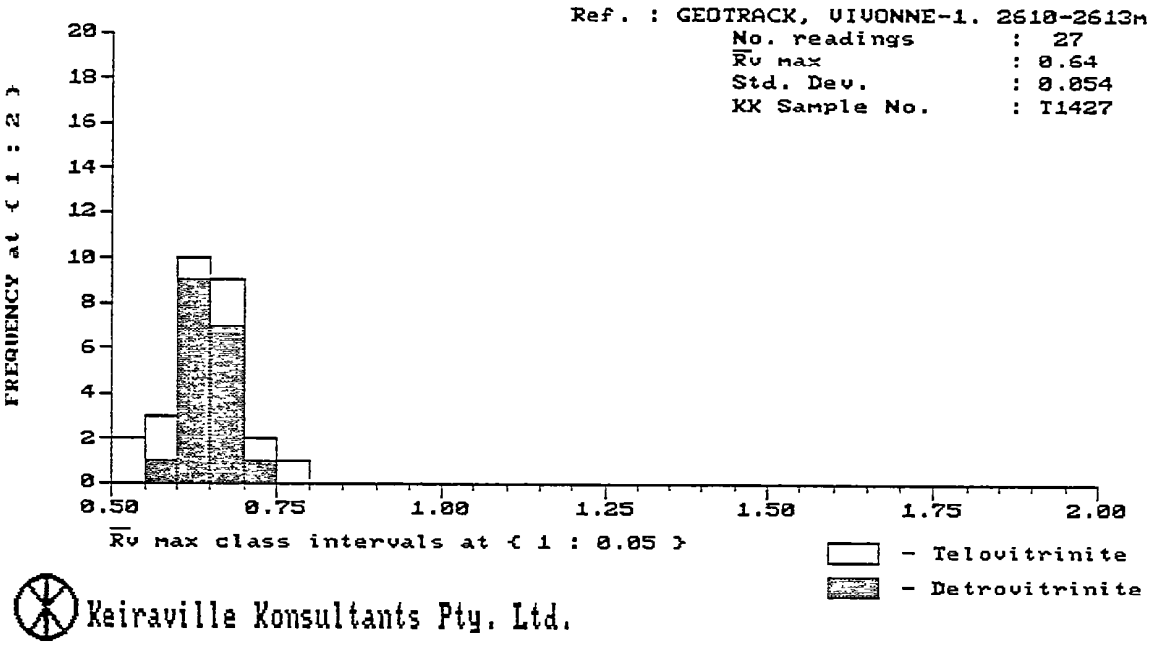

Keiraville Konsultants Pty. Ltd.

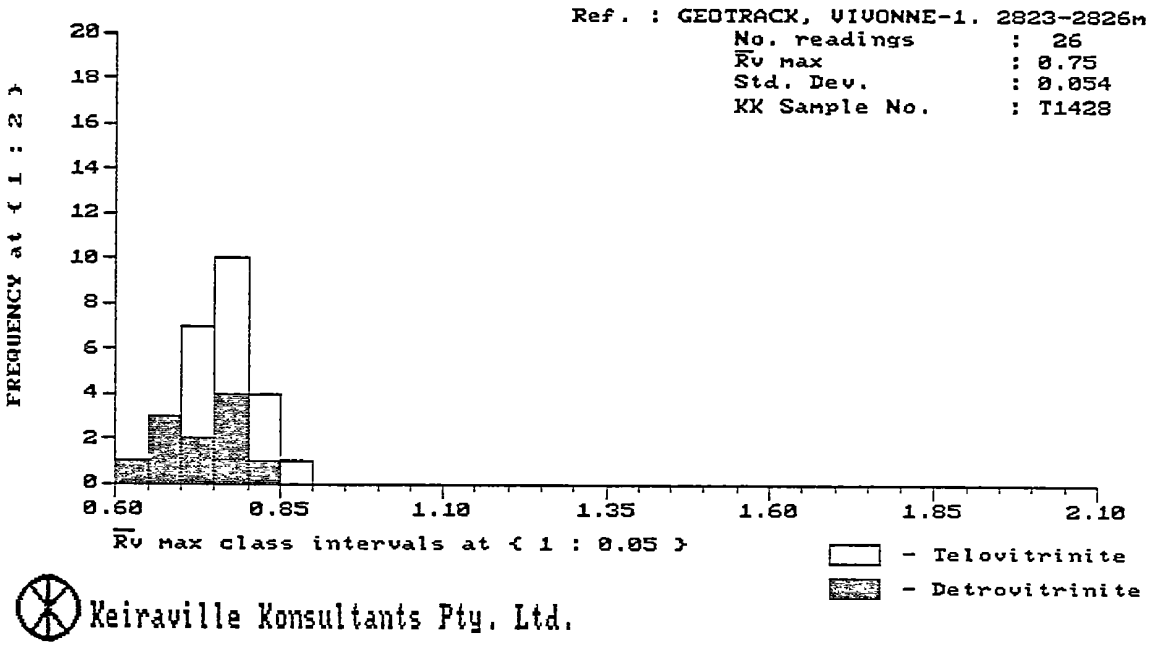
Ref. : GEOTRACK, VIVONNE-1. 2823-2826m
No. readings : 26
Rv max : 0.75
Std. Dev. : 0.054
KK Sample No. : T1428
FREQUENCY at (1 : 2)
20
18
16
14
12
10
8
6
4
2
0
0.60
0.85
1.10
1.35
1.60
1.85
2.10
Rv max class intervals at (1 : 0.05)
- Telovitrinite
- Detrovitrinite
Keiraville Konsultants Pty. Ltd.

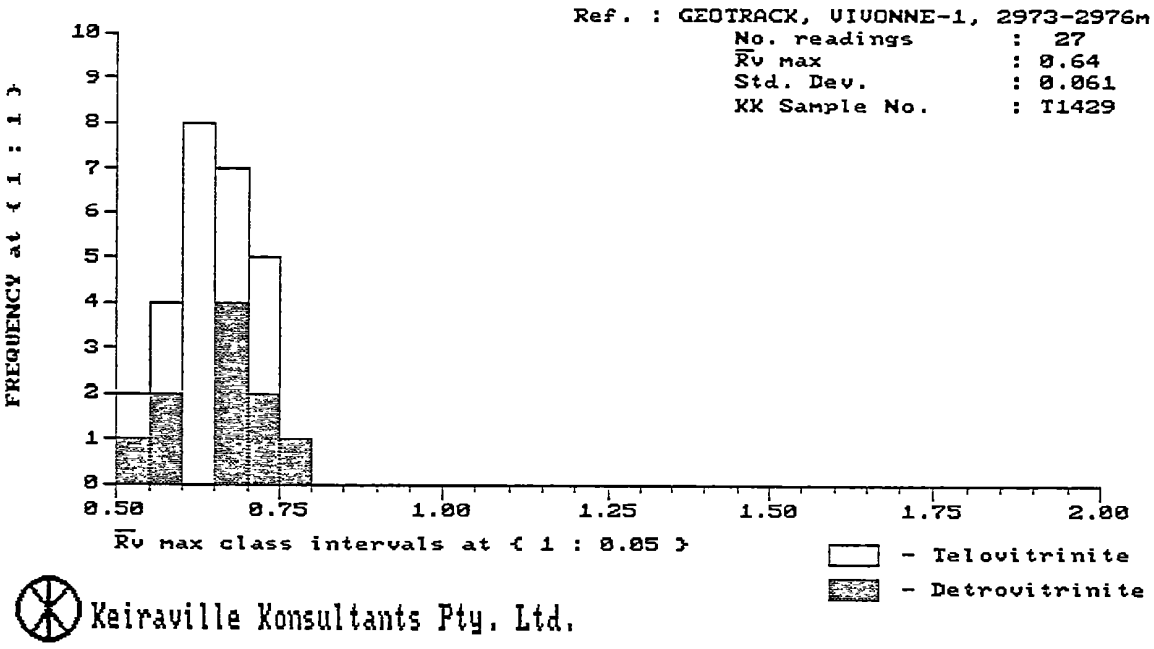

Keiraville Konsultants Pty. Ltd.

JOB # 569, MESA, BORDA-1

KK/Ref. No.	Depth(m) Type	$\bar{R}_v$ max	Range	N	Description Including Liptinite (Exinite) Fluorescence
					WILSON BLUFF
T1408 1.1	1300-1305 Ctgs	0.21	0.17-0.24	6	Rare lamalginite, green to yellow, rare liptodetrinite, yellow. (Carbonate. Dom rare, I=V>L. All three maceral groups rare. Mineral fluorescence pervasive, yellow to orange. Iron oxides rare. Pyrite sparse.)
T1409 2.1	1435-1440 Ctgs	0.28	0.25-0.32	6	Fluorescing liptinite absent. (Carbonate>>calcareous siltstone. Dom rare, V>I. Vitrinite and inertinite rare, liptinite absent. Mineral fluorescence pervasive, yellow. Forams and other fossil fragments sparse. Shell fragments rare. Iron oxides rare. Pyrite abundant.)
T1410 3.1	1620-1625 Ctgs	0.37	0.27-0.48	10	Rare lamalginite and liptodetrinite, greenish yellow. (Carbonate>>calcareous siltstone. Dom rare, V>I=L. All three maceral groups rare. Mineral fluorescence pervasive, yellow to orange. Forams and other fossil fragments abundant. Iron oxides rare. Pyrite abundant.)
T1411 4.1	1830-1835 Ctgs	0.37	0.31-0.51	13	Rare lamalginite and liptodetrinite, greenish yellow. (Carbonate>>calcareous siltstone. Dom rare, I>V=L. All three maceral groups rare. Mineral fluorescence pervasive, yellow to orange. Forams and other fossil fragments common. Iron oxides rare. Pyrite common.)
T1412 5.1	2033-2036 Ctgs	0.41	0.32-0.51	21	Rare lamalginite and liptodetrinite, greenish yellow. (Carbonate>calcareous siltstone. Dom rare, V=L=I. All three maceral groups rare. Mineral fluorescence pervasive, weak greenish yellow. Forams and other fossil fragments common. Iron oxides sparse. Pyrite abundant.)
T1413 6.1	2102-2105 Ctgs	0.39	0.30-0.52	13	Rare lamalginite and liptodetrinite, yellow. (Carbonate> calcareous siltstone. Dom rare, V>I>L. All three maceral groups rare. Mineral fluorescence pervasive, yellow to orange. Forams and other fossil fragments abundant. Iron oxides sparse. Pyrite common.)
					LOWER PIDINGA
T1414 7.1	2174-2177 Ctgs	0.46	0.41-0.49	7	Rare lamalginite, yellow to orange. (Sandstone>siltstone> carbonate. Dom rare, V=I>L. All three maceral groups rare. Mineral fluorescence patchy, yellow to orange. Forams and other fossil fragments sparse. Iron oxides abundant. Pyrite abundant.)
T1415 9.1	2282-2285 Ctgs	0.47	0.41-0.50	3	Rare lamalginite and liptodetrinite, yellow to orange. (Sandstone>siltstone. Dom rare, V>I>L. All three maceral groups rare. Mineral fluorescence pervasive, faint green. Iron oxides abundant. Pyrite abundant.)
T1416 10.1	2360-2363 Ctgs	0.45	0.44-0.45	3	Rare lamalginite and liptodetrinite, yellow, rare sporinite, orange. (Siltstone>sandstone. Dom rare, I>V>L. All three maceral groups rare. Mineral fluorescence pervasive, weak green. Iron oxides major. Pyrite abundant.)

JOB # 569, MESA, BORDA-1

KK/Ref. No.	Depth(m) Type	$\bar{R}_v$ max	Range	N	Description Including Liptinite (Exinite) Fluorescence
					POTOROO
T1417 11.1	2537-2540 Ctgs	0.52	0.45-0.59	15	Rare lamalginite and liptodetrinite, yellow, rare sporinite, dull orange. (Siltstone. Dom sparse, V>I=L. Vitrinite sparse, inertinite and liptinite rare. Mineral fluorescence pervasive, faint green. Iron oxides sparse. Pyrite abundant.)
T1418 12.1	2675-2678 Ctgs	0.53	0.46-0.62	29	Rare lamalginite and liptodetrinite, yellow to orange, rare cutinite, orange. (Siltstone>>sandstone. Dom sparse, V>I=L. Vitrinite sparse, inertinite and liptinite rare. Mineral fluorescence pervasive, weak green. Iron oxides sparse. Pyrite abundant.)

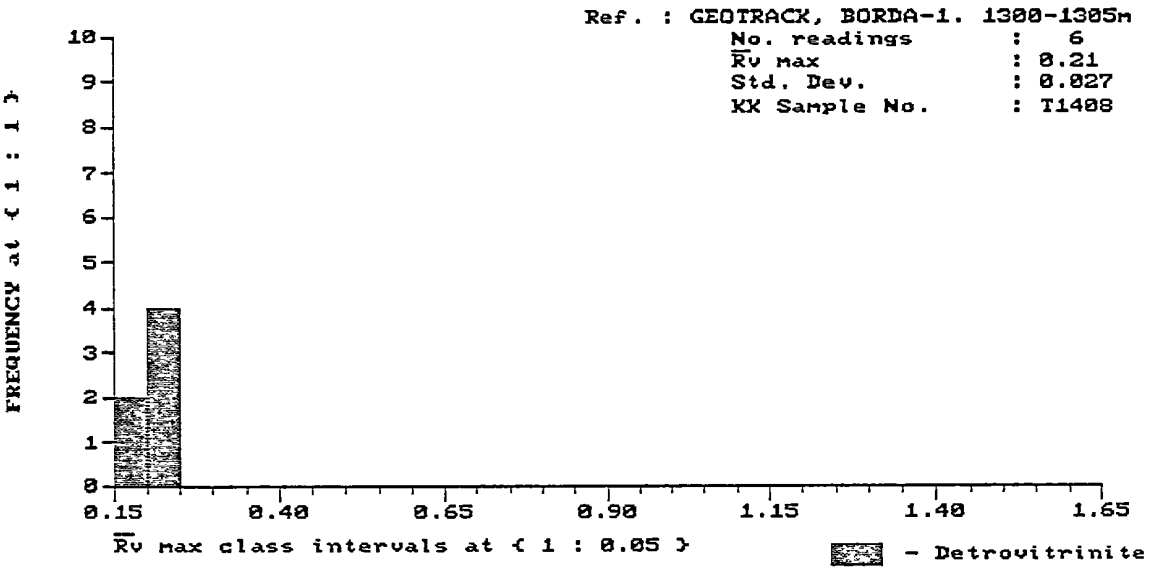

Keiraville Konsultants Pty. Ltd.

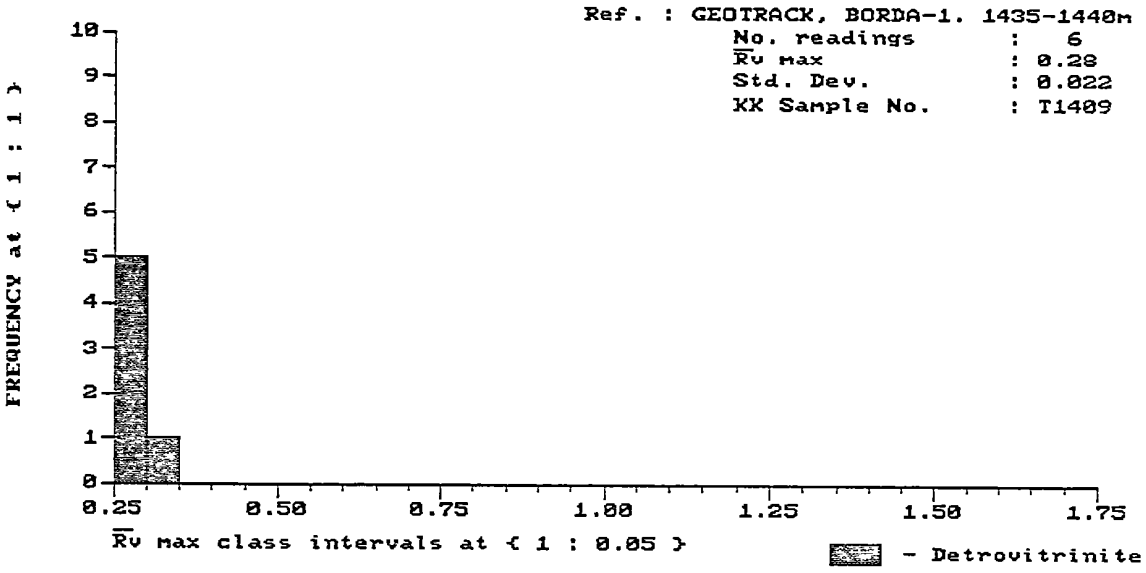

Keiraville Konsultants Pty. Ltd.

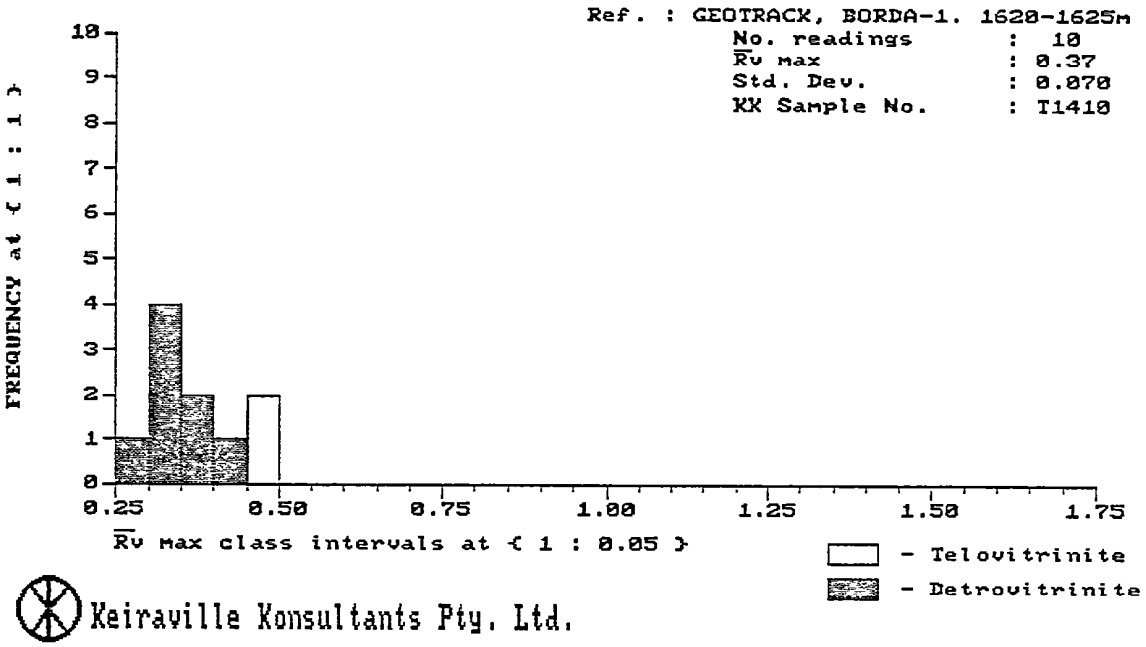
Ref. : GEOTRACK, BORDA-1. 1620-1625m
No. readings : 10
Rv max : 0.37
Std. Dev. : 0.070
KK Sample No. : I1410
FREQUENCY at (1 : 1)
0
1
2
3
4
5
6
7
8
9
10
0.25
0.50
0.75
1.00
1.25
1.50
1.75
Rv max class intervals at (1 : 0.05)
- Telovitrinite
- Detrovitrinite
Keiraville Konsultants Pty. Ltd.

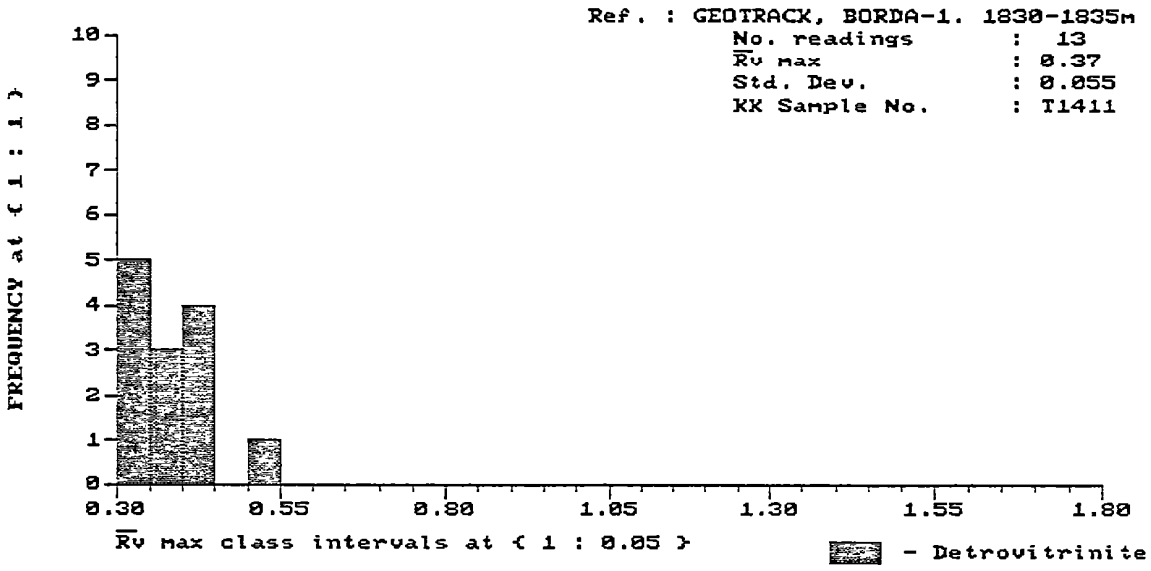

Keiraville Konsultants Pty. Ltd.

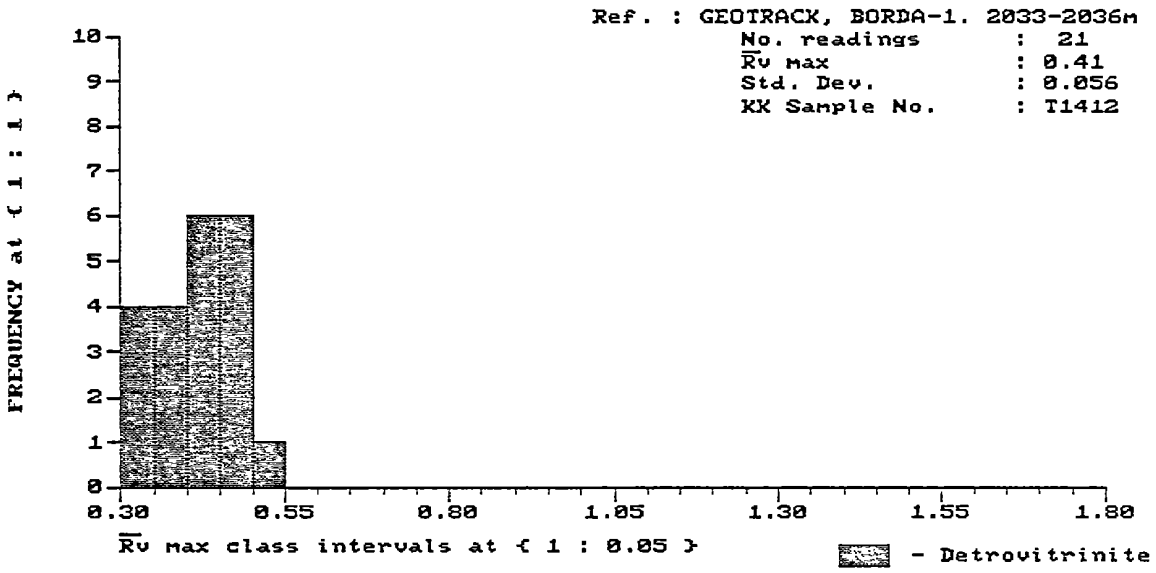

Keiraville Konsultants Pty. Ltd.

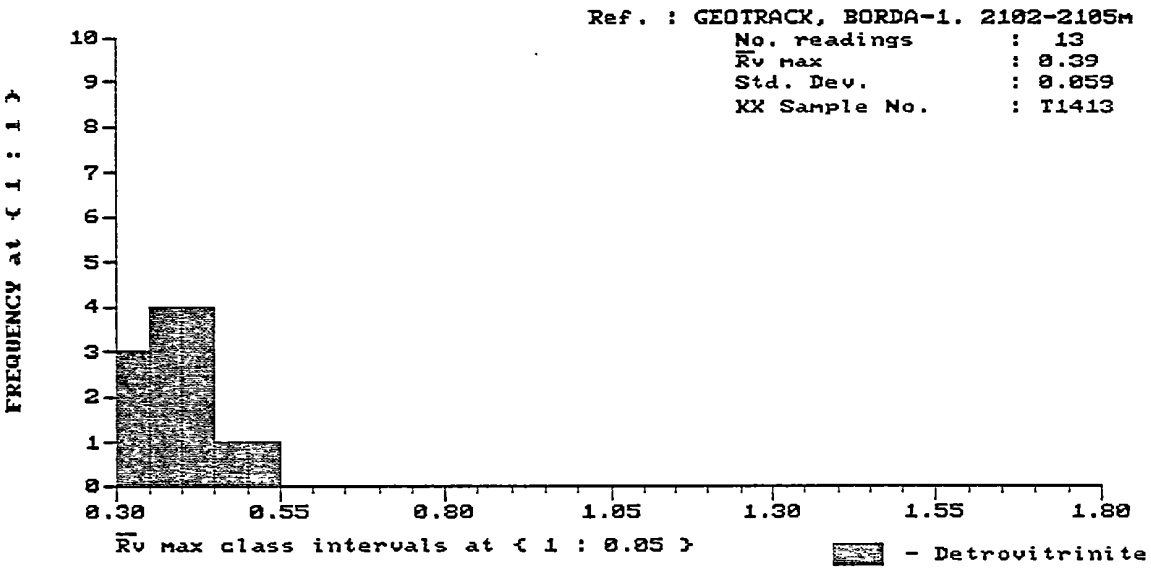

Keiraville Konsultants Pty. Ltd.

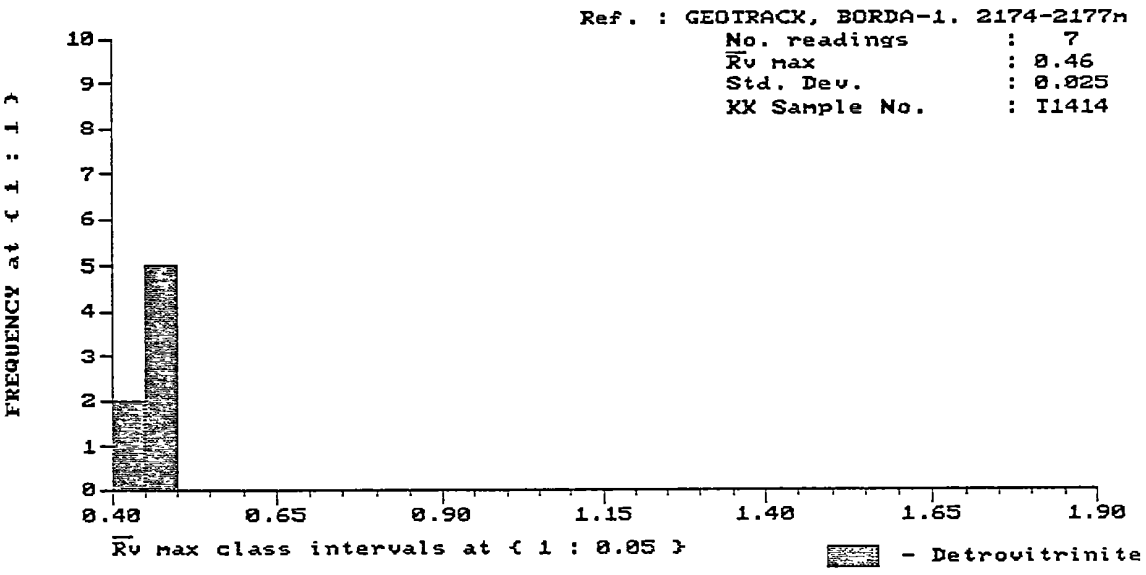

Keiraville Konsultants Pty. Ltd.

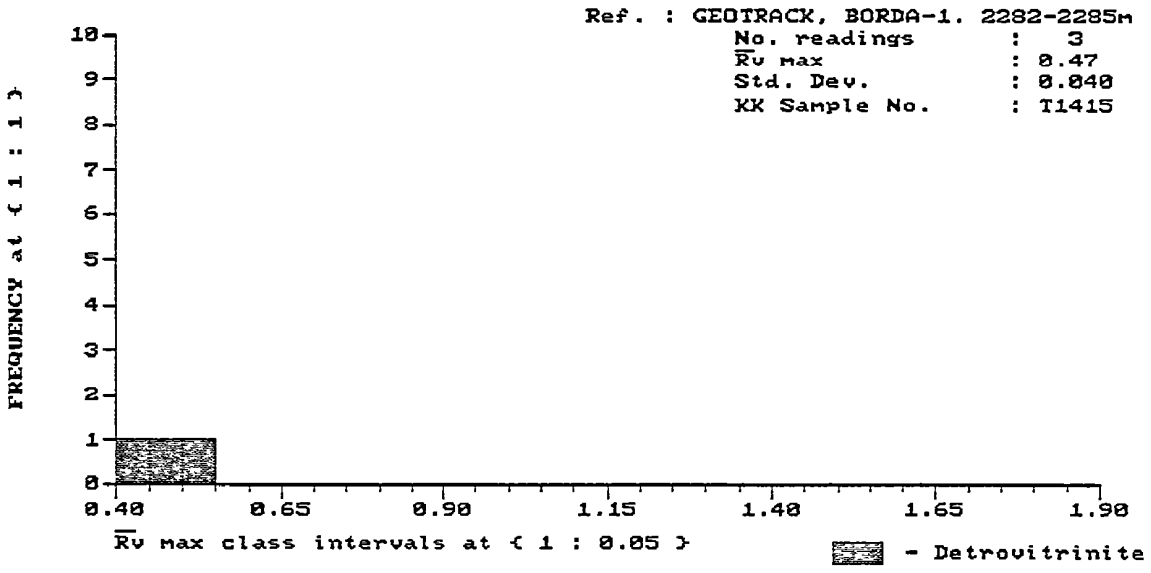

Keiraville Konsultants Pty. Ltd.

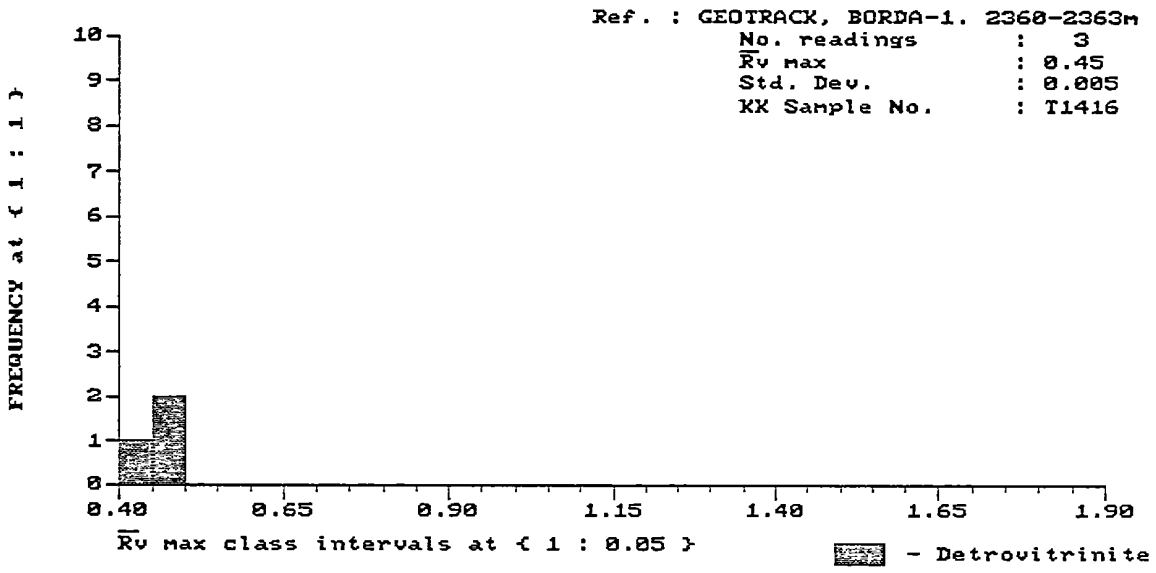

Keiraville Konsultants Pty. Ltd.

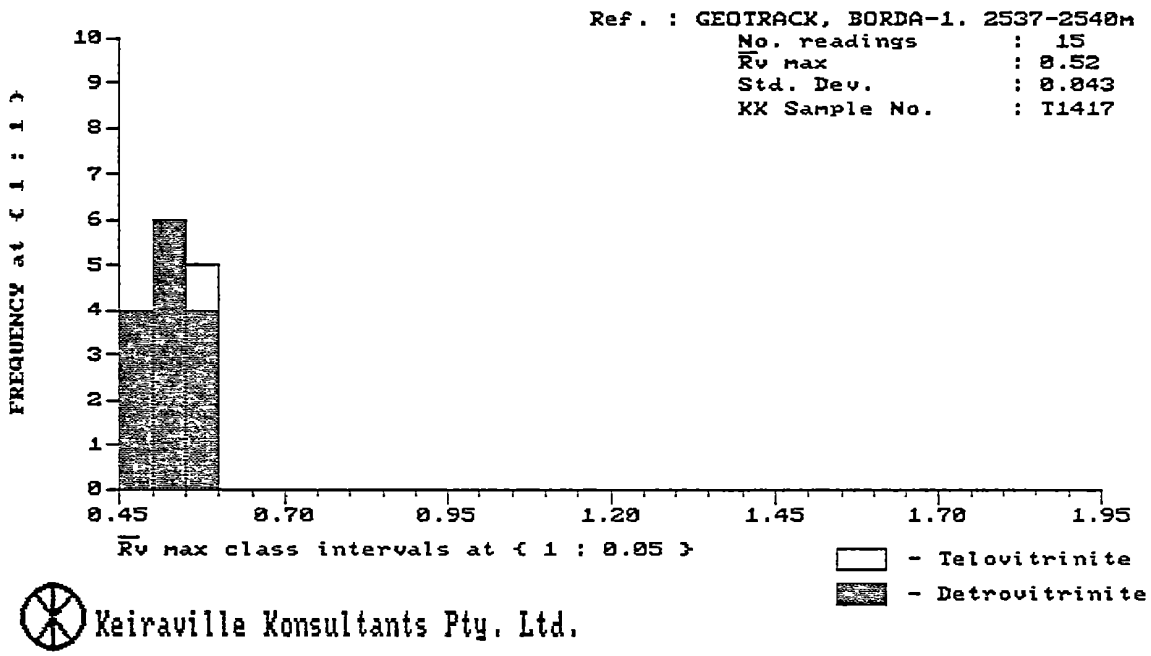

Keiraville Konsultants Pty. Ltd.

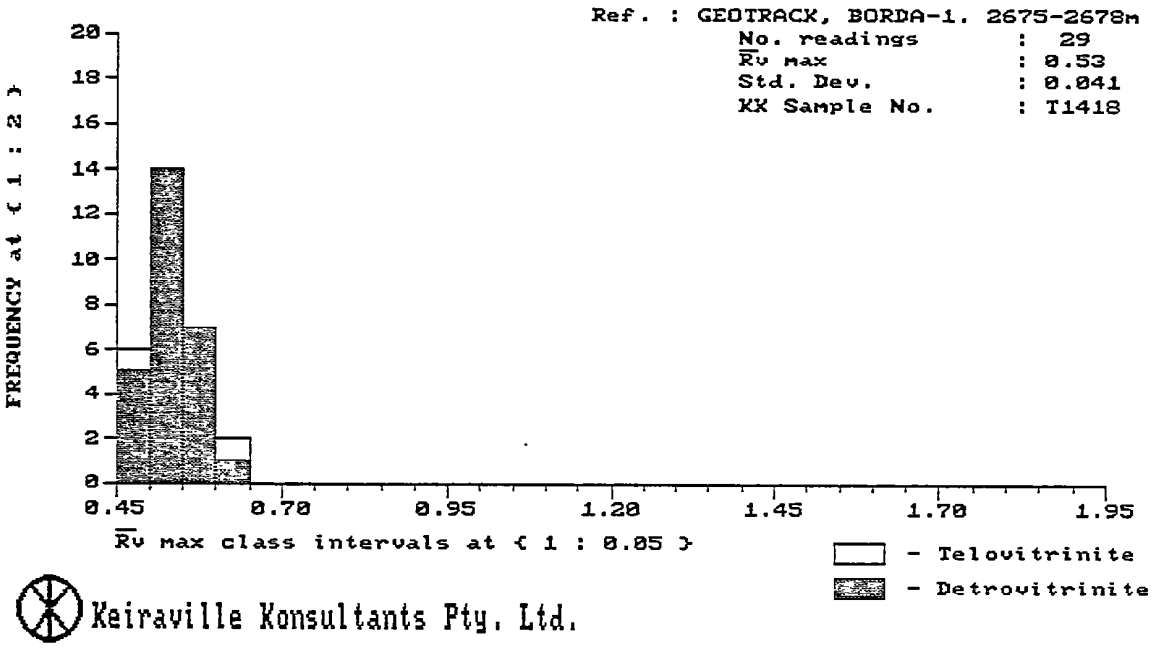

Keiraville Konsultants Pty. Ltd.